AQUEOUS OH PHOTOOXIDATION OF ATMOSPHERICALLY-RELEVANT PRECURSOR-SYSTEMS THROUGH LABORATORY EXPERIMENTS

By

JEFFREY R. KIRKLAND

A dissertation submitted to the

Graduate-School New Brunswick

Rutgers, The State University of New Jersey

in partial fulfillment of the requirements

for the degree of

Doctor of Philosophy

Graduate Program in Environmental Sciences

written under the direction of

Barbara Turpin

and approved by

_____

_____

_____

_____

New Brunswick, New Jersey

October 2014

ABSTRACT OF THE DISSERTATION

Aqueous OH Photooxidation of Atmospherically-Relevant Precursor-Systems through Laboratory Experiments

By JEFFREY R. KIRKLAND

Dissertation Director: BARBARA TURPIN

Chemistry in atmospheric waters (e.g., clouds, fogs, wet aerosols) is a critical component of our complex atmospheric system which affects global environmental health (e.g., climate, air quality). Laboratory, field, and modeling studies have shown that chemistry in atmospheric waters can alter gas-phase budgets of atmospheric oxidants (e.g., HO_2) and change the mass and properties of organic aerosols. However, nearly half of organic matter dissolved in atmospheric waters remains uncharacterized and its chemistry unexplored. The result is error within predictive atmospheric models used to inform policymakers and mitigate harmful gas and particle exposures. To improve model predictions and implement appropriate policies, we must identify and include more detailed chemistry taking place in the atmosphere, specifically in atmospheric waters.

This dissertation is focused on characterizing changes in dissolved organic matter during aqueous-phase chemical reactions (i.e., aqueous processing) and has implications for SOA contributions and atmospheric burdens of gas-phase species. First, the effects of ammonium and nitrate on dilute glyoxal plus hydroxyl radical (OH) chemistry in clouds are explored and support for radical-radical oligomer formation (e.g., tartarate) in wet aerosols is provided. Next, aqueous photooxidation of ambient water-soluble gases collected in the Po Valley, Italy is explored and amines are identified as potentially important participants in aqueous processing. These experiments also demonstrate

formation of particle components (i.e., pyruvate, oxalate) explicitly from aqueous processing of ambient mixtures of water-soluble gases. Finally, aqueous processing of authentic fog waters from Fresno, California and the Po Valley, Italy is explored. Pyruvate and oxalate formation is again observed and precursors to aqueous processing are identified and compared to dissolved organic matter detected by others in fog and rainwater.

This dissertation identifies potentially important precursors and products of aqueous processing; this contributes to an improved understanding of chemistry in atmospheric waters and the related environmental health effects. Precursors identified in this work are likely candidates for future laboratory experiments designed to elicit detailed aqueous chemistry for inclusion in predictive models.

ACKNOWLEDGEMENTS

There are a lot of people to thank for supporting me throughout graduate school. Most importantly and most appreciative of my accomplishments are my parents. I thank Todd and Julie Kirkland, knowing that this is the most important page of my dissertation for them. Of course I also owe the rest of my family and especially my fiancée Lindsey a great deal of thanks. I would be surprised if they read this – but if they do, know that mentioning this sentence is good for a free milkshake (there's no expiration on this voucher). Regardless, my family is an enormous source of motivation.

This page would not be complete without thanks to my advisor Dr. Barbara Turpin for invaluable advice, scientific discussions, mentorship, and general leadership by example. I also want to thank my committee members, Drs. AnnMarie Carlton, John Reinfelder, and Jeff Collett, for their patience through this process since it is so important to each individual student…but they go through the defense process countless times and continue to have patience for every next student. Thank you.

As for the Turpin group past and present, a great deal of thanks is due. Specifically I want to thank Ron Lauck for his continued effort fixing everything in lab that students break. He also has a knack for repairing exhausted brains with a Starbucks latte (mention of this sentence is valid for a latte, or a beverage of equal value, on a mountain at a ski resort somewhere).

TABLE OF CONTENTS

Abstract …… ii

Acknowledgements ……. iv

Table of Contents …… v

List of Tables ……...viii

List of Illustrations ……...ix

Chapter 1: Introduction …….....1

1.1.Motivation ……..1

1.2.Hypothesis and Specific Aims ……3

1.3.Background: Aqueous Processing ..……...4

1.3.1. Secondary Organic Aerosol Formation ...…….4

1.3.2. Gas Budgets …….5

1.3.3. Precursors …….6

1.3.4. OH Radical Reactions in Atmospheric Waters ……7

1.4.Critical Knowledge Gaps ……...8

1.5.Dissertation Overview ……8

1.6.References ……..13

Chapter 2: Glyoxal SOA Chemistry: Effects of dilute nitrate and ammonium and support for organic radical-radical oligomer formation ……..21

2.1.Introduction ……..21

2.2.Experimental …….25

2.2.1. Batch Reactions ……..25

2.2.2. OH Radical Reactions ……26

2.2.3. Product Analysis/Analytical Methods ……26

2.2.4. Quality Control ……...28

2.2.5. Accounting for Nitrate Photolysis ……..29

2.3.Results and discussion ……..29

2.3.1. Dilute glyoxal chemistry in the presence of inorganic nitrogen ……29

2.3.2. Organic nitrogen ……31

2.3.3. Oligomer formation mechanisms for GLY + OH ……..35

2.3.4. Atmospheric Implications ……..37

2.4.References ……38

Chapter 3: Amines, organic acids, and aqueous photooxidation of water-soluble gases from the Po Valley, Italy ……53

3.1.Introduction ……..53

3.2.Approach ……..56

3.2.1. Mist chamber field sampling ……56

3.2.2. Batch OH radical oxidation of field samples in a cuvette chamber ……..57

3.2.3. Analytical methods ……59

3.2.4. Precursor and product identification criteria ……62

3.2.5. Experiment quality control ……...62

3.3.Results and Discussion ……63

3.3.1. Products of aqueous OH photooxidation ……...63

3.3.2. Precursors ……...65

3.3.3. Amines ……...67

3.4.Conclusions and atmospheric implications ……70

3.5.References ……...72

Chapter 4: Characterization of organic precursors and products during aqueous hydroxyl radical oxidation of Po Valley, Italy and Fresno, California fogs ……88

4.1.Introduction ……88

4.2.Methods ……...91

4.2.1. Sample collection ……..91

4.2.2. Batch OH oxidation experiments in a cuvette chamber ……91

4.2.3. Analytical methods ……...94

4.3.Results and Discussion ……...97

4.3.1. Dissolved organic matter in Po Valley and Fresno fogs ……..97

4.3.2. Products of OH oxidation in Po Valley and Fresno fogs ……97

4.3.3. Select precursors in Po Valley and Fresno ……...99

4.4.Atmospheric implications ……...103

4.5.References ……...106

Chapter 5: Implications and future directions ……125

5.1.Summary ……...125

5.2.Implications ……..126

5.3.References ……133

Appendix A: Chapter 2 ……..……138

A.1.Supporting information for Chapter 2 ……138

A.1.1 Measured and modeled H_2O_2 concentrations during H_2O_2 + UV and model reactions used to determine the H_2O_2 photolysis rate constant ……...…..138

A.1.2. Modeled OH concentrations in the presence and absence of HNO_3 ……..…...138

A.1.3. Oxalate concentrations modeled in the presence and absence of HNO_3 …..….139

A.1.4. Modeled nitrate concentrations for GLY + OH + HNO_3 ……..……140

A.1.5. Modeled pH in the presence and absence of HNO_3 using the GLY model and HNO_3 reactions …….…….141

A.1.6. Oxalate concentration measured during GLY + HNO_3 + UV by IC .....……142

A.1.7. Nitrate concentration measured during GLY + HNO_3 + UV by IC …….…….143

A.1.8. Nitrate concentration measured during GLY + OH + HNO_3 by IC ….…….144

A.2.Protocols utilized in Chapter 2 ……145

A.2.1. Batch 1 liter reaction vessel SOP (includes updated sample data sheet)….....145

A.2.2. UV Spectrometry SOP for H_2O_2 + UV experiments ……148

A.2.3. Ion Chromatography SOP (Includes processing of IC/ESI-MS data)…..…….149

Appendix B: Chapter 3 ……150

B.1.Supporting information for Chapter 3 ……...150

B.1.1. Mist chamber sampling times throughout the study ……150

B.1.2. H_2O_2 + UV measurements and model results ……..151

B.1.3. Catalase test results and organic anion recoveries ……...153

B.1.4. ESI-MS detection limits (spectra) ……154

B.1.5. Acetate (+ glycolate) quantification by IC during OH experiments …….155

B.1.6. Formate quantification by IC during OH experiments ……..156

B.1.7. Pyruvate quantification by IC during OH experiments ……....157

B.1.8. Glyoxylate quantification by IC during OH experiments …….....158

B.1.9. Nitrate quantification by IC during OH experiments …….159

B.1.10. Succinate (+ malate) quantification by IC during OH experiments ……...160

B.1.11. Tartarate (+malonate) quantification by IC during OH experiments ……161

B.1.12. Sulfate quantification by IC during OH experiments ……...162

B.1.13. Oxalate quantification by IC during OH experiments ……..163

B.1.14. Product ions identified during OH experiments with mist chamber samples ..164

B.1.15. Product ion trends detected by ESI-MS during OH experiments ……165

B.1.16. Glyoxal (50 μM) + OH test result: oxalate production plot ……166

B.1.17. Fragmentation spectrum for precursor ion m/z+ 304 ……...167

B.1.18. Mechanism that may link precursor ions m/z+ 130 and intermediate/product ion m/z+ 118 ……168

B.1.19. Fragmentation spectrum for intermediate ion m/z+ 118 ……...169

B.1.20. Fragmentation spectrum for intermediate ion m/z+ 162 ……...170

B.2.Protocols used in Chapter 3 ……171

B.2.1. Mist chamber operation SOP ……171

B.2.2. Mist chamber operation field data sheet ……174

B.2.3. Cuvette chamber SOP ……176

B.2.4. Cuvette chamber laboratory sample data sheet ……180

Appendix C: Chapter 4 ……182

C.1.Supporting information for Chapter 4 ……182

C.1.1. Catalase test results and organic anion recoveries ……182

C.1.2. Acetate (+ glycolate) quantification by IC for fog plus OH experiments ……..183

C.1.3. Formate quantification by IC for fog plus OH experiments ……...184

C.1.4. Pyruvate quantification by IC for fog plus OH experiments …….185

C.1.5. Glyoxylate quantification by IC for fog plus OH experiments ……..186

C.1.6. Nitrate quantification by IC for fog plus OH experiments …….187

C.1.7. Succinate (+ malate) quantification by IC for fog plus OH experiments ……...188

C.1.8. Tartarate (+ malonate) quantification by IC for fog plus OH experiments ……189

C.1.9. Sulfate quantification by IC for fog plus OH experiments ……...190

C.1.10. Oxalate quantification by IC for fog plus OH experiments ……191

C.1.11. Fragmentation mechanism and mass spectrum for parent ion(s) detected in Fresno fog samples at unit mass m/z+ 143 …….192

C.1.12. Fragmentation mechanism and mass spectrum for parent ion(s) detected in Fresno fog samples at unit mass m/z+ 167 …….194

C.1.13. Fragmentation mechanism and mass spectrum for parent ion(s) detected in Fresno fog samples at unit mass m/z+ 169 …….195

C.1.14. Fragmentation mechanism and mass spectrum for parent ion(s) detected in Fresno fog samples at unit mass m/z+ 183 …….197

C.1.15. Fragmentation mechanism and mass spectrum for parent ion(s) detected in Fresno fog samples at unit mass m/z+ 185 ……199

C.1.16. Fragmentation mechanism and mass spectrum for parent ion(s) detected in Po Valley fog samples at unit mass m/z+ 113 ……201

C.1.17. Fragmentation mechanism and mass spectrum for parent ion(s) detected in Po Valley fog samples at unit mass m/z+ 153 ……203

C.1.18. Fragmentation mechanism and mass spectrum for parent ion(s) detected in Po Valley fog samples at unit mass m/z+ 167 ……206

C.1.19. Fragmentation mechanism and mass spectrum for parent ion(s) detected in Po Valley fog samples at unit mass m/z+ 169 ……208

C.1.20. Fragmentation mechanism and mass spectrum for parent ion(s) detected in Po Valley fog samples at unit mass m/z+ 183 ……210

C.1.21. Fragmentation mechanism and mass spectrum for parent ion(s) detected in Po Valley fog samples at unit mass m/z+ 185 ……212

LIST OF TABLES

Table 3-1. Mist chamber sample characterization for samples used in OH experiments

……85

Table 3-2. Elemental formulas assigned to precursor ions in July 7^{th},8^{th},9^{th} samples ….86

Table 3-3. Exact masses of precursor ion fragments from analysis of m/z+ 130 ……87

Table 4-1. Fog sample characterization ……118

Table 4-2. Precursors and products identified during OH experiments with Po Valley and Fresno fogs; positive and negative mode ESI-MS analysis ……119

Table 4-3. Exact masses and elemental formulas assigned to parent ions identified during high resolution analysis of fog samples ……..120

Table 4-4. Structures assigned to parent ions using fragmentation information ……...122

LIST OF ILLUSTRATIONS

Figure 2-1. Oxalate production during glyoxal photooxidation experiments ……..46

Figure 2-2. Tartarate production during glyoxal photooxidation experiments ……47

Figure 2-3. Hypothesized organic nitrogen formation reactions ……..48

Figure 2-4. IC-ESI-MS plots for 40 minute samples during glyoxal photooxidation experiments ……..49

Figure 2-5. Relative abundances of tartarate and malonate during glyoxal plus hydroxyl radical ……52

Figure 3-1. Oxalate and pyruvate production during cuvette chamber experiments with July 7th, 8th, 9th samples plus OH radicals ……79

Figure 3-2. Oxalate and pyruvate production during cuvette chamber experiments with June 19th and June 20th samples plus OH radicals ……80

Figure 3-3. Precursor ion trends during cuvette chamber experiments with July 7th, 8th, 9th samples plus OH radicals ……81

Figure 3-4. Precursor ion trends during cuvette chamber experiments with June 19th and 20th samples plus OH radicals ……...82

Figure 3-5. Fragmentation spectrum and structure with noted fragments for m/z+ 130, a precursor in July 7th, 8th, 9th plus OH radical experiments ……83

Figure 4-1. Positive and negative mode ESI-MS spectra at t = 0, 20, 150 minutes into OH radical experiments with Po Valley and Fresno fog samples ……..112

Figure 4-2. Oxalate and pyruvate production during OH experiments with Fresno and Po Valley fog samples ……..114

Figure 4-3. Precursor ion trends during OH experiments with Fresno and Po Valley fog samples ……116

Figure 4-4. Van Krevelen plots of potentially important precursor ions identified during OH experiments with Fresno and Po Valley fog samples ……117

Chapter 1. Introduction

1.1.Motivation

Laboratory, field, and modeling studies have shown that atmospheric aqueous chemistry can alter gas-phase budgets of water-soluble emissions (Nielsen *et al.*, 2012; Ervens *et al.*, 2013; Herckes *et al.*, 2013; Gilardoni *et al.*, 2014) and the mass and properties of organic aerosols (Carlton *et al.*, 2007; Lee *et al.*, 2012; Ortiz-Montalvo *et al.*, 2013). For example, Lee *et al.* (2012) demonstrates volatility changes for dissolved organics undergoing laboratory aqueous processing of cloud and aerosol extracts. Gilardoni *et al.* (2014) monitors gas concentrations before, during, and after fog events to show that scavenging due to fogs leaves interstitial air depleted of water-soluble and oxidized species. Ervens *et al.* (2013) demonstrate gas-phase HO_2 concentrations decrease due to aldehyde oxidation during aqueous processing in clouds/fogs using a box model approach. Atmospheric waters are an important medium through which primary emissions can change during their atmospheric lifetime.

Secondary reactions are a critical component of our complex atmospheric system which affects global environmental health (e.g., climate, air quality). Secondary reactions in the atmosphere play an important role in aerosol production (Hallquist *et al.*, 2009; Ervens *et al.*, 2011). The Intergovernmental Panel on Climate Change (IPCC) continues to report that aerosols contribute the largest uncertainties in global radiative forcing estimates (Stocker, 2013). Since secondary contributions to aerosol mass are difficult to discern and a large source of uncertainty in aerosol predictions (Robinson *et al.*, 2007) and 18-70% of fine particles are organic (by mass), secondary reactions in the gas and aqueous phases are important to improve our understanding of chemical changes

in the atmosphere and the resulting environmental impacts. This dissertation focuses specifically on the aqueous component of secondary reactions.

Atmospheric waters are a platform for water-soluble gaseous and particulate compounds to react forming products with altered properties (e.g., light absorption/scattering, volatility). Notably, aqueous processing contributes to aerosol mass in parallel with gas-phase chemistry, but the precursors to secondary organic aerosol formation through aqueous processing and gas-phase chemistry are fundamentally different. Aqueous processing, for example, requires water-soluble precursors (e.g., low molecular weight species, high O:C ratios). Gas-phase chemistry can occur with primary emissions (e.g., volatile organic compounds, low O:C ratios or hydrocarbons without oxygen) and larger precursors ($>C_7$) are typically needed in order to achieve high yields of secondary organic aerosol through gas phase chemistry and vapor-pressure based partitioning. Thus this process typically produces organic aerosol that has lower O:C ratios and is less hygroscopic than organic aerosol formed through condensed phase chemistry (i.e. chemistry in liquid water or aerosol organic matter). Hygroscopic organic aerosol better act as cloud condensation nuclei and thus, may have greater impacts on climate (Petters and Kreidenweis, 2007; Henning *et al.*, 2014). Oxidant concentrations are strong drivers of gas and aqueous atmospheric chemistry (e.g., O_3, OH, HO_2, NOx, Fe) (Seinfeld and Pandis, 2012). Oxidation reactions lead to increased O:C ratios and water-solubility for emissions as residence time in the atmosphere increases. Oxidant concentrations within atmospheric waters are highly uncertain, and the degree to which oxidants are produced through condensed phase reactions may determine whether oxidation chemistry in wet aerosols exhibits an aerosol

surface area dependence or a liquid water dependence (Ervens *et al.*, 2014). Although inclusion of some precursors to aqueous processing helps link ambient measurements with chemical model predictions, uncertainties in aerosol properties and behavior remain large (Ervens *et al.*, 2011) and nearly half of dissolved organic matter remains uncharacterized in cloud and fog waters (Herckes *et al.*, 2013).

This dissertation explores the aqueous oxidation of atmospherically-relevant mixtures of compounds through controlled experiments. This approach increases our understanding of aqueous processing of previously unstudied, potentially important water-soluble atmospheric species; a critical step to minimize uncertainty in aerosol predictions, identify reactive components of dissolved organic matter, and identify changes in chemical composition due to aqueous processing.

1.2.Hypothesis and Specific Aims

Complex aqueous mixtures explored through laboratory photooxidation experiments will reveal previously unrecognized precursor-product relationships during aqueous processing in real atmospheric waters. The following specific aims are designed to test this hypothesis:

1) Conduct batch aqueous photooxidation experiments with glyoxal, a known participant in aqueous chemistry, in the presence of inorganic nitrogen to understand the effects of ammonium and nitrate on the cloud chemistry of glyoxal.
2) Design and test a new batch reactor capable of conducting reproducible aqueous oxidation experiments with smaller sample volumes (i.e., 33 ml rather than 1 L).

3) Deploy an apparatus for field collection of water-soluble gases and explore the aqueous OH radical oxidation of the ambient matrix of water soluble gases found in the Po Valley, Italy to identify precursors to aqueous oxidation in the ambient environment.
4) Conduct batch aqueous photooxidation experiments with authentic atmospheric waters (i.e., Fresno, CA and Po Valley, IT fog) to identify changes in dissolved organic matter chemical composition and identify previously unstudied precursors to aqueous processing.

1.3.Background: Aqueous Processing

1.3.1. Secondary Organic Aerosol Formation

Secondary formation of aerosol occurs through chemical transformations of primary anthropogenic and biogenic emissions in the atmosphere. Gas phase oxidation of volatile organic compounds (VOC's) creates semi- or low-volatility products that contribute to aerosol mass through nucleation events (Yu and Luo 2009) or condensation onto/into pre-existing particles (Pankow, 1994; Seinfeld and Pankow, 2003; Hallquist *et al.*, 2009). Gas phase oxidative chemistry also cleaves and oxidizes primary emissions producing soluble species capable of partitioning into atmospheric waters (i.e., cloud, fog and aerosol water) where further reactions take place. Water-soluble gaseous organics are ubiquitous throughout the continental troposphere (Carlton and Turpin, 2013). Contributions to aerosol mass from aqueous processing occur when dissolved species react and form low-volatility products that remain in the particle phase after droplet evaporation (Blando and Turpin, 2000; Gelencsér *et al.*, 2003). Contributions to aerosol mass through the latter mechanism are referred to as aqueous SOA (SOA_{aq}). Current

estimates of aqueous SOA demonstrate substantial contributions to total aerosol mass that may rival contributions from gas phase chemistry and vapor pressure based partitioning (Myhre *et al.*, 2009; Ervens *et al.*, 2011; Updyke *et al.*, 2012).

Aqueous processing in clouds and fogs is fundamentally different from aqueous processing in aerosol water. Solutes in clouds and fogs are in dilute solution. Oxidation reactions will dominate in cloud and fog water and radicals formed can be expected to react with dissolved oxygen. This chemistry leads to organic acid formation, for example, from aldehyde oxidation. This chemistry may be oxidant (i.e., OH) limited (Ervens *et al.*, 2014). In contrast, aerosol water contains high organic and inorganic solute concentrations, making non-radical and radical-radical chemistry more favorable. Both mechanisms lead to oligomer formation and in certain cases organosulfate formation or formation of nitrogen-containing organics in wet aerosols (Noziere *et al.*, 2008; Galloway *et al.*, 2009; Perri *et al.*, 2010; Sareen *et al.*, 2010). The focus of this dissertation is cloud/fog-relevant oxidation chemistry to improve our fundamental understanding of aqueous SOA contributions to aerosol mass. While products will be different, we expect that precursors of oxidation chemistry identified herein will also initiate oxidation chemistry in wet aerosols.

1.3.2. Gas Budgets

Atmospheric waters also provide a sink for gases and particles, and thus alter atmospheric budgets of selected species (Collett Jr *et al.*, 2008). Ervens *et al.* (2013) demonstrate that a small percentage (<1%) of dissolved organic carbon (DOC) in atmospheric waters may be an important sink for HO_2 from the gas phase because reaction rates in the aqueous phase are faster than in the gas phase. Similarly, Herckes *et*

al. (2013) provide evidence that more than 50% of dissolved organic matter in clouds and fogs remains uncharacterized. This suggests that the species participating in aqueous processing and the resulting impacts on gas-phase budgets and on atmospheric aerosol mass, composition and properties is poorly understood. The research herein aims to reduce these uncertainties, contribute to the characterization of atmospheric aqueous chemistry, improve mechanistic linkages between controllable emissions and ambient concentrations/composition, and enable the development of more effective air quality management strategies.

1.3.3. Precursors

Organic precursors to aqueous processing (e.g., aldehydes, ketones, monoacids) have been studied for more than a decade (Warneck, 1999; Carlton *et al.*, 2007; Noziere *et al.*, 2008; Paulot *et al.*, 2009; Zhang *et al.*, 2011). More recently it has become apparent that organic chemistry in acidic sulfate aerosols takes place in aerosol water (Zhang *et al.*, 2011), and that aqueous chemistry is important to the formation of SOA from isoprene epoxides (Paulot *et al.*, 2009). Yet a comprehensive characterization of dissolved organic matter and associated chemical changes through aqueous processing does not exist. Chemical changes through aqueous processing have been identified through extensive laboratory and modeling studies (Schwier *et al.*, 2010; Ervens *et al.*, 2011; Ervens *et al.*, 2014). Well-studied precursors include gas-phase oxidation products of isoprene, the most abundant non-methane hydrocarbon (Guenther *et al.*, 2006), namely glyoxal, methylglyoxal, pyruvic acid, acetic acid, glycolaldehyde, methylvinylketone (MVK) and methacrolein (MAC). Atmospheric reactivity of these chemicals has been explored through bulk phase experiments (Carlton *et al.*, 2006; Carlton *et al.*, 2007;

Altieri *et al.*, 2008; Perri *et al.*, 2009; Tan *et al.*, 2010; Zhang *et al.*, 2010; Liu *et al.*, 2012; Tan *et al.*, 2012) and smog chamber experiments (Liggio *et al.*, 2005; Galloway *et al.*, 2009; Nguyen *et al.*, 2013; Zhang *et al.*, 2013) and limited implementation of this chemistry in predictive models has begun (Chen *et al.*, 2007; Myriokefalitakis *et al.*, 2011; Liu *et al.*, 2012). Identification of important precursors, e.g., through methods employed herein, is an important step to improved predictive models. Since models rely on a few important precursors to predict aqueous SOA (Liu *et al.*, 2012) we must identify and include other reactive precursors (e.g., amines) to improve the accuracy of aerosol mass contributions from aqueous processing.

1.3.4. OH Radical Reactions in Atmospheric Waters

OH radical chemistry in atmospheric waters is the focus of this dissertation. Although many oxidants (e.g., O_3, OH, NO_x, Fe, O_2) participate in gas and aqueous atmospheric chemistry (Ervens *et al.*, 2011), OH radicals have rapid reaction rates, versatile reactivity (i.e., H-atom abstraction, double bond addition), and an ability to partition into atmospheric waters from the gas phase (H_{OH} = 30 M atm^{-1}) (Hanson *et al.*, 1992) or form in-situ (Faust and Allen, 1993; Anastasio and McGregor, 2001; Ervens *et al.*, 2014). Since direct measurement of OH radicals in clouds and fogs is not currently possible we rely on proxies for predictions, which suggest that OH radical concentrations could be 10^{-12}-10^{-13}M (Jacob, 1986) in clouds, but may be as low as 10^{-15} M when accounting for organic sinks (Arakaki *et al.*, 2013), and OH estimates may be a major source of uncertainty in aqSOA contributions (Ervens *et al.*, 2014). Furthermore, aqueous OH radical reactions are expected to proceed faster than gas-phase OH chemistry for many species (Atkinson, 1987; Doussin and Monod, 2013).

1.4.Critical Knowledge Gaps

An important goal of the work herein is the identification of reactive water-soluble compounds; possible implications of aqueous processing to atmospheric budgets and environmental health will be discussed. The current state of fog and cloud water analysis is summarized in a recent review by Herckes *et al.* (2013). Briefly, the summary evaluates fog and cloud waters collected across the globe over the past several decades. Herckes *et al.* (2013) critical finding is that cloud and fog waters remain mostly uncharacterized. The authors' summary includes a call for greater efforts to integrate field and laboratory studies to address this deficiency. Ervens *et al.* (2011) provide a review of aqueous processing and focus on contributions to SOA_{aq} mass. Briefly, this review provides evidence that aqueous contributions to organic aerosol mass rival gas-phase contributions, but uncertainties in aqueous processing of organics remain high. We must understand both gas and aqueous chemistry in the atmosphere in order to parameterize this chemistry in such a way as to accurately assess the impacts of controllable emissions on global aerosol budgets (Carlton *et al.*, 2010). This dissertation is focused on characterizing changes in dissolved organic matter during aqueous processing and has implications for aqueous SOA contributions.

1.5.Dissertation Overview

The research reported herein contributes to the growing body of literature exploring chemistry in atmospheric waters. This dissertation explores OH radical photooxidation of complex systems of dissolved organic matter representative of naturally occurring atmospheric cloud/fog waters. Precursors to and products of aqueous processing are discussed in greater detail below. A critical step to mitigation of harmful

effects resulting from controllable emissions and to improved control technologies/strategies is the improved understanding of secondary chemistry in the gas and aqueous phases.

In Chapter 2, the aqueous processing I explore is glyoxal photooxidation by OH in the presence (and absence) of ammonium or nitrate. Glyoxal (GLY) is ubiquitous in the atmosphere and an important aqueous secondary organic aerosol (SOA) precursor (Volkamer *et al.*, 2007; Ortiz-Montalvo *et al.*, 2013). At dilute (cloud-relevant) organic concentrations, OH radical oxidation of GLY has been shown to produce oxalate (Carlton *et al.*, 2007). GLY has also been used as a surrogate species to gain insight into radical and non-radical reactions in wet aerosols, where organic and inorganic concentrations are very high (~M) (Noziere *et al.*, 2008; Galloway *et al.*, 2009; Lim *et al.*, 2010; Lim *et al.*, 2013). The work herein demonstrates, for the first time, that tartarate forms from GLY + OH (Chapter 2) (Kirkland *et al.*, 2013). Tartarate is a key product in a previously proposed organic radical-radical reaction mechanism used to explain the formation of oligomers from GLY oxidation in concentrated (wet aerosol-relevant) solutions (Lim *et al.*, 2010). Making use of this mechanism to better understand differences between oxidation chemistry in wet aerosols and in clouds, Lim *et al.* (2010) concluded that oligomers are major products of OH radical oxidation at high organic concentrations found in wet aerosols. Tartarate measurements herein provide support for this proposed oligomer formation mechanism. This work also demonstrates, for the first time, that dilute (cloud/fog-relevant) concentrations of inorganic nitrogen (i.e., ammonium, nitrate) have little effect on the GLY + OH chemistry leading to oxalate formation in clouds (Kirkland *et al.*, 2013). This, and results from previous experiments conducted with

acidic sulfate, increase confidence that the currently understood dilute GLY + OH chemistry (Lim *et al.*, 2005; Lim *et al.*, 2010) can be used to predict GLY contributions to aqueous SOA through chemistry in clouds and fogs. It should be recognized that organic – inorganic interactions can play an important role in droplet evaporation chemistry (Connelly *et al.*, 2012; Ortiz-Montalvo *et al.*, 2013) and in wet aerosols (Noziere *et al.*, 2008; Galloway *et al.*, 2009; Sareen *et al.*, 2010). The chemistry leading to SOA formation in those environments is complex and remains poorly understood. Note that data produced from chemical models in this chapter is a contribution from Yong Bin Lim.

In Chapter 3, we explore aqueous photooxidation of ambient water-soluble gases to develop insights into potentially important precursors to aqueous processing that may influence aqueous SOA or gas phase budgets. Aqueous OH radical oxidation of several *individual* precursors hypothesized to be important to aqueous SOA formation has been studied in the laboratory (Ervens *et al.*, 2011). In contrast, in this work a mist-chamber (Cofer *et al.*, 1985; Anderson *et al.*, 2008) apparatus was used to collect *atmospheric mixtures* of water-soluble gases from the ambient air at San Pietro Capofiume, Italy during the PEGASOS field campaign. By measuring the concentration dynamics after addition of OH radicals, we were able to develop new insights regarding organic species that initiate aqueous processing. The design and testing of a new reaction vessel that requires smaller water volumes facilitated this research. Specifically, batch aqueous reactions were conducted with 33 ml aliquots of mist-chamber samples and OH radicals in a new low-volume aqueous reaction vessel. Pyruvate and oxalate production was detected in the presence but not in the absence of OH radicals, demonstrating that species

found predominantly in the particle phase in the atmosphere (Saxena and Hildemann, 1996; Kawamura *et al.*, 2003) do form explicitly from aqueous oxidation of atmospheric gases. These compounds are known to form from aldehyde oxidation in the aqueous phase (Carlton *et al.*, 2007; Altieri *et al.*, 2008; Tan *et al.*, 2009; Tan *et al.*, 2010), and could plausibly form from other precursors. Amines and other ions were identified as important precursors to aqueous processing. Amine elemental formulas and chemical structures are reported based upon high-resolution mass spectrometric analysis. Identification of precursors during these experiments demonstrates the removal of water-soluble species from the gas phase in the presence of liquid water where further reactions take place. Note that structural interpretations and the chemical mechanism developed in this chapter were developed with Yong Bin Lim.

In Chapter 4, we induce OH radical chemistry in natural fog waters to improve our current understanding of aqueous processing in authentic atmospheric fog waters. Fog waters naturally accumulate particles and an ambient matrix of water-soluble gases. Further oxidation of these species in the aqueous phase allows us to examine changes in the composition of fog water as it would take place in the atmosphere. Experiments were conducted with winter fog waters collected in Fresno, California and Po Valley, Italy. Batch aqueous photooxidation reactions were conducted in a 33 mL cuvette chamber with fog samples and OH radicals. Pyruvate and oxalate production was again observed. Decreasing ion abundance with increasing reaction times were observed for both types of fogwater in the presence, but not the absence of OH radicals. Elemental formulas and chemical structures for reactants in these fogwaters were compared to past fog and rain water analyses to identify common or unique precursor ions. Precursor and product

characterization in these experiments identifies a complex system of dissolved organic matter in naturally occurring atmospheric waters and provides insight into aqueous processing of water soluble gases and the water-soluble components of particles that partitioned into the bulk aqueous phase during sample collection.

The concluding chapter summarizes the key contributions from this research, limitations, and steps that could improve our current understanding of the results reported herein. The focused implications of this dissertation pertain to budgets of atmospheric gases and contributions to aerosol mass through secondary reactions in atmospheric waters. Broader implications over an extended period of time will include changes in agricultural, industrial, and societal practices as the global population continues to grow. Our current understanding of atmospheric processes, specifically chemistry in atmospheric waters, leaves us unprepared for these changes. This dissertation is a small step towards preparation for future challenges in atmospheric chemistry. Currently our best method of preparation is to accurately characterize, quantify, and understand the modern atmosphere.

1.6.References

Altieri, K.E., S.P. Seitzinger, A.G. Carlton, B.J. Turpin, G.C. Klein and A.G. Marshall, 2008. Oligomers formed through in-cloud methylglyoxal reactions: Chemical composition, properties, and mechanisms investigated by ultra-high resolution ft-icr mass spectrometry. Atmospheric Environment, 42(7): 1476-1490. Available from http://www.sciencedirect.com/science/article/pii/S1352231007010205. DOI http://dx.doi.org/10.1016/j.atmosenv.2007.11.015.

Anastasio, C. and K.G. McGregor, 2001. Chemistry of fog waters in california's central valley: 1. In situ photoformation of hydroxyl radical and singlet molecular oxygen. Atmospheric Environment, 35(6): 1079-1089. Available from http://www.sciencedirect.com/science/article/pii/S1352231000002818. DOI http://dx.doi.org/10.1016/S1352-2310(00)00281-8.

Anderson, C.H., J.E. Dibb, R.J. Griffin, G.S.W. Hagler and M.H. Bergin, 2008. Atmospheric water-soluble organic carbon measurements at summit, greenland. Atmospheric Environment, 42(22): 5612-5621. Available from http://www.sciencedirect.com/science/article/pii/S1352231008002562. DOI http://dx.doi.org/10.1016/j.atmosenv.2008.03.006.

Arakaki, T., C. Anastasio, Y. Kuroki, H. Nakajima, K. Okada, Y. Kotani, D. Handa, S. Azechi, T. Kimura, A. Tsuhako and Y. Miyagi, 2013. A general scavenging rate constant for reaction of hydroxyl radical with organic carbon in atmospheric waters. Environmental Science & Technology, 47(15): 8196-8203. Available from http://dx.doi.org/10.1021/es401927b [Accessed 2014/03/28]. DOI 10.1021/es401927b.

Atkinson, R., 1987. A structure-activity relationship for the estimation of rate constants for the gas-phase reactions of oh radicals with organic compounds. International Journal of Chemical Kinetics, 19(9): 799-828. Available from http://dx.doi.org/10.1002/kin.550190903. DOI 10.1002/kin.550190903.

Blando, J.D. and B.J. Turpin, 2000. Secondary organic aerosol formation in cloud and fog droplets: A literature evaluation of plausibility. Atmospheric Environment, 34(10): 1623-1632. Available from http://www.sciencedirect.com/science/article/pii/S1352231099003921. DOI http://dx.doi.org/10.1016/S1352-2310(99)00392-1.

Carlton, A.G., R.W. Pinder, P.V. Bhave and G.A. Pouliot, 2010. To what extent can biogenic soa be controlled? Environmental science & technology, 44(9): 3376-3380.

Carlton, A.G. and B.J. Turpin, 2013. Particle partitioning potential of organic compounds is highest in the eastern us and driven by anthropogenic water. Atmos. Chem.

Phys., 13(20): 10203-10214. Available from http://www.atmos-chem-phys.net/13/10203/2013/. DOI 10.5194/acp-13-10203-2013.

Carlton, A.G., B.J. Turpin, K.E. Altieri, S. Seitzinger, A. Reff, H.-J. Lim and B. Ervens, 2007. Atmospheric oxalic acid and soa production from glyoxal: Results of aqueous photooxidation experiments. Atmospheric Environment, 41(35): 7588-7602. Available from http://www.sciencedirect.com/science/article/pii/S1352231007004979. DOI http://dx.doi.org/10.1016/j.atmosenv.2007.05.035.

Carlton, A.G., B.J. Turpin, H.-J. Lim, K.E. Altieri and S. Seitzinger, 2006. Link between isoprene and secondary organic aerosol (soa): Pyruvic acid oxidation yields low volatility organic acids in clouds. Geophysical Research Letters, 33(6): L06822. Available from http://dx.doi.org/10.1029/2005GL025374. DOI 10.1029/2005GL025374.

Chen, J., R.J. Griffin, A. Grini and P. Tulet, 2007. Modeling secondary organic aerosol formation through cloud processing of organic compounds. Atmos. Chem. Phys., 7(20): 5343-5355. Available from http://www.atmos-chem-phys.net/7/5343/2007/. DOI 10.5194/acp-7-5343-2007.

Cofer, W.R., V.G. Collins and R.W. Talbot, 1985. Improved aqueous scrubber for collection of soluble atmospheric trace gases. Environmental science & technology, 19(6): 557-560.

Collett Jr, J.L., P. Herckes, S. Youngster and T. Lee, 2008. Processing of atmospheric organic matter by california radiation fogs. Atmospheric Research, 87(3–4): 232-241. Available from http://www.sciencedirect.com/science/article/pii/S0169809507002025. DOI http://dx.doi.org/10.1016/j.atmosres.2007.11.005.

Connelly, B.M., D.O. De Haan and M.A. Tolbert, 2012. Heterogeneous glyoxal oxidation: A potential source of secondary organic aerosol. The Journal of Physical Chemistry A, 116(24): 6180-6187. Available from http://dx.doi.org/10.1021/jp211502e [Accessed 2014/01/10]. DOI 10.1021/jp211502e.

Doussin, J.F. and A. Monod, 2013. Structure–activity relationship for the estimation of oh-oxidation rate constants of carbonyl compounds in the aqueous phase. Atmos. Chem. Phys., 13(23): 11625-11641. Available from http://www.atmos-chem-phys.net/13/11625/2013/. DOI 10.5194/acp-13-11625-2013.

Ervens, B., A. Sorooshian, Y.B. Lim and B.J. Turpin, 2014. Key parameters controlling oh-initiated formation of secondary organic aerosol in the aqueous phase (aqsoa). Journal of Geophysical Research: Atmospheres: 2013JD021021. Available from http://dx.doi.org/10.1002/2013JD021021. DOI 10.1002/2013JD021021.

Ervens, B., B.J. Turpin and R.J. Weber, 2011. Secondary organic aerosol formation in cloud droplets and aqueous particles (aqsoa): A review of laboratory, field and model studies. Atmos. Chem. Phys., 11(21): 11069-11102. Available from http://www.atmos-chem-phys.net/11/11069/2011/. DOI 10.5194/acp-11-11069-2011.

Ervens, B., Y. Wang, J. Eagar, W.R. Leaitch, A.M. Macdonald, K.T. Valsaraj and P. Herckes, 2013. Dissolved organic carbon (doc) and select aldehydes in cloud and fog water: The role of the aqueous phase in impacting trace gas budgets. Atmos. Chem. Phys., 13(10): 5117-5135. Available from http://www.atmos-chem-phys.net/13/5117/2013/. DOI 10.5194/acp-13-5117-2013.

Faust, B.C. and J.M. Allen, 1993. Aqueous-phase photochemical formation of hydroxyl radical in authentic cloudwaters and fogwaters. Environmental science & technology, 27(6): 1221-1224.

Galloway, M.M., P.S. Chhabra, A.W.H. Chan, J.D. Surratt, R.C. Flagan, J.H. Seinfeld and F.N. Keutsch, 2009. Glyoxal uptake on ammonium sulphate seed aerosol: Reaction products and reversibility of uptake under dark and irradiated conditions. Atmos. Chem. Phys., 9(10): 3331-3345. Available from http://www.atmos-chem-phys.net/9/3331/2009/. DOI 10.5194/acp-9-3331-2009.

Gelencsér, A., A. Hoffer, G. Kiss, E. Tombácz, R. Kurdi and L. Bencze, 2003. In-situ formation of light-absorbing organic matter in cloud water. Journal of Atmospheric Chemistry, 45(1): 25-33. Available from http://dx.doi.org/10.1023/A%3A1024060428172. DOI 10.1023/A:1024060428172.

Gilardoni, S., P. Massoli, L. Giulianelli, M. Rinaldi, M. Paglione, F. Pollini, C. Lanconelli, V. Poluzzi, S. Carbone, R. Hillamo, L.M. Russell, M.C. Facchini and S. Fuzzi, 2014. Fog scavenging of organic and inorganic aerosol in the po valley. Atmos. Chem. Phys. Discuss., 14(4): 4787-4826. Available from http://www.atmos-chem-phys-discuss.net/14/4787/2014/. DOI 10.5194/acpd-14-4787-2014.

Guenther, A., T. Karl, P. Harley, C. Wiedinmyer, P.I. Palmer and C. Geron, 2006. Estimates of global terrestrial isoprene emissions using megan (model of emissions of gases and aerosols from nature). Atmos. Chem. Phys., 6(11): 3181-3210. Available from http://www.atmos-chem-phys.net/6/3181/2006/. DOI 10.5194/acp-6-3181-2006.

Hallquist, M., J. Wenger, U. Baltensperger, Y. Rudich, D. Simpson, M. Claeys, J. Dommen, N. Donahue, C. George and A. Goldstein, 2009. Atmos. Chem. Phys., 9: 5155.

Hallquist, M., J.C. Wenger, U. Baltensperger, Y. Rudich, D. Simpson, M. Claeys, J. Dommen, N.M. Donahue, C. George, A.H. Goldstein, J.F. Hamilton, H. Herrmann, T. Hoffmann, Y. Iinuma, M. Jang, M.E. Jenkin, J.L. Jimenez, A. Kiendler-Scharr, W. Maenhaut, G. McFiggans, T.F. Mentel, A. Monod, A.S.H. Prévôt, J.H. Seinfeld, J.D. Surratt, R. Szmigielski and J. Wildt, 2009. The formation, properties and impact of secondary organic aerosol: Current and emerging issues. Atmos. Chem. Phys., 9(14): 5155-5236. Available from http://www.atmos-chem-phys.net/9/5155/2009/. DOI 10.5194/acp-9-5155-2009.

Hanson, D.R., J.B. Burkholder, C.J. Howard and A. Ravishankara, 1992. Measurement of hydroxyl and hydroperoxy radical uptake coefficients on water and sulfuric acid surfaces. The Journal of Physical Chemistry, 96(12): 4979-4985.

Henning, S., K. Dieckmann, K. Ignatius, M. Schäfer, P. Zedler, E. Harris, B. Sinha, D. van Pinxteren, S. Mertes, W. Birmili, M. Merkel, Z. Wu, A. Wiedensohler, H. Wex, H. Herrmann and F. Stratmann, 2014. Influence of cloud processing on ccn activation behaviour in the thuringian forest, germany during hcct-2010. Atmos. Chem. Phys. Discuss., 14(2): 1617-1645. Available from http://www.atmos-chem-phys-discuss.net/14/1617/2014/. DOI 10.5194/acpd-14-1617-2014.

Herckes, P., K.T. Valsaraj and J.L. Collett Jr, 2013. A review of observations of organic matter in fogs and clouds: Origin, processing and fate. Atmospheric Research, 132–133(0): 434-449. Available from http://www.sciencedirect.com/science/article/pii/S016980951300183X [Accessed 2013/11//]. DOI http://dx.doi.org/10.1016/j.atmosres.2013.06.005.

Jacob, D.J., 1986. Chemistry of oh in remote clouds and its role in the production of formic acid and peroxymonosulfate. Journal of Geophysical Research: Atmospheres, 91(D9): 9807-9826. Available from http://dx.doi.org/10.1029/JD091iD09p09807. DOI 10.1029/JD091iD09p09807.

Kawamura, K., N. Umemoto, M. Mochida, T. Bertram, S. Howell and B.J. Huebert, 2003. Water-soluble dicarboxylic acids in the tropospheric aerosols collected over east asia and western north pacific by ace-asia c-130 aircraft. Journal of Geophysical Research: Atmospheres, 108(D23): 8639. Available from http://dx.doi.org/10.1029/2002JD003256. DOI 10.1029/2002JD003256.

Kirkland, J.R., Y.B. Lim, Y. Tan, K.E. Altieri and B.J. Turpin, 2013. Glyoxal secondary organic aerosol chemistry: Effects of dilute nitrate and ammonium and support for organic radical–radical oligomer formation. Environmental Chemistry, 10(3): 158-166. Available from http://www.publish.csiro.au/paper/EN13074. DOI http://dx.doi.org/10.1071/EN13074.

Lee, A.K.Y., K.L. Hayden, P. Herckes, W.R. Leaitch, J. Liggio, A.M. Macdonald and J.P.D. Abbatt, 2012. Characterization of aerosol and cloud water at a mountain site during wacs 2010: Secondary organic aerosol formation through oxidative

cloud processing. Atmos. Chem. Phys., 12(15): 7103-7116. Available from http://www.atmos-chem-phys.net/12/7103/2012/. DOI 10.5194/acp-12-7103-2012.

Liggio, J., S.-M. Li and R. McLaren, 2005. Heterogeneous reactions of glyoxal on particulate matter: Identification of acetals and sulfate esters. Environmental Science & Technology, 39(6): 1532-1541. Available from http://dx.doi.org/10.1021/es048375y [Accessed 2014/04/08]. DOI 10.1021/es048375y.

Lim, H.-J., A.G. Carlton and B.J. Turpin, 2005. Isoprene forms secondary organic aerosol through cloud processing: Model simulations. Environmental Science & Technology, 39(12): 4441-4446. Available from http://dx.doi.org/10.1021/es048039h [Accessed 2014/01/10]. DOI 10.1021/es048039h.

Lim, Y.B., Y. Tan, M.J. Perri, S.P. Seitzinger and B.J. Turpin, 2010. Aqueous chemistry and its role in secondary organic aerosol (soa) formation. Atmos. Chem. Phys., 10(21): 10521-10539. Available from http://www.atmos-chem-phys.net/10/10521/2010/. DOI 10.5194/acp-10-10521-2010.

Lim, Y.B., Y. Tan and B.J. Turpin, 2013. Chemical insights, explicit chemistry, and yields of secondary organic aerosol from oh radical oxidation of methylglyoxal and glyoxal in the aqueous phase. Atmos. Chem. Phys., 13(17): 8651-8667. Available from http://www.atmos-chem-phys.net/13/8651/2013/. DOI 10.5194/acp-13-8651-2013.

Liu, J., L.W. Horowitz, S. Fan, A.G. Carlton and H. Levy, 2012. Global in-cloud production of secondary organic aerosols: Implementation of a detailed chemical mechanism in the gfdl atmospheric model am3. Journal of Geophysical Research: Atmospheres, 117(D15): D15303. Available from http://dx.doi.org/10.1029/2012JD017838. DOI 10.1029/2012JD017838.

Liu, Y., F. Siekmann, P. Renard, A. El Zein, G. Salque, I. El Haddad, B. Temime-Roussel, D. Voisin, R. Thissen and A. Monod, 2012. Oligomer and soa formation through aqueous phase photooxidation of methacrolein and methyl vinyl ketone. Atmospheric Environment, 49: 123-129.

Myhre, G., T. Berglen, M. Johnsrud, C. Hoyle, T. Berntsen, S. Christopher, D. Fahey, I.S. Isaksen, T. Jones and R. Kahn, 2009. Modelled radiative forcing of the direct aerosol effect with multi-observation evaluation. Atmospheric Chemistry & Physics, 9(4).

Myriokefalitakis, S., K. Tsigaridis, N. Mihalopoulos, J. Sciare, A. Nenes, K. Kawamura, A. Segers and M. Kanakidou, 2011. In-cloud oxalate formation in the global troposphere: A 3-d modeling study. Atmos. Chem. Phys., 11(12): 5761-5782.

Available from http://www.atmos-chem-phys.net/11/5761/2011/. DOI 10.5194/acp-11-5761-2011.

Nguyen, T., M. Coggon, R. Flagan and J. Seinfeld, 2013. Reactive uptake and photo-fenton oxidation of glycolaldehyde in aerosol liquid water. Environmental science & technology, 47(9): 4307-4316.

Nielsen, C.J., H. Herrmann and C. Weller, 2012. Atmospheric chemistry and environmental impact of the use of amines in carbon capture and storage (ccs). Chemical Society Reviews, 41(19): 6684-6704. Available from http://dx.doi.org/10.1039/C2CS35059A. DOI 10.1039/C2CS35059A.

Noziere, B., P. Dziedzic and A. Córdova, 2008. Products and kinetics of the liquid-phase reaction of glyoxal catalyzed by ammonium ions (nh4+). The Journal of Physical Chemistry A, 113(1): 231-237.

Ortiz-Montalvo, D.L., S.A.K. Häkkinen, A.N. Schwier, Y.B. Lim, V.F. McNeill and B.J. Turpin, 2013. Ammonium addition (and aerosol ph) has a dramatic impact on the volatility and yield of glyoxal secondary organic aerosol. Environmental Science & Technology, 48(1): 255-262. Available from http://pubs.acs.org/doi/abs/10.1021/es4035667 [Accessed 2014/03/23]. DOI 10.1021/es4035667.

Pankow, J.F., 1994. An absorption model of gas/particle partitioning of organic compounds in the atmosphere. Atmospheric Environment, 28(2): 185-188.

Paulot, F., J.D. Crounse, H.G. Kjaergaard, A. Kürten, J.M.S. Clair, J.H. Seinfeld and P.O. Wennberg, 2009. Unexpected epoxide formation in the gas-phase photooxidation of isoprene. Science, 325(5941): 730-733.

Perri, M.J., Y.B. Lim, S.P. Seitzinger and B.J. Turpin, 2010. Organosulfates from glycolaldehyde in aqueous aerosols and clouds: Laboratory studies. Atmospheric Environment, 44(21–22): 2658-2664. Available from http://www.sciencedirect.com/science/article/pii/S1352231010002578. DOI http://dx.doi.org/10.1016/j.atmosenv.2010.03.031.

Perri, M.J., S. Seitzinger and B.J. Turpin, 2009. Secondary organic aerosol production from aqueous photooxidation of glycolaldehyde: Laboratory experiments. Atmospheric Environment, 43(8): 1487-1497. Available from http://www.sciencedirect.com/science/article/pii/S1352231008011096. DOI http://dx.doi.org/10.1016/j.atmosenv.2008.11.037.

Petters, M.D. and S.M. Kreidenweis, 2007. A single parameter representation of hygroscopic growth and cloud condensation nucleus activity. Atmos. Chem. Phys., 7(8): 1961-1971. Available from http://www.atmos-chem-phys.net/7/1961/2007/. DOI 10.5194/acp-7-1961-2007.

Robinson, A.L., N.M. Donahue, M.K. Shrivastava, E.A. Weitkamp, A.M. Sage, A.P. Grieshop, T.E. Lane, J.R. Pierce and S.N. Pandis, 2007. Rethinking organic aerosols: Semivolatile emissions and photochemical aging. Science, 315(5816): 1259-1262. Available from http://www.sciencemag.org/content/315/5816/1259.abstract. DOI 10.1126/science.1133061.

Sareen, N., A.N. Schwier, E.L. Shapiro, D. Mitroo and V.F. McNeill, 2010. Secondary organic material formed by methylglyoxal in aqueous aerosol mimics. Atmos. Chem. Phys., 10(3): 997-1016. Available from http://www.atmos-chem-phys.net/10/997/2010/. DOI 10.5194/acp-10-997-2010.

Saxena, P. and L. Hildemann, 1996. Water-soluble organics in atmospheric particles: A critical review of the literature and application of thermodynamics to identify candidate compounds. Journal of Atmospheric Chemistry, 24(1): 57-109. Available from http://dx.doi.org/10.1007/BF00053823. DOI 10.1007/BF00053823.

Schwier, A.N., N. Sareen, D. Mitroo, E.L. Shapiro and V.F. McNeill, 2010. Glyoxal-methylglyoxal cross-reactions in secondary organic aerosol formation. Environmental science & technology, 44(16): 6174-6182.

Seinfeld, J.H. and S.N. Pandis, 2012. Atmospheric chemistry and physics: From air pollution to climate change. John Wiley & Sons.

Seinfeld, J.H. and J.F. Pankow, 2003. Organic atmospheric particulate material. Annual Review of Physical Chemistry, 54(1): 121-140.

Stocker, D.Q., 2013. Climate change 2013: The physical science basis. Working Group I Contribution to the Fifth Assessment Report of the Intergovernmental Panel on Climate Change, Summary for Policymakers, IPCC.

Tan, Y., A.G. Carlton, S.P. Seitzinger and B.J. Turpin, 2010. Soa from methylglyoxal in clouds and wet aerosols: Measurement and prediction of key products. Atmospheric Environment, 44(39): 5218-5226. Available from http://www.sciencedirect.com/science/article/pii/S1352231010007399. DOI http://dx.doi.org/10.1016/j.atmosenv.2010.08.045.

Tan, Y., Y.B. Lim, K.E. Altieri, S.P. Seitzinger and B.J. Turpin, 2012. Mechanisms leading to oligomers and soa through aqueous photooxidation: Insights from oh radical oxidation of acetic acid and methylglyoxal. Atmos. Chem. Phys., 12(2): 801-813. Available from http://www.atmos-chem-phys.net/12/801/2012/. DOI 10.5194/acp-12-801-2012.

Tan, Y., M.J. Perri, S.P. Seitzinger and B.J. Turpin, 2009. Effects of precursor concentration and acidic sulfate in aqueous glyoxal−oh radical oxidation and

implications for secondary organic aerosol. Environmental Science & Technology, 43(21): 8105-8112. Available from http://dx.doi.org/10.1021/es901742f [Accessed 2014/01/10]. DOI 10.1021/es901742f.

Updyke, K.M., T.B. Nguyen and S.A. Nizkorodov, 2012. Formation of brown carbon via reactions of ammonia with secondary organic aerosols from biogenic and anthropogenic precursors. Atmospheric Environment, 63: 22-31.

Volkamer, R., F. San Martini, L.T. Molina, D. Salcedo, J.L. Jimenez and M.J. Molina, 2007. A missing sink for gas-phase glyoxal in mexico city: Formation of secondary organic aerosol. Geophysical Research Letters, 34(19).

Warneck, P., 1999. The relative importance of various pathways for the oxidation of sulfur dioxide and nitrogen dioxide in sunlit continental fair weather clouds. Physical Chemistry Chemical Physics, 1(24): 5471-5483. Available from http://dx.doi.org/10.1039/A906558J. DOI 10.1039/A906558J.

Zhang, H., H.M. Parikh, J. Bapat, Y.-H. Lin, J.D. Surratt and R.M. Kamens, 2013. Modelling of secondary organic aerosol formation from isoprene photooxidation chamber studies using different approaches. Environmental Chemistry, 10(3): 194-209. Available from http://www.publish.csiro.au/paper/EN13029. DOI http://dx.doi.org/10.1071/EN13029.

Zhang, H., J.D. Surratt, Y.H. Lin, J. Bapat and R.M. Kamens, 2011. Effect of relative humidity on soa formation from isoprene/no photooxidation: Enhancement of 2-methylglyceric acid and its corresponding oligoesters under dry conditions. Atmos. Chem. Phys., 11(13): 6411-6424. Available from http://www.atmos-chem-phys.net/11/6411/2011/. DOI 10.5194/acp-11-6411-2011.

Zhang, X., Z. Chen and Y. Zhao, 2010. Laboratory simulation for the aqueous oh-oxidation of methyl vinyl ketone and methacrolein: Significance to the in-cloud soa production. Atmospheric Chemistry and Physics, 10(19): 9551-9561.

Chapter 2. Glyoxal SOA chemistry: Effects of dilute nitrate and ammonium and support for organic radical-radical oligomer formation

Material in this chapter is published previously as:

Kirkland, J.R., Y.B. Lim, Y. Tan, K.E. Altieri and B.J. Turpin, 2013. Glyoxal secondary organic aerosol chemistry: Effects of dilute nitrate and ammonium and support for organic radical–radical oligomer formation. Environmental Chemistry, 10(3): 158-166. Available from http://www.publish.csiro.au/paper/EN13074. DOI http://dx.doi.org/10.1071/EN13074.

2.1.Introduction

Atmospheric waters (e.g., clouds, fogs, wet aerosols) serve as a medium in which water-soluble organic compounds react. These water-soluble organics are abundant in the atmosphere due to the gas-phase fragmentation and oxidation of primary emissions. Reactions in atmospheric waters can produce low volatility products that remain in the particle phase upon droplet evaporation (e.g., oxalate, glycolate, oligomers, epoxide sulfates, imidazoles) (Altieri *et al.*, 2006; Carlton *et al.*, 2006; El Haddad *et al.*, 2009; Galloway *et al.*, 2009; Perri *et al.*, 2009; Sun *et al.*, 2010; Surratt *et al.*, 2010; Kamens *et al.*, 2011; Lee *et al.*, 2011; Zhou *et al.*, 2011; Ortiz-Montalvo *et al.*, 2012). As a result, gas-phase followed by aqueous-phase chemistry contributes to secondary organic aerosol (SOA_{aq}) (Blando and Turpin, 2000; Ervens *et al.*, 2011). SOA is also formed when semi- and low-volatility products of gas phase chemistry sorb to particulate organic matter (SOA_{gas}) (Jang *et al.*, 1997; Seinfeld and Pandis, 2012).

While the magnitude of SOA_{aq} remains uncertain, the inclusion of aqueous organic chemistry in global models has led to a substantial enhancement of aerosol

burden, (Fu *et al.*, 2008; Myriokefalitakis *et al.*, 2011; Lin *et al.*, 2012; Liu *et al.*, 2012) improved correlations between models and measurements in the Northeastern United States, (Carlton *et al.*, 2008) and helped to explain the highly-oxidized nature of atmospheric organic aerosols (Lim *et al.*, 2010; Seinfeld and Pandis, 2012). SOA_{gas} is not as oxidized as measured atmospheric aerosol. SOA_{aq} and SOA_{gas} form from different precursors under different atmospheric conditions and have different properties and behavior. For example, since the precursors of SOA_{aq} are water-soluble gases with high O/C ratios, SOA_{aq} is expected to have high O/C ratios, be more hygroscopic, and be better able to serve as cloud condensation nuclei than other organics (Petters and Kreidenweis, 2007). For these reasons, an improved understanding of SOA_{aq} is needed to link emissions to ambient aerosol concentrations, composition, and effects through predictive models that enable the development of effective air quality management strategies. This ultimate goal motivates the work reported herein.

Glyoxal (GLY) is ubiquitous in the atmosphere and an important SOA_{aq} precursor because GLY is highly water soluble, reactive to OH radicals and forms oligomers at high concentrations ($\geq$ mM). GLY is the smallest dicarbonyl and forms through the gas phase photooxidation of alkene and aromatic compounds (Atkinson *et al.*, 2006). The largest global source of GLY is the gas phase oxidation of isoprene (biogenic) (Guenther *et al.*, 2006). A major anthropogenic source of GLY is the oxidation of acetylene (Yeung *et al.*, 2005). Though its marine sources are uncertain, satellite measurements reveal substantial concentrations of GLY in marine air (Wittrock *et al.*, 2006). Acetylene, with an atmospheric lifetime near 18 days (Fu *et al.*, 2008), is one possible GLY source in marine air (Rinaldi *et al.*, 2011). GLY ($3x10^5$ M atm^{-1})(Zhou and Mopper, 1990) readily

partitions into atmospheric waters where it is present at concentrations from one to several hundred μM and can react further (Igawa *et al.*, 1989; Matsumoto *et al.*, 2005; Epstein and Nizkorodov, 2012). GLY can react in atmospheric waters to form lower volatility products (e.g., oxalate, oligomers, organosulfate, imidazole) (Carlton *et al.*, 2007; Noziere *et al.*, 2008; Galloway *et al.*, 2009; Tan *et al.*, 2009; Lee *et al.*, 2011). Since these compounds are found predominantly in the condensed phase in the atmosphere, aqueous oxidation of GLY contributes to SOA_{aq} (Carlton *et al.*, 2007; Tan *et al.*, 2009).[32-33]

Organic nitrogen and sulfur compounds have been observed to form in highly concentrated aqueous solutions relevant to wet aerosols (Noziere *et al.*, 2008; Galloway *et al.*, 2009; Shapiro *et al.*, 2009; Tan *et al.*, 2009; Nozière *et al.*, 2010; Perri *et al.*, 2010).[6, 34-37] Evidence for the photochemical formation of organosulfates from GLY and other aldehydes is provided through studies of bulk sulfate solutions and through smog chamber experiments with acidic sulfate seed particles and UV irradiation(Galloway *et al.*, 2009; Tan *et al.*, 2009; Nozière *et al.*, 2010; Perri *et al.*, 2010).[6, 35-36] Aerosol mimic solutions containing GLY and inorganic ammonium salts have yielded products with carbon-nitrogen bonds in the absence of major atmospheric oxidants (i.e., O_3, OH, NO_3)(Shapiro *et al.*, 2009).[37] In addition, imidazole formation has been detected in (dark) concentrated aldehyde + ammonium sulfate solutions and chamber experiments (Galloway *et al.*, 2009; Tan *et al.*, 2009; Nozière *et al.*, 2010). Inorganic and organic concentrations are orders of magnitude smaller in clouds and fogs. While experiments have been performed to examine the effect of dilute (cloud-relevant) concentrations of acidic sulfate on GLY chemistry (Tan *et al.*, 2009), to our knowledge

the degree to which GLY + OH chemistry is altered by the presence of cloud-relevant concentrations of nitrate or ammonium has not been examined. Inorganic nitrate and ammonium are found in atmospheric cloud and fog waters (e.g., ~1 μM – 3 mM for NO_3^- and NH_4^+ in fogs) (Waldman *et al.*, 1982; Zhang and Anastasio, 2001; Zhang *et al.*, 2007; Altieri *et al.*, 2009), and organic nitrogen species have been measured in California fogs(Mazzoleni *et al.*, 2010) and New Jersey rainwater (Altieri *et al.*, 2009). While organic nitrogen is clearly formed through gas phase chemistry and there is evidence for its formation in aerosols, it could plausibly also form through cloud/fog chemistry. In this work, we conducted chemical modeling and aqueous GLY + OH experiments with cloud/fog-relevant concentrations of inorganic nitrogen (i.e., ammonium sulfate or nitric acid) to determine whether the commonly understood dilute GLY + OH chemistry leading to oxalate (and therefore SOA) is altered by the presence of cloud-relevant concentrations of ammonium sulfate or nitric acid.

Tan *et al.* (2009) studied the aqueous OH radical oxidation of GLY at cloud-relevant and higher concentrations (30-3000 μM). At cloud-relevant (dilute) concentrations, oxalate was the major product and the addition of cloud/fog-relevant concentrations of H_2SO_4 had little impact on the chemistry. At higher (3000 μM) concentrations Tan *et al.* (2009) observed the formation of products with higher carbon numbers than the precursor, GLY. These higher carbon number products only formed in the presence of OH radicals. By accounting for organic radical – radical reactions in the GLY oxidation mechanism, Lim *et al.* (2010) were able to reproduce the concentration dynamics of the major products in the Tan *et al.* (2009) experiments. Using GLY as a surrogate for the behavior of dissolved organics at the high (1-10 M) concentrations

found in wet aerosols, Lim *et al.* (2010) predicted that oligomers would be the main products of organic OH radical oxidation in wet aerosols. Tartarate is a key product in the organic radical-radical mechanism proposed by Lim *et al.* (2010). However, tartarate was not definitively measured in the Tan *et al.* (2009) experiments because tartarate and malonate co-eluted and thus could not be distinguished. In model runs that simulated the experimental conditions and included organic radical-radical chemistry (Lim *et al.*, 2010), tartarate forms early in the experiment, peaking after about 25 minutes. Malonate formation is minor and slower, since it is formed through radical-radical reactions followed by acid catalyzed dehydration. The experimental results reported herein provide definitive evidence for the formation of tartarate from GLY + OH.

This paper examines for the first time the effect of cloud/fog relevant concentrations of inorganic nitrogen on the aqueous oxidation of GLY. The finding that oxalate is not affected by cloud-relevant concentrations of ammonium sulfate and nitric acid increases confidence that the currently understood dilute GLY + OH chemistry can be used to predict GLY SOA formation in clouds and fogs. This paper also provides critical laboratory evidence for oligomer formation through organic radical-radical reactions; this chemistry is evident in 1 mM GLY experiments and is the dominant OH radical oxidation product at the much higher (1-10 M) organic concentrations present in wet aerosols(Lim *et al.*, 2010).

2.2.Experimental

2.2.1. Batch Reactions

Bulk aqueous phase reactions of GLY (1 mM) and hydroxyl radical (~10^{-12} M OH radical, modeled OH) with nitric acid (1.68 mM; HNO_3) or ammonium sulfate (840 μM;

$(NH_4)_2SO_4$) and control experiments were conducted in a 1 L glass reaction vessel, as described in detail elsewhere (Carlton *et al.*, 2006) (Appendix A.2.1). OH radicals were continuously produced *in situ* via direct photolysis of hydrogen peroxide (5 mM; H_2O_2) using a 254 nm mercury lamp (Heraeus Noblelight, Inc. Duluth, GA) placed in a quartz immersion well in the center of the reaction vessel. Surrounding the reaction vessel is a water jacket that maintained a temperature of 26 $\pm$ 2 °C. The reaction vessel was wrapped in aluminum foil to eliminate exposure to ambient light. The following control experiments were conducted: GLY + OH without nitric acid or ammonium sulfate, GLY + HNO_3 + UV, GLY + $(NH_4)_2SO_4$ + UV, GLY + HNO_3 + H_2O_2, GLY + $(NH_4)_2SO_4$ + H_2O_2, GLY + HNO_3, GLY + $(NH_4)_2SO_4$, and H_2O_2 + UV.

2.2.2. OH Radical Concentrations

Aqueous hydroxyl radical concentrations in clouds/fogs are predicted to be $10^{-12} – 10^{-13}$ M (Jacob, 1986). Hydroxyl radical concentrations in these GLY experiments were as follows: $[OH]_{average} = (1\pm2)\ x10^{-12}$ M, $[OH]_{initial} = 7.8x10^{-13}$M, $[OH]_{final} = 6.0x10^{-12}$ M. These concentrations were estimated using the Lim *et al.* (2010) GLY photooxidation model and an H_2O_2 photolysis rate constant (k_1) equal to $1.0x10^{-4}\ s^{-1}$. The value of k_1, which depends on the photon flux of the lamp, was determined by fitting modeled to measured H_2O_2 concentrations in H_2O_2 + UV control experiments (Fig. S1). Hydrogen peroxide was quantified by the triiodide method and analyzed with a UV-vis spectrometer(Klassen *et al.*, 1994) (Appendix: A.2.2).

2.2.3. Product Analysis/Analytical Methods

Discrete samples from aqueous experiments were analyzed via IC (Dionex ICS 3000; IonPac AS11-HC column; 30 °C, AG11-HC guard column; conductivity detector; 35 °C),

IC/ESI-MS (HP – Agilent 1100; negative ion mode), and FT-ICR-MS (Thermo-Finnigan LTQ-XL: positive and negative ion modes, Woods Hole Oceanographic Institution Mass Spectrometry Facility) as described in detail previously and briefly below(Altieri *et al.*, 2009; Tan *et al.*, 2010).[41, 45] Discrete samples for IC and IC/ESI-MS (~1.2 mL) were analyzed immediately (same day), whereas discrete samples for FT-ICR-MS (~5 mL; 40 min time points only) were frozen at -20 °C for later analysis as recommended by Seitzinger *et al.* (2002) for preservation of stored atmospheric water samples for mass spectral analysis (Appendix: A.2.3).

Carboxylic acid and inorganic anions were quantified via IC with five point calibration curves (accept R^2>0.98) developed from authentic standards, including: glycolate (5.8 min), formate (6.7 min), glyoxylate (9.5 min), succinate (20.2 min), tartarate (20.8 min), and oxalate (24.2 min). Note that glycolate co-elutes with acetate, succinate with malate, and tartarate with malonate. These peaks were quantified as glycolate, succinate, and tartarate, respectively. Nitrate (16.7 min) and sulfate (22.8 min) are also detected within the 40 minute IC program.

Negative ionization mode mass spectrometric analysis (50 – 1000 amu) of each peak in the sample chromatograms was performed via IC/ESI-MS as described by Tan *et al.* (2010) (Appendix: SOP). Briefly, the IC conductivity detector effluent (0.4 mL min^{-1}) was directed into the ESI-MS with 40% of 0.05% formic acid in water and 60% methanol mobile phase (0.22 mL min^{-1}). After IC separation, mass spectral analysis was performed with a fragmentor voltage of 40 V and a capillary voltage of 3000 V (nitrogen drying gas; 10 L min^{-1}; 350 °C). Mass assignments were verified with a mixed standard analyzed at the beginning and end of each sequence.

A discrete sample (40 min into the reaction) from each experiment, control experiment, and a 1 mM GLY standard was also analyzed via FT-ICR-MS in positive and negative ionization modes (mass resolution 100,000) to determine elemental formulas of reactions products from 50 to 500 amu. A syringe pump delivered analyte into the spray chamber at 4 µL min^{-1} with a capillary temperature of 260 °C and capillary voltage of -17.50 V. The FT-ICR-MS was calibrated using a Thermo Scientific LTQ-FT external calibration mix. For both positive and negative ion modes, at least 200 scans were collected using the parameters described in Kido Kido Soule *et al.* (2010). The transients were processed using SimStich (Southam *et al.*, 2007) and aligned with MATLAB code provided by Mantini *et al.* (2007) as described in Bhatia *et al.* (2010). Exact masses were processed with Midas Molecular Formula Calculator (v1.1) as described by Altieri *et al.* (2009) to provide elemental formulas of detected species.

2.2.4. Quality Control

Water blanks and dynamic blanks were sampled from the water source (17 MΩ-cm) Barnstead E-Pure milli-q water) and reaction vessel, respectively, and analyzed in the same manner as samples, described above. Blanks had negligible (signal <0.5µS) IC peaks, thus no subtraction is performed. IC/ESI-MS analysis of the blanks revealed that m/z^- 113 has a strong signal (abundance >5000) throughout all spectra and thus was subtracted from spectra. The remaining peaks were small (abundance <2000) and did not interfere with products (abundance of major products >10000; e.g., tartarate, oxalate, nitrate, sulfate). Mixed standards were analyzed with samples to assess the accuracy of quantified organic acids and to check for shifts in retention times. Retention time varied less than 10%. Greater than 20% of samples were run in duplicate. Experiments were run

in triplicate. Error bars for oxalate and tartarate concentrations (Figs. 1-2) are the coefficients of variation across experiments.

2.2.5. Accounting for nitrate photolysis

The effect of OH production via nitrate photolysis on the batch experiments was examined by adding the following reactions to the aqueous GLY + OH chemistry documented in Lim *et al.* (2010):

$HNO_3 \leftrightarrow H^+ + NO_3^-$ K = 22; (Warneck, 1999) (R1)

$NO_3^- + UV \rightarrow O^- + NO_2$ $k = 6.38x10^{-7}$; (Warneck, 1999; Lim *et al.*, 2005) (R2)

$O^- + H_2O \leftrightarrow OH + OH^-$ $k_f=1.7x10^6$, $k_r=1.2x10^{10}$; (Mack and Bolton, 1999) (R3)

$HNO_3 + OH \rightarrow H_2O + NO_3$ $k = 1.0x10^5$; (Neta and Huie, 1986) (R4)

$NO_3^- + OH \rightarrow NO_3 + OH^-$ $k = 1.0x10^5$; (Neta and Huie, 1986) (R5)

$GLY + NO_3 \rightarrow GLYR + HNO_3$ $k = 1.0x10^4$; (Neta and Huie, 1986) (R6)

$OH + NO_2 \rightarrow HNO_3$ $k = 1.3x10^9$; (Lim *et al.*, 2005) (R7)

Nitric acid dissociates to H^+ and nitrate (R1). The photolysis of nitrate produces OH radical (R2 and R3). Nitric acid and nitrate react with OH radicals forming nitrate radicals (R4 and R5). GLY reacts with nitrate radicals by H-atom abstraction ("GLYR" is a GLY radical) and the rate constant is assumed to be $1x10^4$ $M^{-1}s^{-1}$ based on Neta and Huie (1986) (R6). Finally, nitric acid can be regenerated by the reaction of OH radicals with nitrite radicals (R7). This chemistry was used to simulate batch experiments (Figs. S2-S5).

2.3.Results and Discussion

2.3.1. Dilute glyoxal chemistry in the presence of inorganic nitrogen

The addition of ammonium sulfate (840 μM) had no effect on the production of oxalate (Fig. 1), the major product of aqueous GLY photooxidation. The addition of nitric acid (1.68 mM) decreased oxalate production slightly (~10% at peak) when compared to oxalate production in the absence of nitric acid. Mean oxalate concentrations during GLY+OH experiments in the presence of nitric acid are significantly less than (95% confidence) mean oxalate concentrations in GLY+OH experiments at every time point. This finding can be understood by examining model simulations. The addition of HNO_3 decreased oxalate formation (Fig. 1) because HNO_3 lowered the pH (Fig. S5) affecting glyoxylic acid dissociation and subsequently oxalate formation. Simulated OH radical concentrations were unchanged by the addition of HNO_3 (Fig. S2) because OH produced by nitrate photolysis reacts with nitrite radicals to regenerate nitric acid(Mack and Bolton, 1999). The production of oxalate was much slower in GLY+HNO_3+UV control experiments (Fig. S6) compared to OH radical experiments, also suggesting that OH radical production by HNO_3 photochemistry was modest (Fig. S7). Note that simulated and measured nitrate in GLY + OH + HNO_3 remained constant over the course of the reaction (Figs. S4, S8) and no substantial change in other quantified GLY oxidation products (i.e., tartarate plus malonate) was observed either with the addition of ammonium sulfate or nitric acid (Fig. 2). This suggests that the presence of ammonium and inorganic nitrate in clouds and fogs has little impact on the formation of cloud SOA_{aq} from GLY, and supports the use of dilute GLY + OH chemistry (e.g., Lim *et al.* (2010)) to predict GLY cloud SOA.

When beginning this work, we hypothesized that the addition of cloud-relevant concentrations of nitric acid might lead to the formation of organonitrates via radical-

radical reactions or condensation reactions shown in Fig. 3. It is plausible that aqueous nitrate radical chemistry might be a source of oxygenated organic nitrogen compounds measured in fog and rain water(Altieri *et al.*, 2009; Mazzoleni *et al.*, 2010), although these compounds could also have been formed through gas phase chemistry. If the nitrate radicals were formed by photolysis in the aqueous phase and if these reactions occur at dilute concentrations, we should see organonitrate products in experimental samples. Note that uptake from the gas phase provides another source of nitrate radicals in atmospheric waters; this source is not accounted for in our experimental samples. Below we look for evidence of the formation of these and other organic nitrogen products in experimental samples.

2.3.2. Organic nitrogen

Organonitrates are known to form via gas-phase OH radical reactions at high NO_x during the daytime and gas-phase NO_3 radical reactions at night(Gong *et al.*, 2005; Lim and Ziemann, 2005). In the aqueous phase, organonitrates are not expected to form photochemically with NO or NO_2 due to low NO and NO_2 water solubilities (i.e., H_{NO} = $1.9x10^{-3}$ M atm^{-1}, H_{NO2} = $7.0x10^{-3}$ M atm^{-1})(Lim *et al.*, 2005). However, organonitrate formation via NO_3 radical reactions could occur because NO_3 radical is water soluble (H_{NO3} = 2 M atm^{-1}) (Lim *et al.*, 2005) and reactive with respect to organics with rate constants of ~10^3 - ~10^4 M^{-1} s^{-1}(Neta and Huie, 1986). In the nighttime atmosphere, we expect that some NO_3 radical will dissolve in cloud, fog and aerosol liquid water. Photolysis of HNO_3 in the aqueous phase can also form NO_3 radical. In the presence of NO_2, NO_3 radical forms N_2O_5, which is highly water soluble (H_{N2O5} = $1.4x10^{10}$ M atm^{-1})(Lim *et al.*, 2005). HNO_3 forms via hydrolysis when N_2O_5 dissolves in the aqueous

phase. Thus, GLY + OH + HNO_3 is an appropriate system to examine to look for the formation of organonitrates in clouds and fogs.

Experiments conducted with nitric acid versus without nitric acid provide no evidence for organonitrate formation. Modeled (Fig. S4) and measured nitrate (Fig. S8) concentrations show no decrease with time across the experiments. IC/ESI-MS results provide no evidence of unique IC peaks or unique masses during GLY photooxidation in the presence of nitrate or ammonium (Fig. 4c, 4d), when compared to GLY photooxidation without nitrate or ammonium (Fig. 4b). Hypothesized organonitrate products shown in Fig. 3 were not detected by FT-ICR-MS analysis.

IC/ESI-MS results are shown in Fig. 4. Fig. 4a is a mixed standard analyzed via IC/ESI-MS. The lettered peaks in the IC chromatogram at the left of the figure correspond to the mass spectrum labeled with the same letter at the right. Figs. 4b-d show the IC/ESI-MS analysis of 40 minute samples. The IC chromatogram of the 1 mM GLY + OH sample (Fig. 4b) is consistent with the IC chromatogram of similar (3 mM) GLY + OH experiments conducted by Tan *et al.* (2009), showing a large peak with the retention time of oxalate (F) and small peaks with the retention time of malonate + tartarate (E) and with the retention time of mesoxalate (Y). In the 3 mM Tan *et al.* (2009) experiments, an even smaller peak with the retention time of succinate + malate (D) was detectable; this peak was not detected in the current (1 mM) experiments. The mass spectra of Fig. 4b verify that peak F is in fact oxalate (m/z^- 89) and peak Y is mesoxalate (m/z^- 117) as proposed by Tan *et al.* (2009). Both malonate and tartarate are detectable in the 40 min GLY + OH sample (peak E, m/z^- 103 and 149, respectively). The IC/ESI-MS of GLY+OH+HNO_3 (Fig. 4c) and GLY+OH+$(NH_4)_2SO_4$ (Fig. 4d) were identical to that

of GLY+OH with the exception of the nitrate peak (Fig. 4c; peak N; m/z^- 62) and the sulfate peak (Fig. 4d; peak S; m/z^- 97). Thus, the IC/ESI-MS provides no evidence for the formation of organic nitrogen species when GLY is oxidized in the presence of cloud-relevant concentrations of HNO_3 or $(NH_4)_2SO_4$. It is possible that the nitrate peak quantified by the IC includes organic nitrates that formed and elute at the same retention time. However, the IC/ESI mass spectrum for peak N has a single signal at *m/z*- 62, where we expect nitrate ion detection.

Hypothesized organonitrate products shown in Fig. 3 were not detected by FT-ICR-MS analysis. Some nitrogen-containing elemental formulas were identified in samples from experiments conducted both in the presence and in the absence of nitrogen, suggesting the presence of trace nitrogen-containing contaminants. Ultra-high resolution FT-ICR MS has sub ppm mass accuracy and resolution > 100 000, enabling the determination of elemental formulas for thousands of compounds in a complex organic mixture. However, ion abundance depends both on compound concentration and on the matrix of other compounds present. Thus quantification is challenging and the ion abundance above a signal-to-noise threshold is used to determine presence or absence of that compound. In this case, positive/negative mode FT-ICR-MS analyses did not provide definitive evidence for the formation of organic nitrogen species, including those proposed in Fig. 3, in the presence of cloud-relevant concentrations of HNO_3 or $(NH_4)_2SO_4$ when compared to samples from GLY+OH alone.

This finding is, perhaps, not surprising. In order to form organic nitrogen, NO_3 radical reactions (Fig. 3a) require the C=C double bond. The enol form of GLY has this C=C double bond. But since the GLY enol forms from monohydrated or unhydrated

GLY, not dihydrated GLY, the Fig. 3a reaction is unlikely to occur in dilute aqueous solution. Although the nitration of alcohols with HNO_3 is common, there is little evidence of GLY nitration by HNO_3. A recent study suggests that HNO_3 acts as an oxidizing agent that oxidizes GLY to glyoxylic acid, although we did not see evidence of this using cloud-relevant HNO_3 as a source of NO_3 radicals and in the presence of OH radicals (Connelly *et al.*, 2012).

In the daytime atmosphere, NO_3 radical reactions are slow relative to OH radical reactions. In the aqueous phase we expect ~10^{-12} M OH and ~10^{-11} M NO_3. The rate constant for GLY + NO_3 is $1x10^4$ $M^{-1}s^{-1}$(Neta and Huie, 1986). Thus, in the case of GLY, k[NO_3] is ~$1x10^4$ and k[OH] is ~$1x10^9$. For this reason, nitrate radical reactions are unlikely to be important to daytime cloud chemistry. At night, NO_3 radical is taken up into the aqueous phase from the gas phase. It could slowly oxidize organics via hydrogen atom abstraction and peroxy radical formation (e.g., forming glyoxylic acid from GLY) or it could react at the carbon-carbon double bond to form organonitrates. Because the GLY enol forms from monohydrated or unhydrated GLY, not dihydrated GLY, the Fig. 3a reaction is more likely to occur during droplet evaporation or in wet acidic aerosols (De Haan *et al.*, 2009). The nitration of hydrated GLY (diols) with HNO_3 (Fig. 3b) is also more likely to occur in very concentrated solutions, as might be present in evaporating droplets and in wet aerosols.

Likewise, while reactions with NH_4, including formation of imidazole occur in wet aerosols, these reactions are slow relative to OH radical reactions. Our experimental conditions (1 mM GLY + 5 mM H_2O_2 + UV + 840 µM $(NH_4)_2SO_4$) produce hydroxyl radical concentrations ~10^{-12} M at pH = 3 and the rate constant for organic nitrogen

formation (k[GLY + NH_4^+]) given by Noziere *et al.* (2008) is $3.6x10^{-7}$ $M^{-1}s^{-1}$. This is much smaller than the rate constant for GLY + OH ($1.1x10^9$ $M^{-1}s^{-1}$) (Lim *et al.*, 2010). This suggests that the presence of NH_4^+ at cloud-relevant concentrations will not affect GLY + OH chemistry. In addition, we found no evidence of the imidazoles reported by Galloway *et al.* (2009) in the positive mode, by FT-ICR MS.

Organic nitrogen is detected in fine and course particles (Zhang and Anastasio, 2003). Previous studies have reported the formation of nitrogen-containing organics in the gas phase or in the aerosol phase, where concentrations of ammonium and nitrate are quite high. For example, imine and imidazole formation have been observed in chamber studies and bulk aqueous aerosol mimics (Noziere *et al.*, 2008; Galloway *et al.*, 2009; Sareen *et al.*, 2010). Ammonium and nitrate concentrations are several orders of magnitude lower in clouds and in these experiments, and we did not see evidence of such products in the experiments reported herein.

2.3.3. Oligomer formation mechanism for GLY + OH

IC/ESI-MS analysis permits the identification of compounds that co-elute in the IC system, for example, tartarate and malonate. The IC peak at that retention time (21.5 min; tartarate + malonate) is quantified as tartarate throughout these experiments (Fig. 2). Peak E in the IC/ESI-MS of the mixed standard (Fig. 4a) is tartarate. The corresponding mass spectrum of peak E shows that m/z^- 149 (tartarate) is the only major compound detected in the mixed standard. Peak E was not present in blanks. Peak E in Figs. 4b-d is a product of GLY photooxidation and reveals the presence of both tartarate (m/z^- 149) and malonate (m/z^- 103). Thus, both are products formed during GLY photooxidation in the presence and absence of nitric acid and ammonium sulfate. According to the Lim *et*

al. (2010) chemical mechanism, tartarate forms first and malonate forms more slowly during GLY photooxidation. Fig. 5 supports this claim by showing that the abundance of m/z^- 149 in peak E (tartarate) is dominant early in the reaction. The abundance of m/z^- 103 in peak E (malonate) reaches a maximum later in the experiment (between 40 and 120 min) when peak E (tartarate + malonate) is quite small (Fig. 2). Thus, we conclude that peak E is predominantly tartarate.

Verification that tartarate is the major first generation radical-radical product of GLY+OH provides critically important support for the oligomer formation mechanism proposed by Lim *et al.* (2010). While Tan *et al.* (2009) identified a peak with the same IC retention time as tartarate/malonate, the IC/ESI-MS data presented here is the first confirmation that this peak is predominantly tartarate. The slower formation of malonate is also consistent with the organic radical-radical chemistry proposed by Lim *et al.* (2010), since malonate forms through radical-radical reactions followed by acid catalyzed dehydration. Lim *et al.* (2010) proposed that, at the high organic concentrations that are found in wet aerosols (1-10 M), organic radical-radical reactions dominate, producing higher carbon number products. Note that Lim *et al.* (2010) used GLY as a surrogate species to represent total dissolved organics in wet aerosols, in order to better understand the differences in chemistry in clouds and in wet aerosols. It should be recognized that both organics and inorganics are present at high concentrations in wet aerosols. While organic – inorganic interactions do not appear to play an important role in clouds, they can play an important role in droplet evaporation chemistry and in wet aerosols. The chemistry leading to SOA formation in evaporating droplets and in clouds is clearly complex and remains poorly understood.

2.4.Atmospheric Implications

The biogenic and anthropogenic source strengths of isoprene and aromatics and the water-solubility of GLY, a gas phase product of these sources, make GLY a potentially important precursor to SOA_{aq} formation. This research suggests that the currently understood chemistry leading to the formation of SOA through *in-cloud* OH radical oxidation of GLY (Lim *et al.*, 2005; Lim *et al.*, 2010) is robust in the presence of ammonium sulfate and nitric acid. In contrast, others have demonstrated that organic nitrogen products can form at the much higher concentrations found in wet aerosols(Noziere *et al.*, 2008; Galloway *et al.*, 2009). They might also form during cloud/fog droplet evaporation, where GLY may be present in its monohydrated form(De Haan *et al.*, 2009). Detection of tartarate during the GLY + OH experiments herein provides key verification of the organic radical-radical oligomer formation mechanism proposed by Lim *et al.* (2010). This chemistry is detectable in experiments with 1 mM of organic, and is predicted to be dominant at the high (1 – 10 M) concentrations of organics found in wet aerosols. Thus, oxalate is the major product of dilute (in cloud) GLY oxidation and oligomers(Lim *et al.*, 2010) and organic nitrogen(Noziere *et al.*, 2008) are major products of GLY chemistry in wet aerosols.

2.5.References

Altieri, K.E., A.G. Carlton, H.-J. Lim, B.J. Turpin and S.P. Seitzinger, 2006. Evidence for oligomer formation in clouds: Reactions of isoprene oxidation products. Environmental Science & Technology, 40(16): 4956-4960. Available from http://dx.doi.org/10.1021/es052170n [Accessed 2014/01/10]. DOI 10.1021/es052170n.

Altieri, K.E., B.J. Turpin and S.P. Seitzinger, 2009. Oligomers, organosulfates, and nitrooxy organosulfates in rainwater identified by ultra-high resolution electrospray ionization ft-icr mass spectrometry. Atmos. Chem. Phys., 9(7): 2533-2542. Available from http://www.atmos-chem-phys.net/9/2533/2009/. DOI 10.5194/acp-9-2533-2009.

Atkinson, R., D.L. Baulch, R.A. Cox, J.N. Crowley, R.F. Hampson, R.G. Hynes, M.E. Jenkin, M.J. Rossi, J. Troe and I. Subcommittee, 2006. Evaluated kinetic and photochemical data for atmospheric chemistry: Volume ii – gas phase reactions of organic species. Atmos. Chem. Phys., 6(11): 3625-4055. Available from http://www.atmos-chem-phys.net/6/3625/2006/. DOI 10.5194/acp-6-3625-2006.

Bhatia, M.P., S.B. Das, K. Longnecker, M.A. Charette and E.B. Kujawinski, 2010. Molecular characterization of dissolved organic matter associated with the greenland ice sheet. Geochimica et Cosmochimica Acta, 74(13): 3768-3784. Available from http://www.sciencedirect.com/science/article/pii/S0016703710001730. DOI http://dx.doi.org/10.1016/j.gca.2010.03.035.

Blando, J.D. and B.J. Turpin, 2000. Secondary organic aerosol formation in cloud and fog droplets: A literature evaluation of plausibility. Atmospheric Environment, 34(10): 1623-1632. Available from http://www.sciencedirect.com/science/article/pii/S1352231099003921. DOI http://dx.doi.org/10.1016/S1352-2310(99)00392-1.

Carlton, A.G., B.J. Turpin, K.E. Altieri, S. Seitzinger, A. Reff, H.-J. Lim and B. Ervens, 2007. Atmospheric oxalic acid and soa production from glyoxal: Results of aqueous photooxidation experiments. Atmospheric Environment, 41(35): 7588-7602. Available from http://www.sciencedirect.com/science/article/pii/S1352231007004979. DOI http://dx.doi.org/10.1016/j.atmosenv.2007.05.035.

Carlton, A.G., B.J. Turpin, K.E. Altieri, S.P. Seitzinger, R. Mathur, S.J. Roselle and R.J. Weber, 2008. Cmaq model performance enhanced when in-cloud secondary organic aerosol is included: Comparisons of organic carbon predictions with measurements. Environmental Science & Technology, 42(23): 8798-8802.

Available from http://dx.doi.org/10.1021/es801192n [Accessed 2014/01/10]. DOI 10.1021/es801192n.

Carlton, A.G., B.J. Turpin, H.-J. Lim, K.E. Altieri and S. Seitzinger, 2006. Link between isoprene and secondary organic aerosol (soa): Pyruvic acid oxidation yields low volatility organic acids in clouds. Geophysical Research Letters, 33(6): L06822. Available from http://dx.doi.org/10.1029/2005GL025374. DOI 10.1029/2005GL025374.

Connelly, B.M., D.O. De Haan and M.A. Tolbert, 2012. Heterogeneous glyoxal oxidation: A potential source of secondary organic aerosol. The Journal of Physical Chemistry A, 116(24): 6180-6187. Available from http://dx.doi.org/10.1021/jp211502e [Accessed 2014/01/10]. DOI 10.1021/jp211502e.

De Haan, D.O., A.L. Corrigan, K.W. Smith, D.R. Stroik, J.J. Turley, F.E. Lee, M.A. Tolbert, J.L. Jimenez, K.E. Cordova and G.R. Ferrell, 2009. Secondary organic aerosol-forming reactions of glyoxal with amino acids. Environmental Science & Technology, 43(8): 2818-2824. Available from http://dx.doi.org/10.1021/es803534f [Accessed 2014/01/10]. DOI 10.1021/es803534f.

El Haddad, I., L. Yao, L. Nieto-Gligorovski, V. Michaud, B. Temime-Roussel, E. Quivet, N. Marchand, K. Sellegri and A. Monod, 2009. In-cloud processes of methacrolein under simulated conditions – part 2: Formation of secondary organic aerosol. Atmos. Chem. Phys., 9(14): 5107-5117. Available from http://www.atmos-chem-phys.net/9/5107/2009/. DOI 10.5194/acp-9-5107-2009.

Epstein, S.A. and S.A. Nizkorodov, 2012. A comparison of the chemical sinks of atmospheric organics in the gas and aqueous phase. Atmos. Chem. Phys., 12(17): 8205-8222. Available from http://www.atmos-chem-phys.net/12/8205/2012/. DOI 10.5194/acp-12-8205-2012.

Ervens, B., B.J. Turpin and R.J. Weber, 2011. Atmos. Chem. Phys., 11: 11069.

Fu, T.-M., D.J. Jacob, F. Wittrock, J.P. Burrows, M. Vrekoussis and D.K. Henze, 2008. Global budgets of atmospheric glyoxal and methylglyoxal, and implications for formation of secondary organic aerosols. Journal of Geophysical Research: Atmospheres, 113(D15): D15303. Available from http://dx.doi.org/10.1029/2007JD009505. DOI 10.1029/2007JD009505.

Galloway, M.M., P.S. Chhabra, A.W.H. Chan, J.D. Surratt, R.C. Flagan, J.H. Seinfeld and F.N. Keutsch, 2009. Glyoxal uptake on ammonium sulphate seed aerosol: Reaction products and reversibility of uptake under dark and irradiated conditions. Atmos. Chem. Phys., 9(10): 3331-3345. Available from http://www.atmos-chem-phys.net/9/3331/2009/. DOI 10.5194/acp-9-3331-2009.

Gong, H., A. Matsunaga and P.J. Ziemann, 2005. Products and mechanism of secondary organic aerosol formation from reactions of linear alkenes with no3 radicals. The Journal of Physical Chemistry A, 109(19): 4312-4324. Available from http://dx.doi.org/10.1021/jp058024l [Accessed 2014/01/10]. DOI 10.1021/jp058024l.

Guenther, A., T. Karl, P. Harley, C. Wiedinmyer, P.I. Palmer and C. Geron, 2006. Estimates of global terrestrial isoprene emissions using megan (model of emissions of gases and aerosols from nature). Atmos. Chem. Phys., 6(11): 3181-3210. Available from http://www.atmos-chem-phys.net/6/3181/2006/. DOI 10.5194/acp-6-3181-2006.

Igawa, M., J.W. Munger and M.R. Hoffmann, 1989. Analysis of aldehydes in cloud- and fogwater samples by hplc with a postcolumn reaction detector. Environmental Science & Technology, 23(5): 556-561. Available from http://dx.doi.org/10.1021/es00063a007 [Accessed 2014/01/10]. DOI 10.1021/es00063a007.

Jacob, D.J., 1986. Chemistry of oh in remote clouds and its role in the production of formic acid and peroxymonosulfate. Journal of Geophysical Research: Atmospheres, 91(D9): 9807-9826. Available from http://dx.doi.org/10.1029/JD091iD09p09807. DOI 10.1029/JD091iD09p09807.

Jang, M., R.M. Kamens, K.B. Leach and M.R. Strommen, 1997. A thermodynamic approach using group contribution methods to model the partitioning of semivolatile organic compounds on atmospheric particulate matter. Environmental Science & Technology, 31(10): 2805-2811. Available from http://dx.doi.org/10.1021/es970014d [Accessed 2014/01/10]. DOI 10.1021/es970014d.

Kamens, R.M., H. Zhang, E.H. Chen, Y. Zhou, H.M. Parikh, R.L. Wilson, K.E. Galloway and E.P. Rosen, 2011. Secondary organic aerosol formation from toluene in an atmospheric hydrocarbon mixture: Water and particle seed effects. Atmospheric Environment, 45(13): 2324-2334. Available from http://www.sciencedirect.com/science/article/pii/S1352231010009623. DOI http://dx.doi.org/10.1016/j.atmosenv.2010.11.007.

Kido Soule, M.C., K. Longnecker, S.J. Giovannoni and E.B. Kujawinski, 2010. Impact of instrument and experiment parameters on reproducibility of ultrahigh resolution esi ft-icr mass spectra of natural organic matter. Organic Geochemistry, 41(8): 725-733. Available from http://www.sciencedirect.com/science/article/pii/S014663801000135X. DOI http://dx.doi.org/10.1016/j.orggeochem.2010.05.017.

Klassen, N.V., D. Marchington and H.C.E. McGowan, 1994. H2o2 determination by the i3- method and by kmno4 titration. Analytical Chemistry, 66(18): 2921-2925.

Available from http://dx.doi.org/10.1021/ac00090a020 [Accessed 2014/01/10]. DOI 10.1021/ac00090a020.

Lee, A.K.Y., R. Zhao, S.S. Gao and J.P.D. Abbatt, 2011. Aqueous-phase oh oxidation of glyoxal: Application of a novel analytical approach employing aerosol mass spectrometry and complementary off-line techniques. The Journal of Physical Chemistry A, 115(38): 10517-10526. Available from http://dx.doi.org/10.1021/jp204099g [Accessed 2014/01/10]. DOI 10.1021/jp204099g.

Lim, H.-J., A.G. Carlton and B.J. Turpin, 2005. Isoprene forms secondary organic aerosol through cloud processing: Model simulations. Environmental Science & Technology, 39(12): 4441-4446. Available from http://dx.doi.org/10.1021/es048039h [Accessed 2014/01/10]. DOI 10.1021/es048039h.

Lim, Y.B., Y. Tan, M.J. Perri, S.P. Seitzinger and B.J. Turpin, 2010. Aqueous chemistry and its role in secondary organic aerosol (soa) formation. Atmos. Chem. Phys., 10(21): 10521-10539. Available from http://www.atmos-chem-phys.net/10/10521/2010/. DOI 10.5194/acp-10-10521-2010.

Lim, Y.B. and P.J. Ziemann, 2005. Products and mechanism of secondary organic aerosol formation from reactions of n-alkanes with oh radicals in the presence of nox. Environmental Science & Technology, 39(23): 9229-9236. Available from http://dx.doi.org/10.1021/es051447g [Accessed 2014/01/10]. DOI 10.1021/es051447g.

Lin, G., J.E. Penner, S. Sillman, D. Taraborrelli and J. Lelieveld, 2012. Global modeling of soa formation from dicarbonyls, epoxides, organic nitrates and peroxides. Atmos. Chem. Phys., 12(10): 4743-4774. Available from http://www.atmos-chem-phys.net/12/4743/2012/. DOI 10.5194/acp-12-4743-2012.

Liu, J., L.W. Horowitz, S. Fan, A.G. Carlton and H. Levy, 2012. Global in-cloud production of secondary organic aerosols: Implementation of a detailed chemical mechanism in the gfdl atmospheric model am3. Journal of Geophysical Research: Atmospheres, 117(D15): D15303. Available from http://dx.doi.org/10.1029/2012JD017838. DOI 10.1029/2012JD017838.

Mack, J. and J.R. Bolton, 1999. Photochemistry of nitrite and nitrate in aqueous solution: A review. Journal of Photochemistry and Photobiology A: Chemistry, 128(1–3): 1-13. Available from http://www.sciencedirect.com/science/article/pii/S1010603099001550. DOI http://dx.doi.org/10.1016/S1010-6030(99)00155-0.

Mantini, D., F. Petrucci, D. Pieragostino, P. Del Boccio, M. Di Nicola, C. Di Ilio, G. Federici, P. Sacchetta, S. Comani and A. Urbani, 2007. Limpic: A computational

method for the separation of protein maldi-tof-ms signals from noise. BMC Bioinformatics, 8(1): 101. Available from http://www.biomedcentral.com/1471-2105/8/101.

Matsumoto, K., S. Kawai and M. Igawa, 2005. Dominant factors controlling concentrations of aldehydes in rain, fog, dew water, and in the gas phase. Atmospheric Environment, 39(38): 7321-7329. Available from http://www.sciencedirect.com/science/article/pii/S1352231005008058. DOI http://dx.doi.org/10.1016/j.atmosenv.2005.09.009.

Mazzoleni, L.R., B.M. Ehrmann, X. Shen, A.G. Marshall and J.L. Collett, 2010. Water-soluble atmospheric organic matter in fog: Exact masses and chemical formula identification by ultrahigh-resolution fourier transform ion cyclotron resonance mass spectrometry. Environmental Science & Technology, 44(10): 3690-3697. Available from http://dx.doi.org/10.1021/es903409k [Accessed 2014/01/10]. DOI 10.1021/es903409k.

Myriokefalitakis, S., K. Tsigaridis, N. Mihalopoulos, J. Sciare, A. Nenes, K. Kawamura, A. Segers and M. Kanakidou, 2011. In-cloud oxalate formation in the global troposphere: A 3-d modeling study. Atmos. Chem. Phys., 11(12): 5761-5782. Available from http://www.atmos-chem-phys.net/11/5761/2011/. DOI 10.5194/acp-11-5761-2011.

Neta, P. and R.E. Huie, 1986. Rate constants for reactions of nitrogen oxide (no3) radicals in aqueous solutions. The Journal of Physical Chemistry, 90(19): 4644-4648. Available from http://dx.doi.org/10.1021/j100410a035 [Accessed 2014/01/10]. DOI 10.1021/j100410a035.

Noziere, B., P. Dziedzic and A. Córdova, 2008. Products and kinetics of the liquid-phase reaction of glyoxal catalyzed by ammonium ions (nh4+). The Journal of Physical Chemistry A, 113(1): 231-237.

Nozière, B., S. Ekström, T. Alsberg and S. Holmström, 2010. Radical-initiated formation of organosulfates and surfactants in atmospheric aerosols. Geophysical Research Letters, 37(5): L05806. Available from http://dx.doi.org/10.1029/2009GL041683. DOI 10.1029/2009GL041683.

Ortiz-Montalvo, D.L., Y.B. Lim, M.J. Perri, S.P. Seitzinger and B.J. Turpin, 2012. Volatility and yield of glycolaldehyde soa formed through aqueous photochemistry and droplet evaporation. Aerosol Science and Technology, 46(9): 1002-1014. Available from http://dx.doi.org/10.1080/02786826.2012.686676 [Accessed 2014/01/10]. DOI 10.1080/02786826.2012.686676.

Perri, M.J., Y.B. Lim, S.P. Seitzinger and B.J. Turpin, 2010. Organosulfates from glycolaldehyde in aqueous aerosols and clouds: Laboratory studies. Atmospheric Environment, 44(21–22): 2658-2664. Available from

http://www.sciencedirect.com/science/article/pii/S1352231010002578. DOI http://dx.doi.org/10.1016/j.atmosenv.2010.03.031.

Perri, M.J., S. Seitzinger and B.J. Turpin, 2009. Secondary organic aerosol production from aqueous photooxidation of glycolaldehyde: Laboratory experiments. Atmospheric Environment, 43(8): 1487-1497. Available from http://www.sciencedirect.com/science/article/pii/S1352231008011096. DOI http://dx.doi.org/10.1016/j.atmosenv.2008.11.037.

Petters, M.D. and S.M. Kreidenweis, 2007. A single parameter representation of hygroscopic growth and cloud condensation nucleus activity. Atmos. Chem. Phys., 7(8): 1961-1971. Available from http://www.atmos-chem-phys.net/7/1961/2007/. DOI 10.5194/acp-7-1961-2007.

Rinaldi, M., S. Decesari, C. Carbone, E. Finessi, S. Fuzzi, D. Ceburnis, C.D. O'Dowd, J. Sciare, J.P. Burrows, M. Vrekoussis, B. Ervens, K. Tsigaridis and M.C. Facchini, 2011. Evidence of a natural marine source of oxalic acid and a possible link to glyoxal. Journal of Geophysical Research: Atmospheres, 116(D16): D16204. Available from http://dx.doi.org/10.1029/2011JD015659. DOI 10.1029/2011JD015659.

Sareen, N., A.N. Schwier, E.L. Shapiro, D. Mitroo and V.F. McNeill, 2010. Secondary organic material formed by methylglyoxal in aqueous aerosol mimics. Atmos. Chem. Phys., 10(3): 997-1016. Available from http://www.atmos-chem-phys.net/10/997/2010/. DOI 10.5194/acp-10-997-2010.

Seinfeld, J.H. and S.N. Pandis, 2012. Atmospheric chemistry and physics: From air pollution to climate change. John Wiley & Sons.

Seitzinger, S.P., R.M. Styles, R. Lauck and M.A. Mazurek, 2002. Atmospheric pressure mass spectrometry: A new analytical chemical characterization method for dissolved organic matter in rainwater. Environmental Science & Technology, 37(1): 131-137. Available from http://dx.doi.org/10.1021/es025848x [Accessed 2014/01/10]. DOI 10.1021/es025848x.

Shapiro, E.L., J. Szprengiel, N. Sareen, C.N. Jen, M.R. Giordano and V.F. McNeill, 2009. Light-absorbing secondary organic material formed by glyoxal in aqueous aerosol mimics. Atmos. Chem. Phys., 9(7): 2289-2300. Available from http://www.atmos-chem-phys.net/9/2289/2009/. DOI 10.5194/acp-9-2289-2009.

Southam, A.D., T.G. Payne, H.J. Cooper, T.N. Arvanitis and M.R. Viant, 2007. Dynamic range and mass accuracy of wide-scan direct infusion nanoelectrospray fourier transform ion cyclotron resonance mass spectrometry-based metabolomics increased by the spectral stitching method. Analytical Chemistry, 79(12): 4595-4602. Available from http://dx.doi.org/10.1021/ac062446p [Accessed 2014/01/10]. DOI 10.1021/ac062446p.

Sun, Y.L., Q. Zhang, C. Anastasio and J. Sun, 2010. Insights into secondary organic aerosol formed via aqueous-phase reactions of phenolic compounds based on high resolution mass spectrometry. Atmos. Chem. Phys., 10(10): 4809-4822. Available from http://www.atmos-chem-phys.net/10/4809/2010/. DOI 10.5194/acp-10-4809-2010.

Surratt, J.D., A.W.H. Chan, N.C. Eddingsaas, M. Chan, C.L. Loza, A.J. Kwan, S.P. Hersey, R.C. Flagan, P.O. Wennberg and J.H. Seinfeld, 2010. Reactive intermediates revealed in secondary organic aerosol formation from isoprene. Proceedings of the National Academy of Sciences, 107(15): 6640-6645. Available from http://www.pnas.org/content/107/15/6640.abstract. DOI 10.1073/pnas.0911114107.

Tan, Y., A.G. Carlton, S.P. Seitzinger and B.J. Turpin, 2010. Soa from methylglyoxal in clouds and wet aerosols: Measurement and prediction of key products. Atmospheric Environment, 44(39): 5218-5226. Available from http://www.sciencedirect.com/science/article/pii/S1352231010007399. DOI http://dx.doi.org/10.1016/j.atmosenv.2010.08.045.

Tan, Y., M.J. Perri, S.P. Seitzinger and B.J. Turpin, 2009. Effects of precursor concentration and acidic sulfate in aqueous glyoxal−oh radical oxidation and implications for secondary organic aerosol. Environmental Science & Technology, 43(21): 8105-8112. Available from http://dx.doi.org/10.1021/es901742f [Accessed 2014/01/10]. DOI 10.1021/es901742f.

Waldman, J.M., J.W. MUNGER, D.J. JACOB, R.C. FLAGAN, J.J. MORGAN and M.R. HOFFMANN, 1982. Chemical composition of acid fog. Science, 218(4573): 677-680. Available from http://www.sciencemag.org/content/218/4573/677.abstract. DOI 10.1126/science.218.4573.677.

Warneck, P., 1999. The relative importance of various pathways for the oxidation of sulfur dioxide and nitrogen dioxide in sunlit continental fair weather clouds. Physical Chemistry Chemical Physics, 1(24): 5471-5483. Available from http://dx.doi.org/10.1039/A906558J. DOI 10.1039/A906558J.

Wittrock, F., A. Richter, H. Oetjen, J.P. Burrows, M. Kanakidou, S. Myriokefalitakis, R. Volkamer, S. Beirle, U. Platt and T. Wagner, 2006. Simultaneous global observations of glyoxal and formaldehyde from space. Geophysical Research Letters, 33(16): L16804. Available from http://dx.doi.org/10.1029/2006GL026310. DOI 10.1029/2006GL026310.

Yeung, L.Y., M.J. Pennino, A.M. Miller and M.J. Elrod, 2005. Kinetics and mechanistic studies of the atmospheric oxidation of alkynes. The Journal of Physical Chemistry A, 109(9): 1879-1889. Available from

http://dx.doi.org/10.1021/jp0454671 [Accessed 2014/01/10]. DOI 10.1021/jp0454671.

Zhang, Q. and C. Anastasio, 2001. Chemistry of fog waters in california's central valley—part 3: Concentrations and speciation of organic and inorganic nitrogen. Atmospheric Environment, 35(32): 5629-5643. Available from http://www.sciencedirect.com/science/article/pii/S1352231001003375. DOI http://dx.doi.org/10.1016/S1352-2310(01)00337-5.

Zhang, Q. and C. Anastasio, 2003. Free and combined amino compounds in atmospheric fine particles (pm2.5) and fog waters from northern california. Atmospheric Environment, 37(16): 2247-2258. Available from http://www.sciencedirect.com/science/article/pii/S1352231003001274. DOI http://dx.doi.org/10.1016/S1352-2310(03)00127-4.

Zhang, Q., J.L. Jimenez, M.R. Canagaratna, J.D. Allan, H. Coe, I. Ulbrich, M.R. Alfarra, A. Takami, A.M. Middlebrook, Y.L. Sun, K. Dzepina, E. Dunlea, K. Docherty, P.F. DeCarlo, D. Salcedo, T. Onasch, J.T. Jayne, T. Miyoshi, A. Shimono, S. Hatakeyama, N. Takegawa, Y. Kondo, J. Schneider, F. Drewnick, S. Borrmann, S. Weimer, K. Demerjian, P. Williams, K. Bower, R. Bahreini, L. Cottrell, R.J. Griffin, J. Rautiainen, J.Y. Sun, Y.M. Zhang and D.R. Worsnop, 2007. Ubiquity and dominance of oxygenated species in organic aerosols in anthropogenically-influenced northern hemisphere midlatitudes. Geophysical Research Letters, 34(13): L13801. Available from http://dx.doi.org/10.1029/2007GL029979. DOI 10.1029/2007GL029979.

Zhou, X. and K. Mopper, 1990. Apparent partition coefficients of 15 carbonyl compounds between air and seawater and between air and freshwater; implications for air-sea exchange. Environmental Science & Technology, 24(12): 1864-1869. Available from http://dx.doi.org/10.1021/es00082a013 [Accessed 2014/01/10]. DOI 10.1021/es00082a013.

Zhou, Y., H. Zhang, H.M. Parikh, E.H. Chen, W. Rattanavaraha, E.P. Rosen, W. Wang and R.M. Kamens, 2011. Secondary organic aerosol formation from xylenes and mixtures of toluene and xylenes in an atmospheric urban hydrocarbon mixture: Water and particle seed effects (ii). Atmospheric Environment, 45(23): 3882-3890. Available from http://www.sciencedirect.com/science/article/pii/S1352231010010848. DOI http://dx.doi.org/10.1016/j.atmosenv.2010.12.048.

Figure 2-1. Concentration of oxalate (μM) with reaction time (min) for glyoxal (GLY) oxidation experiments: GLY+OH (solid circle), GLY+OH+HNO_3(open circle), and GLY+OH+$(NH_4)_2SO_4$ (asterisk). Error bars represent the coefficient of variation (<10%) across three experiments each.

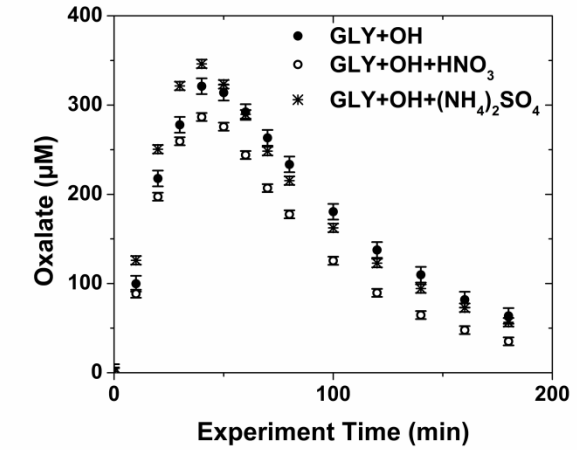

Figure 2-2. Tartarate and malonate detected by ion chromatography for glyoxal (GLY) oxidation experiments: GLY+OH (solid circle), GLY+OH+HNO_3(open circle), and GLY+OH+$(NH_4)_2SO_4$ (asterisk). Note that tartarate and malonate coelute. Error bars represent the coefficient of variation across experiments, 55% for GLY+OH, 49% for GLY+OH+HNO_3, and 38% for GLY+OH+$(NH_4)_2SO_4$.

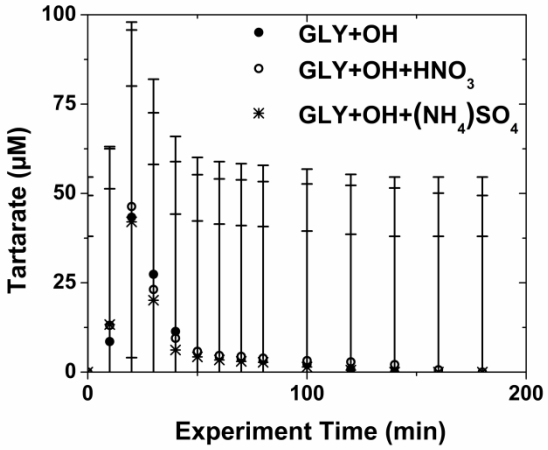

Figure 2-3. Hypothesized reactions and organic nitrogen products.

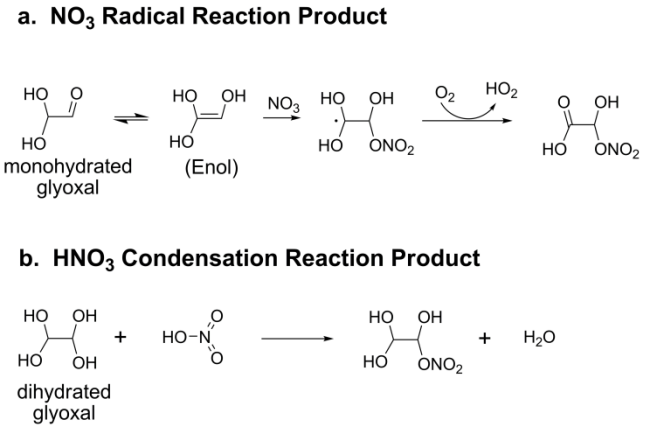

Figure 2-4a-d. Ion chromatography-electrospray ionization mass spectrometry data for the mixed standard (a) and the 40-minute time point samples from glyoxal (GLY) oxidation experiments: GLY+OH (b), GLY+OH+HNO_3(c), and GLY+OH+$(NH_4)_2SO_4$ (d). In each case, the ion chromatogram is shown to the left. The mass spectrum of each lettered peak is shown to the right. The mixed standard contains glycolate (m/z- 75, peak A), formate (m/z- 45, peak B), glyoxylate (m/z- 73, peak C), succinate (m/z- 117, peak D), tartarate (m/z- 149, peak E), and oxalate (m/z- 89, peak F). Note the following organic acid pairs coelute: glycolate + acetate (m/z- 59), succinate + malate (m/z- 133), and tartarate + malonate (m/z- 103). Nitrate (m/z- 62) and sulfate (m/z- 97) are peaks N and S respectively.

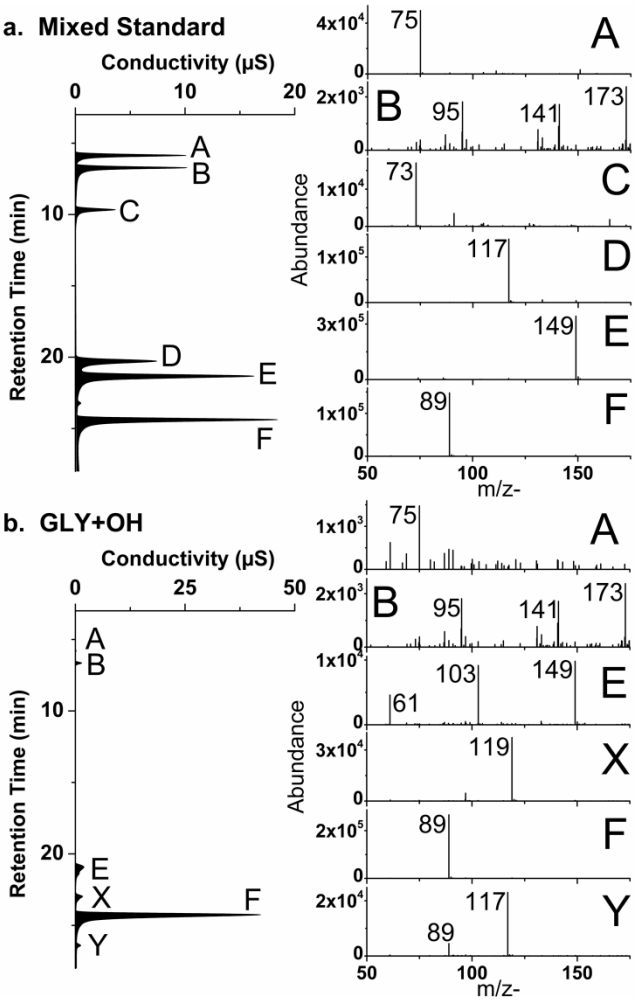
a. Mixed Standard
Conductivity (μS)
0
10
20
Retention Time (min)
10
20
A
B
C
D
E
F
Abundance
4x10^4
75
A
2x10^3
B
95
141
173
1x10^4
73
C
1x10^5
117
D
3x10^5
149
E
1x10^5
89
F
50
100
150
m/z-
b. GLY+OH
Conductivity (μS)
0
25
50
Retention Time (min)
10
20
A
B
E
X
F
Y
Abundance
1x10^3
75
A
2x10^3
B
95
141
173
1x10^4
103
149
61
E
3x10^4
119
X
2x10^5
89
F
2x10^4
117
89
Y
50
100
150
m/z-

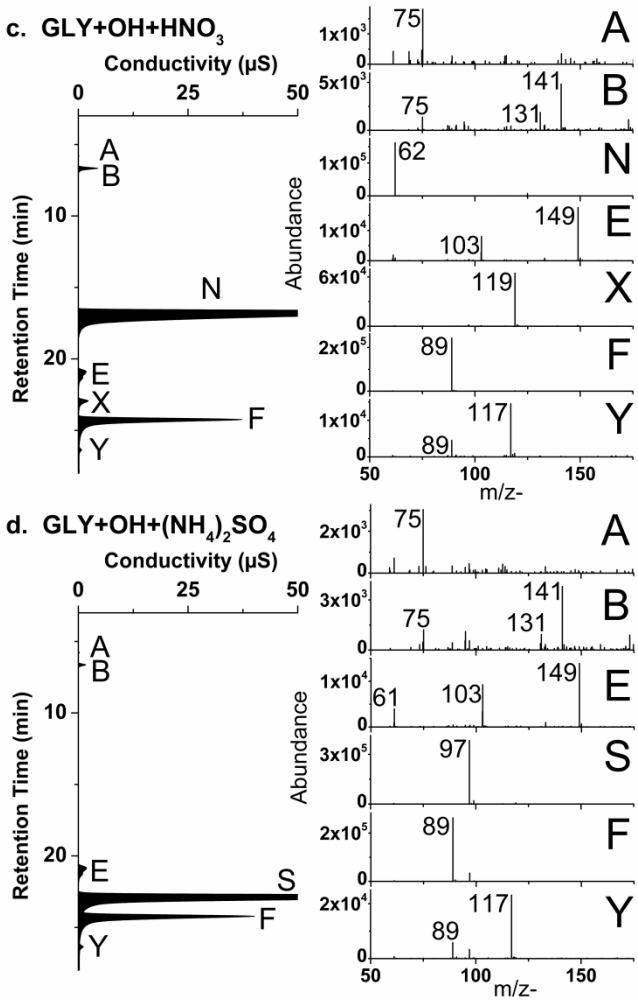
c. GLY+OH+HNO3
Conductivity (μS)
0
25
50
Retention Time (min)
10
20
A
B
N
E
X
F
Y
Abundance
1x10^3
75
A
5x10^3
141
75
131
B
1x10^5
62
N
1x10^4
149
103
E
6x10^4
119
X
2x10^5
89
F
1x10^4
117
89
Y
50
100
150
m/z-
d. GLY+OH+(NH4)2SO4
Conductivity (μS)
0
25
50
Retention Time (min)
10
20
A
B
E
S
F
Y
Abundance
2x10^3
75
A
3x10^3
141
75
131
B
1x10^4
61
103
149
E
3x10^5
97
S
2x10^5
89
F
2x10^4
117
89
Y
50
100
150
m/z-

Figure 2-5. Relative abundances of m/z- 149 (tartarate) and m/z- 103 (malonate) ions in chromatographic peak E as a function of time during the OH radical oxidation of glyoxal are shown here. Because peak E reaches a maximum between 10 and 30 minutes, we conclude that peak E is predominantly tartarate.

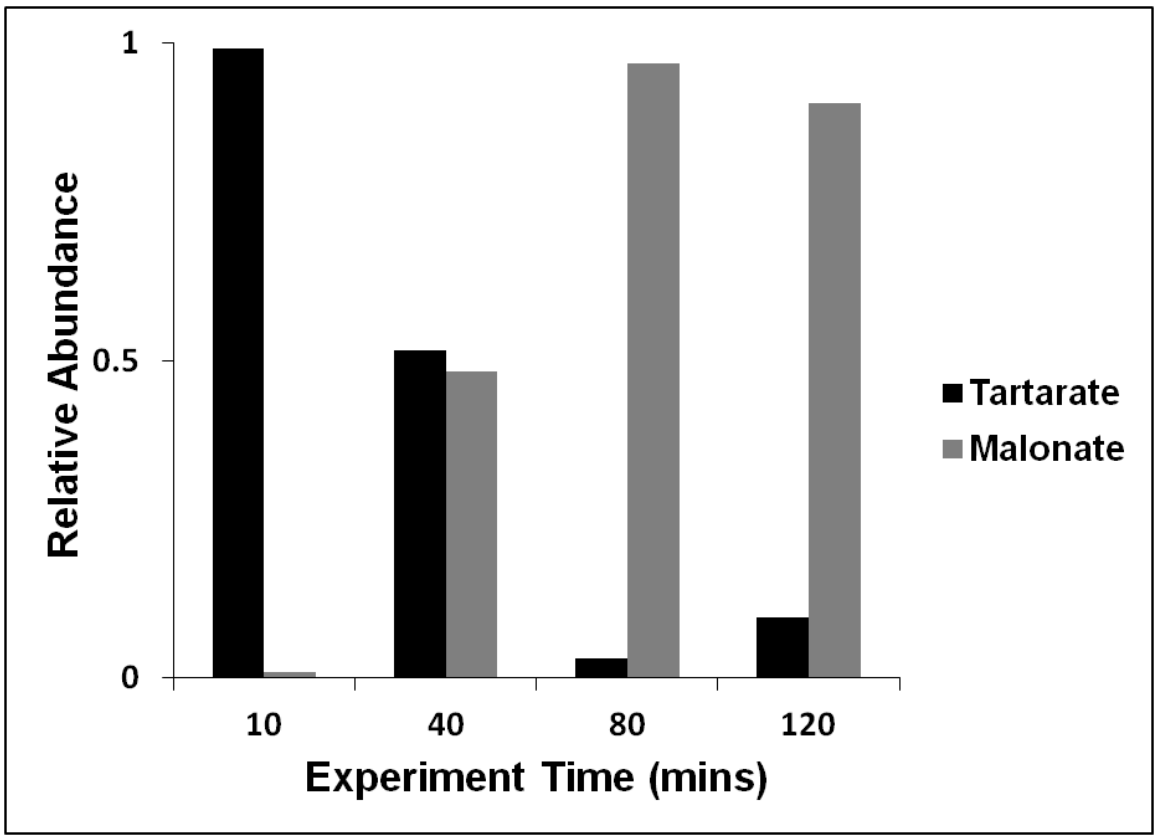

Chapter 3. Amines, organic acids, and aqueous photooxidation of water-soluble gases from the Po Valley, Italy

Material in this chapter will be submitted with the following contributing authors: Kirkland, J.R., Y.B. Lim, A.P. Sullivan, J.L. Collett Jr., F.N. Keutsch, S. Decesari, C.M. Facchini, and B.J. Turpin

3.1.Introduction

There is considerable evidence that chemistry in atmospheric waters (e.g., clouds, fogs, and wet aerosols) alters the composition of organic gases and aerosols (Blando and Turpin, 2000; Herckes *et al.*, 2013). Partitioning of ubiquitous water-soluble gases into atmospheric waters and subsequent reaction has been observed to diminish gas phase oxidant concentration (i.e., HO_2) since aqueous processing of some water-soluble organics is faster than gas-phase oxidation (Ervens *et al.*, 2013). It can also lead to the formation of low volatility products and secondary organic aerosol (SOA). We call this "aqueous SOA" (SOAaq). SOAaq formation helps explain the high oxygen to carbon ratios found in atmospheric aerosols (Aiken *et al.*, 2008; Aiken *et al.*, 2009; Altieri *et al.*, 2009; Lim *et al.*, 2010) and the atmospheric presence of high-molecular weight compounds (Liggio *et al.*, 2005; Altieri *et al.*, 2009; Lim *et al.*, 2010), oxalate (Carlton *et al.*, 2007), and organic sulfate (Nozière *et al.*, 2010; Perri *et al.*, 2010; Ervens *et al.*, 2011; Zhang *et al.*, 2011). Aqueous chemistry has the potential to substantially impact global aerosol budgets (Liu *et al.*, 2012; Barsanti *et al.*, 2013; He *et al.*, 2013). However, to understand the true impact of aqueous chemistry on budgets of reactive gases and aerosols it is important to identify the major precursors. Since hydroxyl radicals are important reactants in clouds and fogs and react more rapidly in the aqueous phase than

in the gas phase (Atkinson, 1987; Doussin and Monod, 2013), we focus on hydroxyl radical chemistry herein. We present for the first time results of aqueous oxidation experiments with ambient mixtures of water-soluble gases.

Laboratory simulations of atmospheric aqueous chemistry have been used to validate and refine aqueous chemical mechanisms for specific precursor compounds in simplified mixtures under a range of atmospherically-relevant concentrations. This validated chemistry has improved global predictions of oxalate and aerosol mass and improved our understanding of chemical transformations that link emissions with ambient measurements (Myriokefalitakis *et al.*, 2011; Liu *et al.*, 2012). These experiments suggest that (dilute) cloud chemistry is an efficient 'cloud processing' medium in which water-soluble gases (e.g. aldehydes) react to form lower volatility products (e.g., organic salts) (Ortiz-Montalvo *et al.*, 2013) through oxidation reactions (e.g., with hydroxyl radicals) (Carlton *et al.*, 2006; Tan *et al.*, 2009; Lee *et al.*, 2011; Kirkland *et al.*, 2013), and non-radical reactions (e.g., forming oligomers) become important during droplet evaporation (Loeffler *et al.*, 2006; De Haan *et al.*, 2009; Connelly *et al.*, 2012). The presence of water also affects the condensed phase chemistry of aerosols, leading to the formation of oligomers, organosulfates, and imidazoles through radical and non-radical reactions (Noziere *et al.*, 2008; Galloway *et al.*, 2009; Lim *et al.*, 2010; Perri *et al.*, 2010; Sareen *et al.*, 2010; Nguyen *et al.*, 2012). However, traditional laboratory simulations do not capture the complex mixture of precursors present in ambient air. In this work, we performed controlled experiments on this natural matrix of water-soluble gases collected in the Po Valley, Italy to identify previously

unstudied precursors to aqueous processing and inform future laboratory experiment design. This motivates the research and results reported herein.

The Po Valley was a logical choice for this work because polluted fogs in this region have been studied for several decades and in the summertime the Po Valley is an area of high photochemical activity and experiences high relative humidities (Fuzzi *et al.*, 1992; Fuzzi *et al.*, 2002; Cappiello *et al.*, 2003). Presumably, then, liquid water concentrations (e.g., wet aerosols and clouds), water-soluble organic concentrations and oxidant concentrations are high. Industrial and agricultural emissions in the Po Valley are trapped by the Alps to the north and Apennines to the south. Organic emissions are fragmented and oxidized photochemically in the summertime. Thus, we expect that water-soluble gases will be abundant. Early exploration of fog chemistry examined temporal variations in gas and particle composition. That is, variation in sulfur and nitrogen species (i.e., NH_4^+, NO_2^-, NO_3^-, SO_4^-), low molecular weight organics (e.g., formaldehyde, acetaldehyde, and formic, acetic, and pyruvic acids), and oxidants (i.e., H_2O_2) in liquid samples (Fuzzi *et al.*, 1992). More recent work includes high-resolution mass spectrometric analysis including mass fragmentation to characterize dissolved organic matter (Cappiello *et al.*, 2003; LeClair *et al.*, 2012; Gilardoni *et al.*, 2014). The work reported herein was conducted as part of a larger campaign, called the Pan European Gas Aerosols Climate Interaction Study (PEGASOS).

In this work we report the novel use of mist chambers to collect the ambient matrix of water-soluble gases from Po Valley, Italy for use in controlled hydroxyl radical photooxidation experiments. Ambient water-soluble gases were scrubbed from Po Valley air during the summer of 2012, subjected to OH photooxidation and analyzed by

ion chromatography and mass spectrometry. During aqueous processing experiments, we observed the oxidation of amines and production of organic anion products (e.g., pyruvate, oxalate) from within the ambient mix of water-soluble gases for the first time. Reactants within the ambient mixture were further examined by high-resolution mass spectrometry to provide insights into the chemical structures of potentially important water-soluble gases present in ambient Po Valley air. Mist chamber samples served as surrogate cloud/fog water enabling the study of aqueous chemistry independent of naturally occurring fog events.

3.2.Approach

3.2.1. Mist chamber field sampling

Water-soluble gases were scrubbed from the ambient air into 17.5 $\pm$ 0.5 MΩ water using mist chambers at the San Pietro Capofiume field site in the Po Valley, Italy (June 12th – July 9th, 2012). Four mist chambers (Cofer *et al.*, 1985; Anderson *et al.*, 2008) were operated in parallel with an air flow rate of 28 $\pm$ 3 L min^{-1}. Air was pulled through each ½ in. Teflon inlet (~3.5 m above ground) and passed through a pre-baked quartz fiber filter (Pall, 47 mm; replaced $\leq$3 days) to remove particles before entering the spray chamber compartment of the apparatus. Water soluble gases accumulated in the liquid water, which refluxed with the aid of a hydrophobic membrane (Zefluor filter, 47 mm) at the top/outlet of the MC. Each mist chamber was initially filled with 30 mL of water; water was added every 15 min as needed to replace evaporative losses. Operation times ranged from 2-4 hours between 5 a.m. and 6 p.m to capture the daytime mixture of water-soluble gases (Appendix B.1.1). This method to collect water-soluble gases has been shown to have high collection efficiencies (>78%) for water-soluble organics (K_H =

~10^3) (Spaulding et al 2002). Aqueous MC samples were composited daily and stored frozen until use in 10 mL and 40 mL aliquots. In a few cases 4 hour morning samples were composited across three days; afternoon samples were separately and similarly composited. Field water blanks were saved, stored, and shipped with each days' samples and handled in the same manner as samples. Each day began with a 5 minute dilute acid (0.025% H_2SO_4) wash followed by a 10 minute water-rinse wash. Next the mist chambers were operated for 2 minutes to collect a dynamic blank and then sample collection began. MC's were cleaned again at the end of each day (Appendix B.2.1 provides the MC operation protocol and B.2.2 the field data sheet). Samples, field water blanks, and dynamic blanks were analyzed for total organic carbon, for total dissolved nitrogen and by mass spectrometry.

OH radical oxidation experiments (Table 3-1) were conducted for days with the highest total organic carbon values (95$\pm$15 µM-C). The composite sample from the mornings of July 7th, 8th, and 9th contained the strongest precursor signals and the highest total dissolved nitrogen (101 µM-N) relative to other samples (mean = 43 µM-N).

3.2.2. Batch OH radical oxidation of field samples in a cuvette chamber

Bulk aqueous phase OH radical oxidation of field samples was carried out in a custom cuvette reaction vessel in which ten cuvettes (with screw caps; Spectrocell Inc., Oreland, PA) each containing 3 mL of sample were held equidistant from a 254 nm mercury lamp (Heraeus Noblelight, Inc. Duluth, GA) housed in a quartz immersion well (Ace Glass Inc., Vineland, NJ). The cuvettes were partially submerged in a temperature controlled (25.0 $\pm$ 0.1 °C) water bath connected to a Fisher Scientific Isotemp 2150 Nano water chiller. The entire chamber was wrapped in aluminum foil to eliminate the

presence of ambient light. OH radicals were continuously produced in the cuvettes *in situ* at a rate of $3.5x10^2$ µM [OH] s^{-1} by photolysis of H_2O_2 (125 µM H_2O_2 was added to each cuvette for this purpose). After removal from the cuvette chamber at t = 10, 20, 30, 40, 40, 60, 80, 100, 120, 150, H_2O_2 in discrete samples (cuvettes) was quenched with 36 µL of 1% catalase solution (Sigma; 40,200 units/mg), thus stopping the reaction. Each discrete sample was analyzed by Ion Chromatography (IC) and Electrospray Ionization Mass Spectrometry (ESI-MS) and 1 mL of sample was frozen for ultra-high resolution Fourier-Transform Ion Cyclotron Resonance Mass Spectrometry (FTICR-MS) discussed below in analytical methods (Appendix B.2.3 provides the Cuvette chamber SOP and B.2.4 the cuvette sample data sheet).

The H_2O_2 photolysis rate constant ($k_1 = 1.0x10^{-4}$ s^{-1}; $R^2 = 0.9405$) for this lamp and chamber were determined from H_2O_2 + UV control experiments (Appendix B.1.2). Specifically, k_1 was determined by fitting H_2O_2 measurements with model predictions using reactions displayed in Appendix A.1.1. The triiodide method (Klassen *et al.*, 1994) was used to measure H_2O_2. H_2O_2 + UV experiments were performed before and after experiments with field water samples. The OH concentration during experiments will depend not only on the OH production rate via H_2O_2 photolysis, but also on the presence of other OH radical sources/sinks in the sample (e.g., Source: collected H_2O_2, Sink: dissolved organic carbon). We expect the average OH radical concentration in field water + OH experiments to be approximately 10^{-12} M determined from the H_2O_2 photolysis model (FACSIMILE) reactions and k_1 determined experimentally, this estimate does not include an OH sink due to reactions with DOC.

In addition to H_2O_2 + UV control experiments, GLY + OH and catalase tests were conducted before and after OH experiments with field water samples. GLY + OH was used to compare performance of the new cuvette chamber with our 1 L reaction vessel which is discussed later with results later (Refer to Chapter 2 for 1L GLY+OH results). The catalase test verified that H_2O_2 was efficiently destroyed when a cuvette was removed from the experiment chamber. In a catalase test, a mixed standard of pyruvate, glyoxylate, and oxalate (50 µM each) was treated as an experimental sample. This mixed standard was spiked with 125 µM H_2O_2, quenched with 4 different amounts of 1% catalase solution (0, 24, 36, and 48 µL) and analyzed by IC to calculate recoveries. Recoveries for pyruvate and glyoxylate, which are known to react with H_2O_2, were greater than 87%. Recoveries for oxalate, which does not, were greater than 95% (Appendix B.1.3).

Field experiments (Field sample + OH) were accompanied by control experiments, specifically: Field sample + H_2O_2, Field Sample + UV, and Water Blank + OH. Field control experiments were used to determine to what extent the chemistry in field sample + OH experiments was the result of OH radical oxidation of water-soluble organics scrubbed from the ambient air, rather than reaction of ambient compounds with UV or H2O2 or the reaction of contaminants.

Batch cuvette chamber experiments and control experiments with field samples are listed in Table 3-1. The table provides sample collection conditions, total organic carbon (TOC) and total dissolved nitrogen (TDN) values for OH experiment samples. Replicate experiments were used to calculate pooled coefficients of variance for IC included with each figure.

3.2.3. Analytical methods

An aliquot from each sampling day was thawed and analyzed for unit mass chemical composition and total organic carbon (TOC; Shimadzu TOC 5000A, Shimadzu Corporation) and total dissolved nitrogen (TDN; Antek PAC 7000B, Antek Instruments). Cuvette samples from experiments and control experiments were analyzed via ion chromatography for organic acids (IC; Dionex ICS 3000; IonPac AS11-HC column; 30 °C, AG11-HC guard column; conductivity detector; 35 °C; milli-q water eluent; KOH gradient method to separate organic acids), and by unit mass ESI-MS (HP – Agilent 1100; positive and negative mode single quadrupole mass spectrometer). A 1 ml aliquot of each sample was stored frozen for later use. Selected aliquots were analyzed by ultra-high resolution MS-MS (Thermo-Finnigan LTQ-XL: positive mode only, Woods Hole Oceanographic Institution Mass Spectrometry Facility; Fourier Transform Ion Cyclotron Resonance, FTICR, MS-MS analysis; Collision Induced Dissociation and Infrared Multi Photon Dissociation fragmentation mechanisms were optimized for each individual ion).

Positive and negative ionization mode mass spectrometric analysis (50 – 1000 amu) of discrete samples was performed with a unit mass resolution ESI-MS. Briefly, 6 injections of 20 µL of sample were analyzed with a 50/50 mixture of 0.05% formic acid in water and methanol (0.22 mL min^{-1}) as described previously by Perri *et al.* (2009). ESI-MS was operated with a fragmentor voltage of 40 V and capillary voltage of 3000 V (nitrogen drying gas; 10 L min^{-1}; 350 °C). This is a soft ionization technique in which mass to charge ratios (m/z) are detected: deprotonated masses in the negative mode (molecular weight minus one) and positively charged adducts in the positive mode (molecular weight plus H+ or Na+ plus other neutral adducts e.g., H_2O, MeOH); detected

masses are not fragments. Mixed standards containing acetic acid, formic acid, pyruvic acid, glyoxylic acid, nitric acid, succinic acid, tartaric acid, ammonium sulfate, and oxalic acid at five concentration levels were also analyzed with each sequence for negative mode to verify mass assignment of these expected products of aqueous processing. Mixed standards containing glyoxal, methylglyoxal, and glycolaldehyde at five concentration levels were analyzed with each sequence for positive mode to verify mass assignment of these expected precursors to aqueous processing. Mass accuracy is checked with caffeine in the positive mode and nitrobenzoic acid in the negative mode.

Ion chromatographic analysis separates carboxylic anions, which were then quantified by IC (i.e., conductivity) with five-point calibration curves (accepted $R^2 >$ 0.98) as described by Tan *et al.* (2009). Standards are produced from commercially available standards of acetate (5.5 min retention time), formate (6.4 min), pyruvate (7.2 min), glyoxylate (9.3 min), nitrate (17.3 min), succinate (20.0 min), tartarate (21.1 min), sulfate (23.1 min) and oxalate (24.5 min). In addition to samples, each sequence included the standard mix (100 μM) of the above compounds (measurement precision for each organic acid <15%), an independent standard mix (100 μM; pyruvate, glyoxylate, oxalate from separate stock; accuracy found to be within 15%), and a water blank injection before and after sample analysis. In addition, 20% of samples were analyzed with a duplicate injection (analytical precision calculated from replicate injections is 25% for oxalate and 87% for pyruvate; other organic acid values included in appendices figure captions).

Selected field samples and selected time points from cuvette chamber photooxidation experiments were analyzed by ultra-high resolution FT-ICR MS^2 (LTQ

FT Ultra; Thermo Scientific) in positive ionization mode. Mass accuracy is checked weekly with caffeine, peptide-MRFA, ultramark, SDS, and sodium taurocholate and found to be within 2ppm. A syringe pump delivered analyte (50% methanol; 50% sample) into the spray chamber at 4 μL min^{-1} with a capillary temperature of 260 °C and spray voltage of 3.8-4.2 kV (solvent blank: 4.5 kV). Target masses were isolated (isolation width: m/z = 2) and fragmented with a collision induced dissociation (CID; helium) in the ion trap (IT) and the resulting ions were detected in the FT-ICR MS. Target masses were isolated in the same manner, transferred to the FT-ICR chamber, and fragmented with an infrared multi photon dissociation (IRMPD; carbon dioxide) laser. Exact masses were processed with Midas Molecular Formula Calculator (v1.1) as described by Altieri *et al.* (2008) to provide elemental formulas of detected species.

3.2.4. Precursor and Product identification criteria

The following criteria were employed to identify precursors and products of OH radical chemistry. Precursor criteria are 1) ion signal greater in the unreacted (t = 0) mist chamber samples and decreasing signal thereafter during OH experiments (and not controls), 2) a reproducible decrease in abundance during multiple OH experiments, 3) constant abundance during control experiments (Field Sample + H_2O_2, Field Sample + UV), 4) ion abundance in Field Water + OH experiment is less than 10% of field sample abundance, 5) ion abundance in field sample is above detection limits calculated from water blanks analyzed with each ESI-MS sequence (Average Signal + 3σ). Product criteria are 1) ion signal increases relative to the unreacted (t = 0) mist chamber samples during OH experiments (and not in controls), 2) a reproducible increase in abundance during multiple OH experiments, 3) ion abundance does not increase during control

experiments (Field Sample + H_2O_2, Field Sample + UV), 4) maximum ion abundance in Field Water + OH is less than minimum detected abundance in OH experiments, 5) ion abundance in field sample is above detection limits calculated from water blanks analyzed with ESI-MS sequence (Average Signal + 3σ).

3.2.5. Experiment Quality Control

In addition, 10% of cuvettes were sampled (two cuvettes removed at one time point) in duplicate and found to be within 15% for every anion measured by IC. Discrete samples from cuvette chamber experiments and standards were analyzed by ESI-MS and 6 injections are averaged, standard deviations calculated, 95% t-test performed, blank is subtracted, 90% t-test is performed and the resulting signals are reported as abundance (Perri *et al.*, 2009).

Water blanks were sampled from the laboratory water source and analyzed in the same manner as samples during cuvette chamber experiments. Since water blanks had negligible IC peaks, no subtraction was performed. Although ESI-MS analysis of water blanks shows variation in abundance across masses, masses selected for further (MS-MS) analysis had negligible or no corresponding signal in water blanks. ESI-MS abundances were considered to be above detection limits when they were greater than the average signal from field and lab water blanks plus three standard deviations (Appendix B.1.4).

3.3.Results and discussion

3.3.1 Products of aqueous OH photooxidation

Oxalate and pyruvate formed during all experiments with OH radicals present and did not form during control experiments (e.g., Figures 3-1 and 3-2; Appendices B.1.5-B.1.13 include IC data for other organic anions quantified). Oxalate and pyruvate

production has been previously observed in laboratory experiments conducted with single precursor compounds (e.g., glyoxal, methylglyoxal, glycolaldehyde, pyruvic acid, acetic acid, methylvinylketone, methacrolein) (Carlton *et al.*, 2006; Carlton *et al.*, 2007; Altieri *et al.*, 2008; Perri *et al.*, 2009; Tan *et al.*, 2010; Zhang *et al.*, 2010; Liu *et al.*, 2012; Tan *et al.*, 2012). Since oxalate and pyruvate are found predominantly in the particle phase in the atmosphere (Saxena and Hildemann, 1996; Kawamura *et al.*, 2003), this finding provides support for aqueous SOA formation in real atmospheric waters. Note that organic carbon concentrations in the mist chamber samples are similar to concentrations found in fogs and ground based clouds (Herckes *et al.*, 2013) and much lower than the concentrations of total dissolved organics in wet aerosols (1-10M) (Lim *et al.*, 2010). While the *precursors* to oxidation chemistry in clouds, fogs and wet aerosols are probably the same, we expect the *products* formed from oxidation in wet aerosols to be different from the products formed in clouds and fogs. Specifically, high concentrations of organic radicals formed from OH oxidation in wet aerosols will react with each other to form oligomeric products (Lim *et al.*, 2010) rather than reacting with O_2. Certainly non-radical reactions (e.g., with inorganics) can also occur in wet aerosols (Noziere *et al.*, 2008; Galloway *et al.*, 2009; Sareen *et al.*, 2010).

Because the Po Valley is a nitrogen-rich region due to local anthropogenic and biogenic sources of ammonia (Crosier *et al.*, 2007) and sulfate concentrations are low, we expect organic acids formed through cloud/fog processing to be present as salts and less volatile than their acid counterparts. For example, the vapor pressure of ammonium oxalate is orders of magnitude lower than that of oxalic acid (Ortiz-Montalvo *et al.*, 2013). Thus, an area like the Po Valley, with abundant ammonia, could have greater

SOAaq mass than another location with comparable organic precursor concentrations and liquid water but less ammonia or more acidic sulfate.

Several products in addition to oxalate and pyruvate were evident based on their increasing ESI-MS ion abundance (Appendix B.1.14). Specifically, the negative mode ions m/z- 73 (e.g., glyoxylate), 87 (e.g., pyruvate), 89 (e.g., oxalate), 103 (e.g., malonate), 117 (e.g., mesoxalate) and 203 and positive mode ions m/z+ 100, 132, 162, and 178 met the described product criteria (Appendix B.1.15).

3.3.2 Precursors

Ions meeting the criteria for precursors were detected during all experiments with OH radicals present (Appendix B.1.5). These identified precursors decrease in the presence of OH and not in the absence of OH (i.e., they do not decrease in field sample + H_2O_2 or field sample + UV control experiments). That is, these masses have strong signals at the start of OH experiments and degrade with continued exposure to OH radicals. The abundance for these masses remains high during Sample+H_2O_2 and Sample+UV. Because the ion abundance decreases in the presence but not the absence of OH, we conclude these ions are reacting with OH radicals.

OH experiments reproducibly show oxalate and pyruvate production despite variations in the identified precursors across sampling days. Thus, it appears that there are multiple sources (precursors) of pyruvate and oxalate present in these mist chamber samples. In addition, ESI-MS (+,-) analysis reveals that more precursor ions were detected during positive mode analysis and more products in negative mode analysis. We expect to detect carboxylic acid, organonitrate, and organosulfate functional groups during negative mode analysis and carbonyl, aldehyde, alcohol, and imine functional

groups during positive mode analysis. This suggests that precursors were mostly water-soluble gases with one or more carbonyl, aldehyde, alcohol, or imine functional groups.

We expected, but did not find evidence for the oxidation of glyoxal (di-hydrate) and methylglyoxal in the field water + OH experiments. ESI-MS abundances at m/z+ 117 (Glyoxal + MeOH), 131, and/or 145, consistent with the presence of glyoxal and/or methylglyoxal were observed in some samples, but precursor trends were not observed. Note that glyoxal and methylglyoxal are products of the gas phase photooxidation of aromatics and alkenes and they are known to form oxalate and pyruvate through aqueous OH radical oxidation (Carlton *et al.*, 2006; Carlton *et al.*, 2007; Altieri *et al.*, 2008; Tan *et al.*, 2009). The reaction of glyoxal (50 µM) plus OH was examined in additional control experiments to gauge how much oxalate would be produced if all of the TOC (~100 µM-C) in mist chamber samples were glyoxal. The maximum oxalate produced during this experiment was 30 µM (Appendix B.1.16). Thus, if the single source of oxalate during mist chamber samples plus OH experiments (~7.5 µM) was glyoxal, we would expect a total of 12 µM glyoxal in our samples. It is possible that the ionization efficiency of glyoxal is suppressed by the matrix of DOC in our samples. However, ESI-MS(+) analysis of several mist chamber samples spiked with 0, 15, and 30 µM glyoxal shows increasing abundance with increasing glyoxal concentration. This suggests our instrument sensitivity is sufficient for detection of glyoxal. Note that 12-15 µM glyoxal is the expected concentration of glyoxal in our mist chamber samples based upon gas-phase glyoxal measurements at the field site and assuming Henry's law equilibrium. Since we know gas-phase glyoxal was present at the site, yet we don't observe a trend indicative of glyoxal during our experiments (i.e. precursor trend at m/z+ 117, 131), we

expect that glyoxal in our samples may be bound to other organic species resulting in 1) no detection at the expected unit masses, 2) bound-glyoxal does not readily react during our experiments, or 3) OH was rapidly consumed by other precursors.

There were two sampling periods with substantial haze based on LIDAR measurements, and 'cyclonic' meteorological conditions (June 18th-19th and July 7th-9th). Air masses were characterized as coming across the Apennine mountains and down through the sampling site (June 18th – 22nd and July 3rd – 8th). We expected the water-soluble components in these air masses to be similar. However, Figures 3-3 and 3-4 show that the strongest observed precursors during these experiments were different. Figures 3-3 and 3-4 show precursor ion trends that best fit the stated criteria detected during OH experiments with July 7th, 8th, 9th and June 19th and June 20th samples. OH experiments with July 7th, 8th, 9th samples show strong initial signals for m/z+ 86, 130, 304 and decreased abundance thereafter. This was not observed in the June OH experiments. OH experiments conducted with June 19th and June 20th samples revealed that m/z+ 137, 179, and 301 (Figure 3-4) follow a precursor trend. Below, we further examine the July 7th, 8th, 9th experiments.

3.3.3 Amines

The even m/z+ ions (86, 130, 304) in the morning mist chamber sample composite collected on July 7th, 8th, and 9th had the strongest precursor ESI-MS(+) signals and the most distinct precursor trends among all OH experiments (Figure 3-3). These ions were only detected in samples collected after July 3rd. In experiments without OH radicals (Sample+H_2O_2 and Sample+UV) the abundances of these ions remained constant throughout the experiment. Even mass ions detected in the positive mode of ESI-MS

analysis suggest the presence of a single nitrogen atom in the elemental formula since nitrogen with an even unit mass (14 amu) can accommodate three bonds with a lone pair of electrons unaffiliated. The presence of nitrogen and the odd numbered bonding results in an even mass when adopting an additional hydrogen during ionization for mass spectrometric detection (e.g., $N + 3H + 1H_{Ionization} = 18$ amu). As an additional example, consider carbon and oxygen. Since carbon (even unit mass, 4 bonds, no lone pairs) and oxygen (even unit mass, 2 bonds, 2 lone pairs) will result in an even unit mass molecular weight, the additional charge resulting from adducts formed in the ionization chamber results in an odd mass to charge ratio. The ion abundances of two other nitrogen-containing ions (m/z+ 118 and 162) increased as m/z+ 86, 130, 304 decreased (Figure 3-3), suggesting that they are intermediates or products of aqueous OH chemistry.

Several pieces of evidence suggest that m/z+ 86, 130, and 304 are amines. Elemental formulas assigned to exact masses (Table 3-2) detected during ultra-high resolution MS isolation suggest that nitrogen functional groups were reduced (i.e., amine, imine), and not oxidized (i.e., nitrate). Greater than a 10 ppm error resulted when the inclusion of an organic nitrate functional group was specified, whereas the elemental formulas reported in Table 3-2 were fit within 1 ppm error and in agreement with the presence of amine functionality. Elemental formulas displayed in Table 3-2 are within 1 ppm error and suggest amine functional groups for m/z+ 86, 118, 130, and 304 since higher O/N ratios are necessary to construct plausible organic nitrate structures. Fragmentation of m/z+ 86 was attempted with IRMPD and CID methods, but did not result in fragments without complete loss of the parent ion signal. However, the elemental formula for m/z+ 86 is a CHN+ compound which eliminates the possibility of

oxidized nitrogen. During fragmentation of m/z+ 130 the parent ion lost a neutral water molecule, suggesting the presence of a hydroxyl functional group, and a CHN+ compound remained. This and further fragmentation provided the structural insights depicted in Figure 3-5 and Table 3-3. Fragmentation of m/z+ 304 yielded one major fragment shown in Appendix B.1.17 which suggest m/z+ 304 is also an amine. The results reported here demonstrate amines were present in the ambient air, able to partition into liquid water and react with OH radicals.

The product ions m/z+ 118 and 162 can be seen increasing during OH radical experiments conducted with July 7^{th}, 8^{th}, 9^{th} composites. Elemental formulas assigned to exact masses detected by ultra-high resolutions FTICR-MS show that m/z+ 118 has an O:N ratio of one and m/z+ 162 has an O:N ratio of three suggesting 118 contains an amine functionality and 162 may contain amine or nitrate functionality. Fragmentation of m/z+ 118 and 162 (t = 30 minute time point saved for fragmentation) reveals that both product ions undergo neutral water losses. It is plausible that these ions result from the OH radical oxidation of our precursor ions. Appendix B.1.18 describes a mechanism by which oxidation of m/z+ 130 could lead to the formation of m/z+ 118. In addition, fragmentation spectra are similar for m/z+ 118 and 162 suggesting structural similarities. Fragmentation of m/z+ 162 includes a fragment with the same exact mass as m/z+ 118 and the difference between the parent ion (m/z+ 162) and daughter ion (m/z+ 118) has the same exact mass as a carboxylic functional group; CO_2 (Appendix B.1.19 = MS^2 m/z+ 118, Appendix B.1.20 = MS^2 m/z+ 162).

This work suggests that liquid water could be a sink for gas-phase amines in the Po Valley atmosphere. This finding is consistent with the concurrently conducted work

of Gilardoni *et al.* (2014), who demonstrated that Po Valley fogs are efficient scavengers of ammonium (efficiency: 68%), nitrate (70%), and organics (50%; including amines). These results are also consistent with Altieri *et al.* (2009), who detected many reduced CHN+ and CHON+ compounds in high-resolution mass spectrometric analysis of rainwater. Nielsen *et al.* (2012) compiled available rate constants for amine + OH radical chemistry in the aqueous phase. This compilation shows that amines react rapidly with OH radicals (10^7 to 10^{10} k $M^{-1}s^{-1}$) in the aqueous phase, within a broad atmospherically relevant pH range (pH 2.0-12.0). Nielsen *et al.* (2012) also calculated lifetimes of specific amines and demonstrated that some species (i.e., alkanol-amines, piperazine) may be completely removed from the gas phase when liquid water is present. Thus, these findings support the aqueous processing results reported herein and suggest that Po Valley fogs and clouds provide an important platform for amines to react. Aqueous amines and their oxidation products are lost through wet deposition. Otherwise they could be released back into the gas phase or incorporated into particulate matter during droplet evaporation. De Haan *et al.* (2009) provide evidence of imidazole and nitrogen-containing oligomer formation during droplet evaporation experiments containing methylglyoxal, amino acids, methylamine, and ammonium sulfate. This chemistry is expected in the nitrogen-rich Po Valley and could have global importance since continental sources of nitrogen species are diverse (e.g., biomass burning, industrial and agricultural processes), but also play an important role in fine particle composition in remote marine environments (Müller *et al.*, 2009).

3.4.Conclusions and atmospheric implications

This work provides evidence for aqueous processing of water-soluble organic gases collected during summer 2012 in the Po Valley, Italy. The period of July 4th-9th resulted in the strongest ion signals that decreased with exposure to OH radicals. Structural insights for these ions (m/z+ 86, 130, 304) suggest that they are amines. Amines, therefore, may be potentially important precursors to aqueous organic processing, and aqueous processing may alter their gas phase budgets as well as particle composition and properties. We report evidence for the production of organic acids that are typically found in atmospheric particles (e.g., oxalate), thus demonstrating that aqueous oxidation of ambient mixtures of water soluble gases can result in secondary organic aerosol formation. This work supports the growing evidence that aqueous organic processing can change chemical characteristics of atmospheric pollutants (e.g., volatility, optical properties). The samples and experiments described here focus on one distinct episode of poor air quality during July which includes reactive amines. Brief results and discussion of OH experiments and analysis from an episode of poor air quality in June suggests that the matrix of water-soluble gases participating in aqueous processing is highly variable and complex. These amine structures and other potentially important precursors to aqueous processing require further exploration to elucidate/validate/refine their aqueous chemical mechanisms and ultimately to improve predictive models used to mitigate the harmful effects of primary emissions.

3.5.References

Aiken, A.C., P.F. DeCarlo, J.H. Kroll, D.R. Worsnop, J.A. Huffman, K.S. Docherty, I.M. Ulbrich, C. Mohr, J.R. Kimmel and D. Sueper, 2008. O/c and om/oc ratios of primary, secondary, and ambient organic aerosols with high-resolution time-of-flight aerosol mass spectrometry. Environmental Science & Technology, 42(12): 4478-4485.

Aiken, A.C., D. Salcedo, M.J. Cubison, J.A. Huffman, P.F. DeCarlo, I.M. Ulbrich, K.S. Docherty, D. Sueper, J.R. Kimmel, D.R. Worsnop, A. Trimborn, M. Northway, E.A. Stone, J.J. Schauer, R.M. Volkamer, E. Fortner, B. de Foy, J. Wang, A. Laskin, V. Shutthanandan, J. Zheng, R. Zhang, J. Gaffney, N.A. Marley, G. Paredes-Miranda, W.P. Arnott, L.T. Molina, G. Sosa and J.L. Jimenez, 2009. Mexico city aerosol analysis during milagro using high resolution aerosol mass spectrometry at the urban supersite (t0) – part 1: Fine particle composition and organic source apportionment. Atmos. Chem. Phys., 9(17): 6633-6653. Available from http://www.atmos-chem-phys.net/9/6633/2009/. DOI 10.5194/acp-9-6633-2009.

Altieri, K.E., S.P. Seitzinger, A.G. Carlton, B.J. Turpin, G.C. Klein and A.G. Marshall, 2008. Oligomers formed through in-cloud methylglyoxal reactions: Chemical composition, properties, and mechanisms investigated by ultra-high resolution ft-icr mass spectrometry. Atmospheric Environment, 42(7): 1476-1490. Available from http://www.sciencedirect.com/science/article/pii/S1352231007010205. DOI http://dx.doi.org/10.1016/j.atmosenv.2007.11.015.

Altieri, K.E., B.J. Turpin and S.P. Seitzinger, 2009. Oligomers, organosulfates, and nitrooxy organosulfates in rainwater identified by ultra-high resolution electrospray ionization ft-icr mass spectrometry. Atmos. Chem. Phys., 9(7): 2533-2542. Available from http://www.atmos-chem-phys.net/9/2533/2009/. DOI 10.5194/acp-9-2533-2009.

Anderson, C.H., J.E. Dibb, R.J. Griffin, G.S.W. Hagler and M.H. Bergin, 2008. Atmospheric water-soluble organic carbon measurements at summit, greenland. Atmospheric Environment, 42(22): 5612-5621. Available from http://www.sciencedirect.com/science/article/pii/S1352231008002562. DOI http://dx.doi.org/10.1016/j.atmosenv.2008.03.006.

Atkinson, R., 1987. A structure-activity relationship for the estimation of rate constants for the gas-phase reactions of oh radicals with organic compounds. International Journal of Chemical Kinetics, 19(9): 799-828. Available from http://dx.doi.org/10.1002/kin.550190903. DOI 10.1002/kin.550190903.

Barsanti, K.C., A.G. Carlton and S.H. Chung, 2013. Analyzing experimental data and model parameters: Implications for predictions of soa using chemical transport models. Atmos. Chem. Phys., 13(23): 12073-12088. Available from

http://www.atmos-chem-phys.net/13/12073/2013/. DOI 10.5194/acp-13-12073-2013.

Blando, J.D. and B.J. Turpin, 2000. Secondary organic aerosol formation in cloud and fog droplets: A literature evaluation of plausibility. Atmospheric Environment, 34(10): 1623-1632. Available from http://www.sciencedirect.com/science/article/pii/S1352231099003921. DOI http://dx.doi.org/10.1016/S1352-2310(99)00392-1.

Cappiello, A., E. De Simoni, C. Fiorucci, F. Mangani, P. Palma, H. Trufelli, S. Decesari, M. Facchini and S. Fuzzi, 2003. Molecular characterization of the water-soluble organic compounds in fogwater by esims/ms. Environmental science & technology, 37(7): 1229-1240.

Carlton, A.G., B.J. Turpin, K.E. Altieri, S. Seitzinger, A. Reff, H.-J. Lim and B. Ervens, 2007. Atmospheric oxalic acid and soa production from glyoxal: Results of aqueous photooxidation experiments. Atmospheric Environment, 41(35): 7588-7602. Available from http://www.sciencedirect.com/science/article/pii/S1352231007004979. DOI http://dx.doi.org/10.1016/j.atmosenv.2007.05.035.

Carlton, A.G., B.J. Turpin, H.-J. Lim, K.E. Altieri and S. Seitzinger, 2006. Link between isoprene and secondary organic aerosol (soa): Pyruvic acid oxidation yields low volatility organic acids in clouds. Geophysical Research Letters, 33(6): L06822. Available from http://dx.doi.org/10.1029/2005GL025374. DOI 10.1029/2005GL025374.

Cofer, W.R., V.G. Collins and R.W. Talbot, 1985. Improved aqueous scrubber for collection of soluble atmospheric trace gases. Environmental science & technology, 19(6): 557-560.

Connelly, B.M., D.O. De Haan and M.A. Tolbert, 2012. Heterogeneous glyoxal oxidation: A potential source of secondary organic aerosol. The Journal of Physical Chemistry A, 116(24): 6180-6187. Available from http://dx.doi.org/10.1021/jp211502e [Accessed 2014/01/10]. DOI 10.1021/jp211502e.

Crosier, J., J.D. Allan, H. Coe, K.N. Bower, P. Formenti and P.I. Williams, 2007. Chemical composition of summertime aerosol in the po valley (italy), northern adriatic and black sea. Quarterly Journal of the Royal Meteorological Society, 133(S1): 61-75. Available from http://dx.doi.org/10.1002/qj.88. DOI 10.1002/qj.88.

De Haan, D.O., A.L. Corrigan, K.W. Smith, D.R. Stroik, J.J. Turley, F.E. Lee, M.A. Tolbert, J.L. Jimenez, K.E. Cordova and G.R. Ferrell, 2009. Secondary organic aerosol-forming reactions of glyoxal with amino acids. Environmental Science &

Technology, 43(8): 2818-2824. Available from http://dx.doi.org/10.1021/es803534f [Accessed 2014/01/10]. DOI 10.1021/es803534f.

Doussin, J.F. and A. Monod, 2013. Structure–activity relationship for the estimation of oh-oxidation rate constants of carbonyl compounds in the aqueous phase. Atmos. Chem. Phys., 13(23): 11625-11641. Available from http://www.atmos-chem-phys.net/13/11625/2013/. DOI 10.5194/acp-13-11625-2013.

Ervens, B., B.J. Turpin and R.J. Weber, 2011. Secondary organic aerosol formation in cloud droplets and aqueous particles (aqsoa): A review of laboratory, field and model studies. Atmos. Chem. Phys., 11(21): 11069-11102. Available from http://www.atmos-chem-phys.net/11/11069/2011/. DOI 10.5194/acp-11-11069-2011.

Ervens, B., Y. Wang, J. Eagar, W.R. Leaitch, A.M. Macdonald, K.T. Valsaraj and P. Herckes, 2013. Dissolved organic carbon (doc) and select aldehydes in cloud and fog water: The role of the aqueous phase in impacting trace gas budgets. Atmos. Chem. Phys., 13(10): 5117-5135. Available from http://www.atmos-chem-phys.net/13/5117/2013/. DOI 10.5194/acp-13-5117-2013.

Fuzzi, S., M. Facchini, G. Orsi, J. Lind, W. Wobrock, M. Kessel, R. Maser, W. Jaeschke, K. Enderle and B. Arends, 1992. The po valley fog experiment 1989. Tellus B, 44(5): 448-468.

Fuzzi, S., M.C. Facchini, S. Decesari, E. Matta and M. Mircea, 2002. Soluble organic compounds in fog and cloud droplets: What have we learned over the past few years? Atmospheric Research, 64(1): 89-98.

Galloway, M.M., P.S. Chhabra, A.W.H. Chan, J.D. Surratt, R.C. Flagan, J.H. Seinfeld and F.N. Keutsch, 2009. Glyoxal uptake on ammonium sulphate seed aerosol: Reaction products and reversibility of uptake under dark and irradiated conditions. Atmos. Chem. Phys., 9(10): 3331-3345. Available from http://www.atmos-chem-phys.net/9/3331/2009/. DOI 10.5194/acp-9-3331-2009.

Gilardoni, S., P. Massoli, L. Giulianelli, M. Rinaldi, M. Paglione, F. Pollini, C. Lanconelli, V. Poluzzi, S. Carbone, R. Hillamo, L.M. Russell, M.C. Facchini and S. Fuzzi, 2014. Fog scavenging of organic and inorganic aerosol in the po valley. Atmos. Chem. Phys. Discuss., 14(4): 4787-4826. Available from http://www.atmos-chem-phys-discuss.net/14/4787/2014/. DOI 10.5194/acpd-14-4787-2014.

He, C., J. Liu, A.G. Carlton, S. Fan, L.W. Horowitz, H. Levy Ii and S. Tao, 2013. Evaluation of factors controlling global secondary organic aerosol production from cloud processes. Atmos. Chem. Phys., 13(4): 1913-1926. Available from

http://www.atmos-chem-phys.net/13/1913/2013/. DOI 10.5194/acp-13-1913-2013.

Herckes, P., K.T. Valsaraj and J.L. Collett Jr, 2013. A review of observations of organic matter in fogs and clouds: Origin, processing and fate. Atmospheric Research, 132–133(0): 434-449. Available from http://www.sciencedirect.com/science/article/pii/S016980951300183X [Accessed 2013/11//]. DOI http://dx.doi.org/10.1016/j.atmosres.2013.06.005.

Kawamura, K., N. Umemoto, M. Mochida, T. Bertram, S. Howell and B.J. Huebert, 2003. Water-soluble dicarboxylic acids in the tropospheric aerosols collected over east asia and western north pacific by ace-asia c-130 aircraft. Journal of Geophysical Research: Atmospheres, 108(D23): 8639. Available from http://dx.doi.org/10.1029/2002JD003256. DOI 10.1029/2002JD003256.

Kirkland, J.R., Y.B. Lim, Y. Tan, K.E. Altieri and B.J. Turpin, 2013. Glyoxal secondary organic aerosol chemistry: Effects of dilute nitrate and ammonium and support for organic radical–radical oligomer formation. Environmental Chemistry, 10(3): 158-166. Available from http://www.publish.csiro.au/paper/EN13074. DOI http://dx.doi.org/10.1071/EN13074.

Klassen, N.V., D. Marchington and H.C.E. McGowan, 1994. H2o2 determination by the i3- method and by kmno4 titration. Analytical Chemistry, 66(18): 2921-2925. Available from http://dx.doi.org/10.1021/ac00090a020 [Accessed 2014/01/10]. DOI 10.1021/ac00090a020.

LeClair, J.P., J.L. Collett and L.R. Mazzoleni, 2012. Fragmentation analysis of water-soluble atmospheric organic matter using ultrahigh-resolution ft-icr mass spectrometry. Environmental science & technology, 46(8): 4312-4322.

Lee, A.K.Y., P. Herckes, W.R. Leaitch, A.M. Macdonald and J.P.D. Abbatt, 2011. Aqueous oh oxidation of ambient organic aerosol and cloud water organics: Formation of highly oxidized products. Geophysical Research Letters, 38(11): L11805. Available from http://dx.doi.org/10.1029/2011GL047439. DOI 10.1029/2011GL047439.

Liggio, J., S.-M. Li and R. McLaren, 2005. Heterogeneous reactions of glyoxal on particulate matter: Identification of acetals and sulfate esters. Environmental Science & Technology, 39(6): 1532-1541. Available from http://dx.doi.org/10.1021/es048375y [Accessed 2014/04/08]. DOI 10.1021/es048375y.

Lim, Y.B., Y. Tan, M.J. Perri, S.P. Seitzinger and B.J. Turpin, 2010. Aqueous chemistry and its role in secondary organic aerosol (soa) formation. Atmos. Chem. Phys., 10(21): 10521-10539. Available from http://www.atmos-chem-phys.net/10/10521/2010/. DOI 10.5194/acp-10-10521-2010.

Liu, J., L.W. Horowitz, S. Fan, A.G. Carlton and H. Levy, 2012. Global in-cloud production of secondary organic aerosols: Implementation of a detailed chemical mechanism in the gfdl atmospheric model am3. Journal of Geophysical Research: Atmospheres, 117(D15): D15303. Available from http://dx.doi.org/10.1029/2012JD017838. DOI 10.1029/2012JD017838.

Liu, Y., F. Siekmann, P. Renard, A. El Zein, G. Salque, I. El Haddad, B. Temime-Roussel, D. Voisin, R. Thissen and A. Monod, 2012. Oligomer and soa formation through aqueous phase photooxidation of methacrolein and methyl vinyl ketone. Atmospheric Environment, 49: 123-129.

Loeffler, K.W., C.A. Koehler, N.M. Paul and D.O. De Haan, 2006. Oligomer formation in evaporating aqueous glyoxal and methyl glyoxal solutions. Environmental Science & Technology, 40(20): 6318-6323. Available from http://dx.doi.org/10.1021/es060810w [Accessed 2014/04/15]. DOI 10.1021/es060810w.

Müller, C., Y. Iinuma, J. Karstensen, D.v. Pinxteren, S. Lehmann, T. Gnauk and H. Herrmann, 2009. Seasonal variation of aliphatic amines in marine sub-micrometer particles at the cape verde islands. Atmospheric Chemistry and Physics, 9(24): 9587-9597.

Myriokefalitakis, S., K. Tsigaridis, N. Mihalopoulos, J. Sciare, A. Nenes, K. Kawamura, A. Segers and M. Kanakidou, 2011. In-cloud oxalate formation in the global troposphere: A 3-d modeling study. Atmos. Chem. Phys., 11(12): 5761-5782. Available from http://www.atmos-chem-phys.net/11/5761/2011/. DOI 10.5194/acp-11-5761-2011.

Nguyen, T.B., P.B. Lee, K.M. Updyke, D.L. Bones, J. Laskin, A. Laskin and S.A. Nizkorodov, 2012. Formation of nitrogen- and sulfur-containing light-absorbing compounds accelerated by evaporation of water from secondary organic aerosols. Journal of Geophysical Research: Atmospheres, 117(D1): D01207. Available from http://dx.doi.org/10.1029/2011JD016944. DOI 10.1029/2011JD016944.

Nielsen, C.J., H. Herrmann and C. Weller, 2012. Atmospheric chemistry and environmental impact of the use of amines in carbon capture and storage (ccs). Chemical Society Reviews, 41(19): 6684-6704. Available from http://dx.doi.org/10.1039/C2CS35059A. DOI 10.1039/C2CS35059A.

Noziere, B., P. Dziedzic and A. Córdova, 2008. Products and kinetics of the liquid-phase reaction of glyoxal catalyzed by ammonium ions (nh4+). The Journal of Physical Chemistry A, 113(1): 231-237.

Nozière, B., S. Ekström, T. Alsberg and S. Holmström, 2010. Radical-initiated formation of organosulfates and surfactants in atmospheric aerosols. Geophysical Research

Letters, 37(5): L05806. Available from http://dx.doi.org/10.1029/2009GL041683. DOI 10.1029/2009GL041683.

Ortiz-Montalvo, D.L., S.A.K. Häkkinen, A.N. Schwier, Y.B. Lim, V.F. McNeill and B.J. Turpin, 2013. Ammonium addition (and aerosol ph) has a dramatic impact on the volatility and yield of glyoxal secondary organic aerosol. Environmental Science & Technology, 48(1): 255-262. Available from http://pubs.acs.org/doi/abs/10.1021/es4035667 [Accessed 2014/03/23]. DOI 10.1021/es4035667.

Perri, M.J., Y.B. Lim, S.P. Seitzinger and B.J. Turpin, 2010. Organosulfates from glycolaldehyde in aqueous aerosols and clouds: Laboratory studies. Atmospheric Environment, 44(21–22): 2658-2664. Available from http://www.sciencedirect.com/science/article/pii/S1352231010002578. DOI http://dx.doi.org/10.1016/j.atmosenv.2010.03.031.

Perri, M.J., S. Seitzinger and B.J. Turpin, 2009. Secondary organic aerosol production from aqueous photooxidation of glycolaldehyde: Laboratory experiments. Atmospheric Environment, 43(8): 1487-1497. Available from http://www.sciencedirect.com/science/article/pii/S1352231008011096. DOI http://dx.doi.org/10.1016/j.atmosenv.2008.11.037.

Sareen, N., A.N. Schwier, E.L. Shapiro, D. Mitroo and V.F. McNeill, 2010. Secondary organic material formed by methylglyoxal in aqueous aerosol mimics. Atmos. Chem. Phys., 10(3): 997-1016. Available from http://www.atmos-chem-phys.net/10/997/2010/. DOI 10.5194/acp-10-997-2010.

Saxena, P. and L. Hildemann, 1996. Water-soluble organics in atmospheric particles: A critical review of the literature and application of thermodynamics to identify candidate compounds. Journal of Atmospheric Chemistry, 24(1): 57-109. Available from http://dx.doi.org/10.1007/BF00053823. DOI 10.1007/BF00053823.

Tan, Y., A.G. Carlton, S.P. Seitzinger and B.J. Turpin, 2010. Soa from methylglyoxal in clouds and wet aerosols: Measurement and prediction of key products. Atmospheric Environment, 44(39): 5218-5226. Available from http://www.sciencedirect.com/science/article/pii/S1352231010007399. DOI http://dx.doi.org/10.1016/j.atmosenv.2010.08.045.

Tan, Y., Y.B. Lim, K.E. Altieri, S.P. Seitzinger and B.J. Turpin, 2012. Mechanisms leading to oligomers and soa through aqueous photooxidation: Insights from oh radical oxidation of acetic acid and methylglyoxal. Atmos. Chem. Phys., 12(2): 801-813. Available from http://www.atmos-chem-phys.net/12/801/2012/. DOI 10.5194/acp-12-801-2012.

Tan, Y., M.J. Perri, S.P. Seitzinger and B.J. Turpin, 2009. Effects of precursor concentration and acidic sulfate in aqueous glyoxal−oh radical oxidation and implications for secondary organic aerosol. Environmental Science & Technology, 43(21): 8105-8112. Available from http://dx.doi.org/10.1021/es901742f [Accessed 2014/01/10]. DOI 10.1021/es901742f.

Zhang, H., J.D. Surratt, Y.H. Lin, J. Bapat and R.M. Kamens, 2011. Effect of relative humidity on soa formation from isoprene/no photooxidation: Enhancement of 2-methylglyceric acid and its corresponding oligoesters under dry conditions. Atmos. Chem. Phys., 11(13): 6411-6424. Available from http://www.atmos-chem-phys.net/11/6411/2011/. DOI 10.5194/acp-11-6411-2011.

Zhang, X., Z. Chen and Y. Zhao, 2010. Laboratory simulation for the aqueous oh-oxidation of methyl vinyl ketone and methacrolein: Significance to the in-cloud soa production. Atmospheric Chemistry and Physics, 10(19): 9551-9561.

Figure 3-1. Oxalate and pyruvate production during OH experiments conducted (in duplicate) with July 7th, 8th, 9th mist chamber sample. Error bars are ±1 coefficient of variation pooled across replicate experiments (23% for oxalate and 78% for pyruvate).

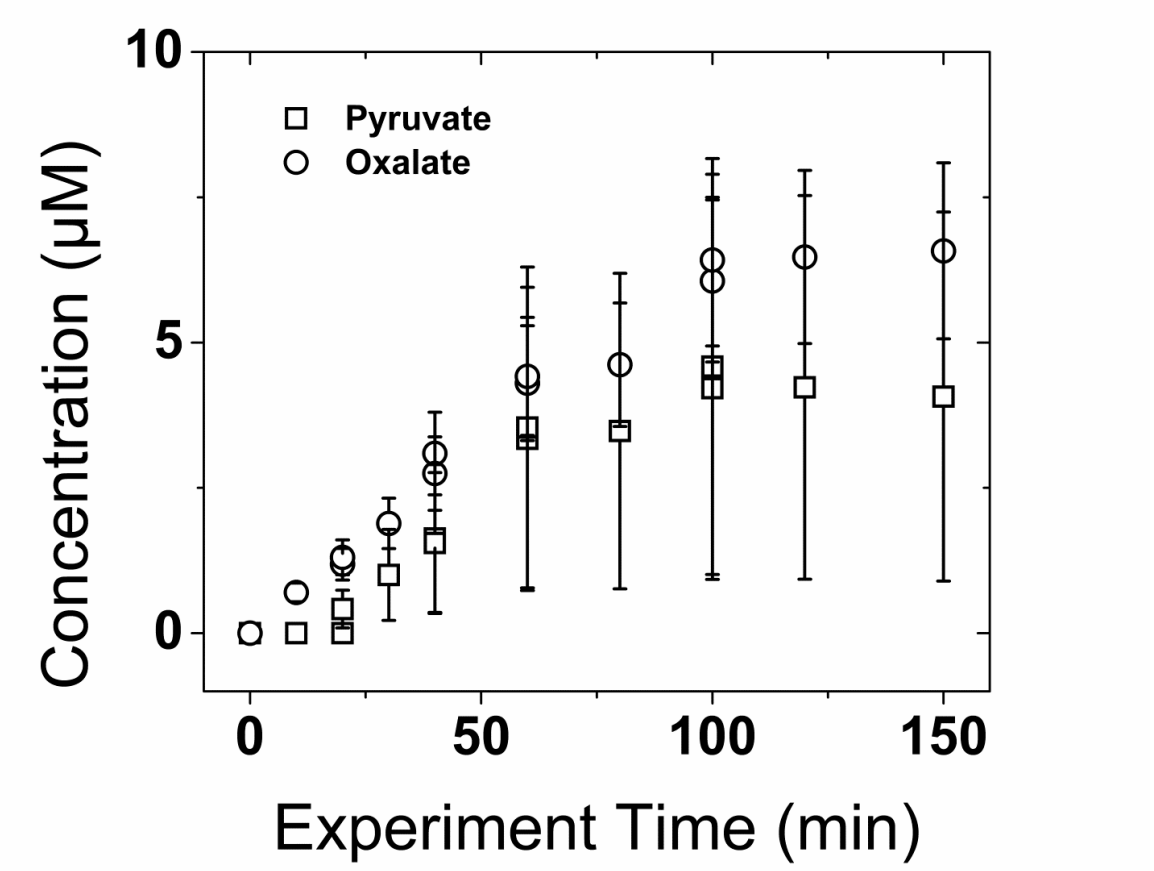

Figure 3-2. Shown here is pyruvate and oxalate production averaged across June 19th+OH and June 20th+OHexperiments with the pooled coefficient of variation calculated based on replicate experiments.

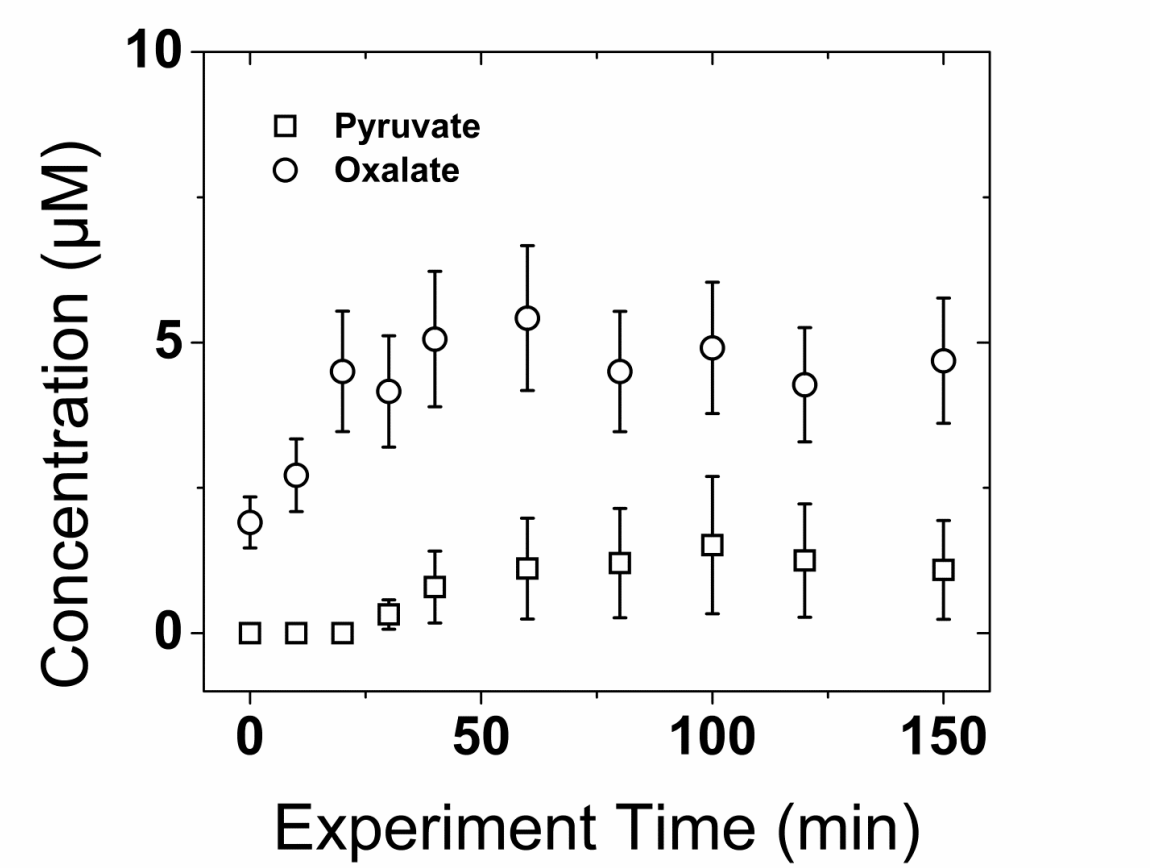

Figure 3-3. Shown here are precursor and intermediate trends for several positive ions detected during two replicate July 7th, 8th, 9th + OH experiments. Precursor ions (m/z+ 86, 130, 304) have abundances that start high and decrease with continued exposure to OH radicals whereas the signal for intermediates (m/z+ 118, 162) increase in the presence of OH radicals and proceed to degrade during our experiment time.

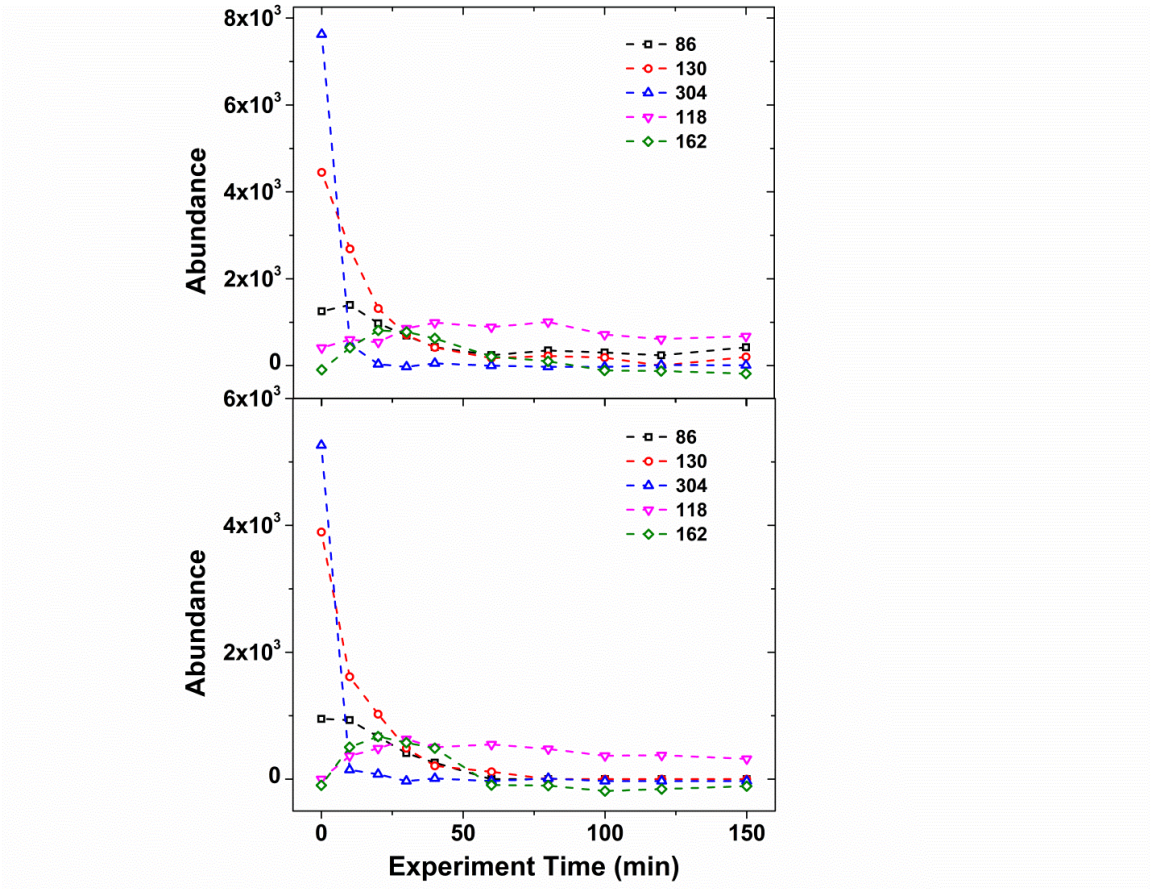

Figure 3-4. Shown here are ions detected in both June 19th and June 20th OH experiments in which these ions follow a trend characteristic of chemicals participating in aqueous processing. June 19th data are shown in the top panel with June 20th in the lower panel. Note that the abundances have been allowed to drop below zero to show some extent of the impact of subtracting detection limits from signals. Also note the starting abundances of these precursor ions are substantially lower than those discussed in greater detail throughout the paper.

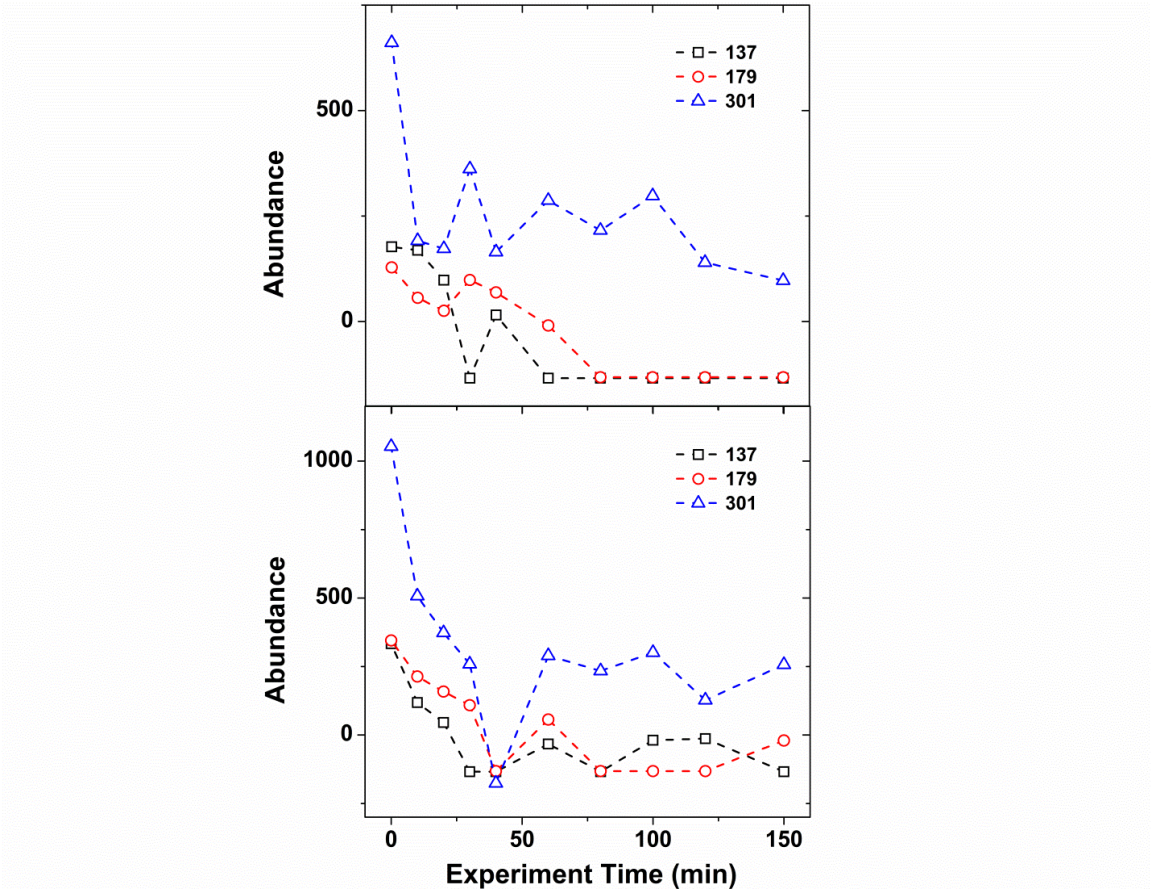

Figure 3-5. Shown here is the fragmentation mass spectrum for precursor ion m/z+ 130 revealing several daughter ions forming when fragmented with the IRMPD method. Amine structures provide the best representation of these exact masses shown here. The exact masses detected are compared to the exact masses of our suggested structures below.

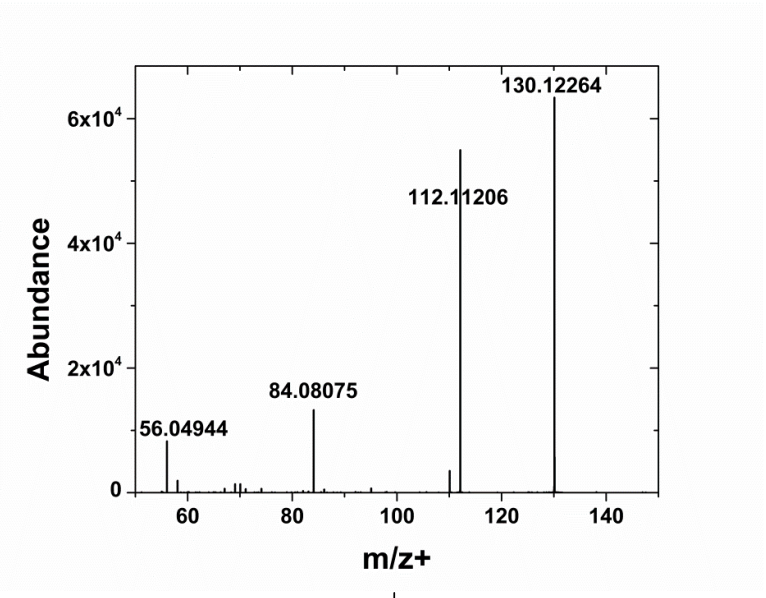

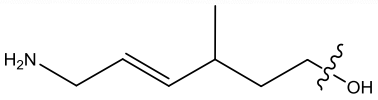

[M+H]+ = 130.12319

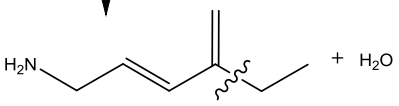

[M+H]+ = 112.11262

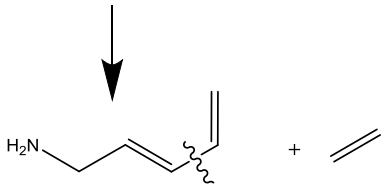

[M+H]+ = 84.08132

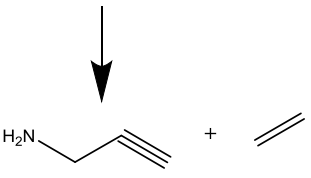

[M+H]+ = 56.05002

Table 3-1. Shown here are sample collection conditions for samples analyzed through experimentation. Included here are sample collection times (of day; T.O.D.) and durations (Mist Chamber; MC Operation Duration), outside temperature and relative humidity, ozone concentrations, Total Organic Carbon (TOC) and Total Dissolved Nitrogen (TDN), and experiments conducted (i.e., controls, replicates). (Note: Incomplete Data = Inc. and Not Applicable = N/A)

Collection Date	**Collection T.O.D.**	**T (°C) Range**	**RH (%) Range**	**O_3 (ppbv)**	**MC Operation Duration**	**TOC (µM-C)**	**TDN (µM-N)**	**Expts (Sample +…)**
June 19th	10am-6pm	24.8-41.0	66-26	65-100	2hr	87	92	OH, H_2O_2, UV
June 20th	10am-6pm	30.5-40.9	52-27	60-100	2hr	91	68	OH
June 25th	10am-6pm	30.6-37.4	47-30	50-85	4hr	98	48	OH
July 1st	5am-11am	20.1-34.2	82-39	50-90	2hr	83	82	OH, OH
July 4th, 5th, 6th	5am-9am	Inc.	Inc.	50-90	4hr	108	68	OH
July 5th, 6th	11am-3pm	Inc.	Inc.	50-90	4hr	108	54	OH
July 7th, 8th, 9th	5am-9am	Inc.	Inc.	50-85	4hr	107	101	OH, OH, H_2O_2, UV
Field Water	N/A	N/A	N/A	N/A	N/A	~3	~3	OH

Table 3-2. The exact masses detected with ultra-high resolution FTICR-MS are reported here with elemental formulas [M-H]+ assigned. These precursor ions and intermediate ions were detected during OH experiments with field samples from July 7th, 8th, 9th and unit mass detection shows these were common in all samples collected after July 3rd.

Exact mass (m/z+)	Elemental Formula [M-H]+	OH Experiment Trend
86.09640	C5H12N1	Precursor
118.12258	C6H16N1O1	Product/Intermediate
130.12260	C7H16N1O1	Precursor
162.11245	C7H16N1O3	Product/Intermediate
304.26378	C20H34N1O1	Precursor

Table 3-3. Amines structures provide the best representation of these exact masses shown here. The exact masses detected are compared to the exact masses of our suggested structures below.

Exact Fragment Mass (m/z+)	Amine Mass [M+H]+
130.12264	**130.12319**
112.11206	**112.11262**
84.08075	**84.08132**
56.04944	**56.04944**

Chapter 4. Characterization of organic precursors and products during aqueous hydroxyl radical oxidation of Po Valley, Italy and Fresno, CA fogs

Material in this chapter will be submitted with the following contributing authors:

Kirkland, J.R., Y.B. Lim, J.L. Collett, M.C. Facchini, and B.J. Turpin

4.1.Introduction

Laboratory experiments, field observations, and modeling studies provide ample evidence that chemistry in atmospheric waters plays an important and complex role in the global atmospheric system (Karamchandani and Venkatram, 1992; Ervens *et al.*, 2011; Herckes *et al.*, 2013). We call this aqueous processing. Aqueous processing alters particle mass concentration, composition, and behavior when low-volatility products remain in the particle phase after water evaporation (Blando and Turpin, 2000; Sareen *et al.*, 2010; Lin *et al.*, 2012; Henning *et al.*, 2014). Aqueous processing also provides a sink for gas phase species. For example, it is well known that SO_2 concentrations are effectively depleted in the presence of liquid water (Jacob et al 1967). And box modeling of aqueous aldehyde oxidation in fogs and intercepted clouds suggests that aqueous processing results in decreased gas-phase HO_2 concentrations (Ervens *et al.*, 2013). Because many water-soluble organics are more reactive in the aqueous phase than in the gas phase, atmospheric waters could also reduce gas phase concentrations of reactive organic gases. Thus, atmospheric aqueous chemistry has the potential to alter the concentrations of products (e.g. O_3) formed through gas phase photochemistry. Laboratory studies with simplified systems have been used to refine our understanding of aqueous processing and further our understanding of aqueous chemical mechanisms (e.g., Whiteaker and Prather, 2003; Carlton *et al.*, 2007; Herckes *et al.*, 2007; Collett Jr *et al.*,

2008; Shapiro *et al.*, 2009; Surratt *et al.*, 2010; Lin *et al.*, 2012). However, limited research explores aqueous chemistry in the complex mixtures found in atmospheric waters. Such studies aid the identification of potentially important precursors to and products of aqueous processing.

Radiation fogs form in the Central Valley of California and the Po Valley, Italy during winter months, capturing gases and particles from traffic emissions, industrial and agricultural processes, biomass burning, and gas-phase oxidation products. Subsequent aqueous processing during condensation-evaporation cycles in atmospheric waters creates a complex mixture of fresh and aged emissions in authentic fog waters. Fogs are a medium in which water-soluble gaseous and particulate compounds react, forming products with altered properties and behaviors. Chemical characterization of authentic atmospheric waters and water-soluble fractions of particles reveals complex mixtures of dissolved organic species. Herckes *et al.* (2013) review field observations of dissolved organic matter (DOM) in clouds and fogs around the world. The authors highlight DOM complexity and observe >50% of dissolved organic matter remains uncharacterized. Recent analysis of Fresno and Po Valley fogs with ultra-high resolution mass spectrometric methods attests to the complexity of DOM with varied functional groups and heteroatoms (Cappiello *et al.*, 2003; Herckes *et al.*, 2006; Mazzoleni *et al.*, 2010; LeClair *et al.*, 2012). Few studies have focused on oxidation of these mixtures and chemical characterization of the resulting DOM. Unlike most studies, which are conducted with single compounds or simple mixtures, Lee *et al.* (2012) photochemically oxidized filter extracts and cloud water from Whistler, British Columbia during the summertime 2010 and found organic aerosol is produced after re-aerosolization which

supports aqueous oxidation as a source of SOA. Ervens *et al.* (2013) used kinetic modeling of a small subset of selected species (i.e., aldehydes) to predict that aqueous processing impacts gas-phase oxidant concentrations (i.e., HO_2). Boris *et al.* (2014) explored aqueous photooxidation of pyruvate added to authentic cloud water to better understand the effects of the matrix of DOM on pyruvate oxidation. Extensive research is needed to develop chemical mechanisms for aqueous processing of known water-soluble atmospheric species and characterization of the remaining 50% of DOM. Specifically, identification and mechanistic understanding of reactive DOM species will improve our understanding of the impacts of aqueous processing on environmental systems.

The work reported herein is part of the continued effort to characterize dissolved organic matter in atmospheric waters and improve estimates of atmospheric impacts (i.e., aqSOA production, gas-phase organic budgets). For the first time we identify reactive species in the complex mixture of dissolved organic matter through controlled OH radical oxidation laboratory experiments with authentic fog waters from the Po Valley, Italy and Fresno, California. Since OH is the most important oxidant in atmospheric waters, DOM is the most important sink (Arakaki *et al.*, 2013) and fogs actively scavenge organic gases and particles (Collett Jr *et al.*, 2008), we expect that OH radical chemistry plays a central role in aqueous fog processing. Anastasio and McGregor (2001) report photoformation of OH ($[3.4\text{-}6.6]\times10^{-16}$ M) after solar spectrum exposure and attribute most OH formation to nitrite photolysis in California winter fog samples. Though not the focus of this research, non-radical chemistry also occurs in atmospheric waters (i.e., in aerosols and during droplet evaporation). This work makes use of fog samples collected in Fresno, CA

in January 2006 and the Po Valley, Italy in winter 2011-2012. Composited fog water samples were subjected to OH photooxidation to identify precursors and products of aqueous processing. Precursors are identified using unit mass and ultra-high resolution mass spectrometric techniques and products identified by unit mass spectrometry and quantified by ion chromatography. Precursors unique to each fog and common across fogs were characterized with high resolution mass spectrometry to illustrate chemical structures and elemental formulas of potentially important participants in aqueous processing.

4.2.Methods

4.2.1. Sample Collection

Fresno fog samples were collected as described previously by Mazzoleni *et al.* (2010). Briefly, a stainless steel Caltech Active Strand Cloudwater Collector (ss-CASCC) was deployed at the California State University experimental farm during January 2006. Cloud/fog droplets were collected by inertial impaction on stainless steel and collected in a pre-baked amber glass bottle. Insoluble particulate matter was removed with a pre-fired quartz fiber filter and fog samples stored in a refrigerator immediately after. The droplet size cut is approximately 6 µm (Herckes *et al.*, 2002). Several January 2006 fog samples (January 7th) were composited to conduct experiments and control experiments with the same water. A field water blank was saved in the field in January 2006 and stored as an authentic sample for quality assurance.

Po Valley fog samples were collected as described by Fuzzi *et al.* (1997). Briefly, an automated active string collector with Teflon and polyethylene components was deployed at the San Pietro Capofiume field site during the winter 2011/2012. Samples

accumulated in pre-baked glass bottles; filtered (pre-fired quartz fiber filters) fogwater samples were stored frozen after collection. Fuzzi *et al.* (1997) predicts the droplet cut point (i.e., 50% collection efficiency) is approximately a 3 μm radius. Several samples (November 27th, November 28th, December 3rd) from winter 2011 were composited and treated the same as Fresno samples. Sample characterization is summarized in Table 4-1.

4.2.2. Batch OH oxidation experiments in a cuvette chamber.

Aqueous OH photooxidation of authentic fog waters was explored (in duplicate) in a cuvette chamber described previously (Kirkland *et al.*, 2013) (See Appendix B.2.3-B.2.4 for cuvette chamber operation information). Briefly, ten cuvettes each containing 3 mL of fogwater are held equidistant from a UV lamp (254 nm; Heraeus Noblelight, Inc. Duluth, GA) and partially submerged in a water-bath for temperature control (25.0 $\pm$ 0.1 °C). The chamber is wrapped in aluminum foil to eliminate the presence of ambient light. OH radicals were continuously produced in situ through direct photolysis of H_2O_2 at a rate of $2.1x10^{-1}$ and $4.2x10^{-1}$ M [OH] s^{-1} for Fresno and Po Valley samples respectively. Fog + OH was conducted in duplicate for Fresno and PO Valley samples. To accomplish this, 750 μM and 1500 μM H_2O_2 were added to Fresno and Po Valley fogwater, respectively. (Note, determination of the photolysis rate constant is provide below.) We aimed to double the OH production rate for the Po Valley fogwater because total organic carbon (TOC) in this composite sample was roughly twice that of the Fresno composite. Cuvettes were removed 10, 20, 30, 40, 40, 60, 80, 100, 120, and 150 minutes after the start of UV illumination, initiating the experiment. A duplicate cuvette is removed at 40 min. An 11th cuvette was treated as a sample, but never placed in the cuvette chamber, this was the zero time point. Catalase was added to all cuvettes

immediately after removing them from the chamber to destroy any remaining H_2O_2 and prevent H_2O_2 reactions from occurring in samples awaiting analysis. For these experiments 75 µL of 1% and 2% catalase solution was used for Fresno and Po Valley experiments, respectively. Note we do not expect H_2O_2 reactions to be important in the chamber itself, since OH radical reactions are faster than H_2O_2 reactions (Tan *et al.*, 2010). However, control experiments were conducted, in part to examine this possibility (see below). Each cuvette served as a discrete sample for analysis with the techniques described below. Analyses were conducted within 24 hours. Sample was also stored frozen for 6 months for future analyses (high resolution MS).

The effective destruction of H_2O_2 by the catalase was verified before and after experiments by adding 750 and 1500 µM H_2O_2 and 75 µL 1% and 2% catalase to a mixed standard containing pyruvic, glyoxylic and oxalic acid (100 µM each). Note that, in the absence of more reactive oxidants, H_2O_2 is known to react rapidly with glyoxylic acid and slowly with pyruvic acid. Recoveries for pyruvate, glyoxalate and oxalate were 87-98%, suggesting that H_2O_2 was effectively quenched. Additional catalase test information is available in Appendix C.1.1.

Control experiments included: Fog + UV, Fog + H_2O_2, and Water Blank + OH. The following were conducted before and after OH experiments: H_2O_2 + UV and a catalase test. Control experiments (i.e., UV, H_2O_2) are used to confirm whether precursors and products identified during OH experiments were explicitly due to OH radical chemistry and not via photolysis or oxidation by H_2O_2. Water Blank + OH results were used to determine whether precursors or products identified during experiments

were the result of chemistry in the authentic fog water and not a result of the oxidation of contaminants in the field samplers.

H_2O_2 + UV results were used to determine the photon flux and photolysis rate constant for the experimental system. In authentic fog water OH is taken up from the gas phase and formed photochemically *in situ* (Anastasio and McGregor, 2001). In contrast, OH in these experiments was formed in the cuvettes through H_2O_2 photolysis. H_2O_2 concentrations as a function of time during H_2O_2 + UV experiments were monitored via UV spectrometry with the triiodide method (Klassen *et al.*, 1994). The H_2O_2 photolysis rate constant (k_1) of $1.0x10^{-4}$ s^{-1} was determined by fitting modeled to measured H_2O_2 concentrations in H_2O_2 + UV experiments using the reactions and rate constants provided in Appendix A.1.1. OH concentrations were approximately 10^{-12} M, estimated by assuming TOC in fog samples can be represented by GLY and using the GLY photooxidation model of Lim et al (2010). [When the initial H_2O_2 was 1500μM, these assumptions yield $[OH]_{initial} = 9.2x10^{-12}$ M, $[OH]_{average} = 8.4x10^{-12}$ M, and $[OH]_{final} = 7.9x10^{-12}$ M. When initial H_2O_2 was 750 μM, these assumptions yield $[OH]_{initial} = 8.7x10^{-12}$ M, $[OH]_{average} = 8.1x10^{-12}$ M, $[OH]_{final} = 7.8x10^{-12}$ M]. OH concentrations used in these experiments constitute a likely upper limit for OH concentrations in fogs. Reactions with dissolved organics in authentic fogs may reduce OH concentrations to 10^{-15} M (Arakaki *et al.*, 2013), unless aqueous phase photochemistry is a more substantial source of OH than currently recognized.

4.2.3. Analytical Methods

An aliquot of each fog sample was analyzed for total organic carbon (TOC; Shimadzu TOC 5000A, Shimadzu Corporation) and total dissolved nitrogen (TDN;

Antek PAC 7000B, Antek Instruments) prior to cuvette chamber experiments, as described by Altieri *et al.* (2009). TOC calibration was performed with potassium hydrogen phthalate solutions (detection limit: 2.08 µM-C) and TDN with urea and nitrate solutions (detection limit: 1.86 µM-N).

Discrete samples from cuvette chamber experiments were analyzed by ion chromatography for organic anion quantification (IC; Dionex ICS 3000; IonPac AS11-HC guard column; conductivity detector; 35 °C; milli-q water eluent; KOH gradient method to separate organic acids), and by electrospray ionization mass spectrometry for unit mass identification (HP – Agilent 1100; positive and negative modes) as described previously (Perri *et al.*, 2009; Tan *et al.*, 2009). A 1 mL aliquot of each discrete sample was stored frozen in a glass IC vial for later use. Both fog samples were analyzed by ultra-high resolution MS-MS (Thermo-Finnigan LTQ-XL: positive mode, Woods-Hole Oceanographic Institution Mass Spectrometry Facility; Ion Trap and Fourier Transform Ion Cyclotron Resonance optimized for each sample through use of Collision Induced Dissociation and Infrared Multi-Photon Dissociation fragmentation mechanisms).

Samples were analyzed by IC for organic anions and quantified with 5 point calibration curves developed by analysis of commercially available solutions (R^2>0.98; 6 µM – 1000 µM concentration range). Organic anion retention times are as follows: acetate (5.6 min), formate (6.2 min), pyruvate (7.1 min), glyoxylate (9.1 min), nitrate (16.2 min), succinate (19.4 min), tartarate (20.5 min), sulfate (22.5 min), oxalate (23.7 min). The IC was operated at 0.4 mL/min for 40 minutes per sample with 25 µL sample injections. Each IC sequence began and ended with the analysis of a water blank, mixed standard (containing all of the organic anions listed above), and an independent standard

(containing pyruvate and oxalate from a different supplier). Replicate analysis of 20% of samples was performed and used to calculate analytical precision (57% for oxalate and 78% for pyruvate). Quantification for each sequence is checked with mixed (100 µM) and independent (100 µM) standards (accepted within 15% of expected values, otherwise all samples and check standards in the run were reanalyzed). Ions listed above were either not detectable or present at concentrations below 1 µM in water blanks.

ESI-MS (+,-) (50-1000 amu) provided unit mass identification of ions present at each time point during experiments. Positive mode analysis detects positively charged adducts (molecular weight plus hydrogen or sodium, sometimes plus waters of hydration) while negative mode analysis detects negatively charge ions (molecular weight minus hydrogen). Each analysis involved 6 injections of 20 µL sample with 0.05% formic acid in water (positive mode) or a 50/50 mixture of 0.05% formic acid in water and methanol (negative mode) operated at a flow rate of 0.22 mL min^{-1}. Additional analytical details are described by Perri *et al.* (2009). Replicate analysis was performed on 20% of samples. For each detected ion, the 6 injections were averaged and the mean absorbance was reported if it was significantly greater than zero with 95% confidence intervals. Each ESI-MS sequence includes water and mixed standards at 5 concentrations levels from 12 - 200 µM in part to verify mass assignment (negative mode: standards listed above plus nitrobenzoic acid; positive mode standards: glyoxal, methylglyoxal, glycolaldehyde, plus caffeine).

The following criteria were used to identify species that were present in the fogwater sample and reactive with respect to OH radicals (i.e., precursors): Precursors are identified through ESI-MS(+) analysis. Precursor criteria are as follows: 1) Ion

abundance > 750 in the unreacted (t = 0) fogwater sample, replicate and control experiments, 2) a reproducible decrease in the ion abundance in the presence of OH in replicate experiments, 3) constant abundance during control experiments (Fog + H_2O_2, Fog + UV), and 4) initial signal is above detection limits (i.e., greater than the mean + 3 standard deviations of the water blank abundance and greater than the Field Water + OH signal). Note the same criteria are used to identify products produced from OH radicals during experiments, with the following changes: 1) Ion abundance is less in the unreacted (t=0) fogwater sample, replicate, and control experiments, 2) a reproducible increase, 3) no abundance or lesser abundance during control experiments, and 4) detected signals (after t = 0) above detection limits.

Precursor ions identified in this way were also analyzed by ultra-high resolution FT ICR MS-MS. MS-MS was conducted in the positive mode only (+) since we expect precursors to aqueous processing to be detected in the positive mode (e.g., aldehydes, amines, alcohols) and the results reported herein support this claim. A syringe pump delivered analyte (50% methanol; 50% sample) into the spray chamber at 4 µL min^{-1} with a capillary temperature of 260 °C and spray voltage 3.8-4.2 kV. Target masses were isolated (isolation width: m/z = 1-2 amu) and fragmentation was optimized for each target mass through CID or IRMPD at 100 k resolution. Exact masses were assigned elemental formulas with Midas molecular formula calculator (v1.1) allowing all combinations of C, H, O, N, S, and Na within 1 ppm error of the positive ion. All parent ions and all fragments with greater than 5% relative signal were assigned elemental formulas. If no elemental formula was assigned within 1 ppm error, the exact mass was

not considered. Each parent ion was then compared to fragments through the identification of lost neutral masses (e.g., H_2O, CO_2, C_2H_4).

4.3.Results and Discussion

4.3.1. Dissolved organic matter in Po Valley and Fresno fogs

Chemical characterization of Po Valley and Fresno fogs (ESI-MS+) demonstrates the complexity of atmospheric dissolved organic matter. Complex DOM has been reported for past analysis of Fresno fog water samples by LeClair *et al.* (2012) and Mazzoleni *et al.* (2010). The complex matrix of DOM is presented in Figure 4-1a for Fresno samples used in this study. DOM characterization has also been reported for Po Valley fogs by Gilardoni *et al.* (2014) and Fuzzi *et al.* (2002); our characterization is shown in Figure 4-1b. Po Valley and California fogs are among the most studied. Several decades of research document relationships between chemical changes in fog water composition and changes in meteorology or physical properties (i.e., droplet size, altitude of formation, temporal variability, etc.; (Herckes *et al.*, 2013) and references therein). The experiments and analysis performed here demonstrate that the fogwater composition undergoes substantive changes with the addition of OH radicals, as seen by ESI-MS(+) spectra for Po Valley and Fresno fogs at times, t = 0, 20, and 150 minutes of OH radical exposure (Figure 4.1).

4.3.2. Products of OH oxidation in Po Valley and Fresno fogs

Oxalate and pyruvate formed during all experiments with authentic fog samples in the presence of OH radicals (Figure 4-2a-d), but not in the absence of OH radicals (i.e., Fog + UV, Fog + H_2O_2). Oxalate production in the field water + OH control experiments was detectable, but small in comparison to production in fog water samples (i.e., 5.8 µM

in Fresno field water and 2.7 μM in Po Valley field water); pyruvate formation was not detected in these control experiments. Oxalate in control experiments is provided in Appendices C.1.2-C.1.8. Recent laboratory experiments have demonstrated oxalate and/or pyruvate production during aqueous processing of several water-soluble organic compounds (e.g., glyoxal, methylglyoxal, glycolaldehyde, acetic acid) (Altieri *et al.*, 2008; Tan *et al.*, 2009; Ortiz-Montalvo *et al.*, 2012). Atmospheric aerosol measurements document that these species remain mostly in the particle phase after droplet evaporation. This suggests that they are present as salts or complexes, which have vapor pressures that are substantially lower than those of organic acids (Ortiz-Montalvo *et al.*, 2013). Oxalate is the most abundant dicarboxylic acid found in atmospheric particles (Saxena and Hildemann, 1996; Kawamura *et al.*, 2003) and recent evidence suggests this is attributed to in-cloud formation mechanisms, making oxalate a globally important species and tracer for aqueous cloud chemistry (Myriokefalitakis *et al.*, 2011). Detection of oxalate and other carboxylic acids in atmospheric waters influenced by diverse biogenic and anthropogenic emission sources (e.g., continental, marine, rural, and urban samples) has been documented for several decades (e.g., Chebbi and Carlier, 1996). Further evidence for oxalate formation through aqueous processing comes from aircraft observations that reveal enhanced oxalate above clouds compared to below clouds (Sorooshian *et al.*, 2006; Sorooshian *et al.*, 2007) and the addition of OH radicals to a water-soluble gases scrubbed ambient air using mist chambers (Chapter 3). Oxalate and pyruvate production in these authentic fog samples are direct evidence for atmospheric aqueous processing of water-soluble organics and SOAaq formation.

4.3.3. Selected precursors in Po Valley and Fresno

Several reactive species were identified in Po Valley and Fresno fog + OH experiments, some in common and some unique to each fog sample (Table 4-2). We observed that precursors were predominantly found in the positive mode and products in the negative mode. Ions presented in Table 4-2 include positive and negative mode ESI-MS analysis. Positive mode analysis includes ions that meet precursor criteria for either fog samples. Negative mode analysis includes ions identified as products according to the above criteria with the exception of one ion identified as a precursor in the Po Valley sample. We expect positive mode analysis to detect ions with carbonyl, aldehyde, amine, and alcohol functional groups since these functional groups readily accept a positive charge (e.g., hydrogen, sodium adducts). Negative mode analysis detects ions with carboxylic, nitrate, and sulfate functional groups since these compounds will readily lose a proton resulting in a negative charge. The temporal evolution of precursor ions that best fit the criteria specified in methods are shown in Figure 4-3. The absorbances of these ions decrease with time in fog+OH and replicate fog+OH experiments and have a steady (unchanging) signal during control experiments (Sample + H_2O_2, Sample + UV). Positive mode unit mass ions exhibiting precursor-like trends (i.e., listed in Figure 4-3) were analyzed by ultra-high resolution FTICR-MS, trapped and fragmented (fragmentation spectra and structural interpretations are available in Appendices C.1.9-C.1.18). These precursor ions are m/z+ 83, 113, 153, 167, 169, 183, 185 in Po Valley fogs and m/z+ 143, 167, 169, 183, 185 in Fresno fogs. Note that these ions were identified with unit mass resolution ESI-MS during laboratory experiments and high resolution mass spectrometry reveals greater insight into elemental formulas for these precursor ions.

Exact masses of the selected unit mass ions are listed in Table 4-3; O:C versus H:C (van Krevelen plot) and N:C versus O:C relationships are provided in Figure 4-4; and possible structures are shown in Table 4.4. In all cases more than one ion (at exact mass) was identified with the same unit mass. Not all of these compounds were present and oxidized by OH radicals, but at least one compound at each unit mass was responsible for the precursor-like trends shown in Figure 4-3. For the most part, the structures in Table 4.4 are unsaturated hydrocarbons with (hydrated) carbonyl or hydroxyl functionalities. Most are larger that C_6 and may have undergone 1-3 oxidation steps. Oxygen-to-carbon ratios were not particularly high (O:C < 0.6). Many exact masses appear to be structurally related, containing aliphatic carbon chains of differing lengths with one or more double bond equivalent (DBE) for OH radical addition (Figure 4-4). Note the slopes in Figure 4-4 are in good agreement with slopes in the van Krevelen plot of the entire mass spectrum (m/z- 100-400) for Fresno fogs presented in Mazzoleni *et al.* (2010).

The complexity of dissolved organic matter in these fog samples is consistent with the findings of LeClair *et al.* (2012) and Mazzoleni *et al.* (2010), who characterized fog samples from the same Fresno, CA field campaign. The DOM in the Po Valley winter fog samples presented here is more complex than the Po Valley summer mist chamber samples discussed in Chapter 3. This is not surprising since naturally occurring fog waters capture water-soluble gases *and* particles, whereas mist chambers explicitly capture water-soluble gases (particles were removed upstream). Additionally, summer versus winter samples likely contribute to different molecular weight-constituents. A large number of the elemental formulas assigned to these exact masses are common in Po

Valley and Fresno fogs. Elemental formulas not detected in 2010, but present in this report may be due to ion affinities in positive and negative modes. That is, common elemental formulas were determined by assigning a neutral mass to the ions detected with the addition or removal of a single hydrogen atom since Mazzoleni *et al.* (2010) performed negative mode (m/z-) analysis and we report positive mode (m/z+) analysis. Common elemental formulas are present in Po Valley and 2010 analysis of Fresno fogs. Some of these elemental formulas are common across all three analyses (Fresno 2010, Fresno here, Po Valley here) and some are unique to Fresno 2010 and Po Valley fogs (Table 4-3). Note that all common elemental formulas between past Fresno analysis and these results are explicitly CHO species. This may suggest variability in aqueous processing of heteroatoms (N, S) or ubiquity in sources of oxidized hydrocarbons. Common structural characteristics include an unsaturated carbon backbone with hydroxyl and carbonyl groups present. Low O:C ratios suggest these species will not be highly water-soluble. However, the presence of oxygenated functional groups will create some affinity for the aqueous phase. This may indicate that these precursors are less likely to diffuse into the bulk cloud water droplet compared to small polar compounds (e.g., C2-C3 aldehydes) and may have a stronger presence at the surface of droplets and thus, this chemistry may be largely dependent on droplet size (Hoag *et al.*, 1999). Interestingly, only one elemental formula in each fog sample (PV and CA) matches an elemental formula detected by Altieri *et al.* (2009) in New Jersey rainwater. A lack of common elemental formulas between rainwater and fogs at different locations may be due to different local and regional emission sources or chemistry or vertical distributions or seasons or scavenging mechanisms.

Fragmentation patterns from MS-MS suggest highly unsaturated structures for the reactive compounds identified in Po Valley and Fresno fogs; nitrogen-containing compounds were more prevalent in Po Valley samples. Multiple parent ions are present in isolation spectra for aqueous processing precursor ions. The difference between elemental formulas assigned to parent ions and fragments were calculated and compared to neutral losses of H_2O, CO_2, C_2H_4, CH_4O, NH_3, CH_3NH_2, $(CH_3)_2NH$, CH_2NH, CH_3CHNH, combinations of these, and subsequent neutral losses of these units. Table 4-4 provides a list of parent ions susceptible to fragmentation and plausible structures to explain the observed neutral losses. Note that the only common elemental formula with detectable fragments between fogs is $C_{10}H_{15}O_2$ and the fragmentation patterns are not the same. OH radical chemistry will progress with sufficient OH until all carbon chains are reduced to basic structures (e.g., CO_2). Thus, small (C_1-C_2) carboxylic acids (e.g., formic, acetic acids) and aldehydes (e.g., formaldehyde, acetaldehyde, glyoxal) are abundant in atmospheric waters. Fragmentation data provide insight into structural characteristics of parent ions. These structural characteristics might highlight the plausibility of OH radical reactions. Note fog samples from the Central Valley in California are representative of urban fogs polluted by emissions from residential and industrial sources as described by Mazzoleni *et al.* (2010) and fog samples from the Po Valley in Italy are representative of fogs polluted by industrial and agricultural emissions (Cappiello *et al.*, 2003). We expect and demonstrate that these fogs have common chemical characteristics.

4.4.Conclusions and Atmospheric Implications

This work demonstrates that aqueous processing in authentic wintertime fog waters collected in the Po Valley, Italy and Fresno, California substantially changes dissolved organic matter. Unit mass ions are identified as precursors to aqueous processing and are most prevalent in positive mode ESI-MS analysis which suggests these structures contain ketone, carbonyl, or hydroxyl functional groups. High resolution analysis of precursor ions shows multiple (exact mass) ions are present at a single unit mass. Elemental formulas assigned to precursor (exact) masses include polyols and nitrogen-containing compounds. We expect aqueous uptake to decrease gas concentrations of these species. The extent to which gas-phase chemistry is altered by this process is yet unknown. In addition, the formation of some particle phase species (e.g., oxalate) suggests the potential for fog chemistry to produce aqueous SOA. Finally, oxidation in the aqueous phase can serve to fragment or functionalize these compounds. Fragmentation of dissolved organic particulate matter can lead to a decrease in organic particulate matter after fog droplet evaporation. Thus, there are several potential implications of fog chemistry. Identification of reactive organic precursors is a first step toward more in depth investigation of the importance of these various effects.

This work demonstrates, through experiments with real fogwaters, that fog processing has the potential to transform atmospheric organic compounds. In the mist chamber experiments presented in Chapter 3, only water-soluble gases were present, whereas in the fog water analyses performed in Chapter 4, dissolved organic particulate matter and gases were present and potentially being attacked. Oxidation can lead to functionalization or fragmentation and can increase or decrease the volatility of the materials. Identified precursors of OH radical oxidation of Po Valley an Fresno fog

water were too large to be volatile organics. These compounds appear to be semi-volatile or of intermediate volatility, and are likely to be found in both the gas and particle phase in the atmosphere. Aqueous oxidation could add oxygen and/or fragment these compounds.

4.5.References

Altieri, K.E., S.P. Seitzinger, A.G. Carlton, B.J. Turpin, G.C. Klein and A.G. Marshall, 2008. Oligomers formed through in-cloud methylglyoxal reactions: Chemical composition, properties, and mechanisms investigated by ultra-high resolution ft-icr mass spectrometry. Atmospheric Environment, 42(7): 1476-1490. Available from http://www.sciencedirect.com/science/article/pii/S1352231007010205. DOI http://dx.doi.org/10.1016/j.atmosenv.2007.11.015.

Altieri, K.E., B.J. Turpin and S.P. Seitzinger, 2009. Oligomers, organosulfates, and nitrooxy organosulfates in rainwater identified by ultra-high resolution electrospray ionization ft-icr mass spectrometry. Atmos. Chem. Phys., 9(7): 2533-2542. Available from http://www.atmos-chem-phys.net/9/2533/2009/. DOI 10.5194/acp-9-2533-2009.

Anastasio, C. and K.G. McGregor, 2001. Chemistry of fog waters in california's central valley: 1. In situ photoformation of hydroxyl radical and singlet molecular oxygen. Atmospheric Environment, 35(6): 1079-1089. Available from http://www.sciencedirect.com/science/article/pii/S1352231000002818. DOI http://dx.doi.org/10.1016/S1352-2310(00)00281-8.

Arakaki, T., C. Anastasio, Y. Kuroki, H. Nakajima, K. Okada, Y. Kotani, D. Handa, S. Azechi, T. Kimura, A. Tsuhako and Y. Miyagi, 2013. A general scavenging rate constant for reaction of hydroxyl radical with organic carbon in atmospheric waters. Environmental Science & Technology, 47(15): 8196-8203. Available from http://dx.doi.org/10.1021/es401927b [Accessed 2014/03/28]. DOI 10.1021/es401927b.

Blando, J.D. and B.J. Turpin, 2000. Secondary organic aerosol formation in cloud and fog droplets: A literature evaluation of plausibility. Atmospheric Environment, 34(10): 1623-1632. Available from http://www.sciencedirect.com/science/article/pii/S1352231099003921. DOI http://dx.doi.org/10.1016/S1352-2310(99)00392-1.

Boris, A.J., Y. Desyaterik and J.L. Collett Jr, 2014. How do components of real cloud water affect aqueous pyruvate oxidation? Atmospheric Research, 143(0): 95-106. Available from http://www.sciencedirect.com/science/article/pii/S0169809514000829. DOI http://dx.doi.org/10.1016/j.atmosres.2014.02.004.

Cappiello, A., E. De Simoni, C. Fiorucci, F. Mangani, P. Palma, H. Trufelli, S. Decesari, M. Facchini and S. Fuzzi, 2003. Molecular characterization of the water-soluble organic compounds in fogwater by esims/ms. Environmental science & technology, 37(7): 1229-1240.

Carlton, A.G., B.J. Turpin, K.E. Altieri, S. Seitzinger, A. Reff, H.-J. Lim and B. Ervens, 2007. Atmospheric oxalic acid and soa production from glyoxal: Results of

aqueous photooxidation experiments. Atmospheric Environment, 41(35): 7588-7602. Available from http://www.sciencedirect.com/science/article/pii/S1352231007004979. DOI http://dx.doi.org/10.1016/j.atmosenv.2007.05.035.

Chebbi, A. and P. Carlier, 1996. Carboxylic acids in the troposphere, occurrence, sources, and sinks: A review. Atmospheric Environment, 30(24): 4233-4249. Available from http://www.sciencedirect.com/science/article/pii/1352231096001021. DOI http://dx.doi.org/10.1016/1352-2310(96)00102-1.

Collett Jr, J.L., P. Herckes, S. Youngster and T. Lee, 2008. Processing of atmospheric organic matter by california radiation fogs. Atmospheric Research, 87(3–4): 232-241. Available from http://www.sciencedirect.com/science/article/pii/S0169809507002025. DOI http://dx.doi.org/10.1016/j.atmosres.2007.11.005.

Ervens, B., B.J. Turpin and R.J. Weber, 2011. Secondary organic aerosol formation in cloud droplets and aqueous particles (aqsoa): A review of laboratory, field and model studies. Atmos. Chem. Phys., 11(21): 11069-11102. Available from http://www.atmos-chem-phys.net/11/11069/2011/. DOI 10.5194/acp-11-11069-2011.

Ervens, B., Y. Wang, J. Eagar, W.R. Leaitch, A.M. Macdonald, K.T. Valsaraj and P. Herckes, 2013. Dissolved organic carbon (doc) and select aldehydes in cloud and fog water: The role of the aqueous phase in impacting trace gas budgets. Atmos. Chem. Phys., 13(10): 5117-5135. Available from http://www.atmos-chem-phys.net/13/5117/2013/. DOI 10.5194/acp-13-5117-2013.

Fuzzi, S., M.C. Facchini, S. Decesari, E. Matta and M. Mircea, 2002. Soluble organic compounds in fog and cloud droplets: What have we learned over the past few years? Atmospheric Research, 64(1): 89-98.

Fuzzi, S., G. Orsi, G. Bonforte, B. Zardini and P.L. Franchini, 1997. An automated fog water collector suitable for deposition networks: Design, operation and field tests. Water Air Soil Pollut, 93(1-4): 383-394.

Gilardoni, S., P. Massoli, L. Giulianelli, M. Rinaldi, M. Paglione, F. Pollini, C. Lanconelli, V. Poluzzi, S. Carbone, R. Hillamo, L.M. Russell, M.C. Facchini and S. Fuzzi, 2014. Fog scavenging of organic and inorganic aerosol in the po valley. Atmos. Chem. Phys. Discuss., 14(4): 4787-4826. Available from http://www.atmos-chem-phys-discuss.net/14/4787/2014/. DOI 10.5194/acpd-14-4787-2014.

Henning, S., K. Dieckmann, K. Ignatius, M. Schäfer, P. Zedler, E. Harris, B. Sinha, D. van Pinxteren, S. Mertes, W. Birmili, M. Merkel, Z. Wu, A. Wiedensohler, H. Wex, H. Herrmann and F. Stratmann, 2014. Influence of cloud processing on ccn

activation behaviour in the thuringian forest, germany during hcct-2010. Atmos. Chem. Phys. Discuss., 14(2): 1617-1645. Available from http://www.atmos-chem-phys-discuss.net/14/1617/2014/. DOI 10.5194/acpd-14-1617-2014.

Herckes, P., H. Chang, T. Lee and J. Collett, Jr., 2007. Air pollution processing by radiation fogs. Water Air Soil Pollut, 181(1-4): 65-75. Available from http://dx.doi.org/10.1007/s11270-006-9276-x. DOI 10.1007/s11270-006-9276-x.

Herckes, P., T. Lee, L. Trenary, G. Kang, H. Chang and J.L. Collett, 2002. Organic matter in central california radiation fogs. Environmental Science & Technology, 36(22): 4777-4782. Available from http://dx.doi.org/10.1021/es025889t [Accessed 2014/03/29]. DOI 10.1021/es025889t.

Herckes, P., J.A. Leenheer and J.L. Collett, 2006. Comprehensive characterization of atmospheric organic matter in fresno, california fog water. Environmental Science & Technology, 41(2): 393-399. Available from http://dx.doi.org/10.1021/es0607988 [Accessed 2014/03/28]. DOI 10.1021/es0607988.

Herckes, P., K.T. Valsaraj and J.L. Collett Jr, 2013. A review of observations of organic matter in fogs and clouds: Origin, processing and fate. Atmospheric Research, 132–133(0): 434-449. Available from http://www.sciencedirect.com/science/article/pii/S016980951300183X [Accessed 2013/11//]. DOI http://dx.doi.org/10.1016/j.atmosres.2013.06.005.

Hoag, K.J., J.J.L. Collett and S.N. Pandis, 1999. The influence of drop size-dependent fog chemistry on aerosol processing by san joaquin valley fogs. Atmospheric Environment, 33(29): 4817-4832. Available from http://www.sciencedirect.com/science/article/pii/S135223109900268X. DOI http://dx.doi.org/10.1016/S1352-2310(99)00268-X.

Karamchandani, P. and A. Venkatram, 1992. The role of non-precipitating clouds in producing ambient sulfate during summer: Results from simulations with the acid deposition and oxidant model (adom). Atmospheric Environment. Part A. General Topics, 26(6): 1041-1052. Available from http://www.sciencedirect.com/science/article/pii/096016869290036K. DOI http://dx.doi.org/10.1016/0960-1686(92)90036-K.

Kawamura, K., N. Umemoto, M. Mochida, T. Bertram, S. Howell and B.J. Huebert, 2003. Water-soluble dicarboxylic acids in the tropospheric aerosols collected over east asia and western north pacific by ace-asia c-130 aircraft. Journal of Geophysical Research: Atmospheres, 108(D23): 8639. Available from http://dx.doi.org/10.1029/2002JD003256. DOI 10.1029/2002JD003256.

Kirkland, J.R., Y.B. Lim, Y. Tan, K.E. Altieri and B.J. Turpin, 2013. Glyoxal secondary organic aerosol chemistry: Effects of dilute nitrate and ammonium and support for

organic radical–radical oligomer formation. Environmental Chemistry, 10(3): 158-166. Available from http://www.publish.csiro.au/paper/EN13074. DOI http://dx.doi.org/10.1071/EN13074.

Klassen, N.V., D. Marchington and H.C.E. McGowan, 1994. H2o2 determination by the i3- method and by kmno4 titration. Analytical Chemistry, 66(18): 2921-2925. Available from http://dx.doi.org/10.1021/ac00090a020 [Accessed 2014/01/10]. DOI 10.1021/ac00090a020.

LeClair, J.P., J.L. Collett and L.R. Mazzoleni, 2012. Fragmentation analysis of water-soluble atmospheric organic matter using ultrahigh-resolution ft-icr mass spectrometry. Environmental science & technology, 46(8): 4312-4322.

Lee, A.K.Y., K.L. Hayden, P. Herckes, W.R. Leaitch, J. Liggio, A.M. Macdonald and J.P.D. Abbatt, 2012. Characterization of aerosol and cloud water at a mountain site during wacs 2010: Secondary organic aerosol formation through oxidative cloud processing. Atmos. Chem. Phys., 12(15): 7103-7116. Available from http://www.atmos-chem-phys.net/12/7103/2012/. DOI 10.5194/acp-12-7103-2012.

Lin, G., J.E. Penner, S. Sillman, D. Taraborrelli and J. Lelieveld, 2012. Global modeling of soa formation from dicarbonyls, epoxides, organic nitrates and peroxides. Atmos. Chem. Phys., 12(10): 4743-4774. Available from http://www.atmos-chem-phys.net/12/4743/2012/. DOI 10.5194/acp-12-4743-2012.

Mazzoleni, L.R., B.M. Ehrmann, X. Shen, A.G. Marshall and J.L. Collett, 2010. Water-soluble atmospheric organic matter in fog: Exact masses and chemical formula identification by ultrahigh-resolution fourier transform ion cyclotron resonance mass spectrometry. Environmental Science & Technology, 44(10): 3690-3697. Available from http://dx.doi.org/10.1021/es903409k [Accessed 2014/01/10]. DOI 10.1021/es903409k.

Myriokefalitakis, S., K. Tsigaridis, N. Mihalopoulos, J. Sciare, A. Nenes, K. Kawamura, A. Segers and M. Kanakidou, 2011. In-cloud oxalate formation in the global troposphere: A 3-d modeling study. Atmos. Chem. Phys., 11(12): 5761-5782. Available from http://www.atmos-chem-phys.net/11/5761/2011/. DOI 10.5194/acp-11-5761-2011.

Ortiz-Montalvo, D.L., S.A.K. Häkkinen, A.N. Schwier, Y.B. Lim, V.F. McNeill and B.J. Turpin, 2013. Ammonium addition (and aerosol ph) has a dramatic impact on the volatility and yield of glyoxal secondary organic aerosol. Environmental Science & Technology, 48(1): 255-262. Available from http://pubs.acs.org/doi/abs/10.1021/es4035667 [Accessed 2014/03/23]. DOI 10.1021/es4035667.

Ortiz-Montalvo, D.L., Y.B. Lim, M.J. Perri, S.P. Seitzinger and B.J. Turpin, 2012. Volatility and yield of glycolaldehyde soa formed through aqueous photochemistry and droplet evaporation. Aerosol Science and Technology, 46(9): 1002-1014. Available from http://dx.doi.org/10.1080/02786826.2012.686676 [Accessed 2014/01/10]. DOI 10.1080/02786826.2012.686676.

Perri, M.J., S. Seitzinger and B.J. Turpin, 2009. Secondary organic aerosol production from aqueous photooxidation of glycolaldehyde: Laboratory experiments. Atmospheric Environment, 43(8): 1487-1497. Available from http://www.sciencedirect.com/science/article/pii/S1352231008011096. DOI http://dx.doi.org/10.1016/j.atmosenv.2008.11.037.

Sareen, N., A.N. Schwier, E.L. Shapiro, D. Mitroo and V.F. McNeill, 2010. Secondary organic material formed by methylglyoxal in aqueous aerosol mimics. Atmos. Chem. Phys., 10(3): 997-1016. Available from http://www.atmos-chem-phys.net/10/997/2010/. DOI 10.5194/acp-10-997-2010.

Saxena, P. and L. Hildemann, 1996. Water-soluble organics in atmospheric particles: A critical review of the literature and application of thermodynamics to identify candidate compounds. Journal of Atmospheric Chemistry, 24(1): 57-109. Available from http://dx.doi.org/10.1007/BF00053823. DOI 10.1007/BF00053823.

Shapiro, E.L., J. Szprengiel, N. Sareen, C.N. Jen, M.R. Giordano and V.F. McNeill, 2009. Light-absorbing secondary organic material formed by glyoxal in aqueous aerosol mimics. Atmos. Chem. Phys., 9(7): 2289-2300. Available from http://www.atmos-chem-phys.net/9/2289/2009/. DOI 10.5194/acp-9-2289-2009.

Sorooshian, A., M.-L. Lu, F.J. Brechtel, H. Jonsson, G. Feingold, R.C. Flagan and J.H. Seinfeld, 2007. On the source of organic acid aerosol layers above clouds. Environmental Science & Technology, 41(13): 4647-4654. Available from http://dx.doi.org/10.1021/es0630442 [Accessed 2014/03/31]. DOI 10.1021/es0630442.

Sorooshian, A., V. Varutbangkul, F.J. Brechtel, B. Ervens, G. Feingold, R. Bahreini, S.M. Murphy, J.S. Holloway, E.L. Atlas, G. Buzorius, H. Jonsson, R.C. Flagan and J.H. Seinfeld, 2006. Oxalic acid in clear and cloudy atmospheres: Analysis of data from international consortium for atmospheric research on transport and transformation 2004. Journal of Geophysical Research: Atmospheres, 111(D23): D23S45. Available from http://dx.doi.org/10.1029/2005JD006880. DOI 10.1029/2005JD006880.

Surratt, J.D., A.W.H. Chan, N.C. Eddingsaas, M. Chan, C.L. Loza, A.J. Kwan, S.P. Hersey, R.C. Flagan, P.O. Wennberg and J.H. Seinfeld, 2010. Reactive intermediates revealed in secondary organic aerosol formation from isoprene. Proceedings of the National Academy of Sciences, 107(15): 6640-6645. Available

from http://www.pnas.org/content/107/15/6640.abstract. DOI 10.1073/pnas.0911114107.

Tan, Y., A.G. Carlton, S.P. Seitzinger and B.J. Turpin, 2010. Soa from methylglyoxal in clouds and wet aerosols: Measurement and prediction of key products. Atmospheric Environment, 44(39): 5218-5226. Available from http://www.sciencedirect.com/science/article/pii/S1352231010007399. DOI http://dx.doi.org/10.1016/j.atmosenv.2010.08.045.

Tan, Y., M.J. Perri, S.P. Seitzinger and B.J. Turpin, 2009. Effects of precursor concentration and acidic sulfate in aqueous glyoxal−oh radical oxidation and implications for secondary organic aerosol. Environmental Science & Technology, 43(21): 8105-8112. Available from http://dx.doi.org/10.1021/es901742f [Accessed 2014/01/10]. DOI 10.1021/es901742f.

Whiteaker, J.R. and K.A. Prather, 2003. Hydroxymethanesulfonate as a tracer for fog processing of individual aerosol particles. Atmospheric Environment, 37(8): 1033-1043. Available from http://www.sciencedirect.com/science/article/pii/S1352231002010294. DOI http://dx.doi.org/10.1016/S1352-2310(02)01029-4.

Figure 4-1. Positive ESI unit mass spectra of (a) CA and (b) PV Fog plus OH radicals at t = 0, 20, and 150 minutes into the experiment. The addition of OH radicals to authentic fog water causes substantive chemical changes to the composition. No subtractions are performed for these spectra. Note that the presence of a strong nitrate signal may suppress ionization in the negative mode, reducing the number of peaks. Negative mode spectra are shown for (c) CA and (d) PV fogs.

(a)

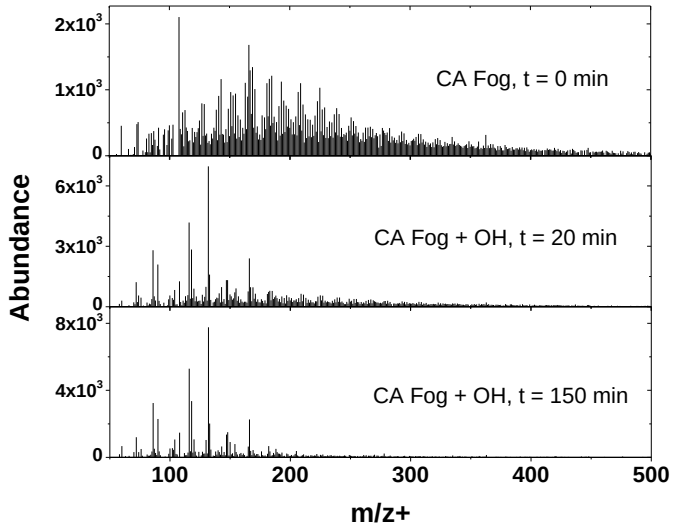

(b)

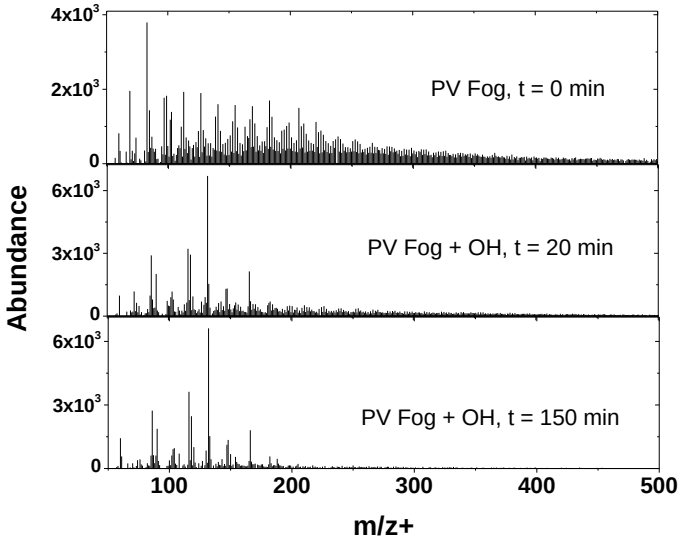

(c)

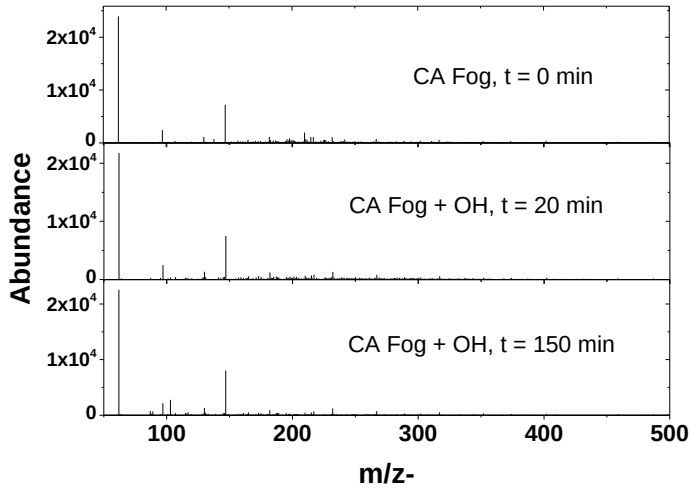
CA Fog, t = 0 min
CA Fog + OH, t = 20 min
CA Fog + OH, t = 150 min
Abundance
m/z-
2x10^4
1x10^4
0
100
200
300
400
500

(d)

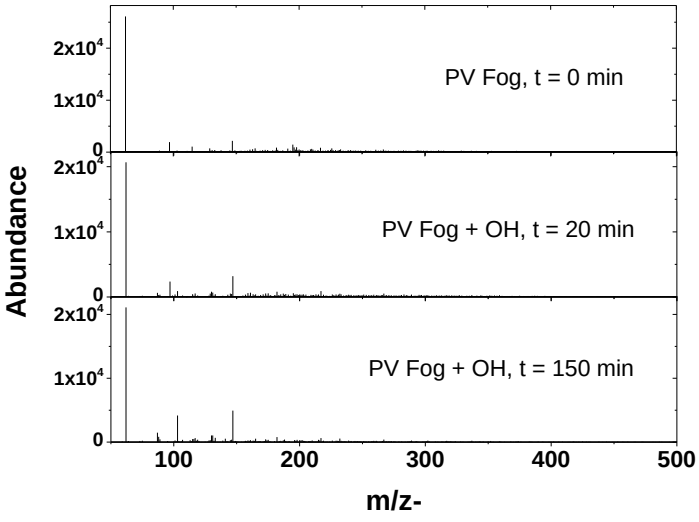
PV Fog, t = 0 min
PV Fog + OH, t = 20 min
PV Fog + OH, t = 150 min
Abundance
m/z-
2x10^4
1x10^4
0
100
200
300
400
500

Figure 4-2. Oxalate and pyruvate production during OH experiments with Fresno and Po Valley fogs: (a) Pyruvate production in replicate Fresno + OH experiments, (b) Oxalate production in replicate Fresno + OH experiments and oxalate formed during a control experiment (Field Water + OH), (c) Pyruvate production in replicate Po Valley + OH experiments, and (d) Oxalate production during replicate Po Valley + OH experiments and oxalate formed during a control experiment (Field Water + OH).

a. Pyruvate formation in Fresno + OH.

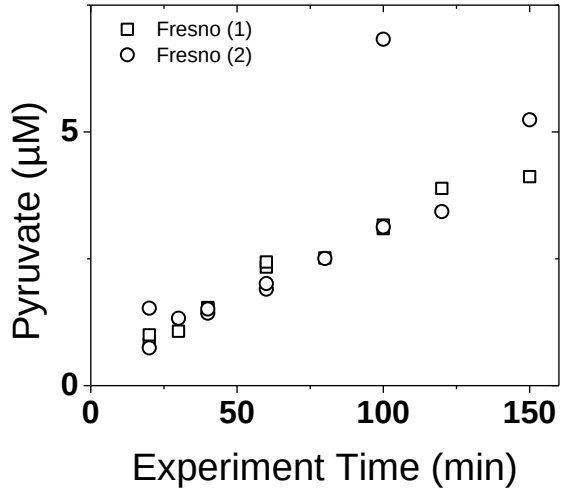

b. Oxalate formation in Fresno + OH.

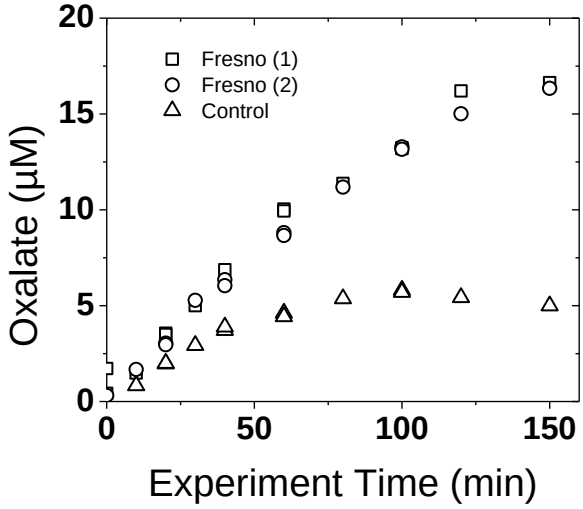

c. Pyruvate formation in Po Valley + OH.

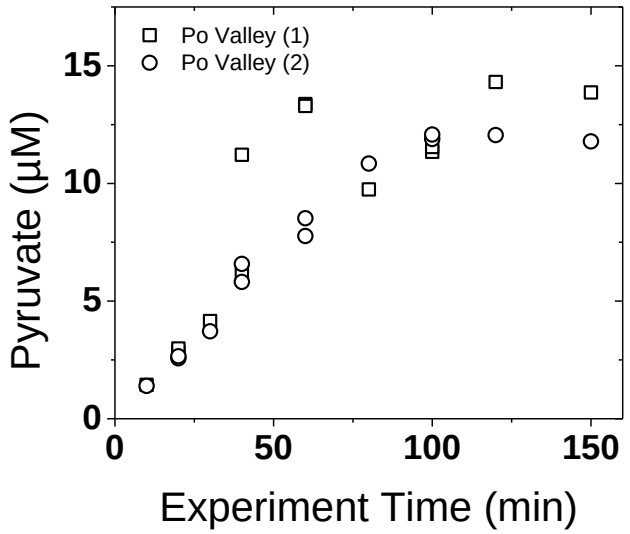

d. Oxalate formation during Po Valley + OH.

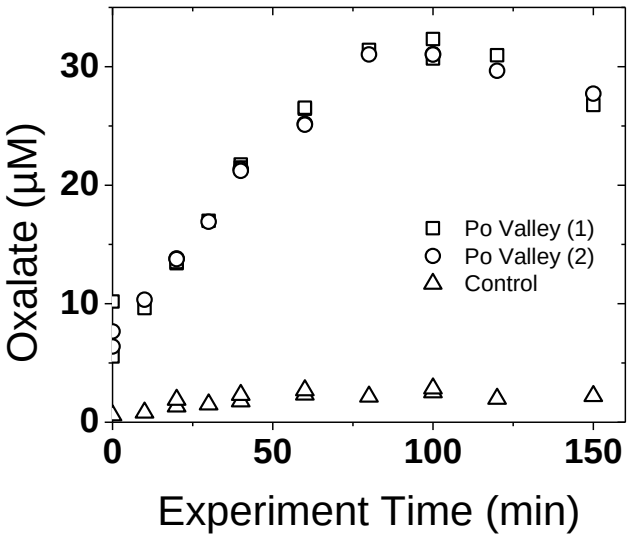

Figure 4-3. Several positive mode ions showing a precursor trend during Fog + OH experiments for (a) Fresno and (b) Po Valley samples.

a. Fresno Precursor Ions (m/z+)

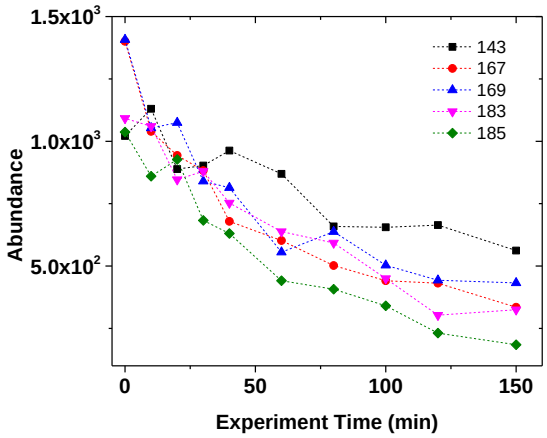

b. Po Valley Precursor Ions (m/z+)

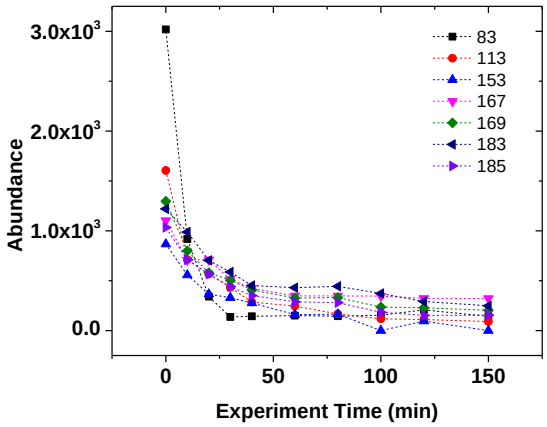

Figure 4-4. van Krevelen plots of exact masses detected with ultra-high resolution FTICR-MS and listed in Table 4.3. These unit mass ions exhibited a precursor trend (Table 4.2). Diagonal lines suggest an elemental relationship between these compounds differing by CH_2 in Po Valley and Fresno samples and are in good agreement with prior analysis of Fresno fog performed by LeClair *et al.* (2012). Additional information about nitrogen containing exact masses is shown.

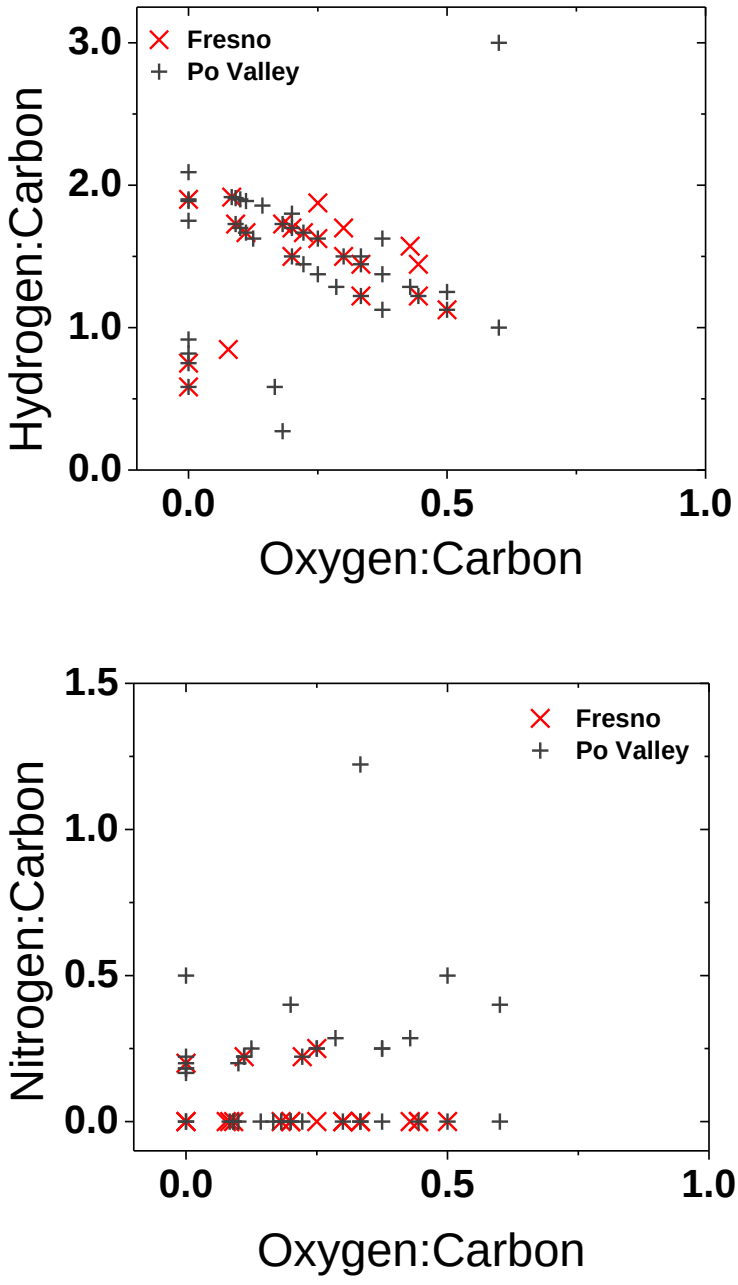

Table 4-1. Characteristics of Fresno and Po Valley fog samples used for OH radical experiments. Characteristic data includes total organic carbon (TOC), total dissolved nitrogen (TDN), pH, nitrate, and sulfate.

Fog Sample	TOC (µM-C)	TDN (µM-N)	pH	NO_3^- (µM)	SO_4^{-3} (µM)
Fresno, CA	607	1622	6.4	551	54
Po Valley, IT	1208	1620	6.4	481	67

Table 4-2. Ions of Interest: Positive and Negative mode Precursors and Products. The ions shown here meet the precursor or product criteria specified in methods. Ions in the positive mode table shown here are identified as precursors with no ions meeting product criteria. Ions in the negative mode table are ions identified as products with one ion meeting precursor criteria in Po Valley fog (noted in parentheses).

Fresno (m/z+)	Po Valley (m/z+)
	83
	99
	113
	127
	139
143	
	153
	155
163	
167	**167**
169	**169**
	171
183	**183**
185	**185**
	207
	221

Fresno (m/z-)	Po Valley (m/z-)
	87
103	**103**
	115 (Precursor)
	117
	131

Table 4-3. Exact masses detected by ultra-high resolution FTICR-MS that correspond to unit mass ions meeting precursor criteria during OH experiments (see Table 4.2). Note that often several exact masses correspond to a single identified unit mass; at least one but not necessarily all of these are actual precursors. Also shown are elemental formulas assigned to exact masses, double bond equivalents (DBE), and notes about detection of these elemental formulas by others (in prior Fresno, CA fog analysis = Mazzoleni et al 2010 identified with "X" or New Jersey rainwater = Altieri et al 2009 identified with "#" or in both fog samples analyzed here, identified with "**β**") or the availability of fragmentation data (*).

Fresno Fog Parent Ion Exact Masses and Elemental Formulas				**Mazz 2010 = X Altieri 2009 = # Po Valley = β Fragments = ***
Class	**m/z+**	**[M+H]+**	**DBE**	**Detected Elsewhere**
CHO	143.07025	$C_7H_{11}O_3$	3	*X #
	143.10663	$C_8H_{15}O_2$	2	*X
	167.07025	$C_9H_{11}O_3$	5	X **β**
	167.10664	$C_{10}H_{15}O_2$	4	***β**
	167.14302	$C_{11}H_{19}O$	3	**β**
	169.04958	$C_8H_9O_4$	5	X **β**
	169.08592	$C_9H_{13}O_3$	4	*X **β**
	169.12232	$C_{10}H_{17}O_2$	3	***β**
	183.06522	$C_9H_{11}O_4$	5	X **β**
	183.08047	$C_{13}H_{11}O$	9	
	183.10158	$C_{10}H_{15}O_3$	4	*X **β**
	183.13798	$C_{11}H_{19}O_2$	3	*X **β**
	183.17435	$C_{12}H_{23}O$	2	**β**
	185.04469	$C_8H_9O_5$	5	X
	185.08088	$C_9H_{13}O_4$	4	*X
	185.11725	$C_{10}H_{17}O_3$	3	*X
CHON	167.11787	$C_9H_{15}N_2O$	4	**β**
	169.09714	$C_8H_{13}N_2O_2$	4	**β**
	183.11282	$C_9H_{15}N_2O_2$	4	**β**
CHN	167.15426	$C_{10}H_{19}N_2$	3	**β**
CHS	183.02642	$C_{12}H_7S$	10	**β**
	185.04205	$C_{12}H_9S$	9	**β**
Po Valley Fog Parent Ion Exact Masses and Elemental Formulas				**Mazz 2010 = X Altieri 2009 = # Fresno = β**
Class	**m/z+**	**[M+H]+**	**DBE**	

CHO	113.02328	$C_5H_5O_3$	4	
	113.05967	$C_6H_9O_2$	3	
	113.09605	$C_7H_{13}O$	2	*
	153.05461	$C_8H_9O_3$	5	X #
	153.09099	$C_9H_{13}O_2$	4	
	153.12738	$C_{10}H_{17}O$	3	*
	167.01278	$C_{11}H_3O_2$	11	
	167.07026	$C_9H_{11}O_3$	5	X **β**
	167.10665	$C_{10}H_{15}O_2$	4	***β**
	167.14303	$C_{11}H_{19}O$	3	**β**
	169.04957	$C_8H_9O_4$	5	X **β**
	169.08592	$C_9H_{13}O_3$	4	X **β**
	169.12231	$C_{10}H_{17}O_2$	3	**β**
	169.15869	$C_{11}H_{21}O$	2	*
	183.04409	$C_{12}H_7O_2$	10	
	183.06521	$C_9H_{11}O_4$	5	X **β**
	183.10158	$C_{10}H_{15}O_3$	4	*X **β**
	183.13797	$C_{11}H_{19}O_2$	3	X **β**
	183.17435	$C_{12}H_{23}O$	2	**β**
CHON	113.03452	$C_4H_5N_2O_2$	4	
	113.0709	$C_5H_9N_2O$	3	*
	153.06584	$C_7H_9N_2O_2$	5	*
	153.10222	$C_8H_{13}N_2O$	4	*
	167.08149	$C_8H_{11}N_2O_2$	5	*
	167.11788	$C_9H_{15}N_2O$	4	**β**
	169.06076	$C_7H_9N_2O_3$	5	*
	169.09714	$C_8H_{13}N_2O_2$	4	***β**
	169.13353	$C_9H_{17}N_2O$	3	*
	183.07642	$C_8H_{11}N_2O_3$	5	
	183.11281	$C_9H_{15}N_2O_2$	4	***β**
	183.1492	$C_{10}H_{19}N_2O$	3	
	185.09211	$C_8H_{13}N_2O_3$	4	*
CHONS	183.07987	$C_5H_{15}N_2O_3S$	0	
CHN	83.06034	$C_4H_7N_2$	3	*
	153.13861	$C_9H_{17}N_2$	3	
	167.15426	$C_{10}H_{19}N_2$	3	**β**
	169.07601	$C_{11}H_9N_2$	9	
	183.09169	$C_{12}H_{11}N_2$	9	
	183.18559	$C_{11}H_{23}N_2$	2	
CHS	183.02641	$C_{12}H_7S$	10	**β**
	185.04205	$C_{12}H_9S$	9	**β**

Table 4-4. Structures derived from exact masses and fragmentation data. Structures were assigned using elemental formulas [M-H]+, DBE, and fragments detected by ultra-high resolution MS-MS. Note that these structures contain the appropriate functional groups and elemental composition, yet exact structures may differ. Note that the absence of N-containing fragments may suggest that these nitrogen-containing functional groups are not terminal in the molecular structure.

Fresno Fog Parent Ion Exact Masses and Elemental Formulas				
Class	**m/z+**	**[M+H]+**	**DBE**	**Neutral Parent Structure**
CHO	143.07025	$C_7H_{11}O_3$	3	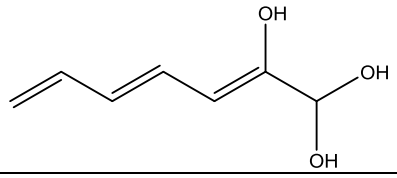
	143.10663	$C_8H_{15}O_2$	2	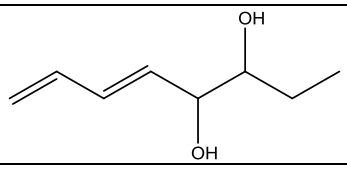
	167.10664	$C_{10}H_{15}O_2$	4	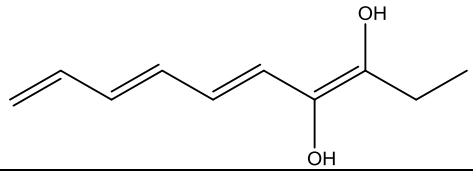
	169.08592	$C_9H_{13}O_3$	4	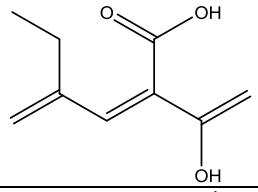
	169.12232	$C_{10}H_{17}O_2$	3	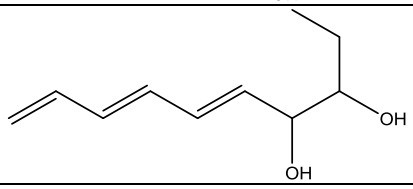
	183.10158	$C_{10}H_{15}O_3$	4	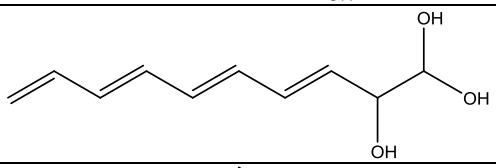
	183.13798	$C_{11}H_{19}O_2$	3	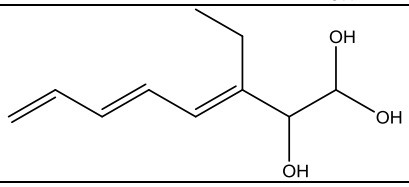

	185.08088	$C_9H_{13}O_4$	4	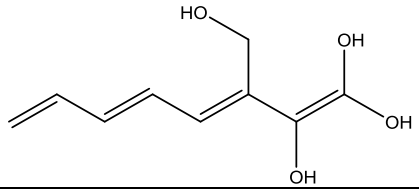
	185.11725	$C_{10}H_{17}O_3$	3	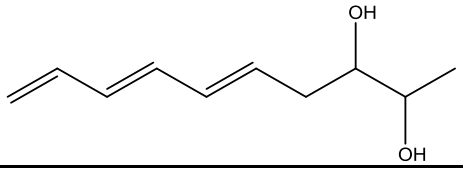

Po Valley Fog Parent Ion Exact Masses and Elemental Formulas				
Class	**m/z+**	**[M+H]+**	**DBE**	**Neutral Parent Structure**
CHO	113.09605	$C_7H_{13}O$	2	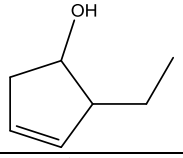
	153.12738	$C_{10}H_{17}O$	3	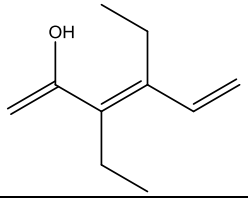
	167.10665	$C_{10}H_{15}O_2$	4	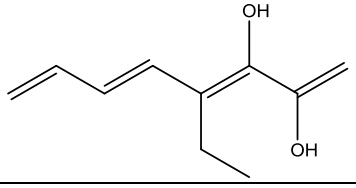
	169.15869	$C_{11}H_{21}O$	2	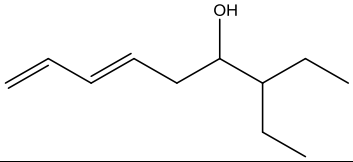
	183.10158	$C_{10}H_{15}O_3$	4	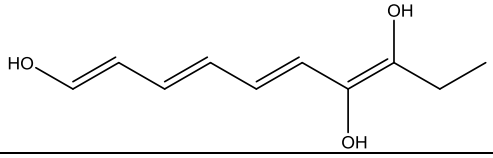
CHON	113.0709	$C_5H_9N_2O$	3	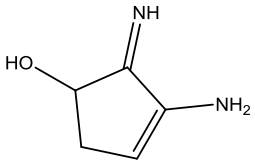

	153.06584	$C_7H_9N_2O_2$	5	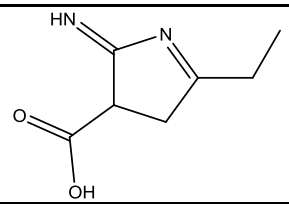
	153.10222	$C_8H_{13}N_2O$	4	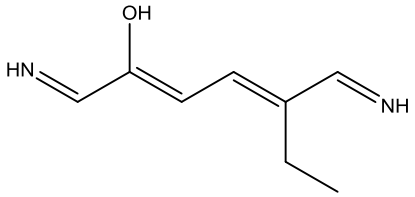
	167.08149	$C_8H_{11}N_2O_2$	5	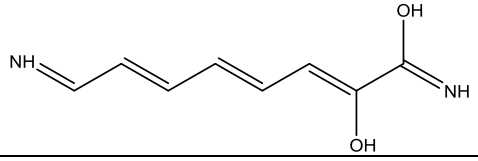
	169.06076	$C_7H_9N_2O_3$	5	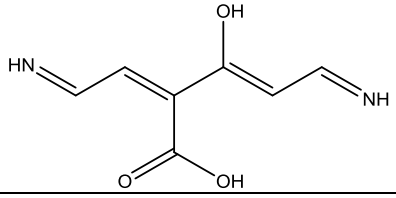
	169.09714	$C_8H_{13}N_2O_2$	4	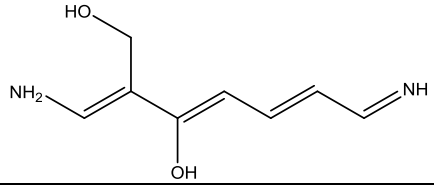
	169.13353	$C_9H_{17}N_2O$	3	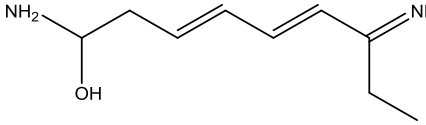
	183.11281	$C_9H_{15}N_2O_2$	4	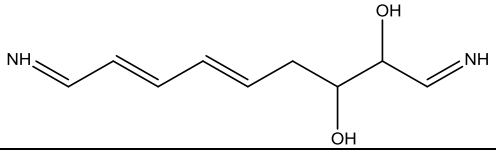
	185.09211	$C_8H_{13}N_2O_3$	4	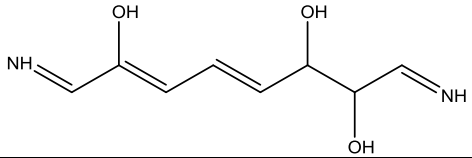
CHN	83.06034	$C_4H_7N_2$	3	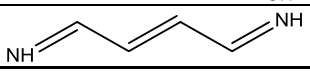

Chapter 5. Implications and Future Directions

5.1.Summary

This dissertation reports advancements in understanding aqueous processing of dissolved organic matter in atmospheric waters. Atmospheric waters provide a medium for a complex system of interactions between water-soluble gases (e.g., SO_2, oxidants, organics, NH_4^+), secondary aqueous reaction products (e.g., SO_4^{2-}, oligomers, organosulfates) and particulate matter (soluble and insoluble). Extracting new information from complex ambient mixtures is integral to advancing our field. This dissertation identifies classes of compounds that are present in the ambient atmosphere and become oxidized when exposed to OH radicals in aqueous solution.

Specifically, this dissertation demonstrates robust glyoxal chemistry in the presence of cloud-relevant concentrations of inorganic nitrogen (NH_4^+ and NO_3^-; Chapter 2), providing further validation for the dilute chemical mechanism documented previously (Lim *et al.*, 2005; Tan *et al.*, 2009). Through OH radical oxidation experiments conducted with authentic fogs and with ambient mixtures of gases, we identify amines and polyols (summer, Po Valley, Italy; Chapter 3), other reduced nitrogen-containing organics and unsaturated aliphatic chains with carbonyl or hydroxyl functionality (winter, Po Valley, Italy and Fresno, California; Chapter 4) as precursors to aqueous processing. As a single body of research, these findings suggest complex temporal variability in aqueous processing influenced by local and regional gas and particle emissions. This dissertation consistently demonstrates production of particle phase components (e.g., oxalate) in all experiments conducted in the presence, but not the absence, of OH radicals. It identifies hitherto uncharacterized participants in aqueous

processing which may be important single precursors for future laboratory studies. Below I place this body of work in the context of related studies and highlight emerging knowledge gaps that warrant attention.

5.2.Implications

Experiments conducted with glyoxal in the presence and absence of nitric acid and ammonium sulfate (Chapter 2)(Kirkland *et al.*, 2013) provide validation that inorganic nitrogen species which are ubiquitous in the atmosphere and can impact chemistry in wet aerosols, have little impact on glyoxal plus OH radical chemistry at cloud/fog-relevant concentrations. Glyoxal is a water-soluble gas-phase reaction product of isoprene and aromatics (Yeung *et al.*, 2005; Guenther *et al.*, 2006). It is also found in the marine environment (Wittrock *et al.*, 2006; Rinaldi *et al.*, 2011). Thus it is ubiquitous, at least during summertime (Fu *et al.*, 2008). Aqueous glyoxal oxidation is known to produce oxalate (Carlton *et al.*, 2007). Since oxalate is predominantly found in the particle phase in the atmosphere (Limbeck *et al.*, 2001; Laongsri and Harrison, 2013), probably as a salt or metal complex (Ortiz-Montalvo *et al.*, 2013), oxalate is aqSOA. Organic nitrates are known to form through gas phase photochemistry (Gong *et al.*, 2005; Lim and Ziemann, 2005). I hypothesized that organic nitrogen also forms through aqueous photochemistry of glyoxal in the presence of inorganic nitrogen species, and that this process contributes to the abundance of organic nitrogen detected in particles and wet deposition (Zhang and Anastasio, 2003; Altieri *et al.*, 2009). Though organic nitrogen was not detected during these experiments, others have shown that light-absorbing organic nitrogen can form from reactions involving ammonium or amines during droplet evaporation and at the high nitrogen concentrations relevant to wet aerosols (Sareen *et*

al., 2010; Nguyen *et al.*, 2012). Additionally, it is possible that organic nitrates could form through aqueous reactions in which NO_3 radicals are formed in the absence of OH radicals, though NO_3 sources may be scarce (Mack and Bolton, 1999; Herrmann *et al.*, 2000). In our experiments, the reactions with OH radicals effectively outcompeted any potential aqueous NO_3 radical chemistry.

This set of experiments advances our knowledge of glyoxal chemistry. These experiments provide critical evidence (i.e., tartarate production) for an organic radical-radical oligomer formation mechanism proposed by Lim *et al.* (2010). This radical-radical mechanism has little impact on product formation in clouds and fogs, but dominates glyoxal oxidation chemistry at the higher concentrations of dissolved organics found in wet aerosols (1-10M). Oxalate is the dominant product of bulk phase glyoxal photooxidation for millimolar and lower organic concentrations. Our oxalate quantification is well captured by the model with nitrogen chemistry included.

Aqueous oxidation experiments conducted with water-soluble gases scrubbed from the ambient air (Po Valley, Italy; Chapter 3) were used to identify reactive precursors to- and products of- aqueous processing. To our knowledge, this is the first time an ambient matrix of water-soluble gases has been captured and its aqueous chemistry explored through OH radical oxidation experiments. Oxalate and pyruvate production during these experiments provides evidence for aqueous SOA formation in real atmospheric waters. This verified, for the first time, that oxalate and pyruvate are produced through OH radical oxidation of an ambient mix of water-soluble gases. Previous experiments investigated the oxidation of single organic precursors (e.g., Carlton *et al.*, 2007; Shapiro *et al.*, 2009; Ervens and Volkamer, 2010; Nozière *et al.*,

2010; Sun *et al.*, 2010). One publication now reports on the oxidation of pyruvic acid in authentic cloud water to discern organic matrix effects and finds slightly slowed pyruvate degradation in cloud water compared to pyruvic acid oxidation alone (Boris *et al.*, 2014). In the work described herein (Chapter 3), precursors were predominantly detected by positive mode electrospray ionization mass spectrometry, suggesting that they were carbonyl compounds, organic peroxides, amines, or alcohols. Previous laboratory experiments have been conducted with individual aldehydes (e.g., glyoxal, methylglyoxal, glycolaldehyde) (Carlton *et al.*, 2007; Altieri *et al.*, 2009; Perri *et al.*, 2009).

Samples collected across the field campaign revealed two distinct sampling periods. Early in the campaign ions exhibiting precursor-like trends had only moderate absorbances and were odd masses. The latter half of the sampling period revealed even ion precursors, specifically amines. Reduced nitrogen functional groups (e.g., imidazoles) have been shown to form during chamber experiments with glyoxal and ammonium sulfate seed at high concentrations relevant to wet aerosols (Galloway *et al.*, 2009) and also form (e.g., imines) in aqueous aerosol mimics (Noziere *et al.*, 2008; Nozière *et al.*, 2010). Laboratory evidence that reduced nitrogen (e.g., amines, ammonium) undergoes further reaction during droplet evaporation is provided by De Haan *et al.* (2009). This and the results in chapter 3 demonstrate that nitrogen-containing organics are not only present in atmospheric waters, which is well documented (Herckes *et al.*, 2013), but they also undergo reactions in that medium. Others have documented the formation of oligomers from amines and aldehydes in evaporating droplets.

A limitation of the current work is the lack of information regarding the relative ESI-MS sensitivity for the compounds making up these ambient mixtures. One implication of this is that we cannot know for sure whether glyoxal and methylglyoxal were not present or not detected because other compounds may have been more readily ionized.

In Chapter 4, experiments conducted with authentic fog waters from the Po Valley, Italy and Fresno, California were used to identify precursors to aqueous processing during wintertime. Oxalate and pyruvate formation during these experiments provide evidence for aqueous SOA formation obtained through controlled experiments with authentic fog waters which agrees with oxidation experiments with Chinese cloud water (Boris *et al.*, 2014). This result is consistent with concurrent fog water analysis in Shanghai during which oxalate was detected throughout 28 fog events (Bian *et al.*, 2014). The strong presence of amine (e.g., CHON+) structures in the Po Valley winter fog samples and summer mist chamber samples and their depletion during OH radical experiments, provide evidence that amines participate in aqueous processing throughout the year. Fresno, CA fogs also included masses that are likely amines. However, the compounds detected in Fresno, CA and Po Valley, Italy have different masses.

It should be noted that, in this work only the most abundant species exhibiting dramatic decreases with exposure to OH radicals were characterized via ultra high-resolution mass spectrometry. A limitation of this research is the use of MS abundance to categorize importance. Since the MS is not fully quantitative, a better understanding of the effect of the matrix on the ionization of individual species would be helpful to identifying the most important aqueous precursors more definitively. These results

contribute to the growing pool of characterized dissolved organic matter in atmospheric waters.

All experiments in this dissertation in the presence of OH radicals demonstrate oxalate production through aqueous processing of: 1) laboratory simulations of atmospheric waters (Chapter 2), 2) surrogate fog waters (Chapter 3), and 3) authentic fog waters (Chapter 4). The work in this dissertation provides support for recent findings linking particulate oxalate measurements with in cloud production mechanisms (Myriokefalitakis *et al.*, 2011). For example, one recent report identifies that cloud processed oxalate is the dominant source of oxalate measured in $PM_{2.5}$ at a rural site in China during warm and cold seasons (Bian *et al.*, 2014) and Tsai and Kuo (2013) demonstrate oxalate is one of the dominant carboxylic acids in fog water, rainwater, and $PM_{2.5}$ in a forest in Taiwan. Oxalate is most often detected in the particle phase (Limbeck *et al.*, 2001) and aqueous processing helps explain abundant oxalate above clouds (Sorooshian *et al.*, 2006; Sorooshian *et al.*, 2007).

This dissertation provides insight into precursors to and products of aqueous processing in real atmospheric waters. It identifies types of compounds whose aqueous chemistry warrants further study because of their potential to form aqueous SOA and because aqueous chemistry reduces their gas phase concentrations. The research presented here contributes to an improved understanding of aqueous processes which can be used to 1) link ambient measurements with primary emissions to develop effective air quality management policy and 2) quantify environmental impacts (e.g., climate, ecological health, formation of light-absorbing material).

Some of the limitations throughout this research may help identify important areas of future research and analytical needs. Quantification of glyoxal and other aldehydes throughout experiments will aid future laboratory studies and field campaigns. Chapters 3 and 4 improve upon this limitation through qualitative evaluation of precursors. Our expected precursors (e.g., glyoxal) do not exhibit the strong presence and precursor trends we hypothesized during mist chamber and fog water photooxidation. However, MS signal trends provide insight into ions participating in aqueous processing; precursors and products. In Chapter 3, low starting TOC values result in MS signals that approach detection limits. This is partially due to the mixture of organic matter present in natural samples with no single, dominant precursor. Furthermore, the strongest ion signal may not participate in aqueous processing. An advantageous improvement upon these experiments is to develop a pseudo-calibration which relates ion abundance to precursor concentration. This is a challenging relationship to understand since ionization efficiency in the electrospray chamber is dependent on the presence of other species. Hence the relationship between laboratory-generated standards and precursor signals in our natural samples would be confined to 'pseudo-calibration'. Precursor ions identified in Chapter 4 come from authentic samples with substantially higher TOC values and resulting MS signals. This research identifies plausible parent ions and categorizes compound classes (i.e., CHO+, CHON+) potentially responsible for the unit mass trends observed. Further photooxidation experiments with single precursor standards could be used to verify parent ions, or families of ions that contribute to the precursor trends detected during OH experiments and to developing a mechanistic understanding of the aqueous chemistry and product formation for these compounds. To my knowledge, the methods and selection

criteria discussed are the best current approach to address our intended science question: what are potentially important precursors to – and products of aqueous processing in real atmospheric waters? As these results and concurrent research (e.g., field campaigns: PEGASOS, SOAS, GOAmazon) become available we expect to encounter an exciting time during which we can develop a more complete and vivid picture of atmospheric chemistry.

5.3.References

Altieri, K.E., B.J. Turpin and S.P. Seitzinger, 2009. Oligomers, organosulfates, and nitrooxy organosulfates in rainwater identified by ultra-high resolution electrospray ionization ft-icr mass spectrometry. Atmos. Chem. Phys., 9(7): 2533-2542. Available from http://www.atmos-chem-phys.net/9/2533/2009/. DOI 10.5194/acp-9-2533-2009.

Bian, Q., X.H.H. Huang and J.Z. Yu, 2014. One-year observations of size distribution characteristics of major aerosol constituents at a coastal receptor site in hong kong – part 1: Inorganic ions and oxalate. Atmos. Chem. Phys. Discuss., 14(2): 1443-1480. Available from http://www.atmos-chem-phys-discuss.net/14/1443/2014/. DOI 10.5194/acpd-14-1443-2014.

Boris, A.J., Y. Desyaterik and J.L. Collett Jr, 2014. How do components of real cloud water affect aqueous pyruvate oxidation? Atmospheric Research, 143(0): 95-106. Available from http://www.sciencedirect.com/science/article/pii/S0169809514000829. DOI http://dx.doi.org/10.1016/j.atmosres.2014.02.004.

Carlton, A.G., B.J. Turpin, K.E. Altieri, S. Seitzinger, A. Reff, H.-J. Lim and B. Ervens, 2007. Atmospheric oxalic acid and soa production from glyoxal: Results of aqueous photooxidation experiments. Atmospheric Environment, 41(35): 7588-7602. Available from http://www.sciencedirect.com/science/article/pii/S1352231007004979. DOI http://dx.doi.org/10.1016/j.atmosenv.2007.05.035.

De Haan, D.O., A.L. Corrigan, K.W. Smith, D.R. Stroik, J.J. Turley, F.E. Lee, M.A. Tolbert, J.L. Jimenez, K.E. Cordova and G.R. Ferrell, 2009. Secondary organic aerosol-forming reactions of glyoxal with amino acids. Environmental Science & Technology, 43(8): 2818-2824. Available from http://dx.doi.org/10.1021/es803534f [Accessed 2014/01/10]. DOI 10.1021/es803534f.

Ervens, B. and R. Volkamer, 2010. Glyoxal processing by aerosol multiphase chemistry: Towards a kinetic modeling framework of secondary organic aerosol formation in aqueous particles. Atmospheric Chemistry and Physics, 10(17): 8219-8244.

Fu, T.-M., D.J. Jacob, F. Wittrock, J.P. Burrows, M. Vrekoussis and D.K. Henze, 2008. Global budgets of atmospheric glyoxal and methylglyoxal, and implications for formation of secondary organic aerosols. Journal of Geophysical Research: Atmospheres, 113(D15): D15303. Available from http://dx.doi.org/10.1029/2007JD009505. DOI 10.1029/2007JD009505.

Galloway, M.M., P.S. Chhabra, A.W.H. Chan, J.D. Surratt, R.C. Flagan, J.H. Seinfeld and F.N. Keutsch, 2009. Glyoxal uptake on ammonium sulphate seed aerosol:

Reaction products and reversibility of uptake under dark and irradiated conditions. Atmos. Chem. Phys., 9(10): 3331-3345. Available from http://www.atmos-chem-phys.net/9/3331/2009/. DOI 10.5194/acp-9-3331-2009.

Gong, H., A. Matsunaga and P.J. Ziemann, 2005. Products and mechanism of secondary organic aerosol formation from reactions of linear alkenes with no3 radicals. The Journal of Physical Chemistry A, 109(19): 4312-4324. Available from http://dx.doi.org/10.1021/jp058024l [Accessed 2014/01/10]. DOI 10.1021/jp058024l.

Guenther, A., T. Karl, P. Harley, C. Wiedinmyer, P.I. Palmer and C. Geron, 2006. Estimates of global terrestrial isoprene emissions using megan (model of emissions of gases and aerosols from nature). Atmos. Chem. Phys., 6(11): 3181-3210. Available from http://www.atmos-chem-phys.net/6/3181/2006/. DOI 10.5194/acp-6-3181-2006.

Herckes, P., K.T. Valsaraj and J.L. Collett Jr, 2013. A review of observations of organic matter in fogs and clouds: Origin, processing and fate. Atmospheric Research, 132–133(0): 434-449. Available from http://www.sciencedirect.com/science/article/pii/S016980951300183X [Accessed 2013/11//]. DOI http://dx.doi.org/10.1016/j.atmosres.2013.06.005.

Herrmann, H., B. Ervens, H.-W. Jacobi, R. Wolke, P. Nowacki and R. Zellner, 2000. Capram2. 3: A chemical aqueous phase radical mechanism for tropospheric chemistry. Journal of Atmospheric Chemistry, 36(3): 231-284.

Kirkland, J.R., Y.B. Lim, Y. Tan, K.E. Altieri and B.J. Turpin, 2013. Glyoxal secondary organic aerosol chemistry: Effects of dilute nitrate and ammonium and support for organic radical–radical oligomer formation. Environmental Chemistry, 10(3): 158-166. Available from http://www.publish.csiro.au/paper/EN13074. DOI http://dx.doi.org/10.1071/EN13074.

Laongsri, B. and R.M. Harrison, 2013. Atmospheric behaviour of particulate oxalate at uk urban background and rural sites. Atmospheric Environment, 71(0): 319-326. Available from http://www.sciencedirect.com/science/article/pii/S1352231013001167. DOI http://dx.doi.org/10.1016/j.atmosenv.2013.02.015.

Lim, H.-J., A.G. Carlton and B.J. Turpin, 2005. Isoprene forms secondary organic aerosol through cloud processing: Model simulations. Environmental Science & Technology, 39(12): 4441-4446. Available from http://dx.doi.org/10.1021/es048039h [Accessed 2014/01/10]. DOI 10.1021/es048039h.

Lim, Y.B., Y. Tan, M.J. Perri, S.P. Seitzinger and B.J. Turpin, 2010. Aqueous chemistry and its role in secondary organic aerosol (soa) formation. Atmos. Chem. Phys.,

10(21): 10521-10539. Available from http://www.atmos-chem-phys.net/10/10521/2010/. DOI 10.5194/acp-10-10521-2010.

Lim, Y.B. and P.J. Ziemann, 2005. Products and mechanism of secondary organic aerosol formation from reactions of n-alkanes with oh radicals in the presence of nox. Environmental Science & Technology, 39(23): 9229-9236. Available from http://dx.doi.org/10.1021/es051447g [Accessed 2014/01/10]. DOI 10.1021/es051447g.

Limbeck, A., H. Puxbaum, L. Otter and M.C. Scholes, 2001. Semivolatile behavior of dicarboxylic acids and other polar organic species at a rural background site (nylsvley, rsa). Atmospheric Environment, 35(10): 1853-1862. Available from http://www.sciencedirect.com/science/article/pii/S1352231000004970. DOI http://dx.doi.org/10.1016/S1352-2310(00)00497-0.

Mack, J. and J.R. Bolton, 1999. Photochemistry of nitrite and nitrate in aqueous solution: A review. Journal of Photochemistry and Photobiology A: Chemistry, 128(1–3): 1-13. Available from http://www.sciencedirect.com/science/article/pii/S1010603099001550. DOI http://dx.doi.org/10.1016/S1010-6030(99)00155-0.

Myriokefalitakis, S., K. Tsigaridis, N. Mihalopoulos, J. Sciare, A. Nenes, K. Kawamura, A. Segers and M. Kanakidou, 2011. In-cloud oxalate formation in the global troposphere: A 3-d modeling study. Atmos. Chem. Phys., 11(12): 5761-5782. Available from http://www.atmos-chem-phys.net/11/5761/2011/. DOI 10.5194/acp-11-5761-2011.

Nguyen, T.B., P.B. Lee, K.M. Updyke, D.L. Bones, J. Laskin, A. Laskin and S.A. Nizkorodov, 2012. Formation of nitrogen- and sulfur-containing light-absorbing compounds accelerated by evaporation of water from secondary organic aerosols. Journal of Geophysical Research: Atmospheres, 117(D1): D01207. Available from http://dx.doi.org/10.1029/2011JD016944. DOI 10.1029/2011JD016944.

Noziere, B., P. Dziedzic and A. Córdova, 2008. Products and kinetics of the liquid-phase reaction of glyoxal catalyzed by ammonium ions (nh4+). The Journal of Physical Chemistry A, 113(1): 231-237.

Nozière, B., S. Ekström, T. Alsberg and S. Holmström, 2010. Radical-initiated formation of organosulfates and surfactants in atmospheric aerosols. Geophysical Research Letters, 37(5): L05806. Available from http://dx.doi.org/10.1029/2009GL041683. DOI 10.1029/2009GL041683.

Ortiz-Montalvo, D.L., S.A.K. Häkkinen, A.N. Schwier, Y.B. Lim, V.F. McNeill and B.J. Turpin, 2013. Ammonium addition (and aerosol ph) has a dramatic impact on the volatility and yield of glyoxal secondary organic aerosol. Environmental Science & Technology, 48(1): 255-262. Available from

http://pubs.acs.org/doi/abs/10.1021/es4035667 [Accessed 2014/03/23]. DOI 10.1021/es4035667.

Perri, M.J., S. Seitzinger and B.J. Turpin, 2009. Secondary organic aerosol production from aqueous photooxidation of glycolaldehyde: Laboratory experiments. Atmospheric Environment, 43(8): 1487-1497. Available from http://www.sciencedirect.com/science/article/pii/S1352231008011096. DOI http://dx.doi.org/10.1016/j.atmosenv.2008.11.037.

Rinaldi, M., S. Decesari, C. Carbone, E. Finessi, S. Fuzzi, D. Ceburnis, C.D. O'Dowd, J. Sciare, J.P. Burrows, M. Vrekoussis, B. Ervens, K. Tsigaridis and M.C. Facchini, 2011. Evidence of a natural marine source of oxalic acid and a possible link to glyoxal. Journal of Geophysical Research: Atmospheres, 116(D16): D16204. Available from http://dx.doi.org/10.1029/2011JD015659. DOI 10.1029/2011JD015659.

Sareen, N., A.N. Schwier, E.L. Shapiro, D. Mitroo and V.F. McNeill, 2010. Secondary organic material formed by methylglyoxal in aqueous aerosol mimics. Atmos. Chem. Phys., 10(3): 997-1016. Available from http://www.atmos-chem-phys.net/10/997/2010/. DOI 10.5194/acp-10-997-2010.

Shapiro, E.L., J. Szprengiel, N. Sareen, C.N. Jen, M.R. Giordano and V.F. McNeill, 2009. Light-absorbing secondary organic material formed by glyoxal in aqueous aerosol mimics. Atmos. Chem. Phys., 9(7): 2289-2300. Available from http://www.atmos-chem-phys.net/9/2289/2009/. DOI 10.5194/acp-9-2289-2009.

Sorooshian, A., M.-L. Lu, F.J. Brechtel, H. Jonsson, G. Feingold, R.C. Flagan and J.H. Seinfeld, 2007. On the source of organic acid aerosol layers above clouds. Environmental Science & Technology, 41(13): 4647-4654. Available from http://dx.doi.org/10.1021/es0630442 [Accessed 2014/03/31]. DOI 10.1021/es0630442.

Sorooshian, A., V. Varutbangkul, F.J. Brechtel, B. Ervens, G. Feingold, R. Bahreini, S.M. Murphy, J.S. Holloway, E.L. Atlas, G. Buzorius, H. Jonsson, R.C. Flagan and J.H. Seinfeld, 2006. Oxalic acid in clear and cloudy atmospheres: Analysis of data from international consortium for atmospheric research on transport and transformation 2004. Journal of Geophysical Research: Atmospheres, 111(D23): D23S45. Available from http://dx.doi.org/10.1029/2005JD006880. DOI 10.1029/2005JD006880.

Sun, Y.L., Q. Zhang, C. Anastasio and J. Sun, 2010. Insights into secondary organic aerosol formed via aqueous-phase reactions of phenolic compounds based on high resolution mass spectrometry. Atmos. Chem. Phys., 10(10): 4809-4822. Available from http://www.atmos-chem-phys.net/10/4809/2010/. DOI 10.5194/acp-10-4809-2010.

Tan, Y., M.J. Perri, S.P. Seitzinger and B.J. Turpin, 2009. Effects of precursor concentration and acidic sulfate in aqueous glyoxal−oh radical oxidation and implications for secondary organic aerosol. Environmental Science & Technology, 43(21): 8105-8112. Available from http://dx.doi.org/10.1021/es901742f [Accessed 2014/01/10]. DOI 10.1021/es901742f.

Tsai, Y.I. and S.-C. Kuo, 2013. Contributions of low molecular weight carboxylic acids to aerosols and wet deposition in a natural subtropical broad-leaved forest environment. Atmospheric Environment, 81(0): 270-279. Available from http://www.sciencedirect.com/science/article/pii/S135223101300681X. DOI http://dx.doi.org/10.1016/j.atmosenv.2013.08.061.

Wittrock, F., A. Richter, H. Oetjen, J.P. Burrows, M. Kanakidou, S. Myriokefalitakis, R. Volkamer, S. Beirle, U. Platt and T. Wagner, 2006. Simultaneous global observations of glyoxal and formaldehyde from space. Geophysical Research Letters, 33(16): L16804. Available from http://dx.doi.org/10.1029/2006GL026310. DOI 10.1029/2006GL026310.

Yeung, L.Y., M.J. Pennino, A.M. Miller and M.J. Elrod, 2005. Kinetics and mechanistic studies of the atmospheric oxidation of alkynes. The Journal of Physical Chemistry A, 109(9): 1879-1889. Available from http://dx.doi.org/10.1021/jp0454671 [Accessed 2014/01/10]. DOI 10.1021/jp0454671.

Zhang, Q. and C. Anastasio, 2003. Free and combined amino compounds in atmospheric fine particles (pm2.5) and fog waters from northern california. Atmospheric Environment, 37(16): 2247-2258. Available from http://www.sciencedirect.com/science/article/pii/S1352231003001274. DOI http://dx.doi.org/10.1016/S1352-2310(03)00127-4.

Appendix A

A.1.1. Measured and modeled H_2O_2 concentration in H_2O_2 + UV control experiment. The concentration of H_2O_2 as a function of time in the H_2O_2 + UV control experiments was modeled (FACSIMILE for Windows Version 4.1.45) using the following reactions and rate constants provided by Lim et al. (2010) with the expection of k_1.

$$H_2O_2 + UV \rightarrow OH + OH; (k_1)$$

$$OH + H_2O_2 \rightarrow HO_2 + H_2O$$

$$HO_2 + H_2O_2 \rightarrow OH + H_2O + O_2$$

$$HO_2 + HO_2 \rightarrow H_2O_2 + O_2$$

$$OH + HO_2 \rightarrow H_2O + O_2$$

$$OH + OH \rightarrow H_2O_2$$

The H_2O_2 photolysis rate constant, $k_1 = 1.0x10^{-4}$ was determined by fitting the model to measured H_2O_2 concentrations. This value of k_1 was then used in the FACSIMILE model for glyoxal to estimate the concentration of OH (M; [OH]initial = $7.8x10^{-13}$, [OH]final = $6.0x10^{-12}$, [OH]average = $(1\pm2)x10^{-12}$) during glyoxal experiments from initial precursor concentrations (e.g., 5 mM H_2O_2, 1 mM GLY).

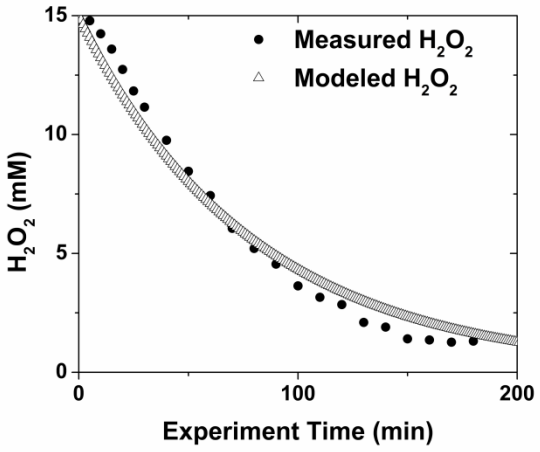

A.1.2. Modeled OH concentration in GLY + OH in the presence and absence of HNO_3. Note OH is formed from H_2O_2 photolysis and reacts with GLY and its reaction products. Inclusion of HNO_3 reactions discussed in the methods does not change [OH] prediction.

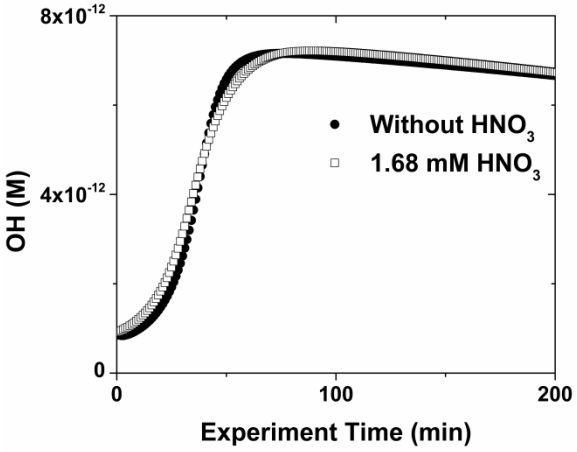

A.1.3. Modeled oxalate concentrations from GLY + OH with and without HNO_3.

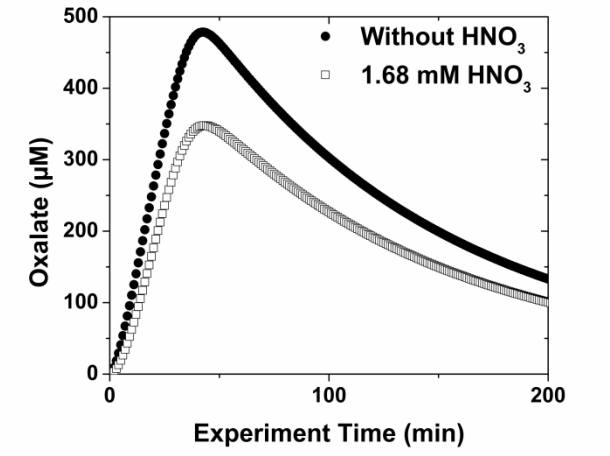

A.1.4. Modeled nitrate concentration in GLY + OH + HNO_3 experiment.

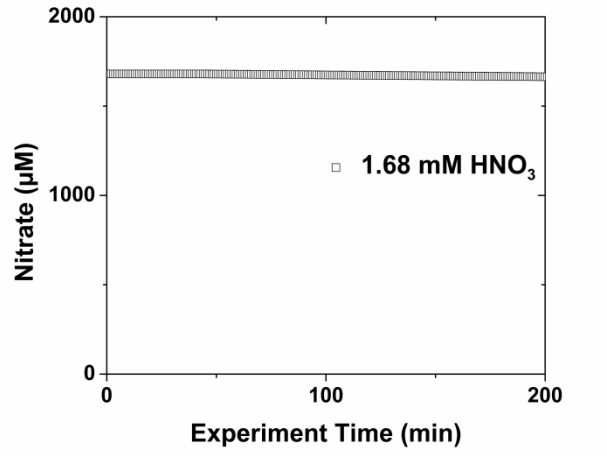

A.1.5. Modeled pH in GLY + OH experiments conducted in the presence and absence of HNO_3.

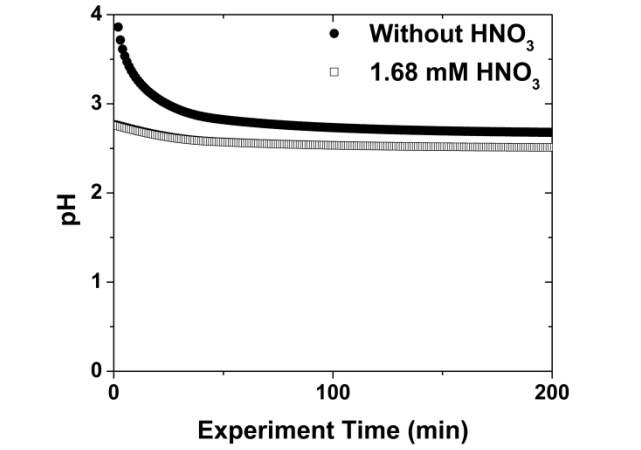

A.1.6. Oxalate concentration measured by IC in GLY + HNO_3 + UV control experiment. Some oxalate formation is seen, but concentrations are much lower and formation is much slower than in GLY + OH + HNO_3 experiments. OH production from HNO_3 + UV is modest.

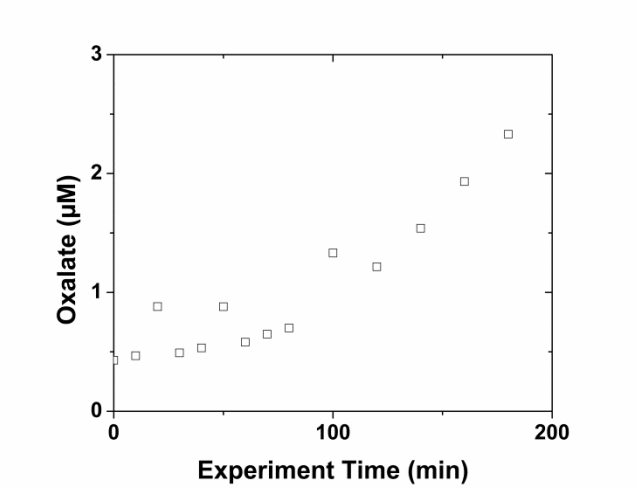

A.1.7. Nitrate concentration measured by IC in GLY + HNO_3 + UV control experiment.

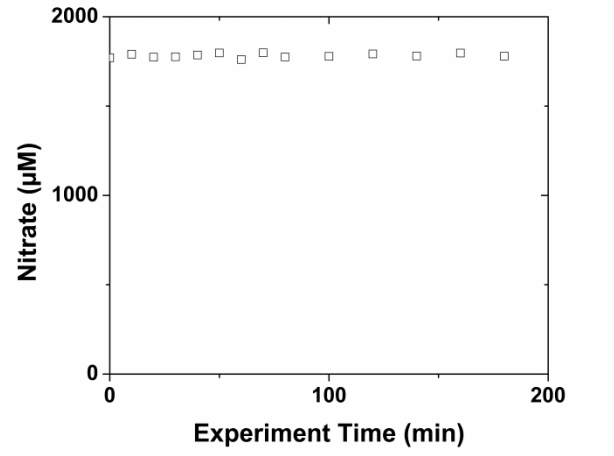

A.1.8. Nitrate concentration measured by IC in GLY + OH + HNO_3 experiment. Error bars represent the coefficient of variation (<1%) across three experiments.

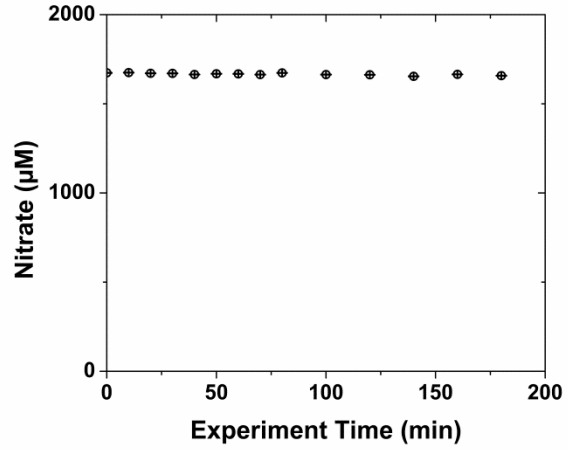

A.2.1. Batch 1L Reaction Vessel SOP and Data Sheet

Aqueous batch reaction SOP

1) Plan experiment
   a. Calculate amount of compounds, determine sampling frequency and volume.
2) Clean all glassware, sampling lines, syringes, thermometers.
3) Wrap reaction vessels in aluminum foil, to block ambient light from vessels
4) Set up reaction vessel
   a. Place reaction vessels in stands on top of stirrer surfaces
   b. Attach tubes for water cooling
      i. Faucet to bottom of reaction vessel
      ii. Top of reaction vessel to control vessel
      iii. Control vessel to drain
      iv. Turn on water
   c. Place magnets inside vessels
   d. Place the immersion well inside the vessel
   e. Attach cooling air tubes
      i. Connect tube to lab vacuum
      ii. Turn on vacuum
   f. Place thermometer and thermometer adapter in vessels
   g. Attach sampling lines and syringes with appropriate adapters
   h. Wrap top of immersion wells in aluminum foil
5) Place UV lamp inside the immersion well. Write down which lamp is used in experiment. Turn on UV lamp and note time on sample data sheets. Warm-up time should be at least 45 minutes.
6) Calibrate pH meter if needed
7) Clean 1L volumetric flask for reaction solution preparation
8) Make reaction and/or control solutions in 1L volumetric flask
9) Experiment and controls
   a. Take the first sample directly from volumetric flask.
   b. Pour solution into reaction vessel and turn stirrer onto to setting4.
   a. Note the time on sample data sheet

i. 2nd sample is taken immediately after solution is placed in vessel. The process may take around 3-5 minutes.
ii. Take samples at similar time points in each experiment.
iii. Pump syringe 3 times before taking each sample.

10) Label all samples with the same experiment code and sample time. Put sample on autosampler and run.

Sample data sheet

Date:		Light turned on:	
Experiment name:		Stirring setting:	

H_2O_2 Conc.: (amount)		Lamp ID:	
Additional Conc.:		Pre-Expt DO:	
Organic Conc.:		Pre-Expt pH:	

Solution Preparation: _____ Solution in vessel: _____

Time	t = min	Sample ID	Temp. (°C)	Comments

Stnd. Mix				Post-Expt DO	
Stnd. Ind'pend't				Post-Expt pH	

A2.2. H_2O_2 + UV SOP

No changes were made to the existing laboratory H_2O_2 + UV SOP which is available upon request and a hard copy available in the laboratory. The data sheet used for this experiment is the same as the Batch 1L Reaction Vessel Data Sheet.

A.2.3. Ion Chromatography SOP

Changes made to the IC SOP include sections “Developing a Calibration Curve” and instructions throughout for operation of IC coupled to ESI-MS and how to process IC and IC/ESI-MS data. This SOP is also available (hard copy) in the laboratory and upon request.

Appendix B

Appendix B.1.1. Shown here is a table of mist chamber collection throughout the campaign with the time of day, mist chamber run time, and total organic carbon concentration displayed. Use of the morning composite of July 7th, 8th, 9th samples provides the best representation of chemistry that rapidly occurs at sunrise before the boundary layer has lifted and diluted our water-soluble species.

	June																						July								
T.O.D.	8	9	10	11	12	13	14	15	16	17	18	19	20	21	22	23	24	25	26	27	28	29	30	1	2	3	4	5	6	7	8	9
5AM										P																						
6										O																						
7										W																						
8										E																						
9										R																						
10																																
11										I																						
12PM										S																						
1										S																						
2										U																						
3										E																						
4										S																						
5																																
6-7																																
Run Time (Hrs)	3	2	2	2	2	2	2	2	2		2	2	2	2	2	2	4	4	3	4	4	2	2	2	2	2	4	4	4	4	4	4
TOCAN (µM-C)	41	33	22	23	19	39	32	48	47		63	87	91	79	59		76	98	50	56	73	44	66	82	73	49		108		107		112

Appendix B.1.2. Shown here is the (average) result of cuvette chamber experiments (before and after) with H_2O_2+UV to determine the OH production rate assuming there are no other OH sources or sinks in our mist chamber samples. The model values are the result corresponding to a hydrogen peroxide photolysis constant of $k = 1.0 \times 10^{-4}$.

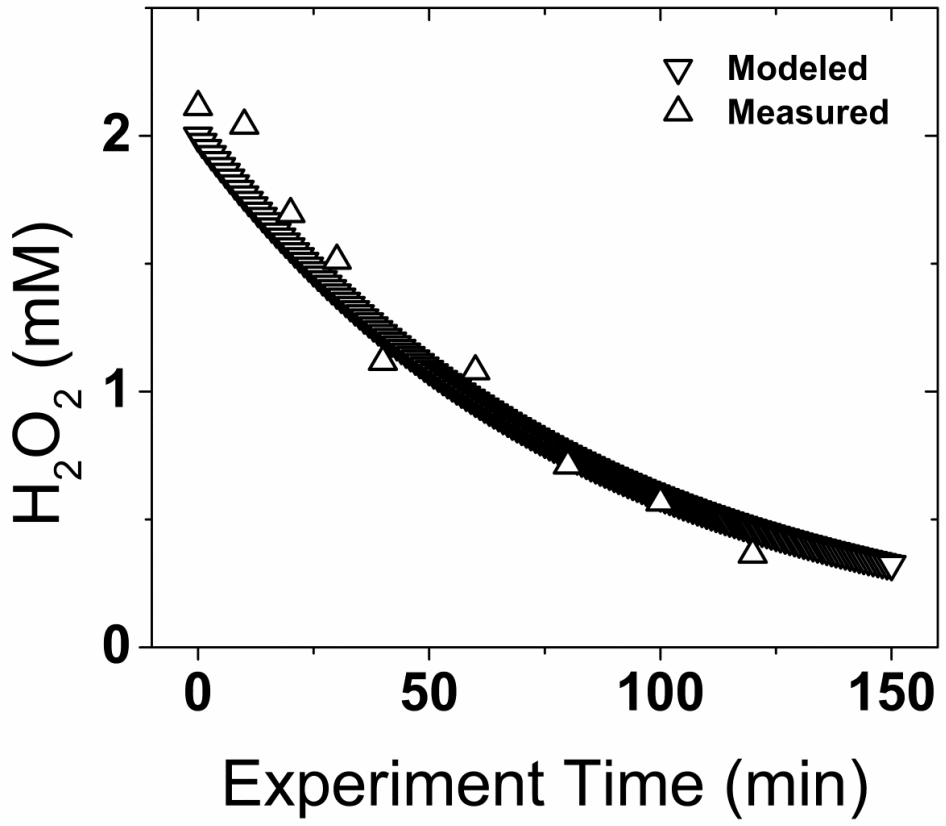

Appendix B.1.3. Shown here are the percent recoveries (range for before and after experiments) acquired through catalase tests during which a 50 µM organic acid mix (pyruvate, glyoxylate, and oxalate) was spiked with H_2O_2 (125 µM) to represent amounts used in OH experiments.

1% Catalase (µL)	**%**		
	Pyruvate Recovered	**Glyoxylate Recovered**	**Oxalate Recovered**
0	92-97	20-39	102-107
6	99-104	70-73	106-106
12	94-96	56-75	103-106
24	95-100	77-83	103-106
36	**94-98**	**77-86**	**99-102**
48	85-97	70-77	97-101

Appendix B.1.4. Shown here are the positive and negative mode ESI-MS detection limits for each mass. Note that a strong signal at m/z- 97 dominates the bottom (negative mode) ESI-MS spectrum and there is no single dominant m/z+ in the top (positive mode) spectrum, but relatively low detection limits across the mass range 50-350 amu.

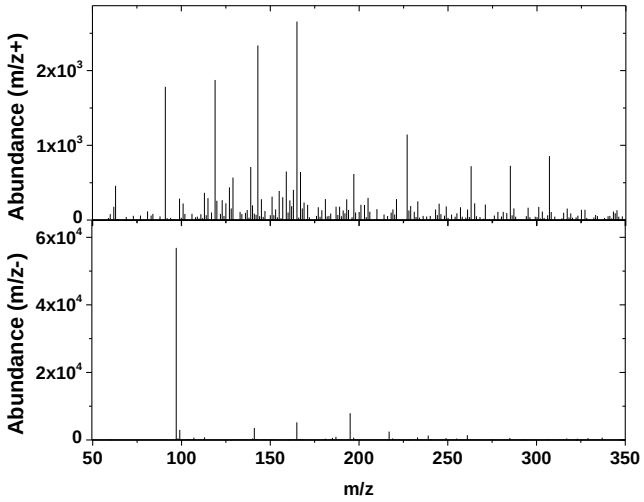

Appendix B.1.5. Shown here is the average **acetate (+glycolate)** formation for all experiments in the presence of OH radicals (Sample + OH), all control experiments (No OH), and an example of a single OH experiment, July 7th, 8th, 9th composite (789+OH) with the pooled coefficient of variation (75%) represented by the error bars. The formula used to calculate the pooled coefficient of variation (CV_{pooled}) is shown below and employed for replicate experiments with the same sample and then pooled.

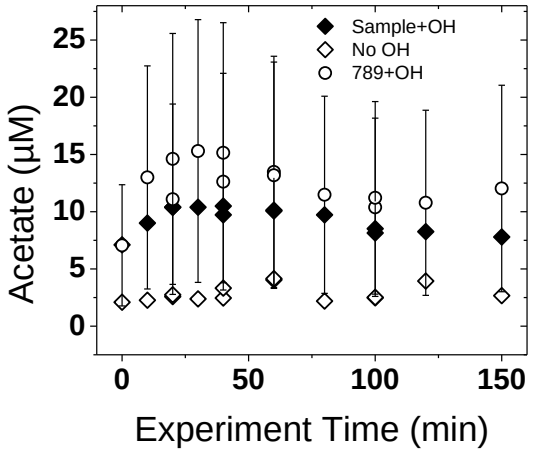

$$CV_{pooled} = \frac{\sigma_{pooled}}{x_{ave}}$$

$$\sigma_{pooled} = \sqrt{\frac{\sum \sigma^2 (N-1)}{\sum (N-1)}}$$

When N = the number of measured values for a single time point

and σ = the standard deviation calculated for measured values at a single time point

Appendix B.1.6. Shown here is the average **formate** formation for all experiments in the presence of OH radicals (Sample + OH; solid diamonds), all control experiments (No OH; open diamonds), and an example of a single OH experiment, July 7th, 8th, 9th composite (789+OH; open circles) with the pooled coefficient of variation (63%) represented by the error bars.

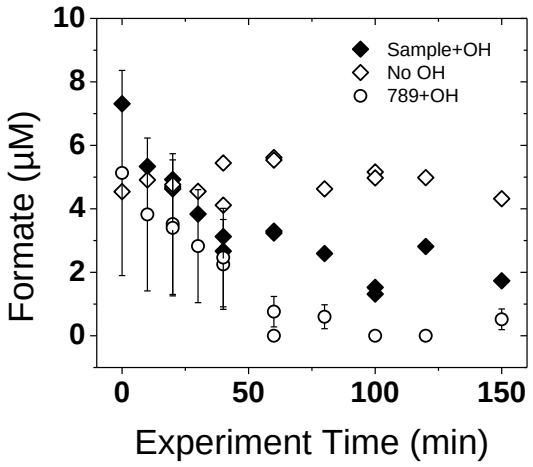

Appendix B.1.7. Shown here is the average **pyruvate** formation for all experiments in the presence of OH radicals (Sample + OH; solid diamonds), all control experiments (No OH; open diamonds), and an example of a single OH experiment, July 7th, 8th, 9th composite (789+OH; open circles) with the pooled coefficient of variation (78%) represented by the error bars.

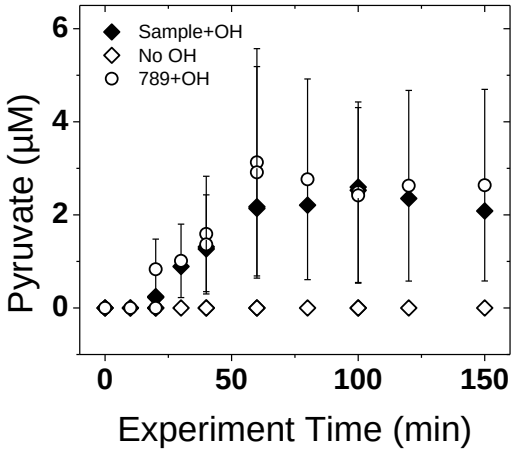

Appendix B.1.8. Shown here is the average **glyoxylate** formation for all experiments in the presence of OH radicals (Sample + OH; solid diamonds) which remains at a value of zero. All control experiments have detect peak area which is quantified as glyoxylate. Note that the concentration in control experiments remains constant suggesting that there may be other chemicals leading to the peak area at the retention time of glyoxylate because we expect glyoxylate to react with H_2O_2 (No OH; open diamonds).

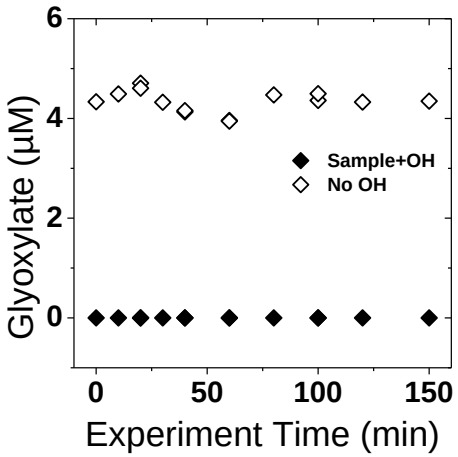

Appendix B.1.9. Shown here is the average **succinate + malate** formation for all experiments in the presence of OH radicals (Sample + OH; solid diamonds), all control experiments (No OH; open diamonds), and an example of a single OH experiment, July 7^{th}, 8^{th}, 9^{th} composite (789+OH; open circles) with the pooled coefficient of variation (198%) represented by the error bars. Note that there is nearly no signal for succinate (which we know coelutes with malate) in the presence and absence of OH radicals which gives rise to a high (198%) error.

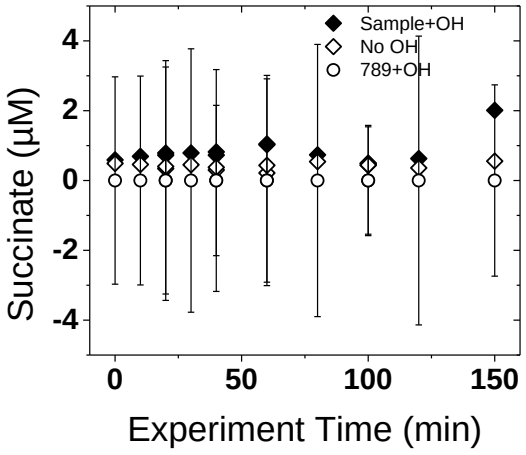

Appendix B.1.10. Shown here is the average **tartarate + malonate** formation for all experiments in the presence of OH radicals (Sample + OH; solid diamonds), all control experiments (No OH; open diamonds), and an example of a single OH experiment, July 7^{th}, 8^{th}, 9^{th} composite (789+OH; open circles) with the pooled coefficient of variation (48%) represented by the error bars. Note that there appears to be a slight increase in tartarate concentration (which we know coelutes with malonate) which occurs during all experiments.

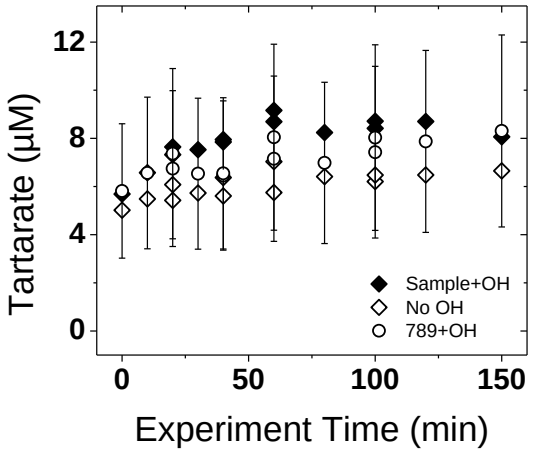

Appendix B.1.11. Shown here is the average **oxalate** formation for all experiments in the presence of OH radicals (Sample + OH; solid diamonds), all control experiments (No OH; open diamonds), and an example of a single OH experiment, July 7th, 8th, 9th composite (789+OH; open circles) with the pooled coefficient of variation (23%) represented by the error bars.

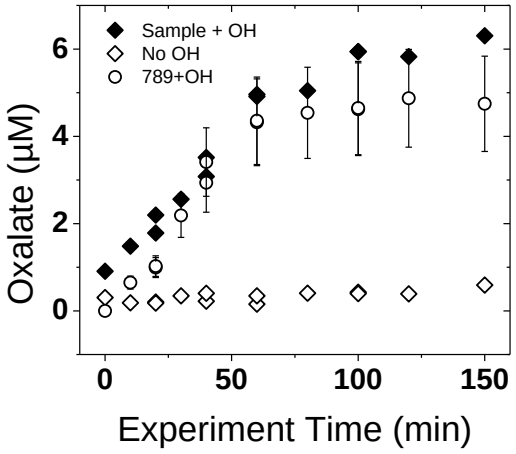

Appendix B.1.12. Shown here is the average **sulfate** formation for all experiments in the presence of OH radicals (Sample + OH; solid diamonds), all control experiments (No OH; open diamonds), and an example of a single OH experiment, July 7th, 8th, 9th composite (789+OH; open circles) with the pooled coefficient of variation (83%) represented by the error bars. It is expected that this sulfate signal is due to the acid washing step during mist chamber sampling preparation.

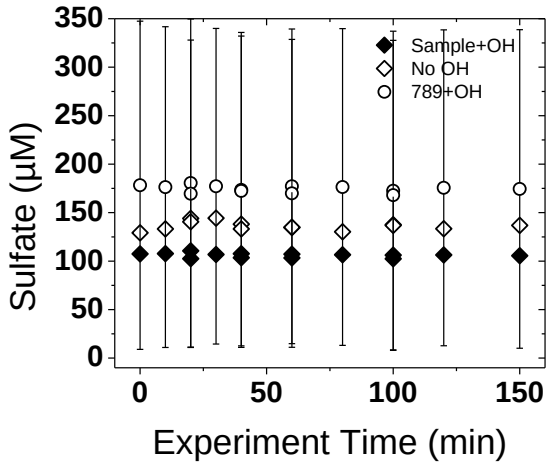

Appendix B.1.13. Shown here is the average **nitrate** formation for all experiments in the presence of OH radicals (Sample + OH; solid diamonds), all control experiments (No OH; open diamonds), and an example of a single OH experiment, July 7th, 8th, 9th composite (789+OH; open circles) with the pooled coefficient of variation (56%) represented by the error bars. Note that there are small amounts of nitrate that are present and unreactive. These differences in nitrate concentrations may be due to the varied influence of gas-phase nitrate sources throughout the study.

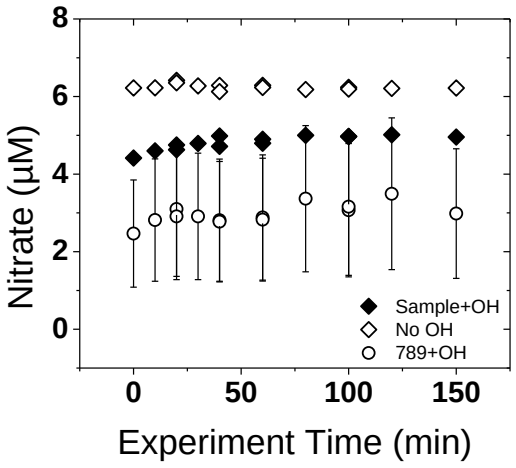

Appendix B.1.14. ESI-MS negative mode analysis is used to identify products. The ions that meet product criteria described in the text are listed below. Most notable are ions with known products of aqueous processing (**bold** ion mass) that appear at the same unit mass. For example, m/z- 73 (glyoxylate), 87 (pyruvate), 89 (oxalate),103 (malonate), and 117 (succinate).

	June			July					
	19	20	25	1	1	56	456	789	789
m/z-				A	B			A	B
73			X	X		X			
87	X		X	X	X	X		X	X
89	X	X		X	X	X			X
103	X	X	X	X	X	X	X	X	X
115									
117	X	X		X	X	X	X	X	X
129						X			
147	X			X					
203			X			X		X	
217									

Appendix B.1.15. Product ion plot for July 5th, 6th afternoon composite plus OH showing ESI-MS abundance throughout experiment time. Note the ions plotted correspond to some known products of aqueous processing (m/z- 73 = glyoxylate, 87 = pyruvate, 89 = oxalate, 103 = malonate, 117 = succinate).

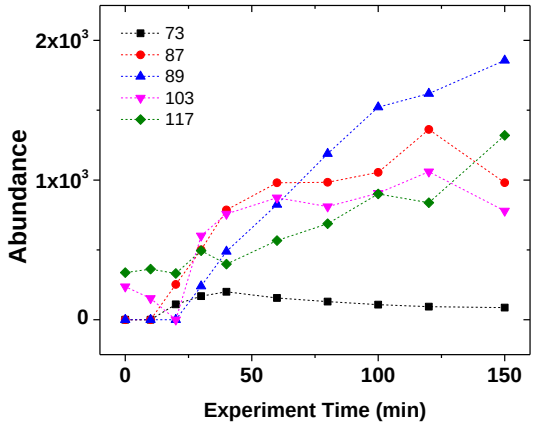

Appendix B.1.16. Shown here is the oxalate production during two (before and after) cuvette experiments with 50µM glyoxal plus 125 µM H_2O_2 to test the reproducibility of cuvette chamber runs and provide a metric of oxalate production if the 100 µM organic carbon in the mist chamber samples were glyoxal.

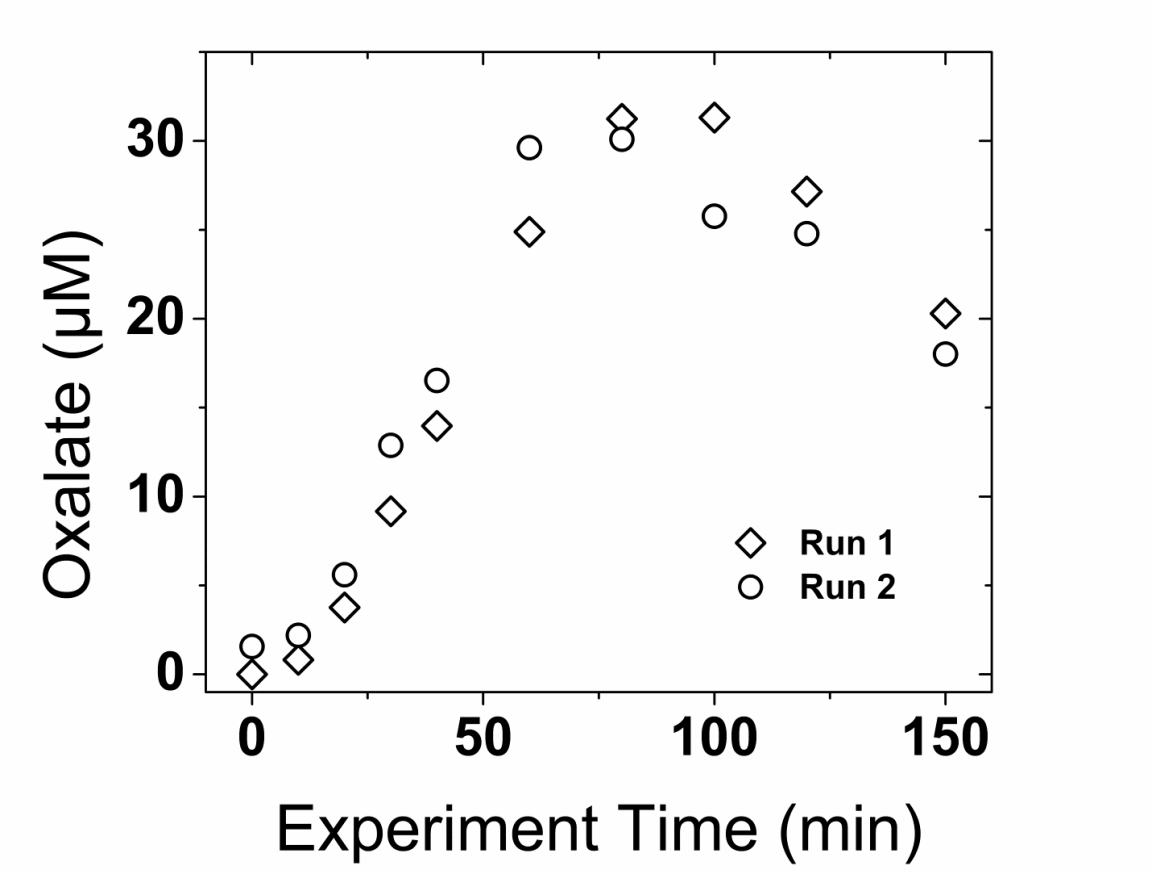

Appendix B.1.17. Displayed is the one major fragment (m/z+219) from m/z+ 304. The elemental formula of m/z+ 304 is $C_{20}H_{34}NO$, m/z+ 219 is $C_{15}H_{23}O$. The difference between these exact masses is 85.08953. This exact mass corresponds to a neutral elemental formula of $C_5H_{11}N$. The separation of N and O atoms during fragmentation supports the claim that m/z+ 304 is an amine since it is unlikely that the link between these fragments was an N-O bond.

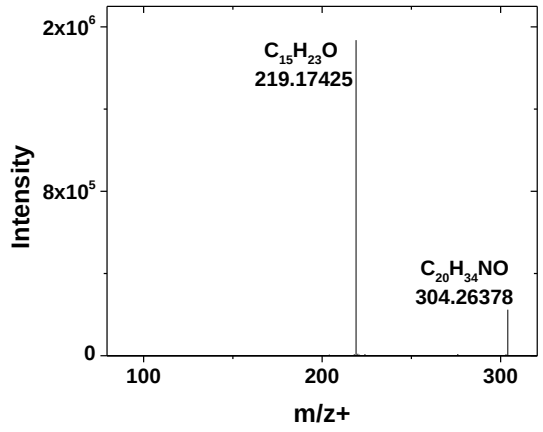

Appendix B.1.18. Mechanism by which m/z+ 130 could form m/z+ 118.

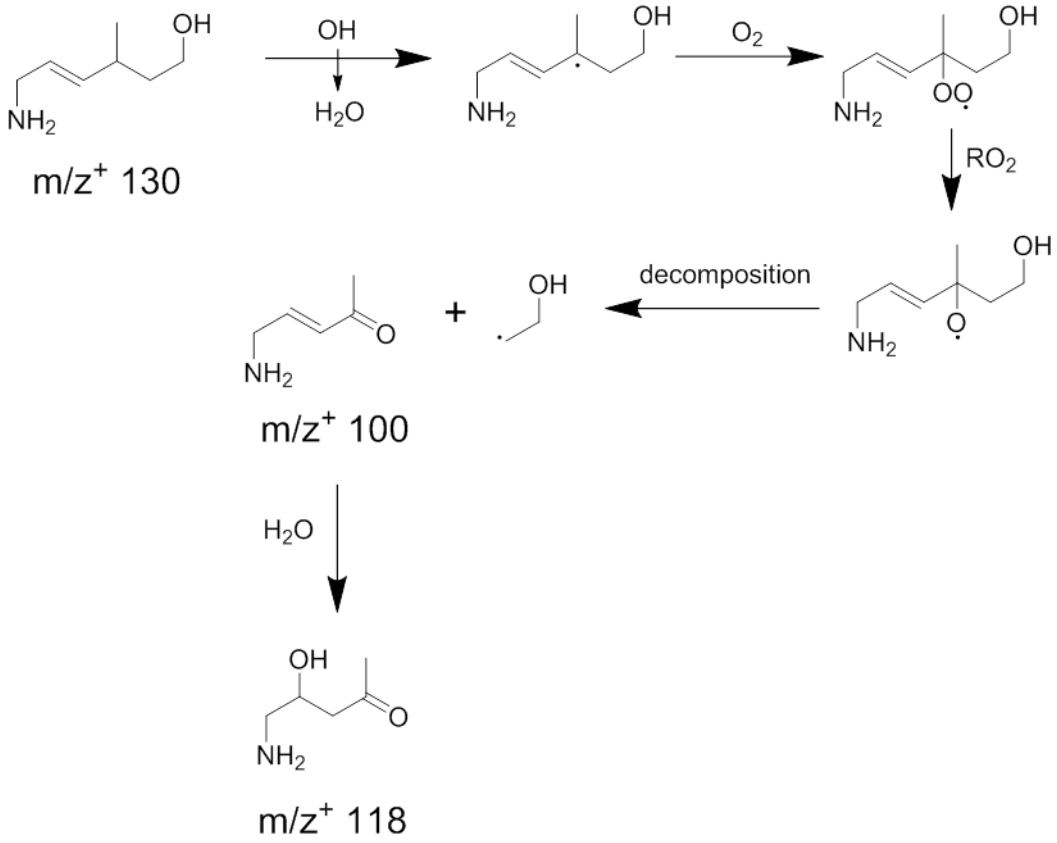

Appendix B.1.19. Shown here is the fragmentation spectrum for parent ion m/z+ 118 which behaves like an intermediate during OH experiments with July 7th, 8th, 9th samples.

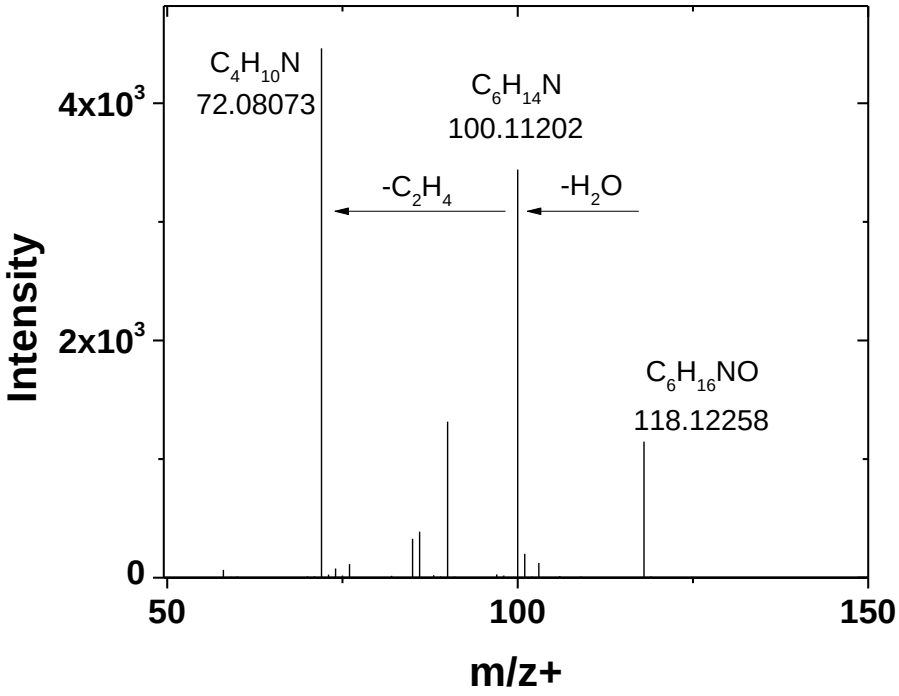

Appendix B.1.20. Shown here is the fragmentation spectrum for parent ion m/z+ 162 which behaves like an intermediate during OH experiments with July 7th, 8th, 9th samples. Note that m/z+ 162 contains a fragment with the same elemental formula as m/z+ 118 and two fragments (m/z+ 100, 72) in common with m/z+ 118 suggesting that m/z+ 118 and 162 may only differ by a CO_2 functional group.

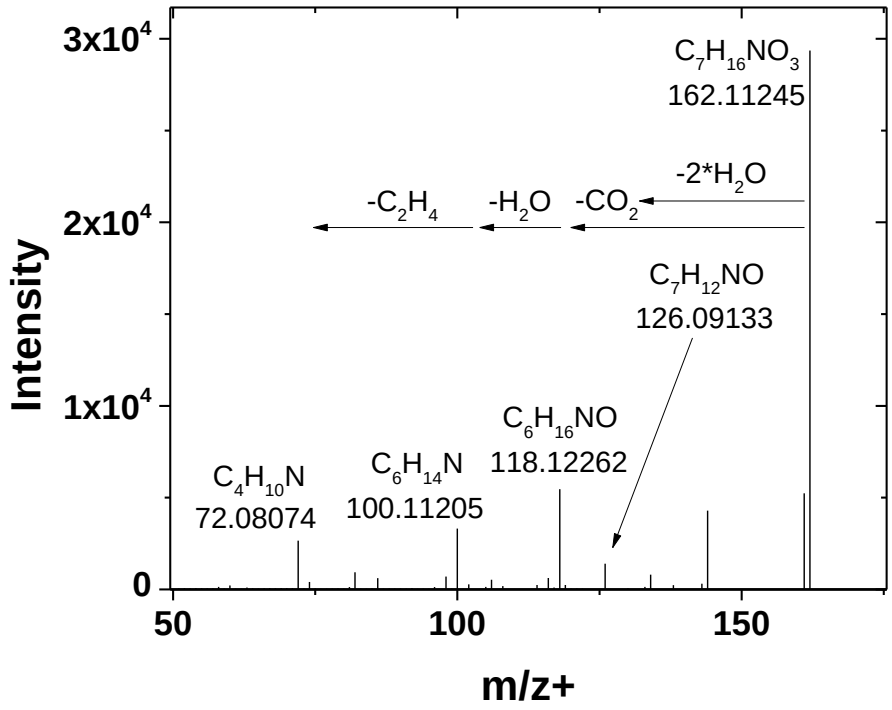

Appendix B.2.1. Shown here is the Mist Chamber operation protocol.

MIST CHAMBER SOP

PREPARATION

1) Clean mist chambers and non-metal parts according to Sonicator SOP
2) Clean metal parts with kimwipes and isopropanol
3) Air tubing is new (Copper, Teflon): No treatment
4) Clean sample tubes, water vessels, syringes, and water tubing according to Acid Wash SOP
5) Quartz fiber filters baked at 500 °C
6) Set up mist chamber scaffolding and pumps as follows:
    a. Bug Screen attached over copper tubing inlet
    b. 3/8 in. Copper tubing runs from outside (~1m above roof) to within 2 ft. of each mist chamber (separate copper tubing for each mist chamber)
    c. Copper tubing coupled to ¼ in. Teflon tubing (Swagelok Reducing Union/McMaster Coupling)
    d. Teflon Tubing swaged to Gelman filter holder
    e. Gelman filter holds 47mm baked quartz fiber filter (fibrous side contacts incoming air first)
    f. Gelman filter holder swaged to bottom of mist chamber (Teflon swagelok ½ in. pipe fitting)
    g. Mist chamber injection port attaches to 60mL syringe
    h. Mist chamber top swaged (Teflon Swagelok ¾ in. pipe fitting) to URG filter pack plug – Tapped and threaded by Piotr)
    i. URG filter pack holds a 47 mm Zefluor filter (no treatment) = hydrophobing membrane
    j. URG filter pack connects to a hose barb adapter for vacuum tubing
    k. Vacuum tubing leads to variable area flow meter (non-digital) – connects via hose barb, bottom port
    l. Top port vacuum tubing leads to a valve
    m. Valve vacuum tubing leads to GAST ¾ HP vacuum pump (oil-less, carbon vane)
    n. Carbon vane pump can be wired for 220V or 110V and connects to power source
    o. Scaffolding should be set-up to minimize torque on the weakest point of the setup; the mist chamber glass
7) BEFORE AND AFTER A SET OF MIST CHAMBER RUNS
    a. Calibrate flow meters with digital TSI flow meter calibrator kit

IN LABORATORY

1) Collect materials:

   a. Cooler with blue ice
   b. 1L milli-q (for syringe fill/re-fill)
   c. 1L 0.25% H_2SO_4 for acid wash
   d. 1L Acid waste bottle
   e. 15 mL milli-q sample from source
   f. 4 x 60mL syringes and tubing
   g. 1L transfer bottle (filled with milli-q as reservoir if needed)
   h. Quartz or Zefluor filters if necessary
   i. 1x 15 mL tube for water sample from bottle
   j. 4x 50 mL tube for water wash sample from each MC
   k. 10x 50 mL tube for composited 'experiment aliquots' (fill to 35-40 mL max to avoid tube breakage = 20% head space)
2) Check "In trailer" list of materials

IN FIELD

1) Materials already in the trailer:
   a. Stationary: field sheets, gloves, kimwipes, labels
   b. Filters/forceps
   c. Hygrometer
   d. Timer/Clock
2) Wearing PPE at all times
   a. Goggles for safety
   b. Gloves for safety and to prevent contamination of the samples
3) Fill syringes with 25 mL (each) 0.25% H_2SO_4
4) Connect syringes to MC's and turn on the pumps with valves halfway open
5) ASAP after pumps are on, add syringe contents to mist chambers
   a. Be careful not to allow solution to drip down onto the quartz filter
   b. Start timer
6) Adjust valves to allow 'sufficient' spray to coat the inside of the mist chamber
7) Allow 5 minutes to pass and switch pumps off
8) Allow the mist chambers to drip for 1 minute
9) Extract the acid and dispose in acid waste bottle
10) Fill syringes with 25 mL (each) milli-q
11) Attach to MC's, turn on pumps as before, start timer, run for 10 mins
12) Extract the water wash and deposit each MC volume in the appropriately labeled 50 mL tube
   a. Example) PV-MC-120701JK-DBa
   b. Po Valley – Mist Chamber – 120701JK – Dynamic Blank a-d (one of four mist chambers)
13) Fill syringes with 60 mL (each) milli-q

14) Attach to MC's, turn on pumps as before, start timer, fill out field sheet, begin 120 min run
15) Monitor MC's flow, spray quality, and record data on the field sheet
    …
16) After 120 mins has passed, extract the sample water and deposit each MC volume into the 1L composite bottle
17) Refill syringes with 60 mL (each) milli-q and repeat 120 min run
18) Repeat runs (4 per day) compositing all sample into the 1L composite bottle
    …
19) When the sampling is complete for the day, conduct an acid wash step and rinse step as performed in steps 3)-11). Do not save the water wash.
20) While the final wash steps are running, split the composite into appropriately labeled 50 mL tubes.
    a. 35-40mL per tube
    b. Label as previously mentioned "PV-MC-120701JK"
    c. 5-7 mL in a 15 mL tube for preliminary TOCAN and ESI-MS characterization
21) Return any supplies (e.g., acid waste) to the laboratory and treat (e.g., neutralize, discard)
22) Sleep. Repeat this tomorrow.

120529JK

Appendix B.2.2. Shown here is the Mist Chamber field data sheet.

PO VALLEY – MIST CHAMBER Checklist

DATE:_____

RUN ID: PV-MC-_____JK

IN LABORATORY

□ Cooler w/ blue ice
□ 1L milli-q
□ 15 mL sample of milli-q
□ 1L 0.25% H_2SO_4
□ 1L Acid Waste Bottle
□ 4x 60 mL syringes
□ 1L Transfer/Composite Bottle
□ Quartz/Zefluor filters
□ 2x 15 mL tube (1 for bottle sample, 1 for composite sample)
□ 4x 50 mL tubes (for water wash)
□ 10x 50 mL tubes (for experimental aliquots)

IN TRAILER

□ Field Sheet
□ 0.25% H_2SO_4 5 min wash
□ Note flow rates, RH, Temp.
□ 10 min water wash
□ Note flow rates, RH, Temp.
□ Water wash saved, labeled
□ **RUN 1: 120 mins - started**
□ Field data sheet filled out
□ Run 1 deposited in composite bottle – returned to cooler
□ **RUN 2: 120 mins – started**
□ Field data sheet filled out
□ Run 2 deposited in composite bottle – returned to cooler
□ **RUN 3: 120 mins – started**
□ Field data sheet filled out
□ Run 3 deposited in composite bottle – returned to cooler
□ **RUN 4: 120 mins – started**
□ Field data sheet filled out
□ Run 4 deposited in composite bottle – returned to cooler
□ 0.25% H_2SO_4 5 min wash
□ Note flow rates, RH, Temp.
□ 10 min water wash
□ Note flow rates, RH, Temp.
□ 5-7 mL of composite saved in 15 mL tube, labeled
□ 35-40 mL of composite split into __ x 50 mL tubes, labeled
□ Samples in freezer rack

RUN ID RANGE: PV-MC-_____JK

NB_____-NB_____

Date	
MC Run	PV-MC-_____JK

PV-MC-_____JK-BL
PV-MC-_____JK-DB;A-D
15 mL Composite Saved

(From Bottle)
(Water Wash)
(for TOCAN, MS)

Collection ID Range
NB_____-NB_____
_____x 50 mL Tubes Saved
15 mL Composite Saved

LOCAL					Flow (LPM)				Volume (mL)[ex. MC+Syringe]				
Expt Time (mins)	Time of Day	RH (%)	T (°C)	MC-A	MC-B	MC-C	MC-D	MC-A	MC-B	MC-C	MC-D	Comments
0												RUN____(# of 4)
15												
30												
35												
45												
60												
75												
90												
105												
120												
0												
15												RUN____
30												
35												
45												
60												
75												
90												
105												
120												
5 min Acid Wash 10 min Water Wash												**AM OR PM** (Circle One)

	Flow	CalKit	MC-A	MC-B	MC-C	MC-D
Calibrator Kit Measurement (LPM)	1					
	2					
	3					
	4					
	5					

Flowmeter Comments/Notes:

Appendix B.2.3. Shown here is the Cuvette Chamber reaction SOP.

Aqueous cuvette reaction SOP (IC and ESI-MS) for (PV) field samples

Cuvette experiments are designed for investigating aqueous-phase OH radical reactions of water soluble organic compounds (WSOCs; e.g., GLY or MGLY) present in [mist chamber] field samples. Ten cuvettes are filled with 3mL each of field sample solution and H_2O_2. Each cuvette faces directly toward the 254nm UV lamp so that the same OH radical production via H_2O_2 photolysis is allowed to occur in all cuvettes. Catalase, which destroys peroxides, is immediately added after completion of cuvette reaction because in the cuvette there always exist excess amounts of H_2O_2, which degrades common organic products like glyoxylic acid (rapidly) and pyruvic acid (less rapid) (See Tan et al., 2010).

Experimental Plan:

A. *H_2O_2 plus UV (photon flux quantification) Experiment: Lamp QC*
B. *Catalase Test (glyoxylic acid+pyruvic acid+oxalic acid+catalase+H_2O_2): Catalase QC*
C. *Two Experiments: 10 time points including t = 0, and 1 duplicate = 11 cuvettes for any given experiment.*
D. *Experiment One: IC (1mL) and ESI-MS(+)/ESI-MS(-) (1mL) and Freeze (1mL)*
E. *Experiment Two: IC(1mL) and ESI-MS(-)/ESI-MS(+) (1mL) and Freeze (1mL)*
F. *IC/ESI-MS: for later analysis*
G. *Control Experiments: Field Sample + UV and Field Sample + H_2O_2 (Field Water Blank Experiment?)*
H. *Repeat C-G*
I. *Repeat A, B within 2 months*

The Experiment

1) One day before the Cuvette Chamber Run
    a. Turn on IC according to the IC SOP
    b. Clean (11) cuvettes, (11) caps, and glassware according to the Sonicator SOP
    c. Make sure acid washed 100 mL glassware is available (If not, prepare according to the Acid Wash SOP)
2) Plan Experiment
    a. Calculate amount of H_2O_2 to add based on TOCAN data (Refer to Appendix A; Obtain photolysis rate constant from H_2O_2 experiment – Refer to H_2O_2 SOP)
    b. Calculate amount of catalase to add (Refer to Appendix B)
3) Start up ESI-MS according to ESI-MS Startup/Shutdown SOP
4) Create an IC and ESI-MS sequence (Refer to the IC SOP and the ESI-MS Discrete Sample SOP)
    a. ESI-MS important note: 6 injections per sample, 20% of samples in replicate
    b. IC important note: 20% of samples in replicate
5) Thaw the appropriate 50 mL centrifuge tube containing mist chamber field sample

6) Warm up UV lamp at least 45 minutes prior to placement in the immersion well (shield UV output with foil-wrapped spare immersion well (Wear protective gear – UV goggles/face shield, lab coat/long sleeves)
    a. During lamp warm up time – set up cuvette chamber, make solutions
    b. Label properly: Make sure sample ID's are unique, and/or documented in the comments section of the sequence table. And include collection ID/ collection date, etc.
7) Prepare 5 point pseudo-calibration on the ESI-MS of expected compounds.
8) Begin ESI-MS blanks: (see step 9)
9) Begin IC blanks: lab water blank (milli-q), field DI water, mist chamber dynamic blank (2 min. run), field composite sample (No H_2O_2), standards (calibration-mix), and independent standards (3 organic acids; different batch) on the IC as described in the IC SOP (Note: Describe samples in the comments section of the sequence table in Chromeleon)
10) Use rinsed, acid washed "transfer" bottle (100mL pyrex bottle) to prepare solution
11) Prepare REACTION SOLUTION (UV + H_2O_2 + Field Sample) and place the cuvettes filled with the reaction solution into the reaction vessel:
    a. Make 33mL of field sample + H_2O_2 solution in the transfer bottle (NOTE: DO NOT LET THIS SIT: USE IMMEDIATELY).
    b. Fill each cuvette with 3 mL of solution mix prepared in the transfer bottle, then place 10 CAPPED cuvettes (FUV facing center) in the reaction vessel. Wipe Non-frosted face of cuvette with kimwipe prior to placement. IMPORTANT! Once H_2O_2 is added, start reaction ASAP to minimize H_2O_2 oxidation (i.e., H_2O_2 + Glyoxylic Acid), which is not photooxidation.
    c. When the lamp is introduced to the cuvette chamber (step 13), add catalase to the 11^{th} cuvette containing field sample + H_2O_2. This is 't = 0 mins'
12) Set up cuvette chamber reaction vessel
    i. Attach tubes for WATER cooling in the following manner:
        v. Faucet to bottom of reaction vessel
        vi. Top of reaction vessel to sink (see point iv. here)
        vii. Control flow/monitor water level inside chamber (Water level should not exceed cuvette caps, but cuvettes must be partially submerged)
        viii. Topic of further discussion: chiller flow control
    j. Place the immersion well inside the reaction vessel
    k. Attach cooling AIR tubes in the following manner:
        iii. Connect tube to lab vacuum
        iv. Turn on vacuum (enough for audible air flow)
    l. Place thermometer and thermometer adapter in thermometer port on top of the reaction vessel. Record temperature. (Contact Piotr)
13) Wrap cuvette chamber in aluminum foil.
14) Begin the cuvette photo reaction by inserting the lamp. Make sure you are wearing UV goggles!
15) Remove a cuvette at: t = 10, 20, 30, 40, 40b, 60, 80, 100, 120, 150 mins

16) Add x µL of 1% catalase (as determined in Appendix B - step 2) to the 3mL cuvette to quench H_2O_2. Mix catalase solution (pump 1mL pipette 5 times).
17) Split 3mL cuvette volume into 1mL – ESI-MS vial, 1mL – IC vial, 1mL IC vial for freezing
18) Label all samples with the same experiment code and sample time (Refer to Sample Data Sheet). And prepare IC/ESI-MS samples in between each sampling
19) Analyze 1st (IC) vial and 2nd (MS) vial immediately following catalase addition. Freeze the 3rd (IC) vial and save for further analysis. **Do not use plastic storage containers with any hydrogen peroxide-containing samples.** (Be careful, some vials may break during storage.)
20) Measure and record temperature after the cuvette photoreaction.
21) Clean up requires the following:
    a. Start the cleaning procedure for the cuvettes, caps, etc.
    b. Turn off the lamp, the vacuum, and the water flow
    c. Put the lamp back in its Styrofoam sleeve
    d. Monitor the instruments to make sure fluids, etc. are sufficient to finish analyzing all the samples in the sequences

Appendix A: H_2O_2 Use

Determine concentrations of WSOC in the fields sample and calculate H_2O_2 concentrations necessary for OH radical reactions

b. Obtain the concentration of WSOCs: TOCAN analysis provides the concentration of WSOCs in terms of total organic carbon (TOC) in µM-C.
c. Calculate amount of H_2O_2 required:
    a. $H_2O_2 = 5\times$ [(#TOC) µM-C × ¼] = [5/4 x TOC]µM H_2O_2
        i. Assumption (1): All WSOCs in the field samples are C_2; $0.5TOC \approx C_2$
        ii. Assumption (2): Half of the C_2-equivalent is as reactive as GLY
        iii. Example
            1. Sample = ***100 µM-C***
            2. Sample = 50 µM C_2 equivalent
            3. Sample = 25 µM reactive GLY equivalent
            4. Thus, 5 x 25 µM = ***125 µM H_2O_2***

Appendix B: Catalase Use

A. Catalase test
    a. Use the same concentration of H_2O_2 as in experiments
    b. Test Instructions (Analyzed by IC; Refer to IC SOP):
        i. Create Solution with:
            1. 50 µM Pyruvic Acid
            2. 50 µM Glyoxylic Acid
            3. 50 µM Oxalic Acid
            4. Same [µM] as H_2O_2 Experiment (Added last)

ii. Pipette 3 mL of the above solution into cuvettes
iii. Allow approximately 3 minutes to pass after the H_2O_2 is added (equivalent to the time that passes when a cuvette is taken from the chamber and catalase is added)
iv. Add 0.1% Catalase solution as follows into 3 cuvettes each
    1. 0 µL 1% Catalase (Vial 1)
    2. 6 µL 1% Catalase (Vial 2)
    3. 12 µL 1% Catalase (Vial 3)
    4. 24 µL 1% Catalase (Vial 4)
    5. 36 µL 1% Catalase (Vial 5)
    6. 48 µL 1% Catalase (Vial 6)
v. Run IC and determine the volume of 0.1% catalase solution and calculate recoveries of oxalic, pyruvic, and glyoxylic acids
    1. NOTE: Provide catalase "calibration curve" for volume added and recoveries for the H_2O_2 concentration in the experiment
vi. Previous experiments suggest that 36 µL of 0.1% catalase solution is required to destroy 150 µM H_2O_2 solution in a 3mL volume.

120810JK, BJT, YBL, RJL, DLO

Appendix B.2.4. Shown here is the cuvette chamber sample data sheet.

Sample data sheet

Experiment Date:		Light turned on (time):	
Experiment name:	Field+	Field ID:	PV-MC-_____JK

H_2O_2 Conc.: (5/4xTOC)µM		Lamp ID:	☐Little Lambda
Additional Conc.(e.g., HNO_3):		Collection date and Collection ID (Sticker):	
TOC Result (µM-C):			

H_2O_2 Added (Time): _____ UV added (Time): _____

Time of Day	t = min	Sample ID (Include Cuvette #)	Temp. (°C)	Comments (experiment, operator, sample, etc.)
	PRE-0			Field Sample Only – No H_2O_2 Added
	0			
	10			
	20			
	30			
	40a			
	40b			
	60			
	80			
	100			
	120			
	150			

Other Notes:

- ☐ Lamp warm up time 45 mins
- ☐ 1% Catalase Added (Volume = _____µL per 3mL Cuvette)
- ☐ ESI-MS : 5 point calibration prior to start (50µM Org Acids)
- ☐ ESI-MS : 6 Injections
- ☐ IC Calibration Method: _____

Stnd. Mix				

Appendix C

Appendix C.1.1. Shown here are the percent recoveries (range for before and after experiments) acquired through catalase tests during which a 100 µM organic acid mix (pyruvate, glyoxylate, and oxalate) was spiked with H_2O_2 (700 µM or 1500 µM) to represent amounts used in OH experiments.

1-2% Catalase (µL)	**%**		
	Pyruvate Recovered	**Glyoxylate Recovered**	**Oxalate Recovered**
0	71-87	22-43	96-103
50	84-88	48-95	93-95
75	**87-92**	**87-98**	**93-98**
100	78-86	71-96	86-94
150	87-89	79-96	95-98

Appendix C.1.2. Shown here is **acetate** (**+ glycolate**; coelute) quantified by IC during two OH experiments and controls (UV, H_2O_2) for California and Po Valley fogs. Error bars represent the pooled coefficient of variation (46%) calculated from repeated experiments. Filled circles and open squares are OH experiments with open triangles (up) Fog + UV and filled triangles (down) Fog + H_2O_2.

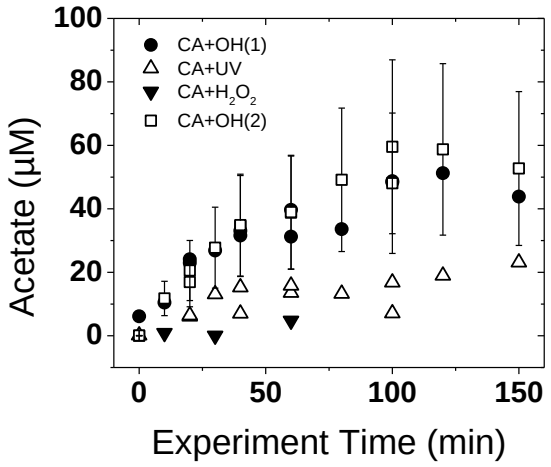

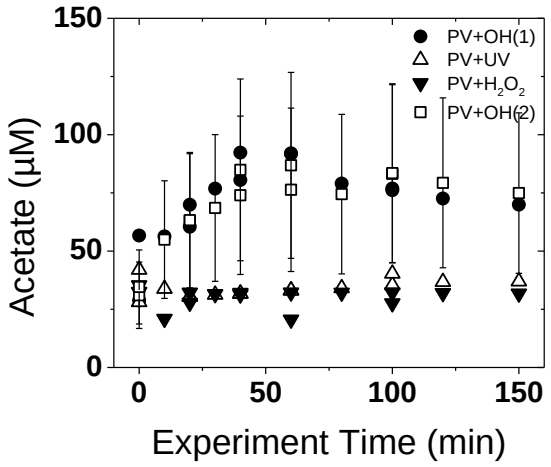

Appendix C.1.3. Shown here is **formate** quantified by IC during two OH experiments and controls (UV, H_2O_2) for California and Po Valley fogs. Error bars represent the pooled coefficient of variation (53%) calculated from repeated experiments. Filled circles and open squares are OH experiments with open triangles (up) Fog + UV and filled triangles (down) Fog + H_2O_2.

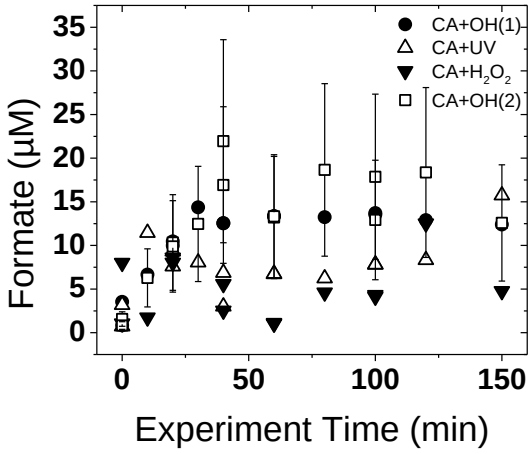

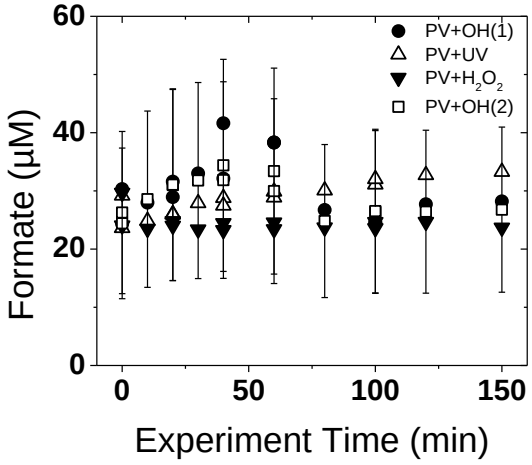

Appendix C.1.4. Shown here is **pyruvate** quantified by IC during two OH experiments and controls (UV, H_2O_2) for California and Po Valley fogs. Error bars represent the pooled coefficient of variation (68%) calculated from repeated experiments. Filled circles and open squares are OH experiments with open triangles (up) Fog + UV and filled triangles (down) Fog + H_2O_2.

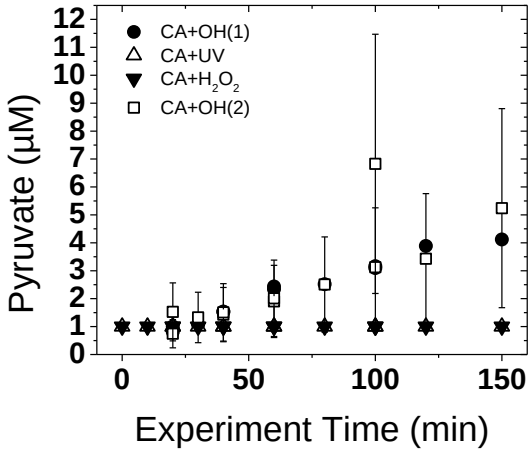

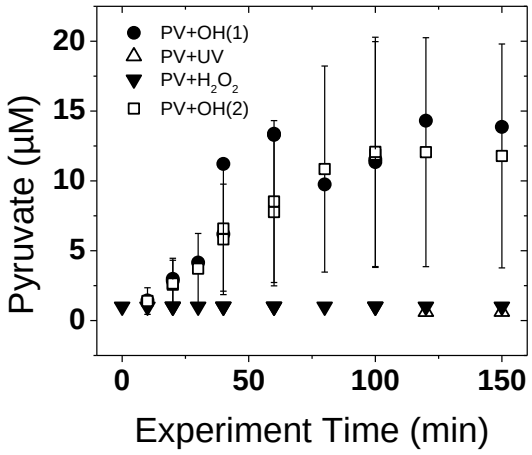

Appendix C.1.5. Shown here is **glyoxylate** quantified by IC during two OH experiments and controls (UV, H_2O_2) for Po Valley fog experiments since no signal is detected in Fresno fog experiments. Error bars represent the pooled coefficient of variation (9%) calculated from the two Po Valley + OH experiments. Filled circles and open squares are OH experiments with open triangles (up) Fog + UV and filled triangles (down) Fog + H_2O_2.

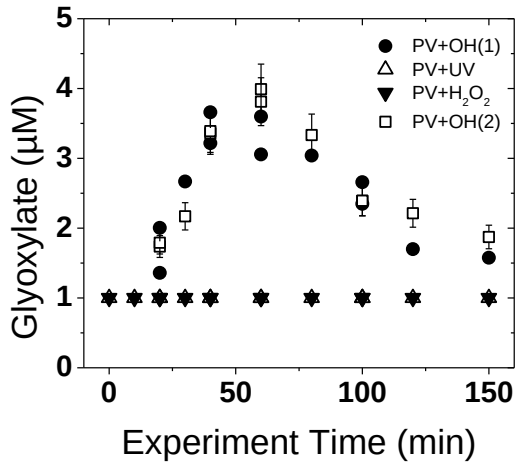

Appendix C.1.6. Shown here is **nitrate** quantified by IC during two OH experiments and controls (UV, H_2O_2) for California and Po Valley fogs. Error bars represent the pooled coefficient of variation (9%) calculated from repeated experiments. Filled circles and open squares are OH experiments with open triangles (up) Fog + UV and filled triangles (down) Fog + H_2O_2.

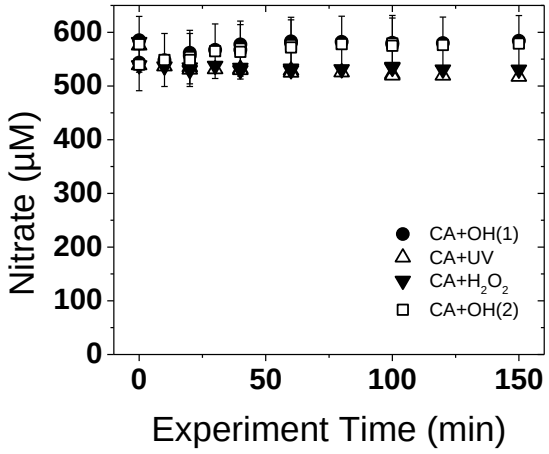

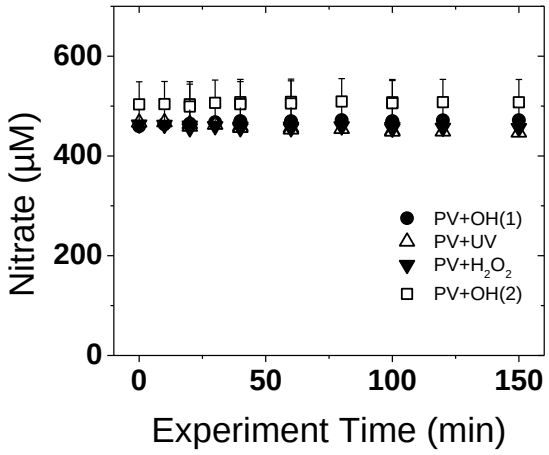

Appendix C.1.7. Shown here is **succinate** (**+ malate**; coelute) quantified by IC during two OH experiments and controls (UV, H_2O_2) for California and Po Valley fogs. Error bars represent the pooled coefficient of variation (41%) calculated from repeated experiments. Filled circles and open squares are OH experiments with open triangles (up) Fog + UV and filled triangles (down) Fog + H_2O_2.

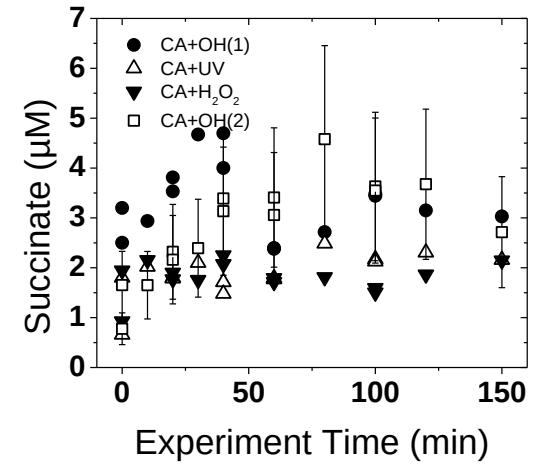

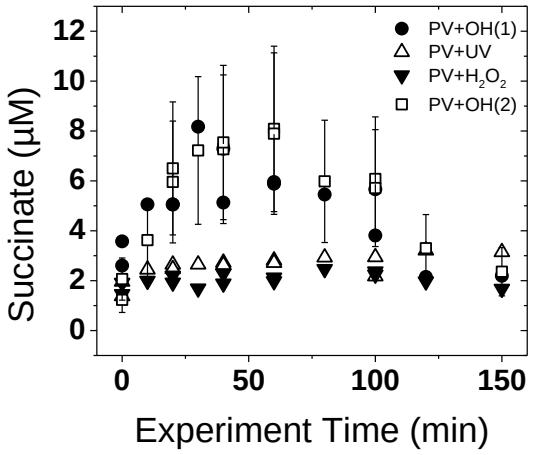

Appendix C.1.8. Shown here is **tartarate** (**+ malonate**; coelute) quantified by IC during two OH experiments and controls (UV, H_2O_2) for California and Po Valley fogs. Error bars represent the pooled coefficient of variation (50%) calculated from repeated experiments. Filled circles and open squares are OH experiments with open triangles (up) Fog + UV and filled triangles (down) Fog + H_2O_2. Field water + OH experiments had an appreciable tartarate signal which is shown here with the asterisk.

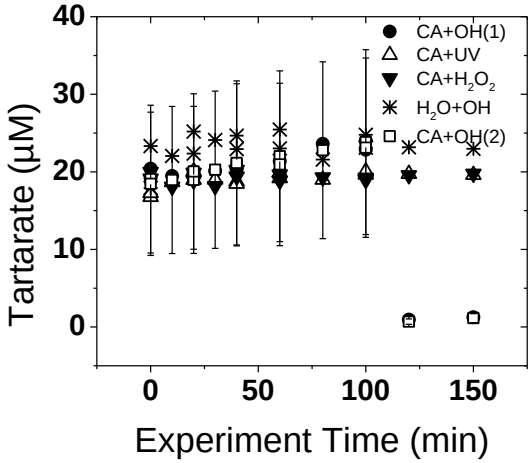

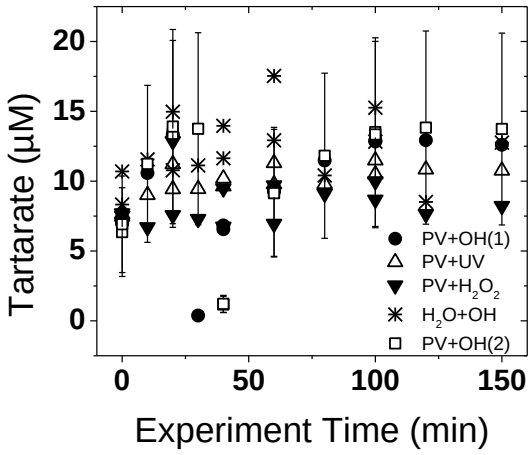

Appendix C.1.9. Shown here is **sulfate** quantified by IC during two OH experiments and controls (UV, H_2O_2) for California and Po Valley fogs. Error bars represent the pooled coefficient of variation (17%) calculated from repeated experiments. Filled circles and open squares are OH experiments with open triangles (up) Fog + UV and filled triangles (down) Fog + H_2O_2.

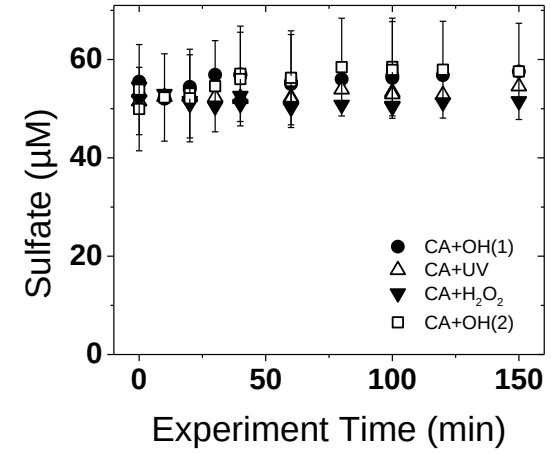

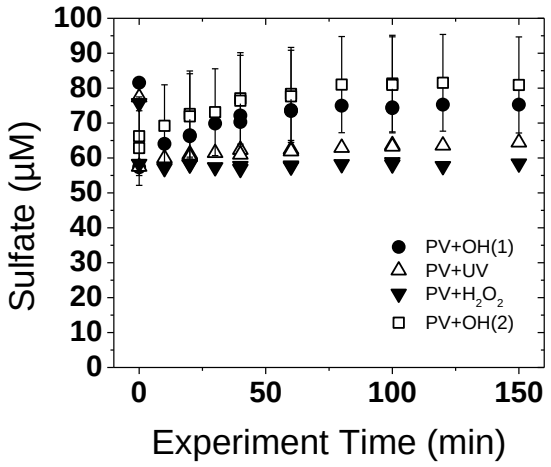

Appendix C.1.10. Shown here is **oxalate** quantified by IC during two OH experiments and controls (UV, H_2O_2) for California and Po Valley fogs. Error bars represent the pooled coefficient of variation (55%) calculated from repeated experiments. Filled circles and open squares are OH experiments with open triangles (up) Fog + UV and filled triangles (down) Fog + H_2O_2. Note that figures in chapter 4 include Field water + OH data for oxalate.

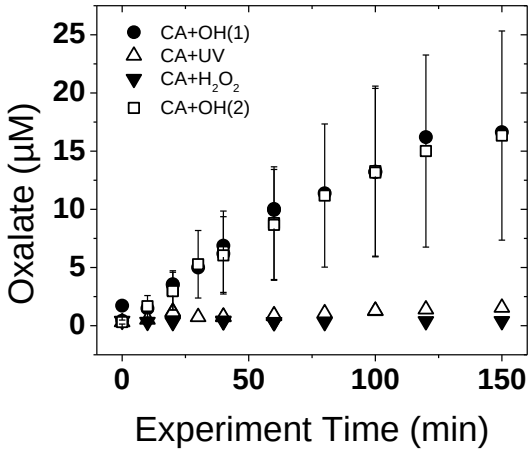

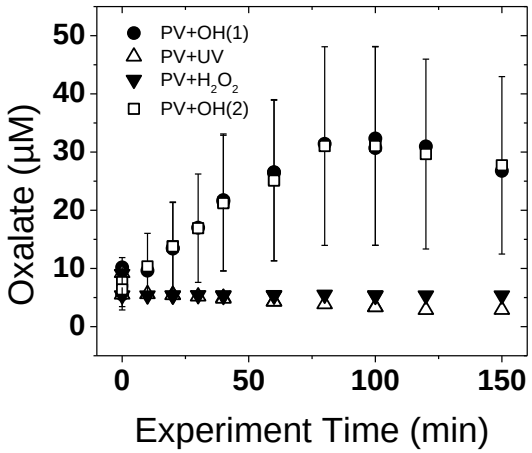

Appendix C.1.11. Shown here are the plausible structures for exact masses (2) detected at unit mass m/z+ 143 in Fresno fog. The fragmentation pattern is shown with the exact mass of the neutral molecule lost in bold text and the measured difference in plain text. Also shown is the fragmentation mass spectrum with the relevant exact masses shown.

CAfog_m/z+143 (1 of 2)

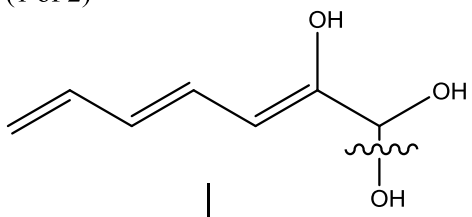

143.07019

Exact Mass
Measured Difference

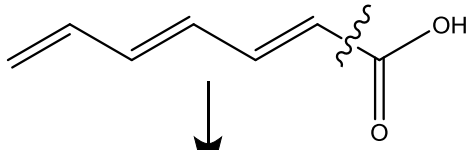

125.05963

$+H_2O$

H2O 18.010565
Diff 18.01056

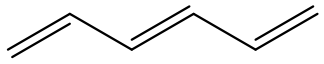

81.06982

$+CO_2$

CO2 43.989829
Diff 43.98981

CAfog_m/z+143 (2 of 2)

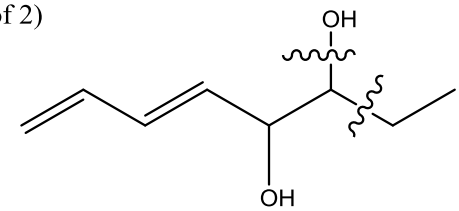

143.10663
$C_8H_{15}O_2$

H2O+C2H4 46.041865
Diff 46.04191

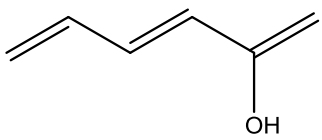

97.06472

$+H_2O + C_2H_4$

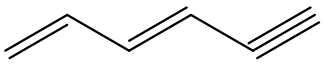

79.05416

$+H_2O$

H2O 18.010565
Diff 18.01056

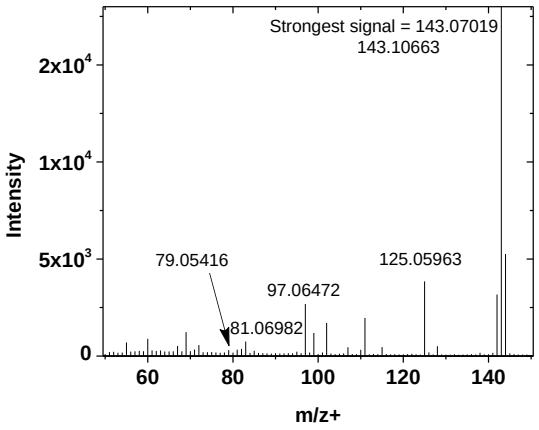
Strongest signal = 143.07019
143.10663
2x10^4
1x10^4
5x10^3
0
Intensity
79.05416
97.06472
81.06982
125.05963
60
80
100
120
140
m/z+

Appendix C.1.12. Shown here are the plausible structures for exact masses detected at unit mass m/z+ 167 in Fresno fog. The fragmentation pattern is shown with the exact mass of the neutral molecule lost in bold text and the measured difference in plain text. Also shown is the fragmentation mass spectrum with the relevant exact masses shown.

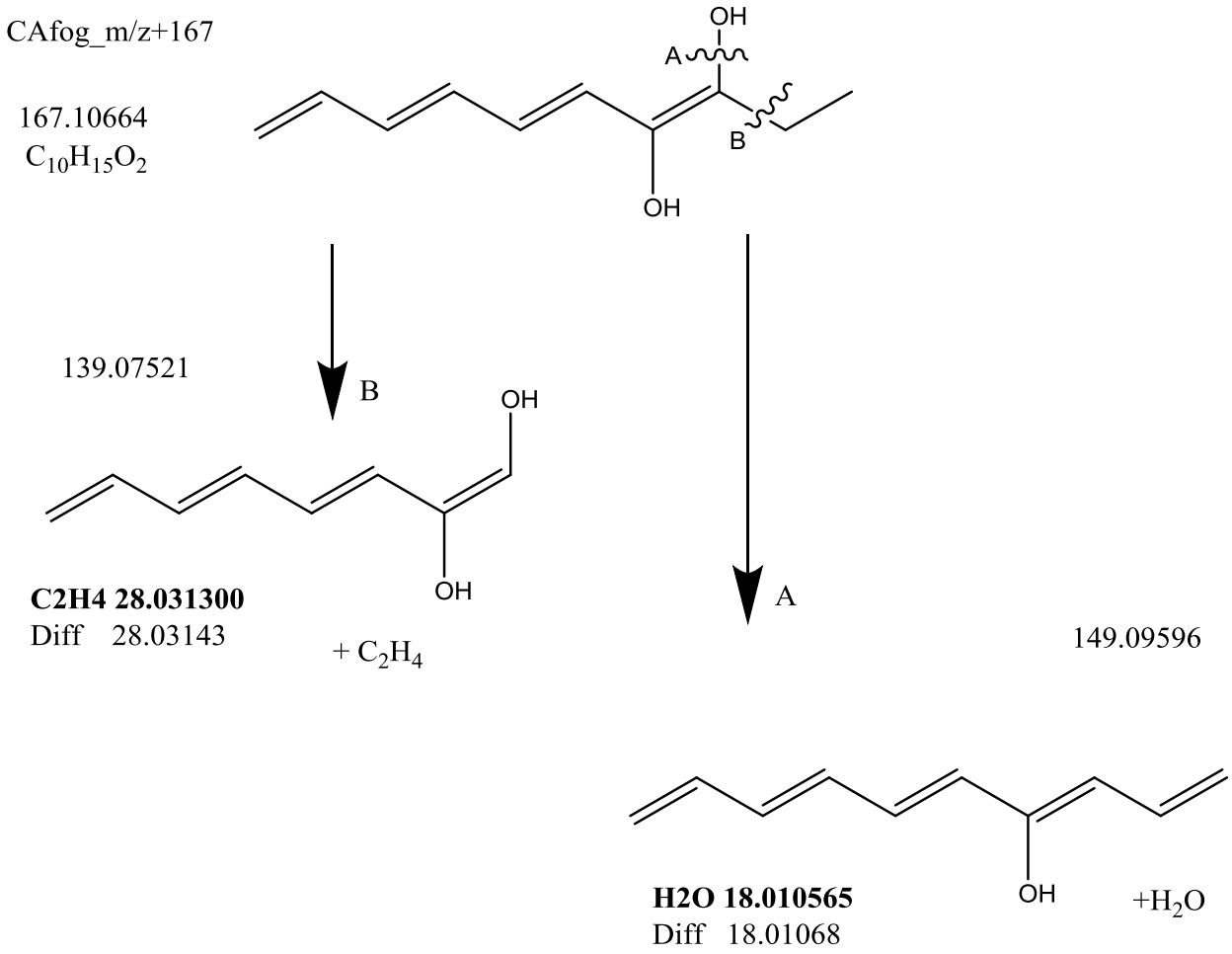

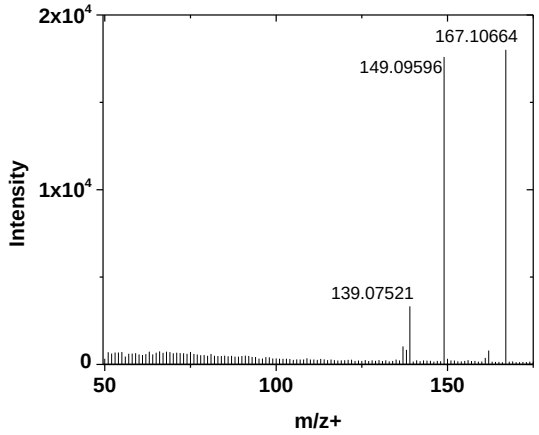

Appendix C.1.13. Shown here are the plausible structures for exact masses (2) detected at unit mass m/z+ 169 in Fresno fog. The fragmentation pattern is shown with the exact mass of the neutral molecule lost in bold text and the measured difference in plain text. Also shown is the fragmentation mass spectrum with the relevant exact masses shown.

CAfog_m/z+169 (1 of 2)

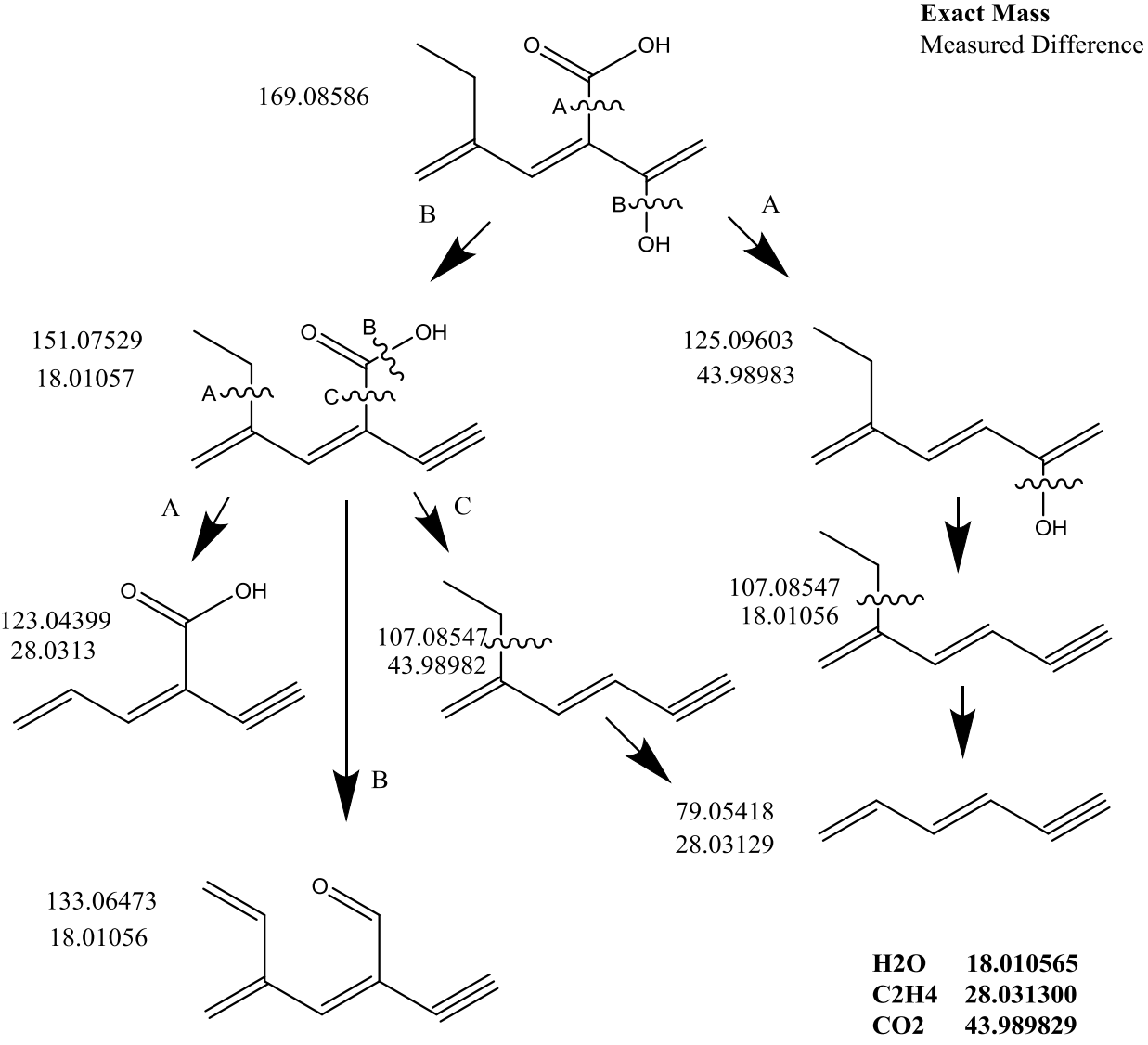

CAfog_m/z+169 (2 of 2)

169.12232

$C_{10}H_{17}O_2$

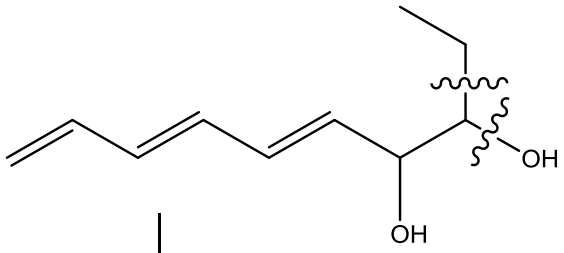

123.08038

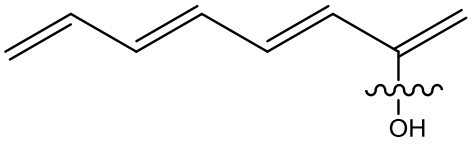

$+H_2O + C_2H_4$

H2O+C2H4 46.041865
Diff 46.04194

105.06982

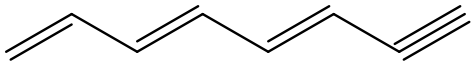

$+H_2O$

H2O 18.010565
Diff 18.01056

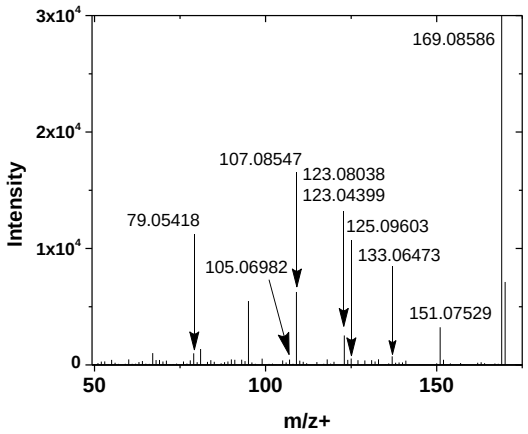

Appendix C.1.14. Shown here are the plausible structures for exact masses (2) detected at unit mass m/z+ 183 in Fresno fog. The fragmentation pattern is shown with the exact mass of the neutral molecule lost in bold text and the measured difference in plain text. Also shown is the fragmentation mass spectrum with the relevant exact masses shown.

CAfog_m/z+183 (1 of 2)

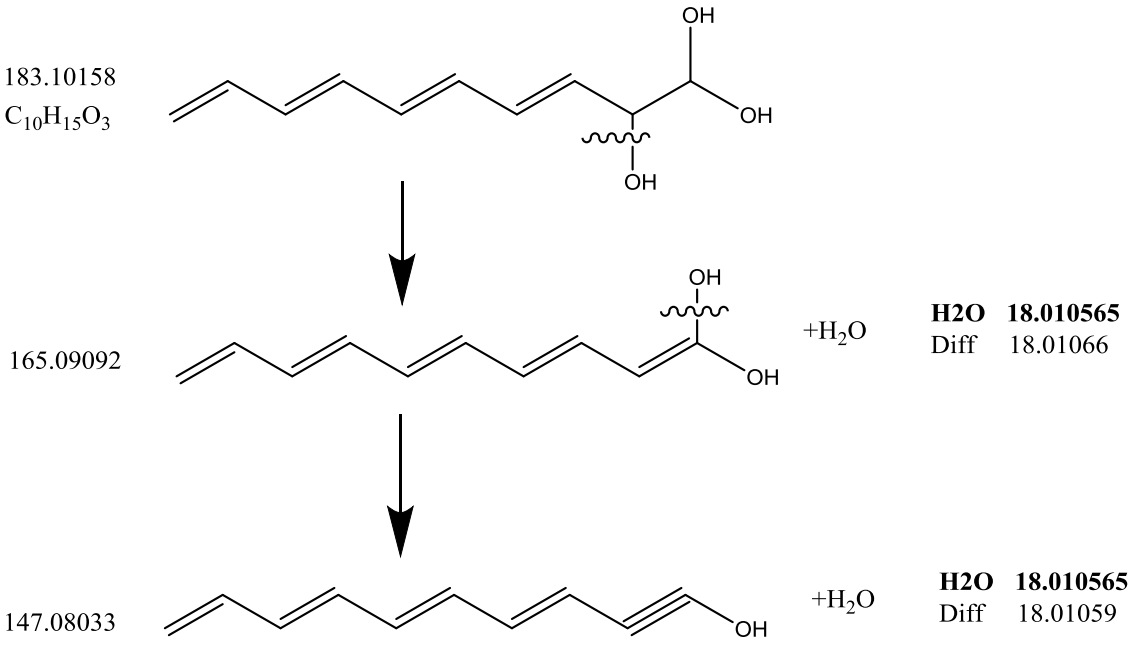

CAfog_m/z+183 (2 of 2)

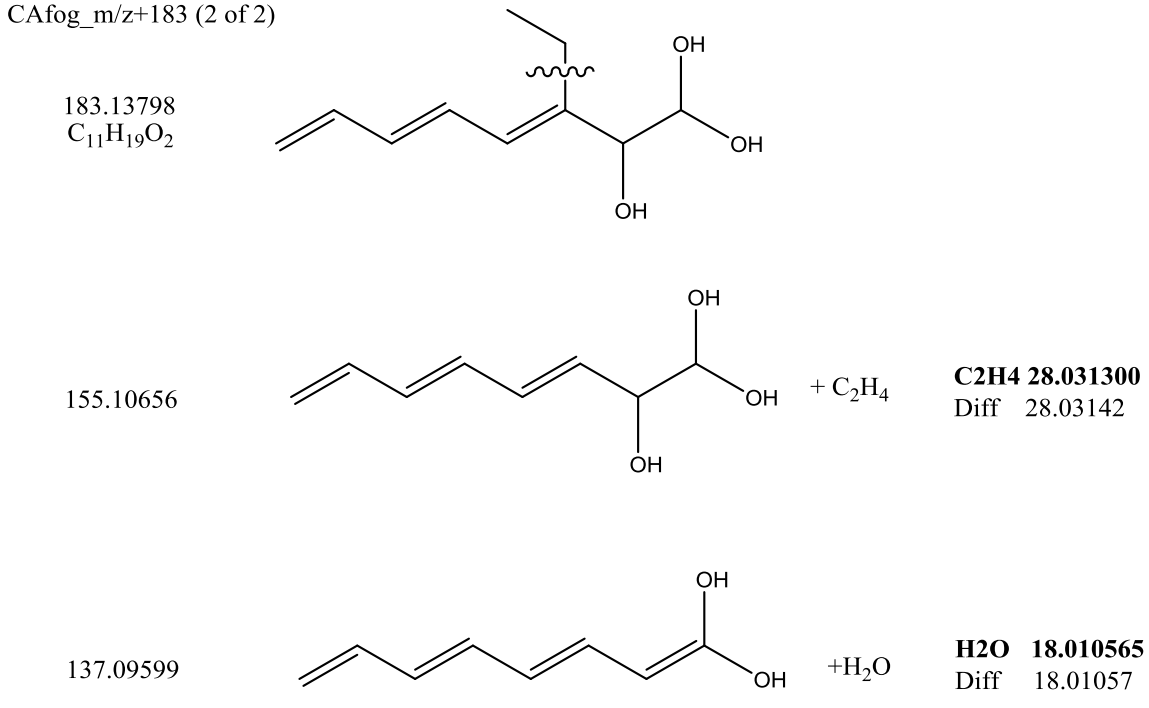

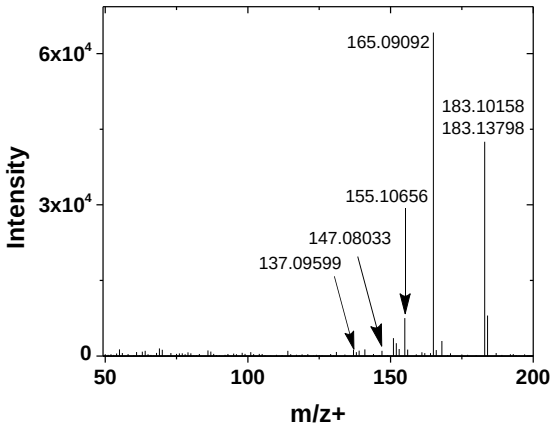
6x10^4
3x10^4
0
Intensity
50
100
150
200
m/z+
165.09092
183.10158
183.13798
155.10656
147.08033
137.09599

Appendix C.1.15. Shown here are the plausible structures for exact masses (2) detected at unit mass m/z+ 185 in Fresno fog. The fragmentation pattern is shown with the exact mass of the neutral molecule lost in bold text and the measured difference in plain text. Also shown is the fragmentation mass spectrum with the relevant exact masses shown.

CAfog_m/z+185 (1 of 2)

185.08088
$C_9H_{13}O_4$

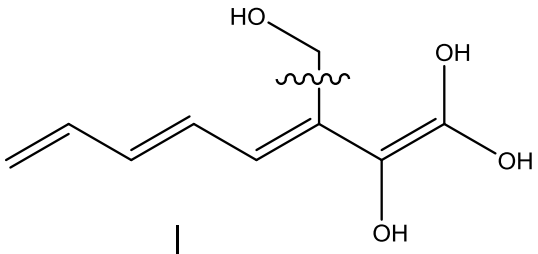

153.05452

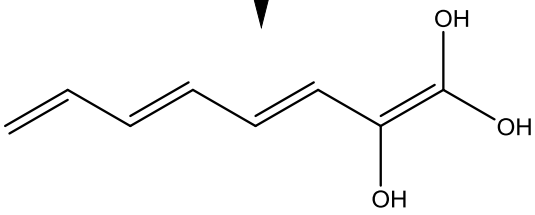

$+CH_3OH$

CH3OH 32.026215
Diff 32.02636

CAfog_m/z+185 (2 of 2)

185.11725
$C_{10}H_{17}O_3$

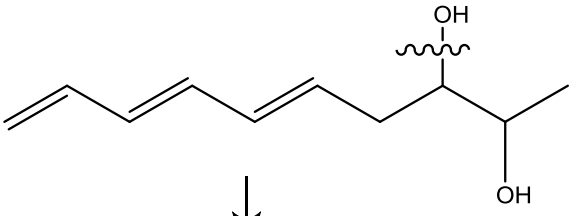

167.10657

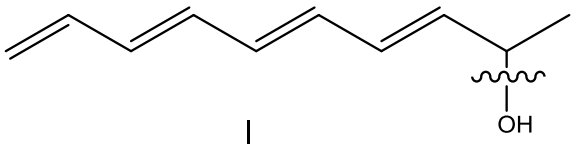

$+H_2O$

H2O 18.010565
Diff 18.01068

149.09596

$+H_2O$

H2O 18.010565
Diff 18.01061

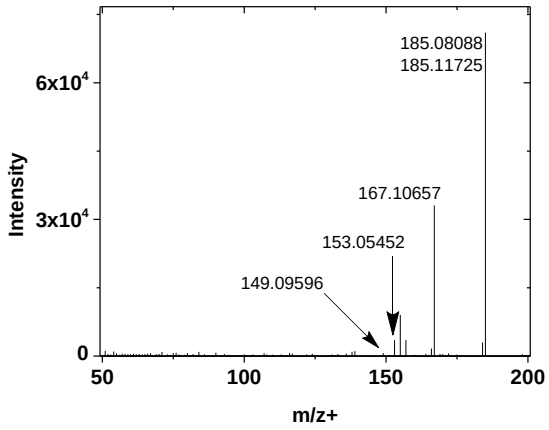
185.08088
185.11725
167.10657
153.05452
149.09596
6x10^4
3x10^4
0
Intensity
50
100
150
200
m/z+

Appendix C.1.16. Shown here are the plausible structures for exact masses (2) detected at unit mass m/z+ 113 in Po Valley fog. The fragmentation pattern is shown with the exact mass of the neutral molecule lost in bold text and the measured difference in plain text. Also shown is the fragmentation mass spectrum with the relevant exact masses shown.

PVfog_m/z+113 (1 of 2)

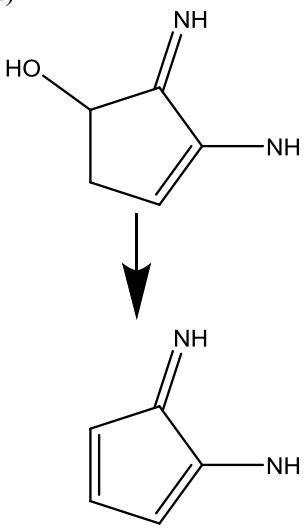

113.07089

95.06032

+H_2O

Exact Mass
Measured Difference

H2O 18.010565
Diff 18.01057

PVfog_m/z+113 (2 of 2)

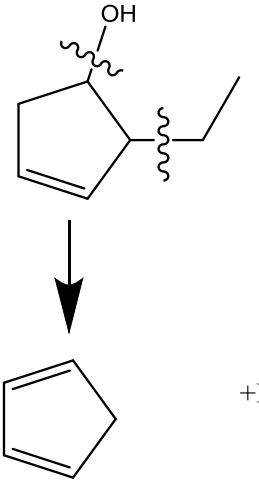

113.09605
$C_7H_{13}O$

67.05419

+H_2O +C_2H_4

H2O+C2H4 46.041865
Diff 46.04186

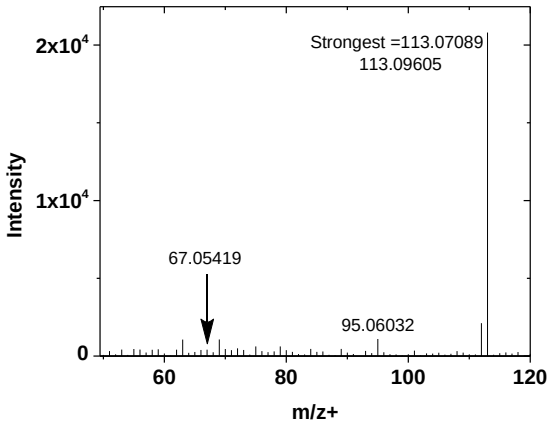
Strongest =113.07089
113.09605
67.05419
95.06032
Intensity
2x10^4
1x10^4
0
60
80
100
120
m/z+

Appendix C.1.17. Shown here are the plausible structures for exact masses (3) detected at unit mass m/z+ 153 in Po Valley fog. The fragmentation pattern is shown with the exact mass of the neutral molecule lost in bold text and the measured difference in plain text. Also shown is the fragmentation mass spectrum with the relevant exact masses shown.

PVfog_m/z+153 (1 of 3)

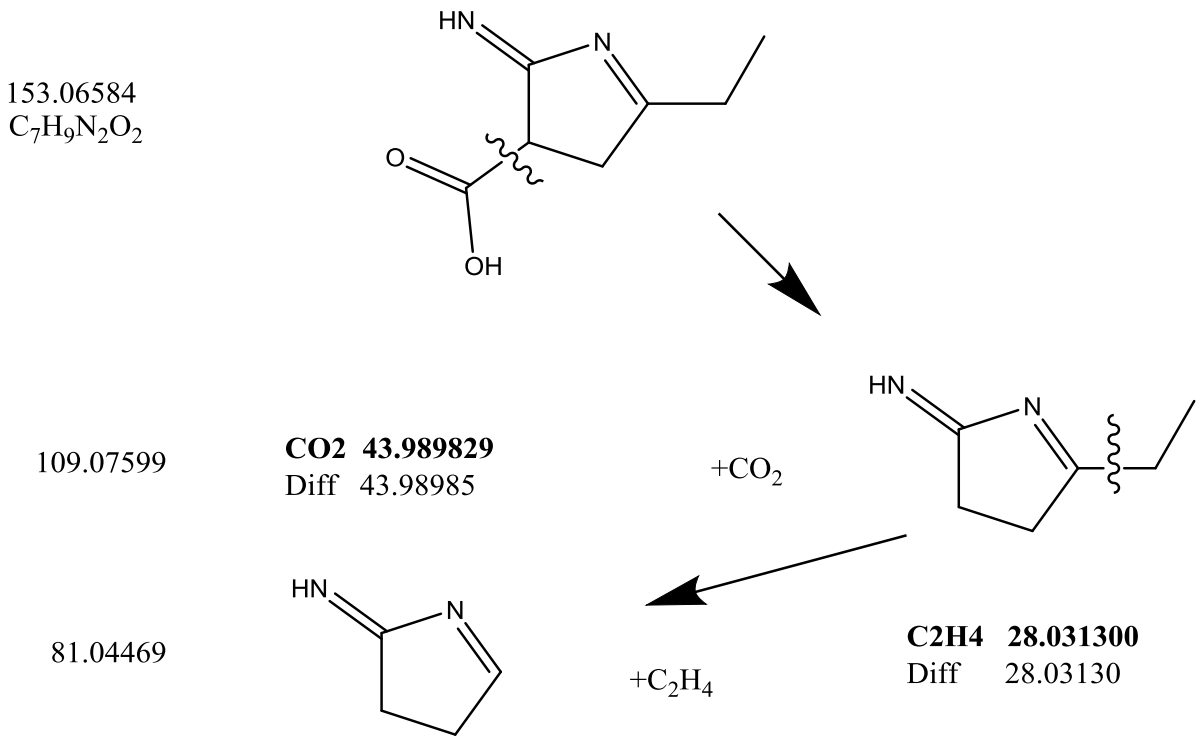

PVfog_m/z+153 (2 of 3)

Exact Mass
Measured Difference

153.10221

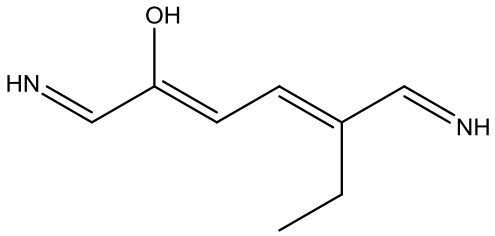

135.09164

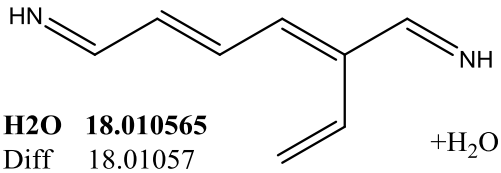

H2O 18.010565
Diff 18.01057

$+H_2O$

125.07090

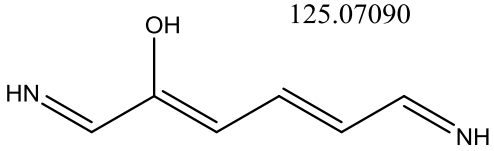

$+C_2H_4$

C2H4 28.031300
Diff 28.03131

107.06034

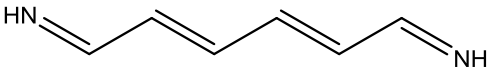

C2H4 28.031300
Diff 28.03130

$+C_2H_4$

PVfog_m/z+153 (3 of 3)

153.12738
$C_{10}H_{17}O$

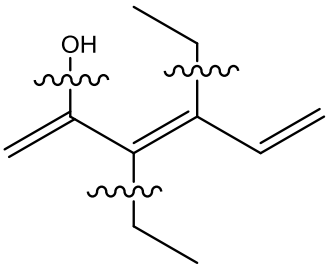

79.05419

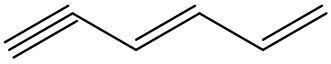

H2O,C2H4,C2H4 74.073165
Diff 74.07319

$+H_2O + 2(C_2H_4)$

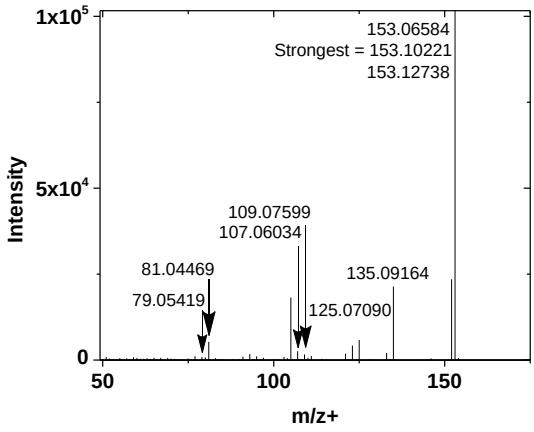
1x10^5
5x10^4
0
Intensity
153.06584
Strongest = 153.10221
153.12738
109.07599
107.06034
81.04469
79.05419
135.09164
125.07090
50
100
150
m/z+

Appendix C.1.18. Shown here are the plausible structures for exact masses (2) detected at unit mass m/z+ 167 in Po Valley fog. The fragmentation pattern is shown with the exact mass of the neutral molecule lost in bold text and the measured difference in plain text. Also shown is the fragmentation mass spectrum with the relevant exact masses shown.

PVfog_m/z+167 (1 of 2)

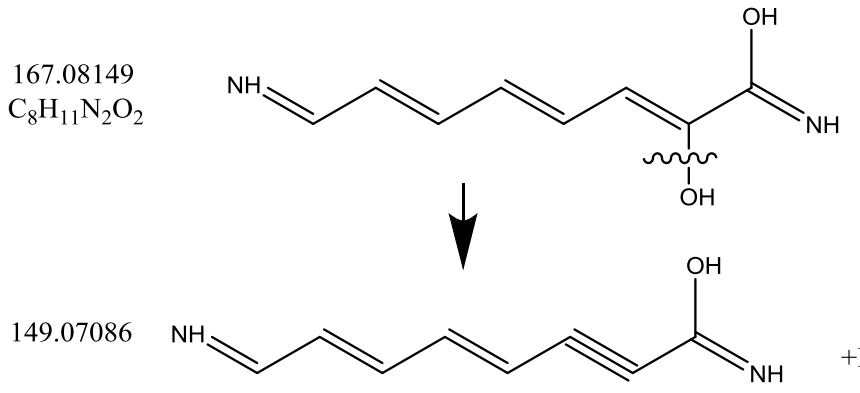

H2O 18.010565
Diff 18.01063

PVfog_m/z+167 (2 of 2)

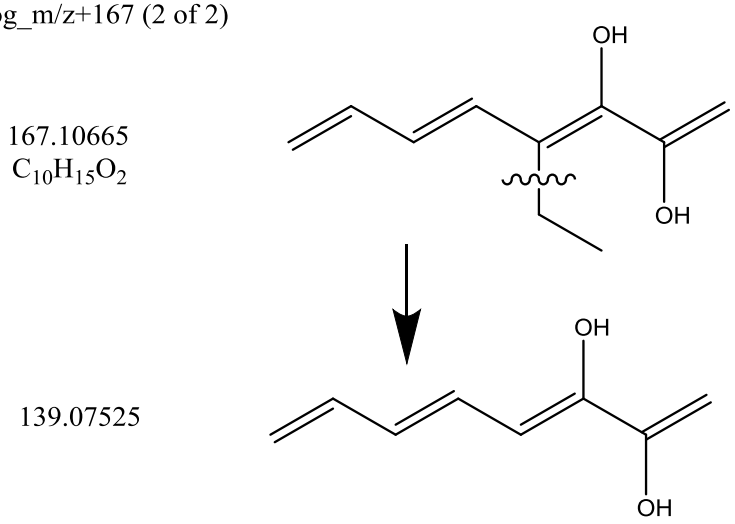

C2H4 28.031300
Diff 28.03140

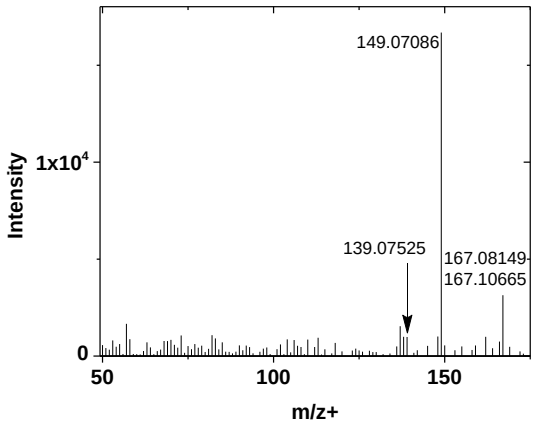
149.07086
Intensity
1x10^4
139.07525
167.08149
167.10665
0
50
100
150
m/z+

Appendix C.1.19. Shown here are the plausible structures for exact masses (4) detected at unit mass m/z+ 169 in Po Valley fog. The fragmentation pattern is shown with the exact mass of the neutral molecule lost in bold text and the measured difference in plain text. Also shown is the fragmentation mass spectrum with the relevant exact masses shown.

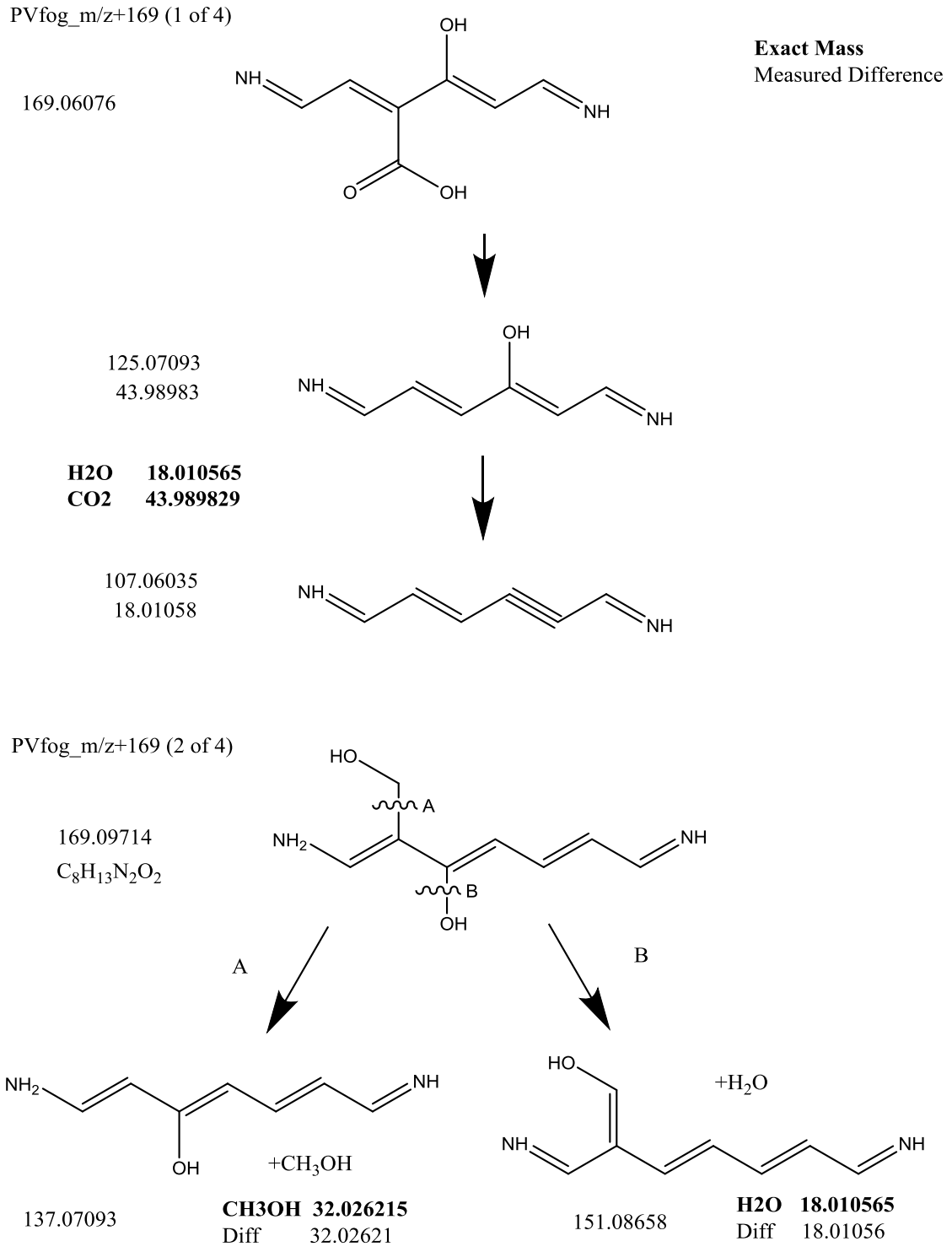

PVfog_m/z+169 (3 of 4)

169.13353
$C_9H_{17}N_2O$

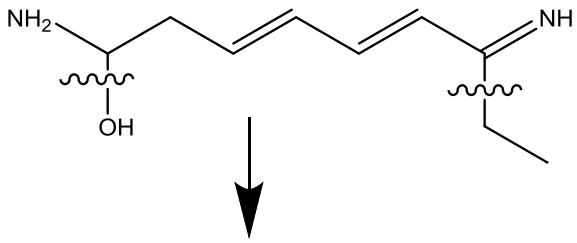

123.09166

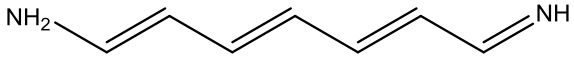

+ H_2O + C_2H_4

H2O, C2H4 46.041865
Diff 46.04187

PVfog_m/z+169 (4 of 4)

169.15869
$C_{11}H_{21}O$

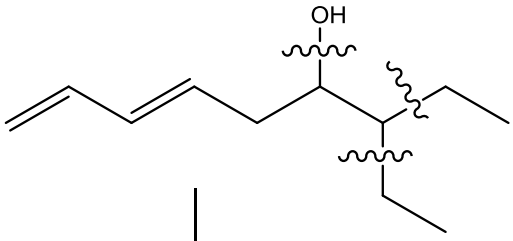

95.08550

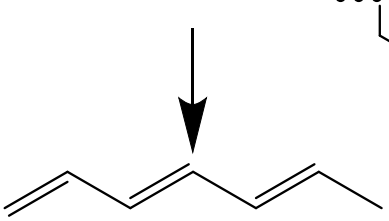

+ H_2O + C_2H_4 + C_2H_4

H2O, C2H4, C2H4 74.073165
Diff 74.07319

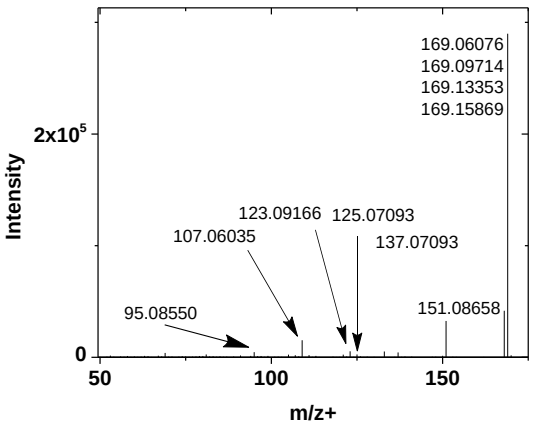

Appendix C.1.20. Shown here are the plausible structures for exact masses (2) detected at unit mass m/z+ 183 in Po Valley fog. The fragmentation pattern is shown with the exact mass of the neutral molecule lost in bold text and the measured difference in plain text. Also shown is the fragmentation mass spectrum with the relevant exact masses shown.

PVfog_m/z+183 (1 of 2)

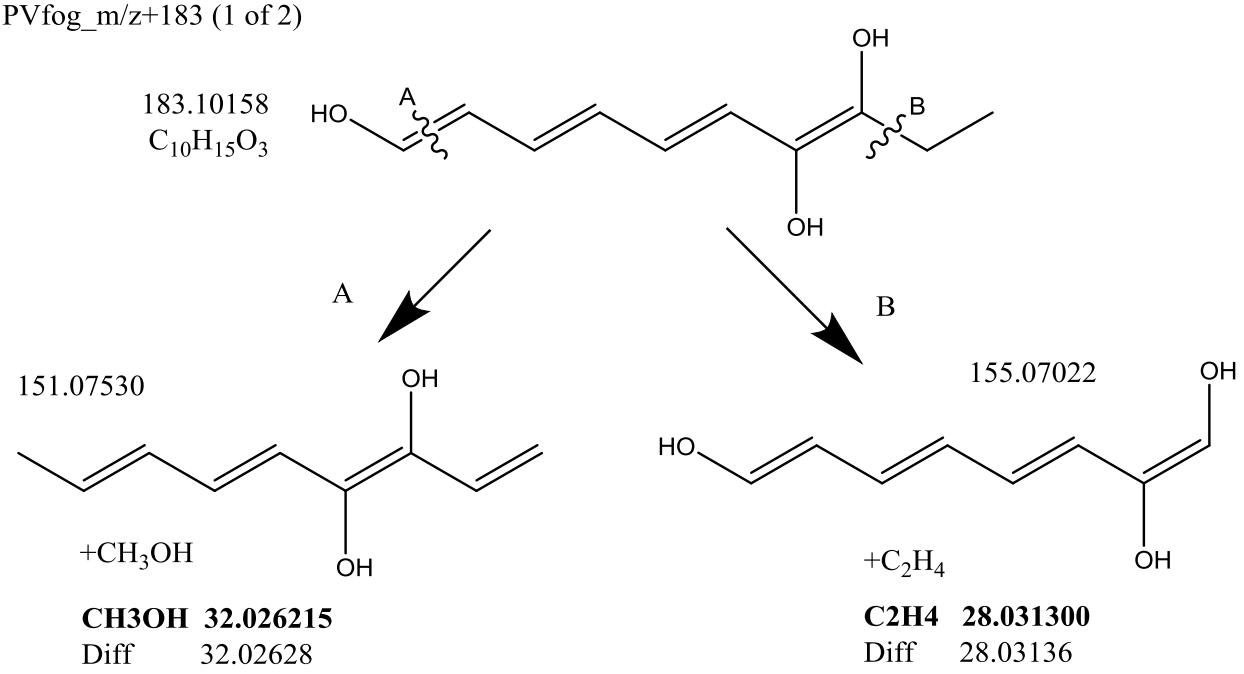

CH3OH 32.026215
Diff 32.02628

C2H4 28.031300
Diff 28.03136

PVfog_m/z+183 (2 of 2)

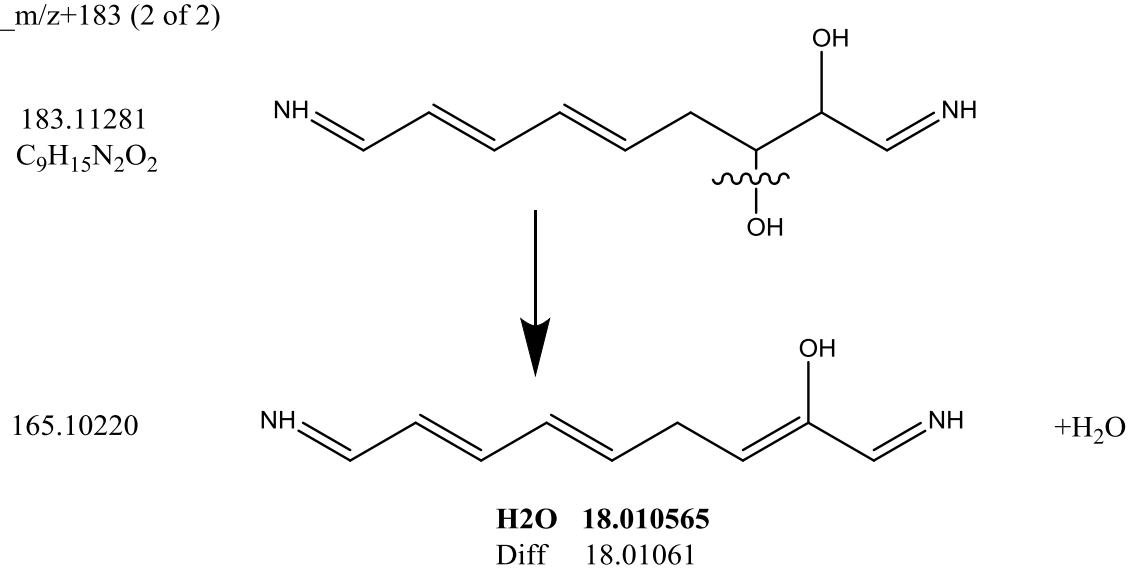

H2O 18.010565
Diff 18.01061

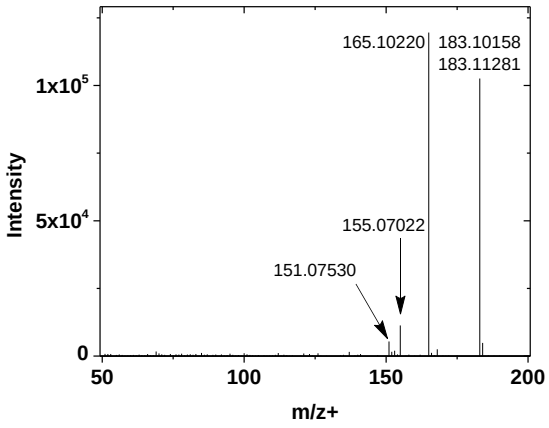
165.10220
183.10158
183.11281
155.07022
151.07530
1x10^5
5x10^4
0
Intensity
50
100
150
200
m/z+

Appendix C.1.21. Shown here are the plausible structures for exact mass detected at unit mass m/z+ 185 in Po Valley fog. The fragmentation pattern is shown with the exact mass of the neutral molecule lost in bold text and the measured difference in plain text. Also shown is the fragmentation mass spectrum with the relevant exact masses shown.

PVfog_m/z+185

185.09211
$C_8H_{13}N_2O_3$

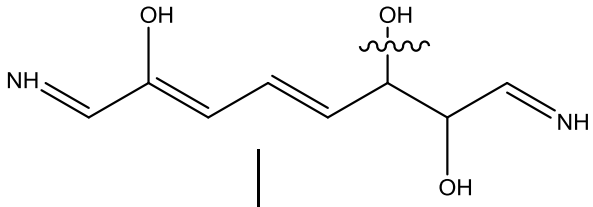

167.08147

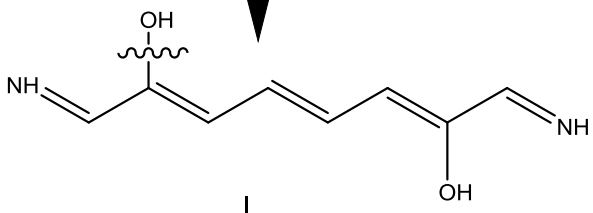

$+H_2O$

H2O 18.010565
Diff 18.01064

149.07085

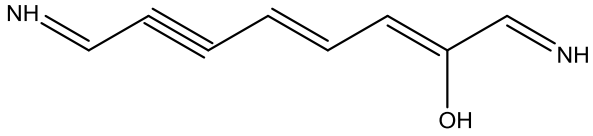

$+H_2O$
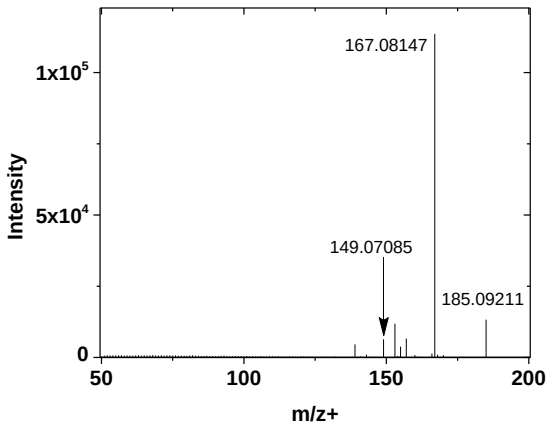
H2O 18.010565
Diff 18.01062